Photochromic glycomacrocycles : synthesis, characterization and light-controlled stereoselective glycosylation investigation

Jinbiao Jiao

▶ **To cite this version:**

Jinbiao Jiao. Photochromic glycomacrocycles : synthesis, characterization and light-controlled stereoselective glycosylation investigation. Organic chemistry. Université Paris-Saclay, 2022. English. NNT : 2022UPASF064 . tel-04762934

HAL Id: tel-04762934
https://theses.hal.science/tel-04762934v1

Submitted on 1 Nov 2024

HAL is a multi-disciplinary open access archive for the deposit and dissemination of scientific research documents, whether they are published or not. The documents may come from teaching and research institutions in France or abroad, or from public or private research centers.

L'archive ouverte pluridisciplinaire **HAL**, est destinée au dépôt et à la diffusion de documents scientifiques de niveau recherche, publiés ou non, émanant des établissements d'enseignement et de recherche français ou étrangers, des laboratoires publics ou privés.

THÈSE DE DOCTORAT

NNT : 2022UPASF064

université PARIS-SACLAY

Photochromic glycomacrocycles: synthesis, characterization and light-controlled stereoselective glycosylation investigation

Glycomacrocycles photocommutables : synthèse, caractérisation et étude de la stéréosélectivité de glycosylation contrôlée par la lumière

Thèse de doctorat de l'Université Paris-Saclay

École doctorale n° 571 Sciences Chimiques : Molécules, Matériaux, Instrumentation et Biosystèmes (2MIB)
Spécialité de doctorat : Chimie
Graduate School : Chimie. Référent : ENS Paris-Saclay

Thèse préparée dans l'unité de recherche **PPSM (Université Paris-Saclay, ENS Paris-Saclay, CNRS)**, sous la direction de **Joanne XIE**, professeure, le co-encadrement de **Stéphane MAISONNEUVE**, ingénieur de recherche

Thèse soutenue à Paris-Saclay, le 30 septembre 2022, par

Jinbiao JIAO

Composition du Jury

Membres du jury avec voix délibérative

Samir MESSAOUDI Directeur de Recherche, Université Paris-Saclay (Laboratoire BioCIS, UMR CNRS 8076)	Président
Véronique BONNET Maître de Conférences, HDR, Université de Picardie Jules Vernes (Laboratoire LG2A, UMR CNRS 7378)	Rapportrice & Examinatrice
Nadège LUBIN-GERMAIN Professeure, CY Cergy-Paris Université (Laboratoire BioCIS, UMR CNRS 8076)	Rapportrice & Examinatrice
Mickaël MENAND Maître de Conférences, Sorbonne Université (IPCM, UMR CNRS 8232)	Examinateur

ACKNOWLEDGEMENTS

This dissertation is accomplished in the « Laboratoire de Photophysique et Photochimie Supramoléculaires et Macromoléculaires (PPSM) » in École Normale Supérieure Paris-Saclay (ENS Paris-Saclay), Université Paris-Saclay. I express my sincere gratitude to all the people for giving me the help and supports during the journey to finish the thesis.

First and foremost, I would like to express my gratitudes to my advisors, Pr. Joanne Xie and Dr. Stéphane Maisonneuve. They offered me the opportunity to study at ENS de Cachan (2018.09-2020.03) and latter relocated ENS Paris-Saclay (2020.03-2022.09).

Second, I also would like to express my gratitudes to China Scholarship Council (CSC). They gave me the opportunity and scholarship to help me to study at ENS Paris-Saclay.

When I study at PPSM, my advisors, Pr. Joanne Xie and Dr. Stéphane Maisonneuve gave me lots of constructive guidance from laboratory synthetic and the spectroscopic perspectives. They also gave me lots of help in my life. I sincerely thank them for their help in my work and life. I also owe my sincere gratitude to my colleagues, Chaoqi, Jonathan, Clément, Yang, Zhaoxin, Gaoyu, Aurélie, Suzanne, Nawel, Elodie and all the PPSM's members who gave me their help.

Last my thanks would go to my beloved family for their living considerations and great support in my PhD's studying.

For this dissertation, I would like to thank the committee members: Véronique BONNET, Nadège LUBIN-GERMAIN, Mickaël MENAND and Samir MESSAOUDI.

ACRONYMS, NOTATIONS & ABBREVIATIONS

Å	ångström, a length unit, 0.1 nm
Abs	absorption
Ac	acetyl
$[\alpha]_D$	specific rotation degrees, under the wavelength of sodium D ray
Bn	benzyl
BSP	1-benzenesulfinyl piperidine
Bz	Benzoyle
t-Bu	*tert*-butyl
C	concentration
Cal	calculated
CD	circular dichroism
CIPs	contact ion pairs
CSA	camphorsulfonic acid
CuAAC	Cu(I)-catalyzed azide/alkyne cycloaddition
d	doublet (NMR) or days
DBU	1,8-diazabicyclo[5.4.0]undec-7-ene
DCC	N,N′-Dicyclohexylcarbodiimide
DCM	dichloromethane
DFT	density functional theory
DIPEA	*N*,*N*-diisopropylethylamine
DMAP	dimethylaminopyridine
DMF	*N*,*N*-dimethylformamide
DMTST	dimethyl(methylthio)sulfonium trifluoromethanesulfonate
ε	molar absorption coefficient
equiv.	equivalence
ESI	electrospray Ionization
Et	ethyl
FWHM	full width at half maxium
Glc	Glucosyl
GM	Glycomacrocycles
h	hour(s)
Hex	n-hexyl
HFIP	Hexafluoropropan-2-ol
HRMS	High Resolution Mass Spectrometry
Hyp	hydroxyproline
Hz	Hertz
IAD	intramolecular aglycone delivery
J	coupling constant
λ	wavelength, nm
LC	liquid crystal
m	multiplet (NMR)

M	$mol \cdot L^{-1}$
Man	mannosyl
Me	methyl
Mp	melting point
MS	molecular sieve
NIS	*N*-iodosuccinimide
NMR	nuclear magnetic resonance
PE	petroleum ether
Pg	protecting group
PGM	Photochromic glycomacrocycles
Ph	phenyl
ppm	parts per million
Py	pyridyl
Rf	retention factor
RT	room temperature
s	singlet (NMR)
SSIPs	solvent separated ion pairs
TBAF	tetrabutylammonium fluoride
TBAI	tetrabutylammonium iodide
TBDPS	*tert*-butyldiphenylsilyl
TD-DFT	time-dependent density functional theory
TEA	triethylamine or tetraethylammonium
TFA	Trifluoroacetic acid
TFE	2,2,2-trifluoroethanol
TfOH	triflic acid, , *a.k.a* trifluoromethanesulfonic acid
THF	tetrahydrofurane
TLC	thin layer chromatography
TMS	trimethylsilyl or tetramethylsilane (NMR)
TMSOTf	trimethylsilyl trifluoromethanesulfonate
p-TsOH	*p*-toluenesulfonic acid
UV	ultraviolet
Vis	visible

TABLE OF CONTENTS

GENERAL INTRODUCTION

Photochromic molecules are bistable molecules featuring different structural and/or electronic properties which may be reversibly isomerized by light, with the possibility to cycle up to one million "round trips". They offer numerous opportunities for reversibly photomodulating chemical, biological or pharmacological activities or proprieties. Light is generally noninvasive and orthogonal toward most elements of living systems. It can be easily and precisely controlled in time, location, wavelength and intensity, thus enabling the precise activation and deactivation of biological function. It offers also the potential to change the properties of defined molecules in biological systems with minimal disturbance to the rest of the system. There is increasing use of the photoisomerization to control the conformation as well as the activities of nucleic acids, peptides, proteins or ionic canals. As molecular photoswitch, azobenzene offers numerous opportunities for the applications thanks to its small size, its large conformational change induced by the photoisomerization, the availability of numerous synthetic methods, as well as the various possibilities of strutural modification to tune the photophysical properties.

As the most abundant renewable biomass on the earth, carbohydrates are enantiomerically pure and biodegradable. They represent highly valuable chiral compounds to be conjugated with photochromic compounds as chiral molecular photoswitches. Furthermore, spatiotemporally controlling the structure and functions of carbohydrates by light would be particularly interesting since carbohydrates are optically transparent. However, introducing a photochromic unit on the carbohydrates represents a relatively under-explored approach to developing new chemical tools for different applications.

Glycosyl azobenzenes have been developed as photocontrollable surfactants, for chiral discrimination or reversible switching of bacterial adhesion, and so on. Photoswitchable glycomacrocycles have also been reported since 2017, showing excellent photoswitching properties, large conformational changes and very interesting chiroptical properties. As a continuing interest in the development of photoswitchable glycomacrocycles of our group, this PhD thesis is devoted to the investigation of the photocontrol of the stereochemistry of glycosylation through 'intramolecular aglycon delivery' by using azobenzene-based photoswitchable tether, and generating new photoswitchable glycomacrocycle so as to study their photoswitching, chiroptical and ion-complexation properties.

This dissertation is composed of three chapters. **Chapter I** of this manuscript is devoted to the bibliographic work covering the knowledge of glycosylation, glycomacrocycles, photochromism and photoswitchable glycomacrocycles of the whole work. The **Chapter II** is devoted to synthesize photochromic glycomacrocycles containing the triazole linkers through the intramolecular glycosylation, and to study the influence of the configuration the azobenzene tether on the outcome and the stereoselectivity of glycosylation by light illumination. In the **Chapter III**, we focus on the photochromic and chiroptical properties investigation of the glycomacrocycles, as well as their ion recognition properties.

Chapter I

Chapter I - INTRODUCTION TO GLYCOSYLATION, GLYCOMACROCYCLES AND PHOTOCHROMISM

1. Glycosylation

Carbohydrates, or sugars, are among the most important biomolecules in life science. Carbohydrates exist as glycosides, polysaccharides, or glycoconjugates in nature. Carbohydrates are not only used to store energy or as a structural component of the cell wall, but also mediate various biological processes, such as immune response, fertilization, cell growth and communication.[1] Carbohydrates play a vital role in many pathological processes, including inflammation, bacterial infection, virus invasion, cancer metastasis, etc.[2] Undoubtedly, understanding the mechanism of carbohydrate participation in pathological processes would facilitate the development of detection and treatment of related diseases.

Obviously, the prerequisite for research in glycobiology is to obtain a sufficient amount of pure carbohydrates. One method is to isolate them from natural sources. This method is difficult and cumbersome because of the low abundance and heterogeneity in nature. Therefore, sophisticated carbohydrates are usually obtained through chemical synthesis. In fact, whether it is an oligosaccharide, a polysaccharide, or a glycoconjugate, glycosidic bonds represent the main linkage between sugars units and other biomolecules. So the formation of glycosidic bonds from glycosylation is one of the most important reactions in the field of glycoscience.

Glycosylation is a coupling reaction to form the new glycosidic linkage between glycosyl donor and glycosyl acceptor. The glycosyl donor is usually equipped with an anomeric leaving group, whose activation can trigger the glycosylation. The glycosyl acceptor is usually equipped with a hydroxyl group, which can make the nucleophilic attack on the activated anomeric center to terminate the glycosylation. Generally, to have the glycosidic linkage at a particular position, all other functional groups of glycosyl donor and glycosyl acceptor need to be protected.

The general mechanism of glycosylation is illustrated in ***Scheme 1***. The promoter A-B can activate the leaving group of the glycosyl donor to get the activated donor which, after the dissociation, leads to glycosyl cation, or oxacarbenium ion or other intermediates. Then the nucleophilic attack of glycosyl acceptor from the top or the bottom face on the activated anomeric center forms a mixture of α- and β-glycosides.[3,4,5]

[1] C. R. Bertozzi, L. L. Kiessling, *Science* **2001**, *291*, 2357-2364.
[2] V. Ajit, C. Richard, E. Jeffrey, F. Hudson, H. Gerald, M. Jamey, Essentials of glycobiology, *Cold Spring Harb. Lab. Press N. Y.* **2009**.
[3] L. K. Mydock, A. V. Demchenko, *Org. Biomol. Chem*. **2010**, *8*, 497-510.
[4] D. Crich, *Acc. Chem. Res.* **2010**, *43*, 1144-1153.
[5] T. G. Frihed, M. Bols, C. M. Pedersen, *Chem. Rev*. **2015**, *115*, 4963-1153.

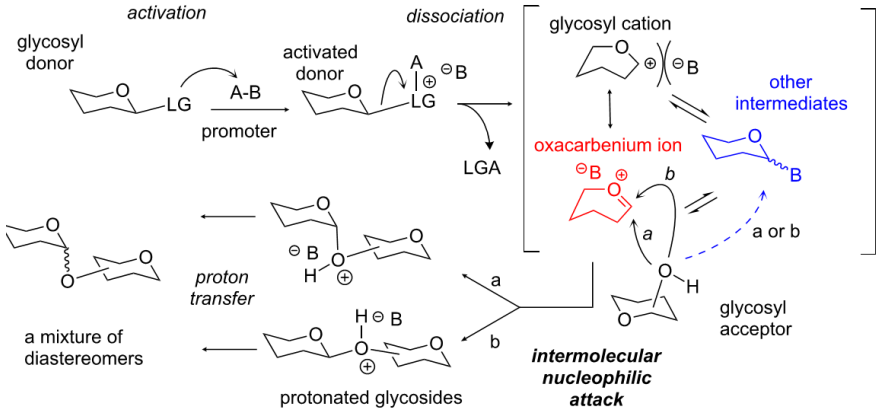

Scheme 1. *Mechanistic outline of the intermolecular glycosylation reaction*[6]

Recent investigations have demonstrated that the promoter can activate the leaving group of the glycosyl donor to form several intermediates species, including activated donor (α- or β-form), contact ion pairs (CIPs, α- or β-form) and solvent separated ion pairs (SSIPs).[7,8,9] The nucleophilic attack of the glycosyl acceptor on the activated anomeric center of the glycosyl acceptor could follow S_N2-like or S_N1-like mechanism on oxocarbenium ions (CIPs and SSIPs), forming β-glycoside if the attacking takes place from the top face and α-glycoside from the bottom side (**Scheme 2**).

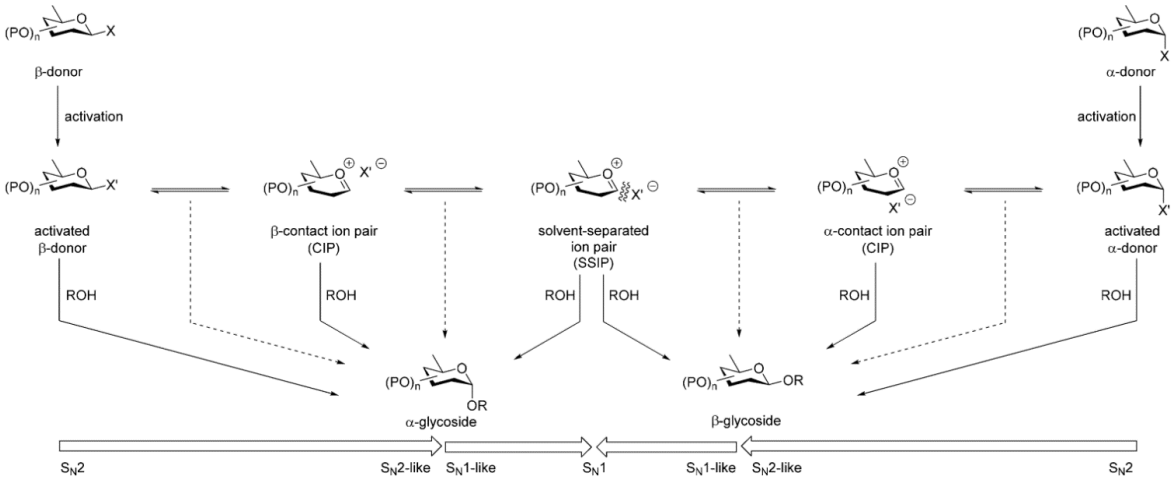

Scheme 2. *General mechanism of the glycosylation*[3,4,5,7]

There are four different kinds of linkages found in nature: manno-type β-linkage, manno-type α-linkage, gluco-type α-linkage and gluco-type β-linkage. According to the orientations of functional groups at C-1 and C-2, it has two forms: 1,2-cis and 1,2-trans (**Figure 1**).[10] As we know, the anomeric configuration has a huge influence on the molecular structure, properties and biological functions. For example, amylose and cellulose, which are anomeric diastereoisomers composed both of glucose unit, have a different biological role: the first one is a food source and the second a structural component of wood. Carbohydrate and their conjugates remain challenging

[6] X. G. Jia, A. V. Demchenko, *Beilstein J. Org. Chem*. **2017**, *13*, 2028-2048.
[7] L. Bohé, D. Crich, *Comptes Rendus Chim*. **2011**, *14*, 3-16.
[8] L. Bohé, D. Crich, *Carbohydr. Res*. **2015**, *403*, 48-59.
[9] P. O. Adero, H. Amarasekara, P. Wen, L. Bohe, D. Crich, *Chem. Rev*. **2018**, *118*, 8242-8284.
[10] R. A. Mensink, T. J. Boltje, *Chem. Eur. J.* **2017**, *23*, 17637-17653.

targets for chemists due to the requirement for elaborate protecting and leaving group manipulations to control the stereoselectivity of glycosylation, functionalization, tedious purification, and sophisticated characterization. Achieving high stereocontrol in glycosylation reactions is still challenging despite various developed glycosylation methods and strategies.

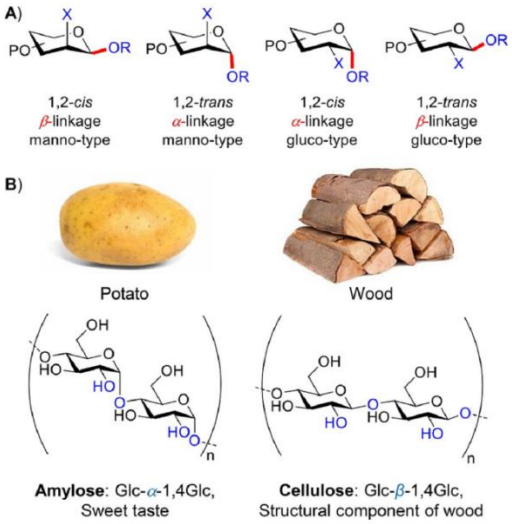

Figure 1. *Structures of anomeric linkages*[7]

1.1. Different glycosyl donors

For the glycosyl donor, the leaving group and the protecting groups (mostly of hydroxyls) have influence on the outcome of glycosylation.[11,12] For the glycosylation, the leaving group of the glycosyl donor can determine the activating mode of the glycosylation and also can determine the reactivity. The common leaving group and reaction method are listed in **Table 1**.

Table 1. *Common leaving groups of the glycosyl donors*

Type of Donors/Method	Structure	Reaction conditions
The Koenigs-Knorr method[13,14]	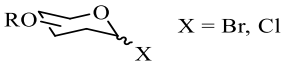 X = Br, Cl	R'OH Silver salts or Mercury salts or Lewis acid
Glycosyl fluoride[15,16]		R'OH, silver salts (Lewis acid)
Glycosyl trichloroacetimidate[17,18]	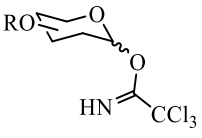	R'OH Lewis acid

[11] S. C. Ranade, A. V. Demchenko, *J. Carbohydr. Chem.* **2013**, *32*, 1-43.
[12] J. Guo, X.-S. Ye, *Molecules* **2010**, *15*, 7235-7265.
[13] H. Paulsen, *Angew. Chem. Int. Ed. Engl*. **1982**, *21*, 155-173.
[14] H. Paulsen, *Chem. Soc. Rev*. **1984**, *13*, 15-45.
[15] K. C. Nicolaou, R. E. Dolle, D. P. Papahatjis, *J. Am. Chem. Soc*. **1984**, *106*, 4189-4192.
[16] T. Matsumoto, H. Maeta, K. Suzuki, G. Tsuchihashi, *Tetrahedron Lett.* **1988**, *29*, 3567-3570.
[17] R. R. Schmidt, J. Michel, *Angew. Chem. Int. Ed. Engl*. **1980**, *19*, 731-732.
[18] R. R. Schmidt, *Angew. Chem. Int. Ed. Engl.* **1986**, *25*, 212-235.

Thioglycoside[19,20]		R'OH $Hg(OAc)_2$ or NBS or DMTST or IDCP or NIS/TfOH
Glycosyl silyl ether[21]	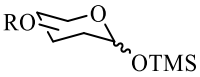	R'OH TMSOTf
Glycosyl sulfoxide[22,23]	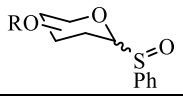	R'OH DTBMP, Tf_2O
Glycosyl hydroxide[24]	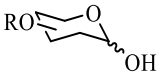	R'OH Ph_2SO, Tf_2O

Since the development of these glycosylation methods, their activation conditions (reagents or catalysts) have been generalized. Obviously, the orientation of the leaving group has little effect on the glycosylation through S_N1 mechanism. Some glycosyl donors generated excellent stereoselectivity. For example, the Koenigs-Knorr method[25,26], thioglycoside[17,27], and glycosyl trichloroacetimidate[18,19] have good *1,2-cis* selectivity. However, it is generally difficult to have a good stereocontrol of the anomeric configuration. The activating system and the reaction conditions can also influence the stereoselectivity and the yield of the glycosylation.

1.2. Participating groups on the glycosyl donors

Sometime, the neighboring protecting groups can participate the reaction and influence on the stereoselectivity of the glycosylation (**Scheme 3**). Without neighboring protecting groups, *1,2-cis* glycoside is usually the main product due to the anomeric effect. In the presence of participating group, for example, an ester function on the 2-position, *1,2-trans* glycoside is obtained as the main product.

[19] K. C. Nicolaou, S. P. Seitz, D. P. Papahatjis, *J. Am. Chem. Soc*. **1983**, *105*, 2430-2434.
[20] J. D. C. Codée, R.E. J. N. Litjens, L. J. Bos, H. S. Overkleefta, G. A. Marel, *Chem. Soc. Rev.* **2005**, *34*, 769-782.
[21] L. F. Tietze, P. Fischer, H. J. Guder, *Tetrahedron Lett.* **1982**, *23*, 4661-4664.
[22] D. Kahne, S. Walker, Y. Cheng, D. V. Engen, *J. Am. Chem. Soc*. **1989**, *111*, 6881-6882.
[23] D. Crich, S. Sun, *J. Am. Chem. Soc*. **1998**, *120*, 435-436.
[24] B. A. Garcia, J. L. Poole, D. Y. Gin, *J. Am. Chem. Soc*. **1997**, *119*, 7597-7598.
[25] H. Paulsen, *Chem. Soc. Rev*. **1984**, *13*, 15-45.
[26] K. C. Nicolaou, R. E. Dolle, D. P. Papahatjis, *J. Am. Chem. Soc*. **1984**, *106*, 4189-4192.
[27] T. Matsumoto, H. Maeta, K. Suzuki, G. Tsuchihashi, *Tetrahedron Lett.* **1988**, *29*, 3567-3570.

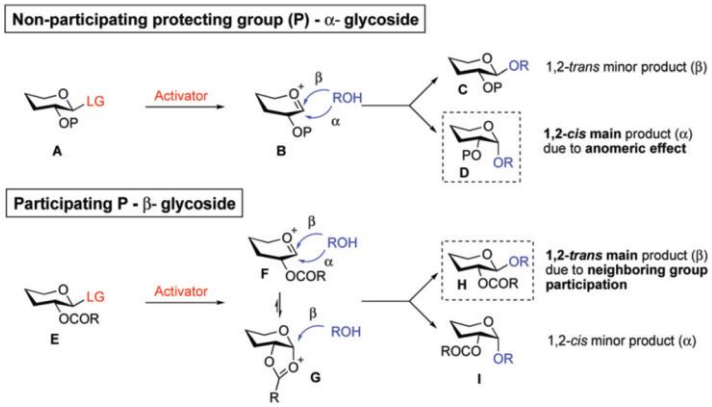

Scheme 3. *Strategies accessing 1,2-cis- and trans-glycosides*[28]

For instance, for the glycosyl donor with a participating group at C-2 position (**Scheme 4**), the promoter can activate the leaving group, leading to the acyloxonium as the major intermediate which favors the nucleophlic attack from the opposite β-face, forming the β-glycoside.

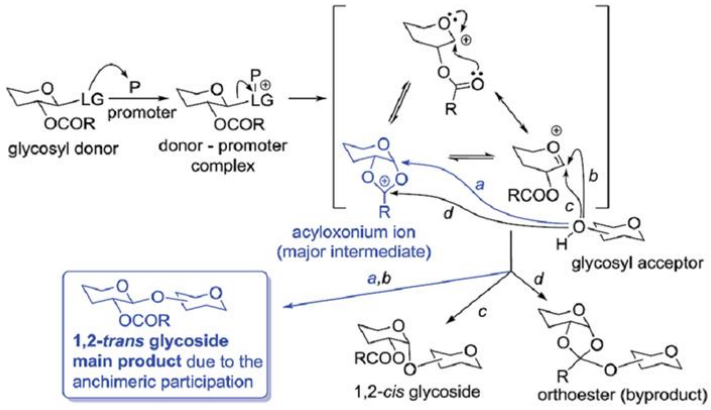

Scheme 4. *Mechanism of glycosylation with a participating group at C-2 position*[4]

1.3. Effect of the glycosyl acceptor

The reactivity of glycosyl acceptors is relatively poorly understood, contrary to the glycosyl donors. Axial OH of the sugar is bulkier, and usually less reactive than equatorial OH. If all the hydroxyls are at equatorial position in an aldopyranoside, the order of the reactivity is as follows: 6-OH > > 3-OH > 2-OH > 4-OH.[30] Generally, before doing the glycosylation, the non-reacting hydroxyl groups of the glycosyl acceptor should be protected to avoid the formation of mixtures of regioisomers. The sugar configuration, the number and the position of the hydroxyl groups and the nature of the protecting group could affect the yield and selectivity.[30]

For example, Sinaÿ and co-workers have carried out the influence of the protecting groups of the acceptor on the results of glycosylations of galactosyl bromide **#1** (**Table 2**).[29,30] The results showed that the reactions have good yields for the acceptors with an *O*-benzyl (**#2**) or *O*-allyl (**#3**, **#4**) group at the C-3 position. Comparing the glycosylation of the acceptor **#5** with that of the

[28] G. Bati, J.-X. He, K. B. Pal, X.-W. Liu, *Chem. Soc. Rev*. **2019**, *48*, 4006-4018.
[29] P. Sinaÿ, *Pure Appl. Chem.* **1978**, *50*, 1437-1452.
[30] S. Vorm, T. Hansen, J. Hengst, H. S. Overkleeft, J. D. C. Codée, *Chem. Soc. Rev.* **2019**, *48*, 4688-4706.

acceptor **#2** or **#3**, the yield of the reaction dropped to a mere 5% because of an *O*-acetyl group at the C-3 position of the acceptor **#5**.

Table 2. *Influence of protecting groups of acceptor on the glycosylation yield*[29]

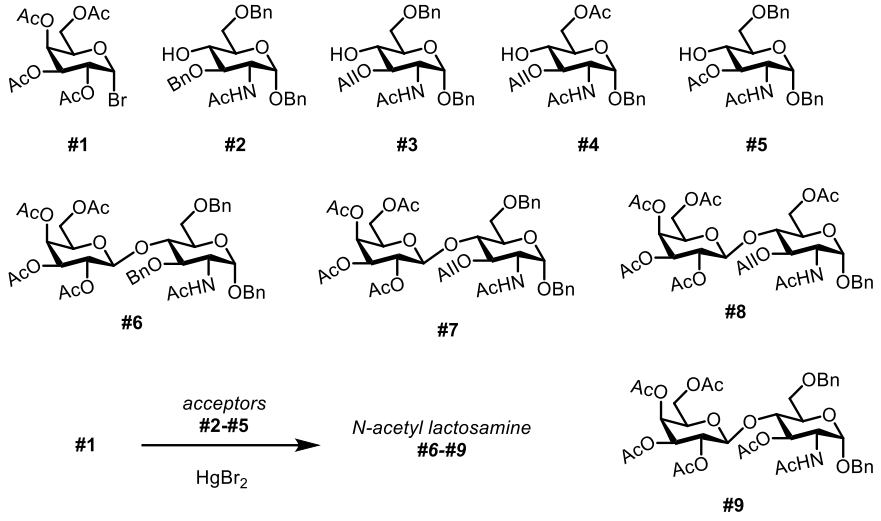

Glycosyl donor	Product	Yield (%)
#1	**#2**	87
#1	**#3**	77
#1	**#4**	78
#1	**#5**	5

All glycosylations proceeded with exclusive β-selectivity

1.4. General methods of intramolecular glycosylation

Intramolecular glycosylation is a strategy developed to control the stereoselectivity of the glycosylation. By linking the glycosyl donor-acceptor pairs together, it's possible to increase the efficiency and selectivity of the glycosylation by bringing the reaction counterparts in close distance and in orientated conformation. The desired saccharide can be obtained after the tether removal (***Scheme 5***).[31]

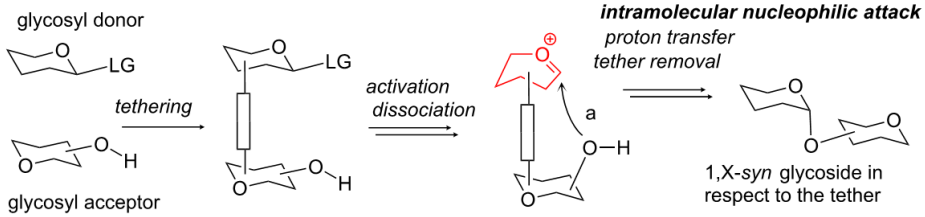

Scheme 5. *The mechanistic outline of intramolecular glycosylation reaction*[31]

In order to realize intramolecular glycosylation, it's firstly necessary to construct the glycosyl donor-acceptor pairs by using the tethers to link the glycosyl donor and glycosyl acceptor, then do the intramolecular glycosylation to get the corresponding glycomacrocycles. There are three general strategies to achieve intramolecular glycosylations: 'molecular clamp' concept with the attachment of the glycosyl donor and acceptor away from the reactive centers (**Figure 2**A); intramolecular aglycone delivery (IAD) where the glycosyl donor is tethered directly via the hydroxy group of the glycosyl acceptor to be glycosylated (**Figure 2**B); and leaving group-based

method with the glycosyl acceptor linked to the leaving group of the glycosyl donor (**Figure 2**C).[31] The 'molecular clamp' concept has been mostly developed. The flowing presentation will focus on this approach.

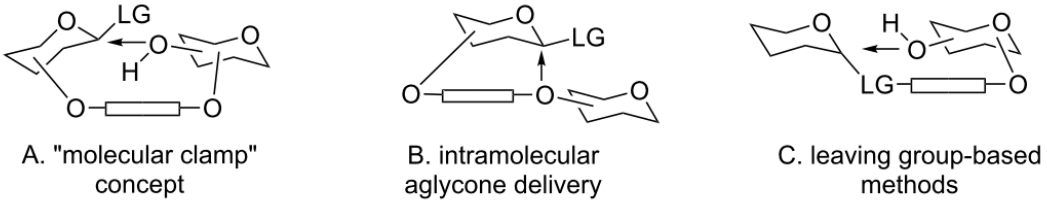

Figure 2. *Three general concepts for intramolecular glycosylation reactions*[31]

Kusumoto et al. found that the glycosylation between the glycosyl donor **#10** and glycosyl acceptor **#11** not working (**Scheme 6**).[32] Then they used muramic acid as a shorter linker to link the glycosyl donor **#10** (at the position 6) and glycosyl acceptor **#11** (at the position 3) to get the glycosyl donor-acceptor pair **#12** which, after TsOH-catalyzed intramolecular glycosylation, ester bond cleavage and protections step, furnished the target disaccharide **#13**. This is the first exemple of intramolecular glycosylation using the molecular clamping strategy.

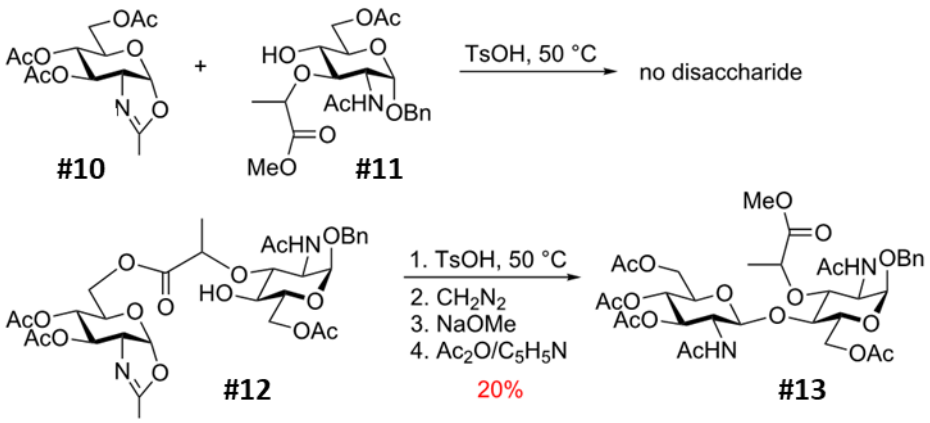

Scheme 6. *First intramolecular glycosylation using the molecular clamping*[32]

Since then, different tethers have been developed for the intramolecular glycosylation, such as flexible succinoyl[33] and related tethers,[34] carbonate,[35] as well as oxalic,[33] malonic[33,36,37], and glutaric,[38] dicarboxylic acids, phthaloyl and related tethers, xylylene tether, and peptide template and so on.[31] Following are some examples.

Ziegler et al. has designed the glycosyl donor-acceptor pair **#16** with succinoyl group as tether to link the glycosyl donor **#14** (at the position 2) and glycosyl acceptor **#15** (at the position 3)

[31] X. G. Jia, A. V. Demchenko, Beilstein *J. Org. Chem*. **2017**, *13*, 2028-2048.
[32] S. Kusumoto, M. Imoto, T. Ogiku, T. Shiba, *Bull. Chem. Soc. Jpn*. **1986**, *59*, 1419-1423.
[33] S. Valverde, A. M. Gómez, A. Hernández, B. Herradón, J. C. López, *J. Chem. Soc., Chem. Commun*. **1995**, 2005-2006.
[34] H. Yamada, K. Imamura, T. Takahashi, *Tetrahedron Lett*. **1997**, *38*, 391-394.
[35] G. Lemanski, T. Ziegler, *Tetrahedron* **2000**, *56*, 579.
[36] R. Lau, G. Schüle, U. Schwanaberg, T. Ziegler, *Liebigs Ann*. **1995**, 1745-1754.
[37] G. Lemanski, T. Ziegler, *Helv. Chim. Acta*. **2000**, *83*, 2655-2675.
[38] M. Wakao, K. Fukase, S. Kusumoto, *Synlett* **1999**, 1911-1914.

(**Scheme 7**).[39] Then they used #**16** to do the intramolecular glycosylation to get the *1,2-trans* glycoside **#17**. After ester bond cleavage with NaOMe, the target compound **#18** with a *1,2-trans* configuration was obtained after per-benzoylation.

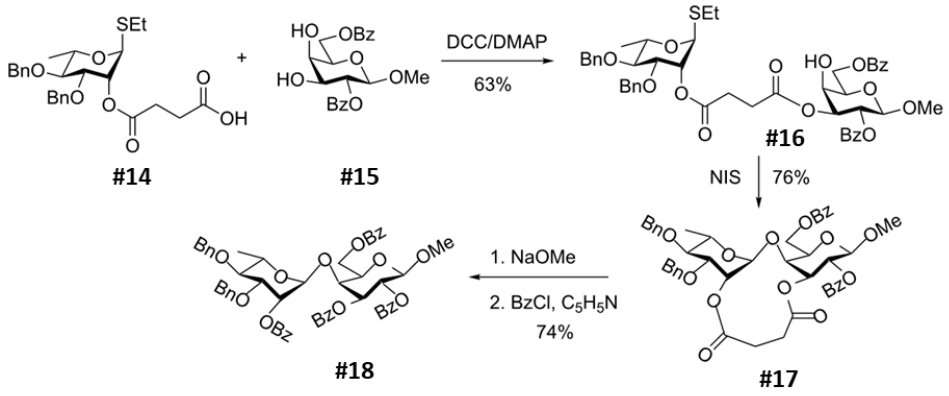

Scheme 7. *Succinoyl as a flexible linker for intramolecular glycosylation of prearranged glycosides*[39]

Lemanski et al. have synthesized a series of glycosyl donor-acceptor pairs by using linkers with different lengths.[40,41] When the succinoyl or malonyl linker is attached to the 6-OH of mannopyranosyl donor, mixtures of α- and β-anomers were obtained, except for the acceptor **#19c** that furnished the β-anomer **#22c**(**Figure 3**). In the case of thio-mannosides **#20**, a linker with minimum 3 atoms is necessary to achieve the intramolecular glycosylation, leading to a mixture of α- and β-anomers in favor of the α-anomer. However, with sulfoxide as the glycosyl donor (**#21**), the shorter linker (carbonyl and oxalyl) led only to the α-glycosylation products **#24a,b**, while the succinoyl linker gave a mixture of α- and β-anomers.

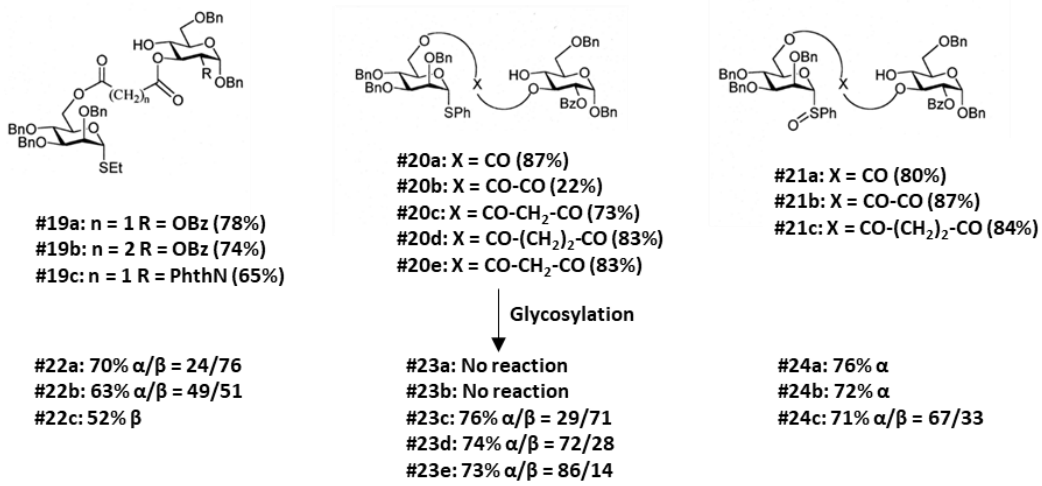

Figure 3. *Intramolecular glycosylation reported by Lemanski et al.*[40,41]

Valverde et al. have designed new glycosyl donor-acceptor pairs **#25** and **#28** by using the phthaloyl as the tether.[33] The phthaloyl linker is linked to the C-6 position of thiomannosides **#25** and **#28** respectively (**Scheme 8**). Intramolecular glycosylation of **#25** and **#28** in the presence of NIS/TfOH led to the glycomacrocycles **#26** and **#29** respectively, which furnished the corresponding (1-3') and (1-4') linked *1,2-trans* disaccharides after linker removal and acetylation.

[39] T. Ziegler, R. Lau, *Tetrahedron Lett.* **1995**, *36*, 1417-1420.
[40] G. Lemanski, T. Ziegler, *Tetrahedron* **2000**, *56*, 563-579.
[41] G. Lemanski, T. Ziegler, *Helv. Chim. Acta.* **2000**, *83*, 2655-2675.

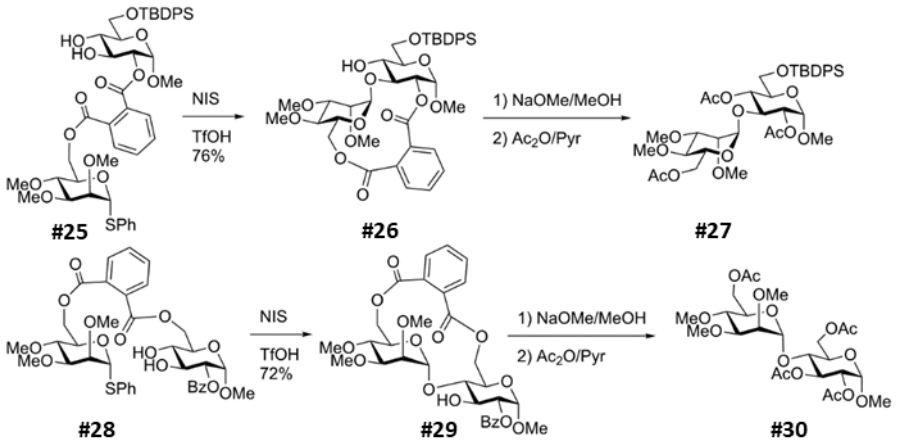

***Scheme 8**. Intramolecular glycosylation reported by Valverde et al.*[33]

Generally, for the intramolecular glycosylation, with more rigid linkers, small macrocycle will form with more selectictvity. An example of this approach is given below that has been successfully applied to the synthesis of *1,2-cis* glycosides with complete selectivity. Schmidt and coworkers have designed a new glycosyl donor-acceptor pair **#34**. [42] First, they use *α,α'*-dibromoxylene as the tether to link the glycosyl donor at C-3 position and the glycosyl acceptor **#33** at the C-6 position to get **#34** (**Scheme 9**). Intramolecular glycosylation followed by hydrogenolysis and acetylation furnished the glycomacrocycle **#36** with *1,2-cis* stereoselectivity.

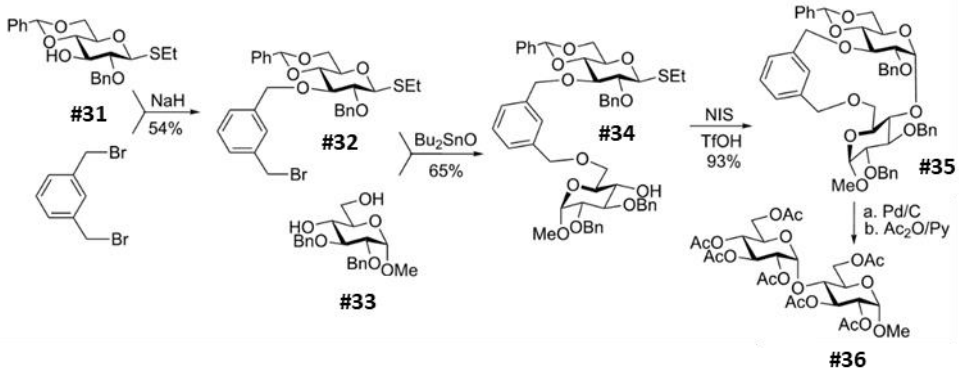

***Scheme 9.** Intramolecular glycosylation reported by Schmidt and coworkers* [42]

Warriner and coworkers used the peptide template as a new method of intramolecular glycosylation (**Scheme 10**).[43] They synthesized the glycopeptide **#37** and then used the NIS/TfOH to realise the glycosylation to get the (1-4)-linked disaccharide **#39** with high α-selectivity (*α/β* = 8:1) for the glucosyl acceptor, and lower α-selectivity (*α/β* = 1.8:1) for galactosyl acceptor after removal of peptide tether (Scheme 10). Interestingly, starting from the glycopeptide **#38** with the position of glycosyl donor and acceptor reversed on the peptide linker compared to **#37**, the intramolecular glycosylation led to the (1-4)-linked disaccharide **#39** with *α/β* = 1:1 for the glucosyl acceptor and high α-selectivity (*α/β* = 9:1) for the galactosyl acceptor. Consequently, both the nature of the glycosyl acceptor and the position of linkage of both glycosyl donor and acceptor can influence the stereoselectity in peptide templated synthesis.

[42] M. Müller, U. Huchel, A. Geyer, R. R. Schmidt, *J. Org. Chem.* **1999**, *64*, 6190-6201.
[43] D. R. Greenwell, A. F. Ibnouzaki, S. L. Warriner, *Angew. Chem., Int. Ed.* **2002**, *41*, 1215-1218.

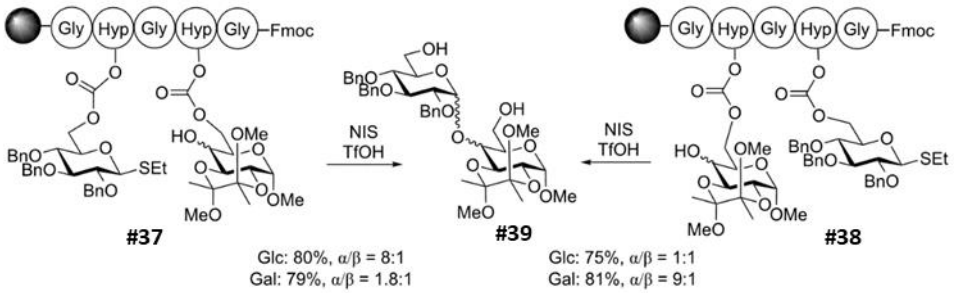

Scheme 10.*Positioning effect of donor and acceptor in peptide templated synthesis*[43]

2. Glycomacrocycle

Macrocyclic compounds represent a unique class of molecules because of their natural existence and unique structural, physicochemical, and biological properties as well as their potential applications in nanotechnology, biology, and drug delivery [44] Development of sugar-based macrocycles is of particular interest for chemical, supramolecular, analytical, and biological applications because carbohydrates are readily available, cheap, enantiomerically pure and multifunctional building blocks.[45]

2.1. Natural carbohydrate-containing macrocycles

Glycomacrocycles are existing in nature. Complex carbohydrate-containing macrocyclic compounds isolated from plants or microorganisms, usually in the ring of hydroxylated fatty acids (for complex glycolipids, including resin glycosides) or benzoic acid (for 4-glycosyloxybenzoates) dimers) are usually flanked by several monosaccharides or oligosaccharides arranged in 18- to 46-membered macrolide rings (**Figure 4**). These carbohydrate-containing macrocylic compounds exhibit various biological activities, such as plant growth regulation, cytotoxicity against human breast cancer cell lines, antiviral, and ionophoresis activities. An intact macrolide ring is essential for its biological activity.[46,47]

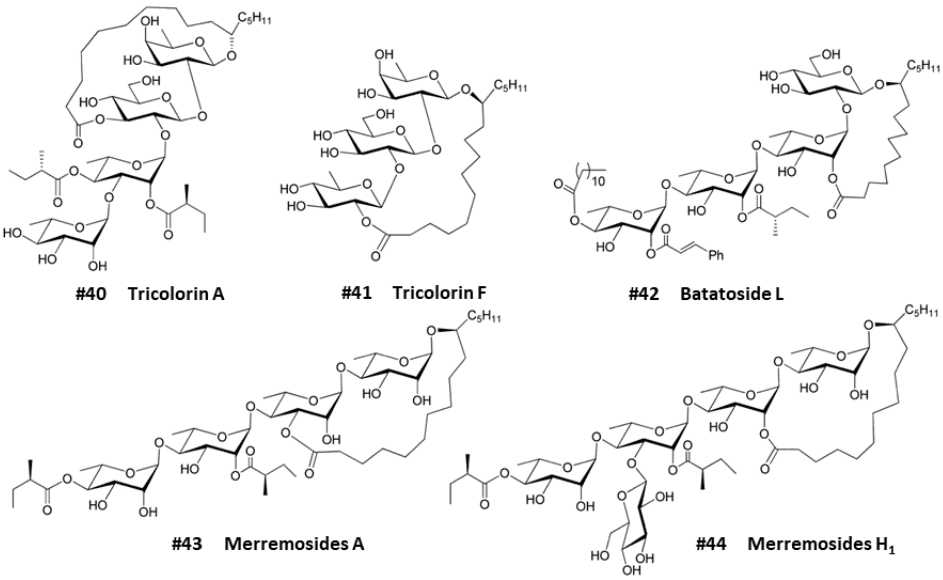

Figure 4. *Structure of some resin glycosides from the morning glory family*[45]

Tricolorin A, a plant used in traditional Mexican agriculture to suppress the growth of invasive weeds, is a 19-membered macrolide which was isolated from Ipomoea tricolor cav (Convolvulaceae) in 1993. Since 1996, several syntheses of the tricolorin A have been reported, involving macrolactonization or intramolecular glycosylation strategies, as shown in retrosynthetic

[44] E. A. Villar, D. Beglov, S. Chennamadhavuni, J. A. Porco, Jr., D. Kozakov, S. Vajda, A. Whitty, *Nat. Chem. Biol*. **2014**, *10*, 723-731.
[45] J. Xie, N. Bogliotti, *Chem. Rev.* **2014**, *114*, 7678-7739.
[46] T. Fujioka, Y. H. Kashiwada, K. Okabe, K. H. B. Lee, *Med. Chem. Lett.* **1996**, *6*, 2807-2810.
[47] A. Fürstner, M. Albert, J. Mlynarski, M. Matheu, E. DeClercq, *J. Am. Chem. Soc*. **2003**, *125*, 13132-13142.

Scheme 11. The compound **#46** has been selected as a key intermediate product to synthesize tricolorin A by the Heathcock[48,49] and Yu and Hui[50,51] followed by macrolactonization. The compound **#47** was the kay intermediate to synthesize tricolorin A followed by the intramolecular glycosylation strategies by Saikari's group.[52]

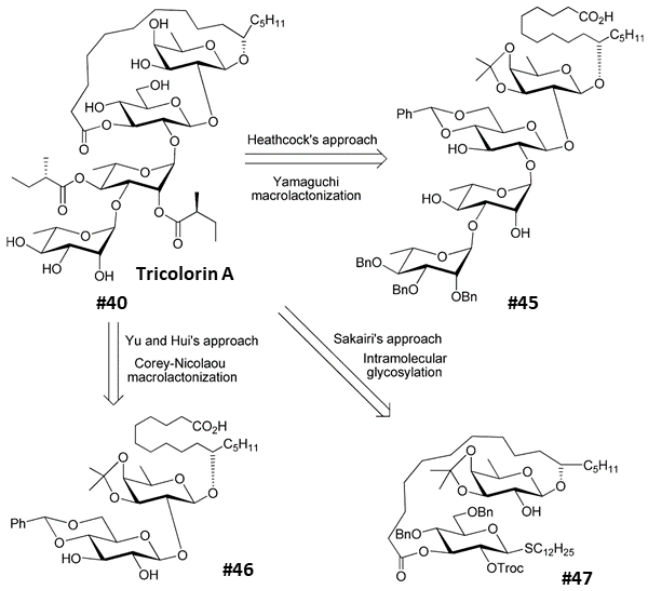

Scheme 11. *Retrosynthesis of Tricolorin A*[45]

For example, the glycoside **#50** was first prepared by glycosylation of thiogalactoside **#48** with alcohol **#49**, followed by the Zemplan transesterification (**Scheme 12**). After saponification, compound **#50** was coupled to the C-3 position of thioglucoside **#51** to give the dissacharide **#47**. MeOTf-promoted intramolecular glycosylation of **#47** provided the disaccharide macrolactone **#52** in 67% yield.

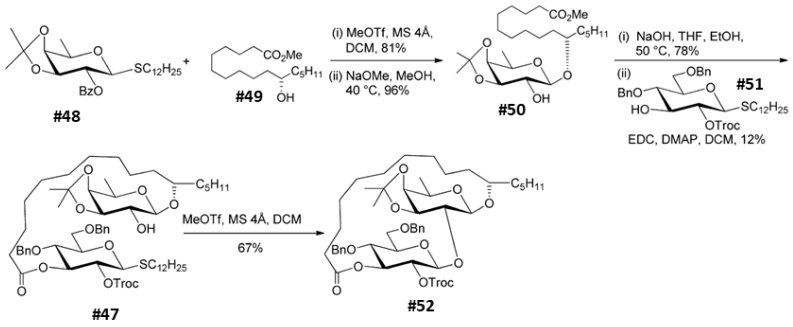

Scheme 12. *Synthesis of the macrolactone core of Tricolorin A by Sakairi's Group.*[52]

Tricolorin F is a 21-membered trisaccharide macrolide. Heathcock's group53 reported the first total synthesis of Tricolorin F in 2004 by using a similar strategy as for their synthesis of tricolorin A. Glycosylation of #50 coupling with D-glucosyl trichloroacetimide #53 followed by deacetylation afforded the disaccharide #54, which was further glycosylated with quinosyl

[48] D. P. Larson, C. H. Heathcock, *J. Org. Chem.* **1996,** *61*, 5208-5209
[49] D. P. Larson, C. H. Heathcock, *J. Org. Chem.* **1997**, *62*, 8406-8418.
[50] S.-F. Lu, Q. O'yang, Z.-W. Guo, B. Yu, Y.-Z. Hui, *Angew. Chem., Int. Ed.* **1997**, *36*, 2344-2346.
[51] S.-F. Lu, Q. O'yang, Z.-W. Guo, B. Yu, Y.-Z. Hui, *J. Org. Chem*. **1997**, *62*, 8400-8405.
[52] S.-H. Son, N. Yanagiya, J. Furukawa, N. Sakairi, *Synlett* **2009**, *18*, 2957-2960.
[53] M. Brito-Arias, R. Pereda-Miranda, C. H. Heathcock, *J. Org. Chem*. **2004**, *69*, 4567-4570.

trichloroacetimidate #55 (Scheme 13). After saponification, the resulting carboxylic acid #56 was macrocyclized using Yamaguchi's procedure to give the target trichrome F after debenzylation.

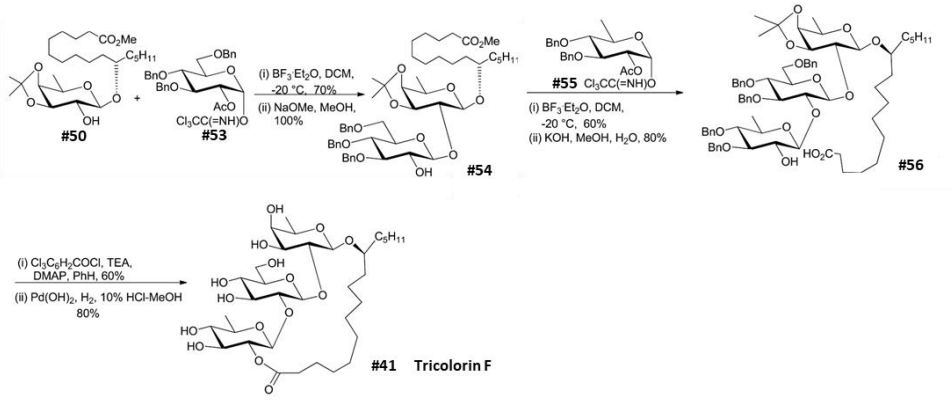

Scheme 13. *Total Synthesis of Tricolorin F by Heathcock's Group*[53]

2.2. Synthetic Glycomacrocycles

Glycomacrocycles containing various linkage as alkyne, amide, amine, carbamate, ester, ether, thiourea, triazole or urea have been designed and synthesized as biomolecule-mimetics, carbohydrate ligands for carbohydrate-protein or carbohydrate-nucleic acid interaction, enzyme inhibitors, as well as artificial receptors.[45] In the following, synthesis and applications of some carbohydrate-containing macrocycles will be presented.

The water-soluble glycophane **#65** (the term glycophane was employed by Wilcox to name cyclodextrin-cyclophane hybrid receptor[54]) was synthesized by *C*-arylation of ribofuranolactone **#59** with diorganolithium **#58**, followed by stereoselective reduction of bis(hemiacetal), introduction of amino function on the ribofuranoside, macrocyclization with terephthaloyl chloride, and final deprotection (**Scheme 14**).[55]

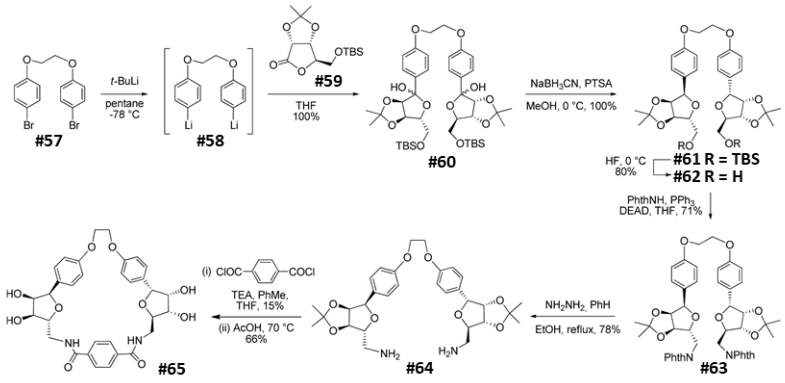

Scheme 14. *Synthesis of glycophanes from ribonolactone*[55]

[54] R. R. Bukownik, C. S. Wilcox, *J. Org. Chem.* **1988**, *53*, 463-471.
[55] C. S. Wilcox, M. D. Cowart, *Carbohydr. Res.* **1987**, *171*, 141-160.

Penades' group has prepared several other glycophane by nucleophilic substitution of α,α'-trehalose ditriflate **#67** with 2,7-dihydroxynaphthalene **#68** or 4,4′-isopropylidenediphenol **#70** (**Scheme 15**).[56,57] Water-soluble glycophane **#69** is able to complexe electron-deficient aromatic guests such as dinitrophenol or trinitrophenol in aqueous methanol (1:1) or borate buffer. Compound **#69** also exhibited chiral discrimination against racemic 2,4-dinitrophenyl amino acid derivatives with enantioselectivities ranging from 5% to 40%. Investigation of carbohydrate-carbohydrate interactions in water has demonstrated that the macrocycle **#69** has a stereospecific interaction towards 4-nitrophenyl α-glycosides.[58]

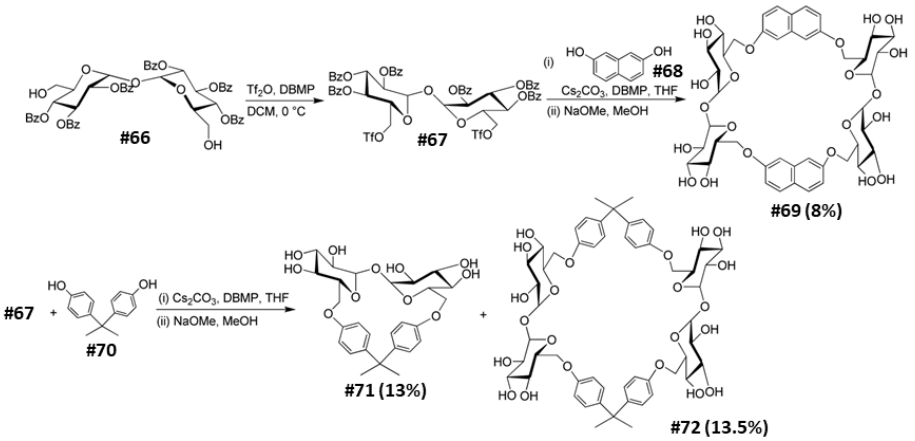

Scheme 15. *Synthesis of glycophanes from α,α'-trehalose*[56,57]

Dondoni's group has studied sugar calix arene-conjugated macrocyclic compounds.[59] Bridged and double calixsugars have been prepared through ester and amide linkages between α,α'-trehalose diols **#71**, **#77** or diamine **#78** and calixarene diacid 1,3-dichloride **#74** (**Scheme 16**). Among the synthesized glycomacrocycles **#75**, **#76**, **#79**-**#82**, compound **#76** shows selective recognition of imidazole.

[56] S. Penadés, J. M. Coterón, *J. Chem.* Soc., *Chem. Commun*. **1992**, *9*, 683-684.
[57] J. M. Coterón, C. Vicent, C. Bosso, S. Penadés, *J. Am. Chem. Soc*. **1993**, *115*, 10066-10076.
[58] J. Jiménez-Barbero, E. Junquera, M. Martín-Pastor, S. Sharma, C. Vicent, S. Penadés, *J. Am. Chem. Soc.* **1995**, *117*, 11198-11204.
[59] A. Dondoni, X. Hu, A. Marra, H. D. Banks, *Tetrahedron Lett*. **2001**, *42*, 3295-3298.

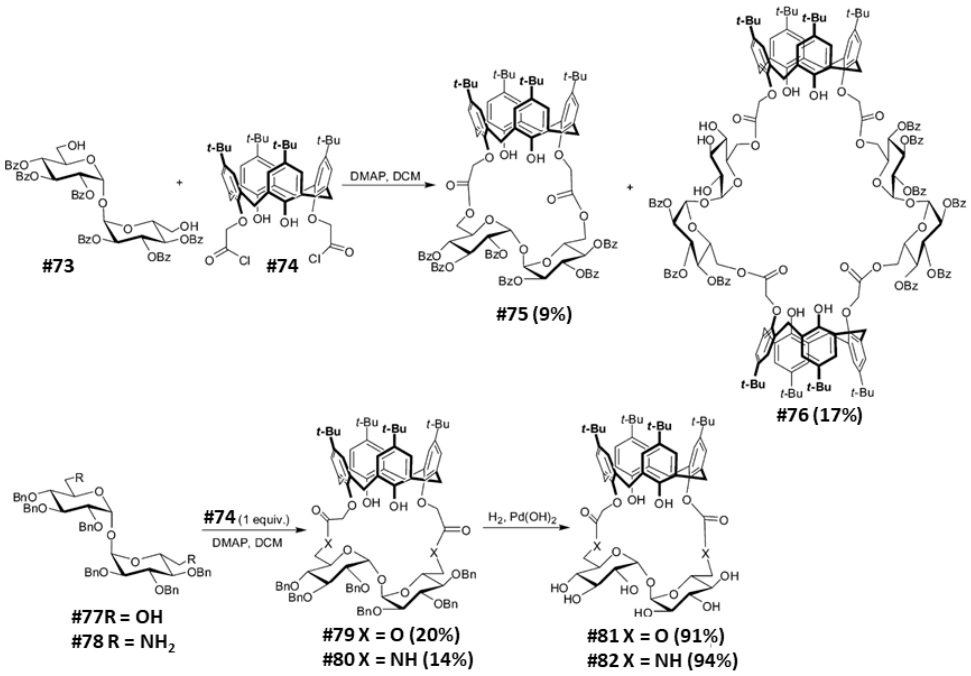

Scheme 16. *Synthesis of bridged and double calixsugars*[59]

Triazole-containing glycomacrocycles have been developed by using copper-catalyzed alkyne and azide cycloaddition (CuAAC), a very popular "click" reaction widely used in many research fields.[60,61] Over the years, the 1,2,3-triazole moiety formed in this process has become more than just a passive linker because it can form complexes with ionic species.[62,63] These interesting properties stimulate the incorporation of triazoles in carbohydrate-derived macrocyclic compounds.

Gin and colleagues reported the synthesis of cyclodextrin analogs by cyclic dimerization of appropriately substituted trisaccharides.[64] The azido- and propargyl-functionalized trisaccharide **#83** underwent the cyclization by using CuI and DBU, affording the cyclic dimer **#84** after hydrogenolysis (**Scheme 17**). This macrocycle is able to bind to 8-anilino-1-naphthalenesulfonate (ANS) in water with a binding constant of 38 ± 10 M^{-1}, probably by forming an inclusion complex.

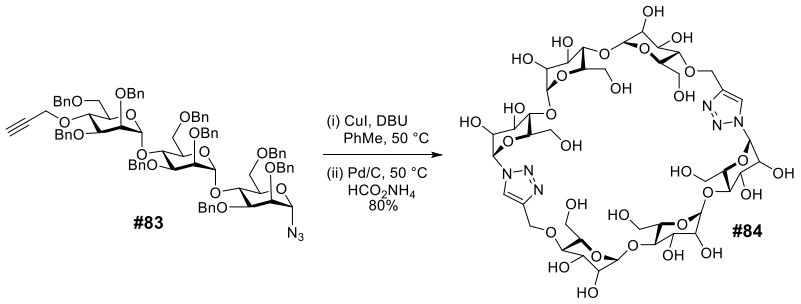

Scheme 17. *Gin's cyclodextrin analogue obtained by cyclodimerization of a trimannoside*[64]

[60] H. C. Kolb, M. G. Finn, K. B. Sharpless, *Angew. Chem., Int. Ed*. **2001**, *40*, 2004-2021.
[61] M. Meldal, C. W. Tornøe, *Chem. Rev*. **2008**, *8*, 3295-3298.
[62] H. Struthers, T. L. Mindt, R. Schibli, *Dalton Trans.* **2010**, *39*, 675-696.
[63] S. G. Agalave, S. R. Maujan, V. S. Pore, *Chem. Asian J.* **2011**, *6*, 2696-2718.
[64] K. D. Bodine, D. Y. Gin, M. S. Gin, *J. Am. Chem. Soc*. **2004**, *126*, 1638-1639.

Billing and Nilsson reported a method for synthesis of macrocyclic carbohydrate/peptide hybrids by using CuAAC.[65] Click reaction of azido propargyl aminoglucopyranoside #**85** followed by deacylation afforded the macrocyclic dimer #**86** (**Scheme 18**).

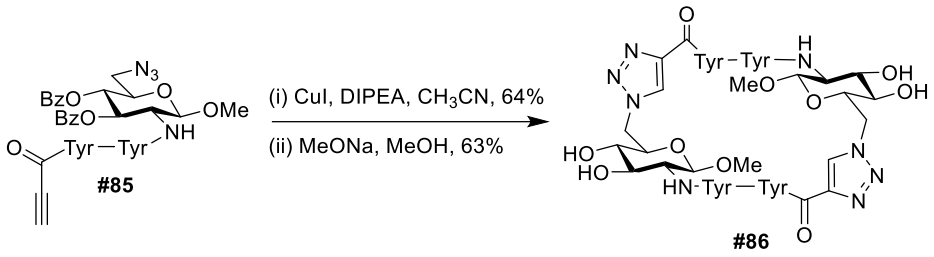

Scheme 18. *Billing and Nilsson's macrocyclic carbohydrate/peptide hybrids*[65]

Plantier-Royon' group reported another macrocycle derived from galacturonic acid, containing an amide function and a triazole ring.[66] The results of CuAAC of the compound **#87** strongly depend on the reaction conditions (**Scheme 19**). In the presence of ascorbic acid/$CuSO_4$, the monomeric macrocycle **#88** was isolated as the major product, whereas only the cyclic dimer **#89** is formed when CuI/DIPEA is used in water. The complexation of **#88** with Cu(II) was investigated by EPR, UV/vis spectroscopy, and mass spectrometry analysis, indicating the formation of the species [**#88·Cu**], involving a five-coordinated copper center.

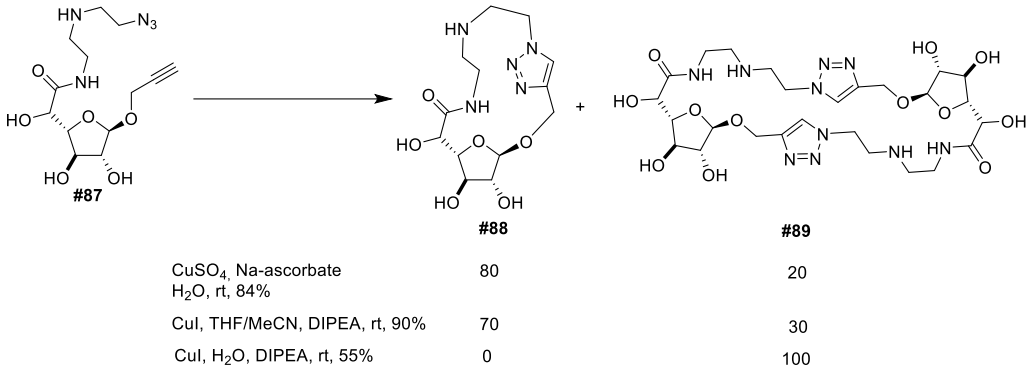

Scheme 19. *Plantier-Royon's "click" reaction of galacturonic acid-derived azido-alkyne*

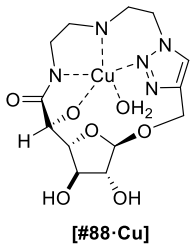

Figure 5. *Proposed structure of complexe* ***#88·Cu***[66]

Chen' group have synthesized up to 78-membered glycomacrocycles with click chemistry (**Scheme 20**).[67] By using chemoenzymatic method, different azido-, alkyne-functionalized sialic acid derivatives have been synthesized. Intramolecular CuAAC-macrocyclization led to a variety of

[65] J. F. Billing, U. J. Nilsson, *J. Org. Chem.* **2005**, *70*, 4847-4850.
[66] A. Allam, L. Dupont, J.-B. Behr, R. Plantier-Royon, *Eur. J. Org. Chem.* **2012**, *4*, 817-823.
[67] S. Muthana, H. Yu, H. Cao, J. Cheng, X. Chen, *J. Org. Chem.* **2009**, *74*, 2928-2936.

macrocyclic oligosaccharides **#91-#98** in 30-91% yields. These compounds have high solubility in water and interact with small hydrophobic molecules such as *para*-toluene sulfonate or *para*-methyl benzoate in a size-dependent manner.

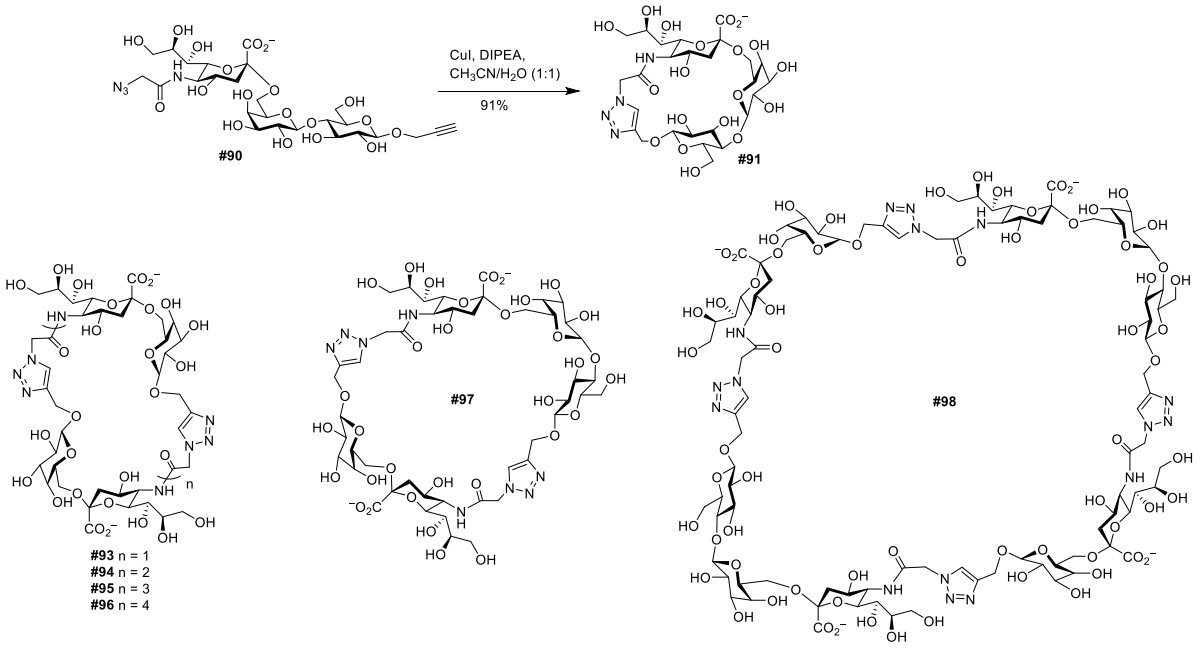

Scheme 20. *Synthesis of sialic acid-containing macrocycles*

Murphy and coll. reported a similar approach to obtain glucotriazolophane. The bisazide **#100**, obtained in three steps from the glycosyl azide **#99**, underwent intermolecular CuAAC with **#101** to give the macrocycle **#102** in 56% yield (**Scheme 21**).[68]

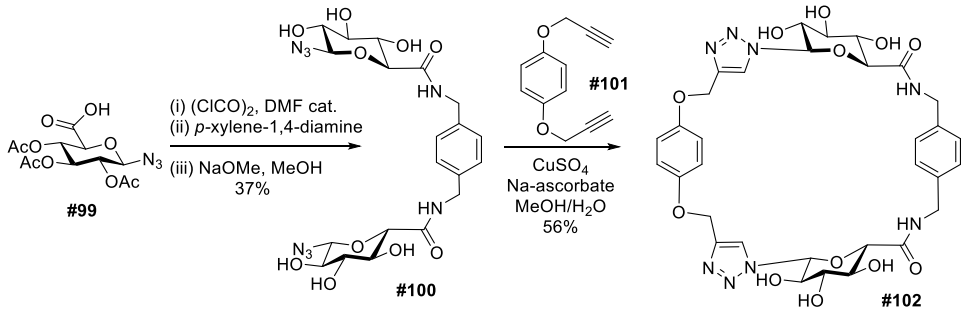

Scheme 21. *Synthesis of Murphy's glycotriazolophane*[68]

[68] R. Leyden, P. Murphy, *Synlett* **2009**, *12*, 1949-1950.

3. Photochromism

Photochromism is defined as a photoinduced reversible transformation of the chemical species between two isomers with the different absorption spectra, molecular geometry and physicochemical properties.[69,70] The common photochromic molecules are shown in Figure 6. Photochemical isomerization of photochromic molecules can be classified into two main types: *trans* ↔ *cis* or *E* ↔ *Z* isomerization through N=N or C=C double bonds such as azobenzenes, stilbenes, hemithioindigos; and photochemical cyclization reaction, such as thisphenefulgides, diarylethenes and spiropyrans (Figure 6).

	Photoswitches	Isomerization	λ_1/λ_2	polarity change
A	Azobenzenes	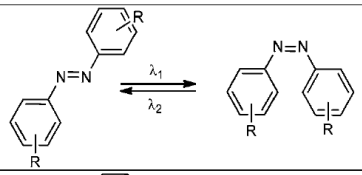	UV/VIS (ΔT)	medium (Δμ = ~3 D)
B	Stilbenes	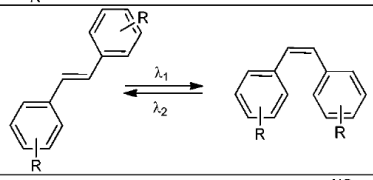	UV/UV	small
C	Spiropyrans	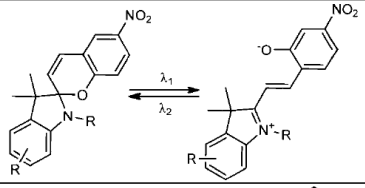	UV/VIS (ΔT) or VIS/UV	large (Δμ = 8-15 D)
D	Diarylethenes	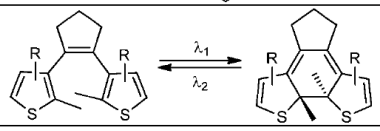	UV/VIS	small
E	Thiophenefulgides	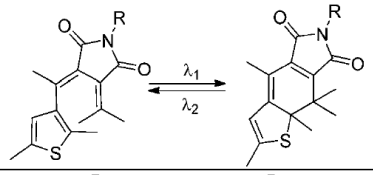	UV/VIS	small
F	Hemithioindigos	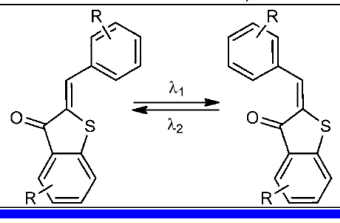	VIS/VIS (ΔT)	medium (Δμ = ~1.6 D)

Figure 6. *Examples of the photochromic molecules*[71]

Photochromic compounds can also be divided into *T*-type or *P*-type photoswitches. The *T*-type are sensitive to the light and the temperature, like the *Z*-isomers of azobenzenes and hemithioindigos, as well as the merocyanines (the open form of spiropyrans) which can be thermally converted back to the corresponding *E*-isomers or to spiropyrans respectively, without illumination.

[69] M. Irie, *Chem. Rev*. **2000**, *100*, 1683-1684.
[70] H. Dürr, H. Bouas-Laurent, Photochromism: *Molecules and Systems, Elsevier*, **2003**.
[71] W. Szymański, J. M. Beierle, H. A. V. Kistemaker, W. A. Velema, B. L. Feringa, *Chem. Rev*. **2013**, *113*, 6114-6178.

The P-type photochromes such as thisphenefulgides and diarylethenes are only switchable under light irradiation. In recent years, investigation of photochromic molecules has increased enormously for applications in the storage materials,[72] in super-resolution imaging,[73] for remote controlling of chemical reactivity,[74] photopharmacology,[75] supramolecular chemistry,[76] and so on.

Azobenzene is a stimuli-responsive molecule with a long history. It was first discovered in 1834,[77] and the photoisomerization of azobenzene has been reported in 1937 by the Hartley.[78] In-depth development of the azobenzene derivatives has revealed their excellent photophysical and chemical properties as a functional material, or for biomedical and material applications.[79]

Azobenzene is a diazene (HN=NH) derivative, with the two hydrogens replaced by phenyl groups, which has the *cis* (*Z*) or *trans* (*E*) isomer (**Figure 7**). Isomerization of the *trans* to *cis*-isomer can occur by the irradiation with UV-visible light,[80,81] mechanical stress[82] or electrostatic stimulation.[83,84] Isomerization of *cis* to *trans* occurs spontaneously in the dark owing to the higher thermodynamic stability of the *trans*-isomer or under visible light (420-490 nm). For unsubstituted azobenzene, the ratio of *cis*/*trans* isomers under UV light (340-380 nm) can reach approximately 80/20.[85] The *E*-azobenzene is usually more stable than the *Z*-isomer which has a half-life of about 2 days.[86] The *E*-azobenzene displays a strong $\pi \rightarrow \pi^*$ transition near 320 nm and a weak $n \rightarrow \pi^*$ transition around 450 nm (**Figure 7**). Compared to the *E*-isomer, Z-azobenzene shows a stronger $n \rightarrow \pi^*$ transition near 450 nm, and weaker $\pi \rightarrow \pi^*$ transition at 280 and 250 nm.

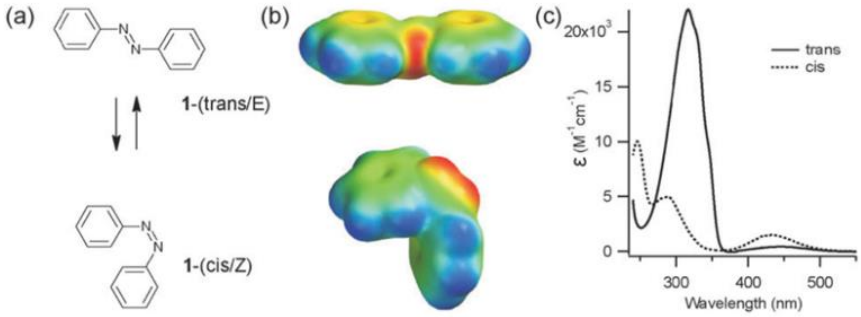

Figure 7. *(a) Structures of trans and cis isomers of azobenzene. (b) Spacefilling models colored by electrostatic potential (red-negative to blue-positive). (c) Absorption spectra of the trans and cis isomers of azobenzene in ethanol.*[87]

[72] S. Kawata, Y. Kawata, *Chem. Rev*. **2000**, *100*, 1777-1788.
[73] T. Ozawa, H. Yoshimura, S. B. Kim, *Anal. Chem*. **2013**, *85*, 590-609.
[74] R. Gostl, A. Senf, S. Hecht, *Chem. Soc. Rev*. **2014**, *43*, 1982-1996.
[75] M. M. Lerch, M. J. Hansen, G. M. van Dam, W. Szymanski, B. L. Feringa, *Angew. Chem. Int. Ed.* **2016**, *55*, 10978-10999.
[76] D. H. Qu, Q. C. Wang, Q. W. Zhang, X. Ma, H. Tian, *Chem. Rev*. **2015**, *115*, 7543-7588.
[77] Demselben, *Ann. Pharm*. **1834**, *12*, 311-314.
[78] G. S. Hartley, *Nature* **1937**, *140*, 281-281.
[79] A. A. Beharry, G. A. Woolley, *Chem. Soc. Rev*. **2011**, *40*, 4422-4437.
[80] H. Rau, *Photoreact. Org. Thin Films*, **2002**, 3-47
[81] H. Rau, E. Lueddecke, *J. Am. Chem. Soc*., **1982**, *104*, 1616-1620.
[82] R. Turansky, M. Konopka, N. L. Doltsinis, I. Stich, D. Marx, *Phys. Chem. Chem. Phys.*, **2010**, *12*, 13922-13932.
[83] J. Henzl, M. Mehlhorn, H. Gawronski, K.-H. Rieder, K. Morgenstern, *Angew. Chem., Int. Ed.*, **2006**, *45*, 603-606.
[84] X. Tong, M. Pelletier, A. Lasia, Y. Zhao, *Angew. Chem., Int.Ed.*, **2008**, *47*, 3596-3599.
[85] E. Fischer, *J. Am. Chem. Soc*. **1960**, *82*, 3249-3252.
[86] H. M. Bandara, S. C. Burdette, *Chem. Soc. Rev*. **2012**, *41*, 1809-1825.
[87] A. A. Beharry, G. A. Woolley, *Chem. Soc. Rev*. **2011**, *40*, 4422-4437.

The photoisomerization of azobenzenes is extremely fast, occurring on a timescale of hundreds of femtoseconds to picoseconds.[88,89] *The* E→Z *photoisomerization of azobenzenes occurs through either* S_0 *(singlet ground state)* ⟶ S_1 *(first singlet excited state) or* $S_0 \rightarrow S_2$ *(second singlet excited state) excitation. Different isomerization mechanisms following* $n–\pi^*$ *or* $\pi–\pi^*$ *excitation, either* through the reversal of one of the N–C bonds or by the rotation of the N=N double bond (**Figure 8**). The nonbonding electron pair of each nitrogen atom may lead to one $n \rightarrow \pi^*$ electronic transition ($S_0 \rightarrow S_1$) with inversion at the nitrogen atom (inversion mechanism), while the rotation mechanism involves a $\pi \rightarrow \pi^*$ transition ($S_0 \rightarrow S_2$).[90]

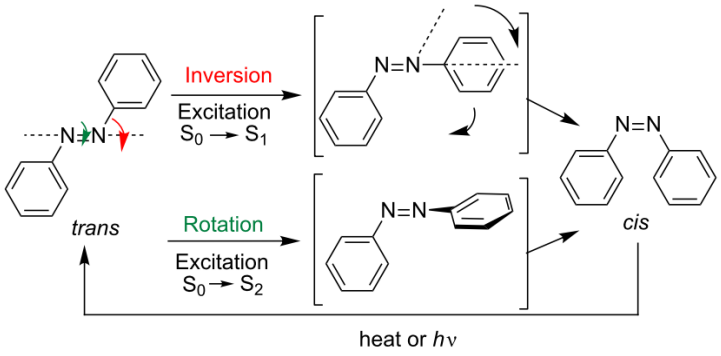

Figure 8. *Mechanistic proposals for the isomerization of azobenzenes*[90]

A great number of azobenzene derivatives have been reported.[91,92] Modification, mainly in the *ortho* and *para* positions, with different substituents can result in major changes in absorption, emission, and photochemical properties.

Thanks to its small size and easy functionalization, azobenzenes have been widely used as light-sensitive tools to investigate biological phenomena or for photopharmacology. For exemple, Maglia and co-workers[93] have prepared azobenzene-functionalized Fragaceatoxin C (a toxin that upon binding to the surface of sphingomyelin-rich cells leads to the assembly of nanopores at the cell membrane and causes cell death) (**Figure 9**). The affinity of modified toxin for biological membranes can be activated or deactivated by irradiation, allowing pore formation to be reversibly controlled by light. This study opens the perspective to use light-controlled Fragaceatoxin C in photopharmacology for cancer therapy and for fabrication of nanopore arrays in nanopore sensing devices, where the reconfiguration of individual nanopores must be controlled with high spatiotemporal precision.

[88] M. Quick, A. L. Dobryakov, M. Gerecke, C. Richter, F. Berndt, I. N. Ioffe, S. A. Kovalenko, *J. Phys. Chem. B* **2014**, *118*, 8756-8771.
[89] C. J. Otolski, A. M. Raj, V. Ramamurthy, C. G. Elles, *Chem. Sci*. **2020**, ***11***, 9513-9523.
[90] E. Merino, M. Ribagorda, *Beilstein J. Org. Chem*. **2012**, *8*, 1071-1090.
[91] J. Calbo, A. R. Thawani, R. S. Gibson, A. J. White, M. J. Fuchter, *Beilstein J. Org. Chem*. **2019**, *15*, 2753-2764.
[92] F. A. Jerca, V. V. Jerca, R. Hoogenboom, *Nat. Rev. Chem*. **2022**, *6*, 51-69.
[93] N. L. Mutter, J. Volaric, W. Szymanski, B. L. Feringa, G. Maglia, *J. Am. Chem. Soc*. **2019**, *141*, 14356-14363.

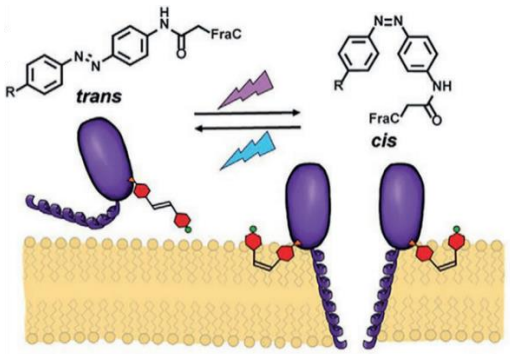

Figure 9. *FraC modified with a photoswitch (red) does not bind to the surface of the cell when the azobenzene is in the trans state, while the azobenzene can be reversibly switched to the cis state upon irradiation with light to stabilize the mature pore structure.*[93]

Betancourt and co-workers[94] prepared and characterized light-responsive hydrogels (named as PR-Hgel) prepared by cross-linking of di-NHS esters of azobenzoic acid with tetravalent amine-terminated poly(ethylene glycol) (**Figure 10**). Exposure of PR-Hgels to UV light leads to photoisomerization of the azobenzene crosslinker and reduction of the hydrogel size. UV-triggered hydrogel size reduction was accompanied by increased release of the near-infrared fluorescent dye Alexa Fluor 750 (AF750). This work demonstrates that this kind of system could be applied as reversible photoresponsive potential of biomaterials.

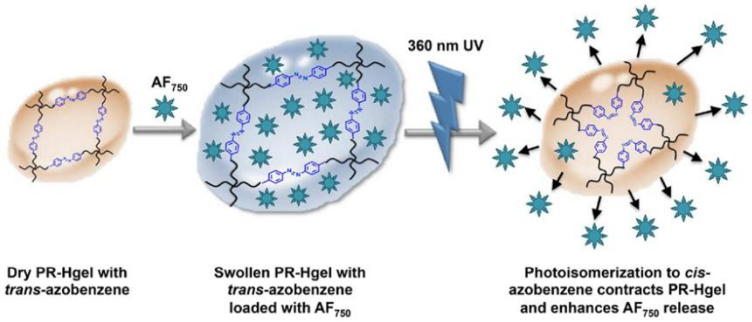

Figure 10. *Photoresponsive hydrogels prepared by cross-linking of di-NHS ester of azobenzoic acid and four-armed, amine-terminated poly (ethylene glycol).*[94]

Zhang and co-worker[95] reported a NIR light-sensitive drug delivery system (DDS) named UCNP@AzoLipo, which is consisted of novel liposomes based on UCNP (upconversion nanoparticle)-encapsulated azobenzene liposome nanostructures (**Figure 11**). Azobenzene liposomes can be formed by using 1,2-distearoyl-*sn*-glycero-3-phosphocholine (DSPC) phospholipids and amphiphilic azobenzene derivatives. As NIR-triggered components in the entire DDS, core/shell UCNPs were synthesized in a layer-by-layer manner with oleic acid (OA) as a stabilizer. The OA-terminated UCNP phase was transferred between the water and oil phases via van der Waals interactions. Then, doxorubicin (DOX, an anticancer drug) and UCNPs were used to encapsulate hybrid azobenzene liposome vesicles. Under intermittent 2.2 W cm^{-2} and 7.8 W cm^{-2}

[94] S. K. Rastogi, H. E. Anderson, J. Lamas, S. Barret, T. Cantu, S. Zauscher, W. J. Brittain, T. Betancourt, *ACS Appl. Mater. Interfaces* **2018**, *10*, 30071-30080.
[95] C. Yao, P. Wang, X. Li, X. Hu, J. Hou, L. Wang, F. Zhang, *Adv. Mater*. **2016**, *28*, 9341-9348.

NIR light (980 nm) laser irradiation, the DOX release reached 57 wt% and over 90 wt% within 6 h, respectively. So switchable NIR-triggered precise drug release can be achieved.

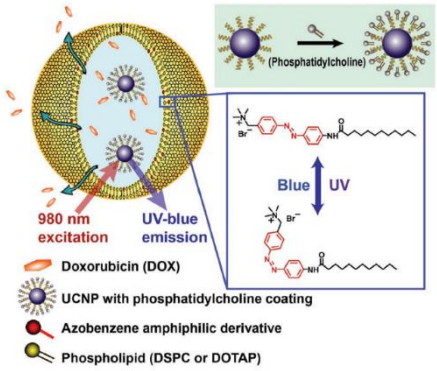

Figure 11. *NIR/visible light sensitive azobenzene: NIR triggered azobenzene-liposome/upconversion nanoparticle hybrid vesicles for controlled drug delivery*[95]

4. Photoswitchable macrocycles

As presented in the **Chapter 1.2**, glymacrocycles represent a unique class of molecule which has many interesting properties and applications like chiral catalysis, chiral recognition, and so on. Introducing a photochromic unit into the glycomacrocycles could enable the reversible photocontrol of their conformation and different properties light illumination. Photoswitchable glycomacrocycles could bring new applications as chiral dopants for liquid crystals, photoswitchable gels, photoswitchable catalyst, photocontrol of biological activities, photopharmacology and so on.

Despras and coworkers has reported the first two photoswitchable glycomacrocycles in 2017.[96] These two macrocycles are composed of symmetrical azobenzene bis-glycoside units linked with piperazine through thiourea bridges (**Figure 12**a). Both compounds show interesting reversible shape switching upon photoirradiation or heating (**Figure 12**b), and interesting chiroptical properties with chirality transfer from the disaccharide to azobenzene moiety.

[96] G. Despras, J. Hain, S. Jaeschke, *Chem. Eur. J.* **2017**, *23*, 10838-10847.

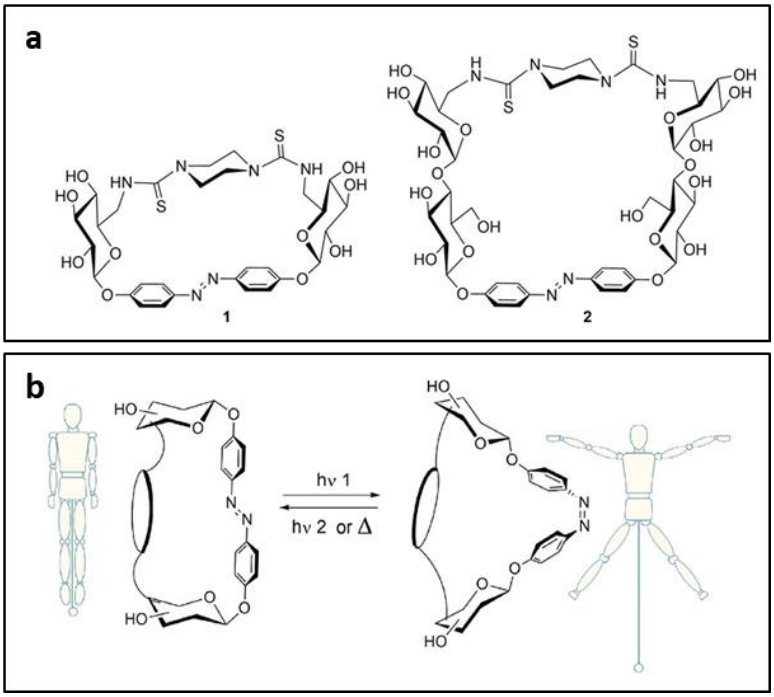

Figure 12. *a. Structures of the targeted photoswitchable glycomacrocycles. b. Reversible shape switching of glycoazobenzene macrocycles upon photoirradiation or heating*[96]

One year later, the same group reported another glycoazobenzene macrocycle,[97] containing 4,4'-dihydroxyazobenzene linked to the 6-position of two mannosides, and alkyne function at anomeric position (**Figure 13**a). This macrocycle also displays reversible shape-switching during the *E*↔*Z* isomerization, and chiroptical properties (**Figure 13**c). Interestingly, the solubility in water can also be reversibly tuned. Irradiation of *E*-macrocycle at 365 nm for 3 min led to the *Z*-isomer (*Irr365*) which shows a limpid solution in water (**Figure 13**b). Further irradiation at 525 nm during 10 min converted the *Z*-isomer back to the *E*-isomer (*Irr525*), and the solution became cloudy again (**Figure 13**b).

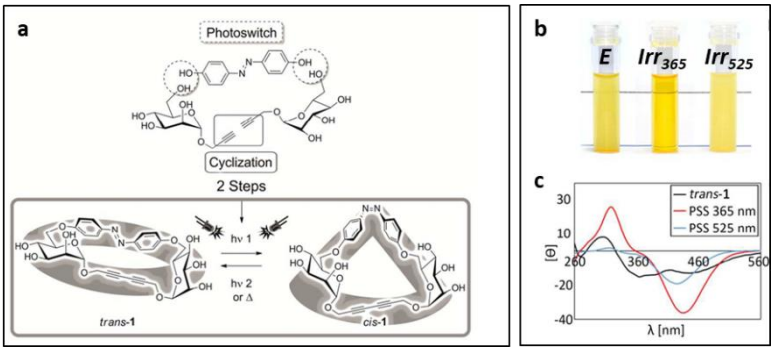

Figure 13. *a. Reversible trans/cis isomerisation of the azobenzene unit leads to shape-switching of the macrocycle. b. Reversible switching of the solubility. c. CD spectra of glycomacrocycle.*[97]

In the same period, our group has also reported photoswitchable glycomacrocycles, [98,99] which contain 2,2'-dihydroxyazobenzene linked to the 2,3- or 4,6- positions of manno- or gluco-

[97] J. Hain, G. Despras, *Chem. Commun*. **2018**, *54*, 8563-8566.

[98] C. Lin, S. Maisonneuve R. Métivier, J. Xie, *Chem. Eur. J.* ***2017***, *23*, 14996-15001.
[99] C. Lin, S. Maisonneuve, C. Theulier, J. Xie, *Eur. J. Org. Chem*. **2019**, 1770-1777.

pyranosides (**Figure 14**). The synthesized macrocycle can be reversibly isomerized between *E* and *Z* isomers upon UV or visible irradiation with excellent photostability and thermal stability (for the *Z* isomer), and chiroptical properties. Interestingly, the macrocycle **#103** is able to form organogel in cyclohexane and ethanol. The formed organogel in cyclohexane can be reversibly tuned to the liquid state by heating or shaking (**Figure 14**). Irradiation at 365 nm led to the *Z*-isomer which precipitated in the apolar cyclohexane.

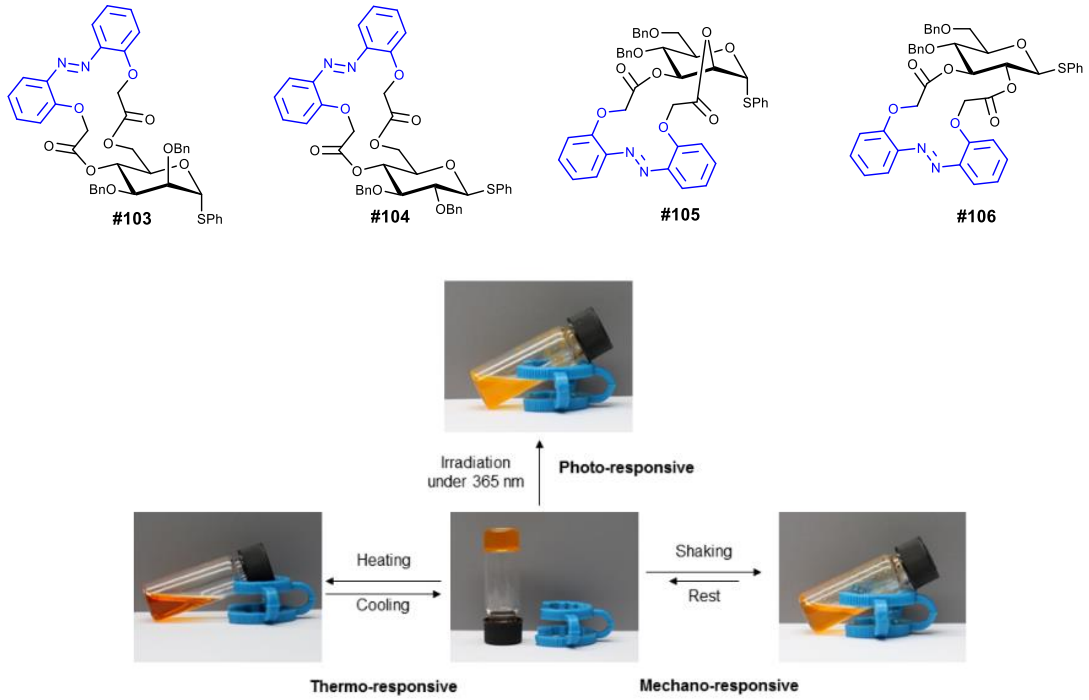

Figure 14. *Structure of the photoswitchable glycomacrocycles, and pictures demonstrating the multistimuli-responsive behavior of #**103** gel in cyclohexane*[98]

Thanks to the chiroptical property of these photoswitchable glycomacrocycles, their use as photocromic chiral dopant for the liquid crystals has been recently investigated by the group of Y. Kim.[100] They have demonstrated that cholesteric liquid crystals (CLCs) doped with photochromic glycomacrocycles **#103** and **#106** provided dynamic control of helical superstructures in response to a light stimulus. An unprecedented shortening of the helical pitch length and the empowerment of helical twisting power up to 500% are observed upon $E \rightarrow Z$ photoisomerization. These glycomacrocyclic azobenzene-based CLCs can also drive the mechanical movement of micro-objects., with two modes of rotation two-directional or one-directional rotational motion (crankshaft mode) are realized (**Figure 15**).

[100] Y. Kim, N. Mafy, S. Maisonneuve, C. Lin, N. Tamaoki, J. Xie, *ACS Appl. Mater. Interfaces*, **2020**, *12*, 52146-52155.

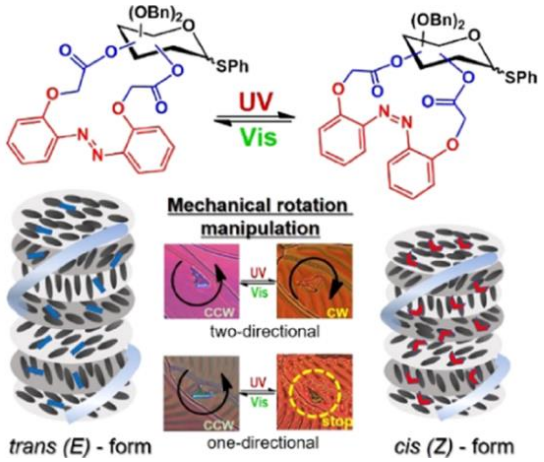

Figure 15. *Reversible tuning of helical superstructure by the photochemical reaction of chiral dopants*[100]

The last reported photochromic glycomacrocycle is realized by Jarosz and coworkers.[101] This glycomacrocycle, prepared by a high-yield Cs_2CO_3-templated macrocyclization between iodine-functionalized sucroside and 2,2'-dihydroxyazobenzene (**Figure 16**). *E*-macrocycle can be transformed readily into *Z*-isomer upon irradiation with green light, and the backward transformation is triggered by blue light. Both isomers have cation binding ability, with a preference for potassium among alkali metal cations. Moreover, the *Z*-macrocycle binds cations stronger than the *E*-isomer ($K_{cis}/K_{trans} \leq 4.1$).

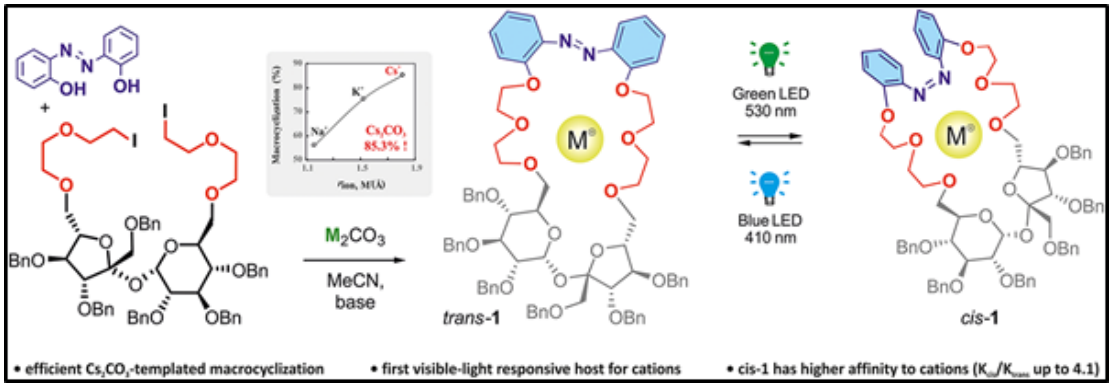

Figure 16. *Synthesis and cation complexation of the photochromic glycomacrocycle*[101]

Our group has reported a new intramolecular glycosylation strategy to synthesize a series of new glycoazobenzene macrocycles *E*-#**107** - *E*-#**113**,[102] containing *p,p'*- and *o,o'*-dihydroxy azobenzenes, with rigid (phthalic acid) and/or flexible (succinic acid) linkers as the photochromic template to realize the intramolecular glycosylation, as shown in **Scheme 22**. Excellent α-stereoselectivity has been obtained after NIS/TfOH promoted intramolecular glycosylation (**Figure 17**), with higher yields (45-60%) for more rigid phthaloyl-linked compounds. No influence of azobenzene configuration (*E* or *Z*-isomers) on the stereoselectivity of the glycosylation has been observed, with however lower yield (30 % max.) for the *Z*-azobenzene-linked substrates.

[101] P. S. Owska, K, Dąbrowa, S. Jarosz, *Org. Lett.* **2021**, *23*, 2687-2692.
[102] C. Lin, J. Jiao, S. Maisonneuve, J. Malletroit, J. Xie, *Chem. Commun*. **2020**, *56*, 3261-3264.

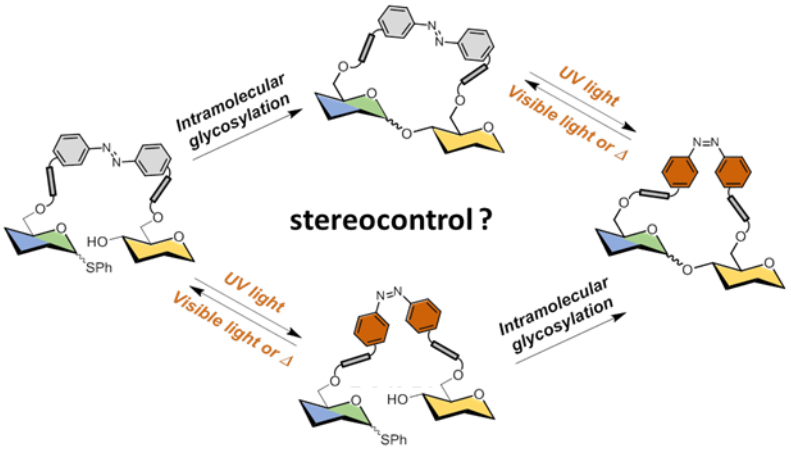

Scheme 22. *Photoswitchable glycomacrocycles through intramolecular glycosylation approach*

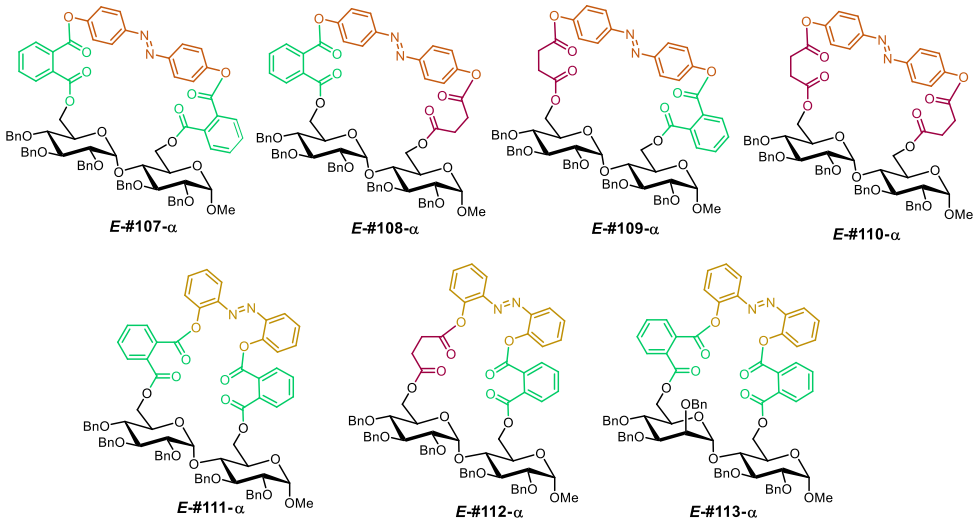

Figure 17. *Synthesized glycomacrocycles by using the photochromic template*[102]

5. Objectives of thesis

Up to date, only a limited number of photochromic glycomacrocycles have been reported.[96,97,98,101,102] Beside their excellent photoswitching properties, these glycomacrocycles displayed very interesting reversible shape switching, solubility switching, ions complexation, chirality transfer, as well as multi stimuli-responsive self-assembly properties. Since photoisomerization of azobenzene from *E*- to *Z*-isomer induced large geometrical and conformational changes, we will continue to investigate the stereoselectivity of the intramolecular glycosylation through photochromic template approach. The sugar moiety will be linked to the azobenzene by using CuAAC. The nature and the length of the azobenzene linker will be optimized to improve the yield and the stereoselectivity of glycosidic macrocyclisation. These studies will be described in Chapter II (*Scheme 23*). Chapter III will describe the photochromic properties of synthesized azobenzene-based glycomacrocycles, as well as the chirality transfer and host-guest investigation with different metal ions.

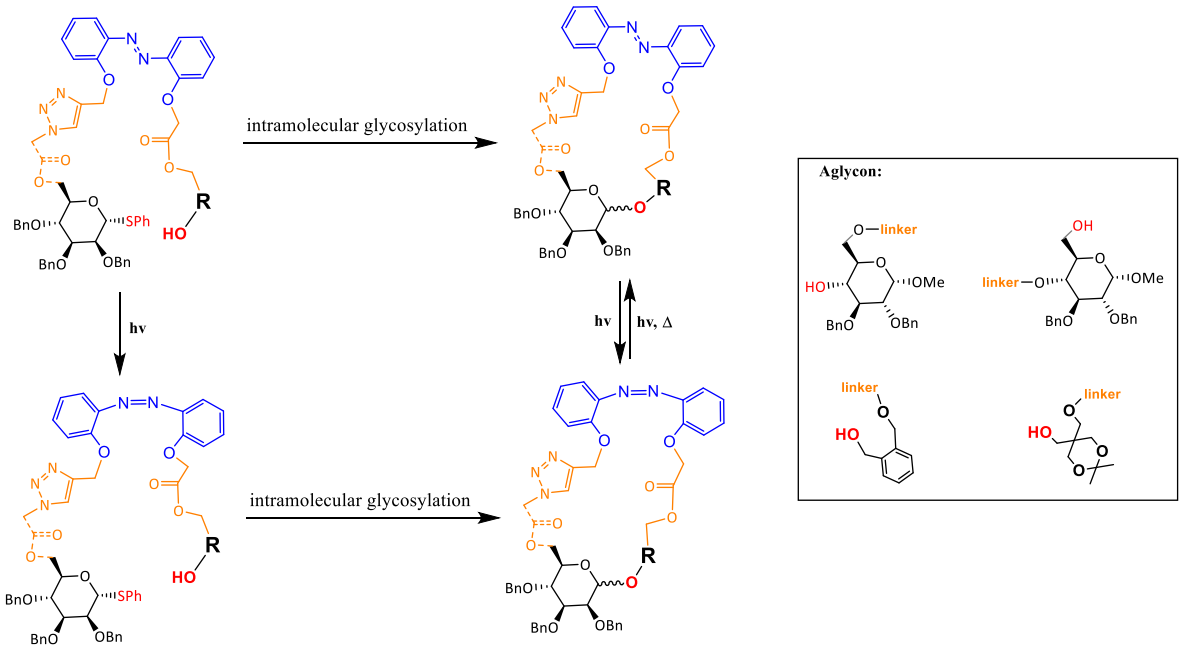

Scheme 23. *Designed triazole-linked photoswitchable glycosyl donor-acceptor pairs for intramolecular glycosylation investigation.*

Chapter II

Chapter II - SYNTHESIS OF PHOTOCHROMIC GLYCOMACROCYCLES THROUGH INTRAMOLECULAR GLYCOSYLATION

1. Principle of using azobenzene as photochromic linker for intramolecular glycosylation

The aim of this thesis is to design, synthesize and investigate novel photochromic glycomacrocycles (PGMs) through intramolecular glycosylation reaction by using azobenzene as photochromic template (**Scheme 24**). Glycosyl donor and acceptor are linked together via non-reacting centre to a photochromic template. As molecular photoswitch, azobenzene has been chosen because of its small size, its excellent photostability and the large changes in molecular size and shape induced by the photoisomerization between the thermodynamically favoured *E*-isomer and the energetically higher *Z*-isomer.[103] The *Z*-isomer can thermally return to the more stable *E*-isomer. It's expected that photoisomerization of the photochromic template would induce large concomitant geometrical change and the disposition between the glycosyl donor and glycosyl acceptor, and consequently influence the efficiency and the stereoselectivity of the macrocyclization by stereoelectronic and conformational effects.

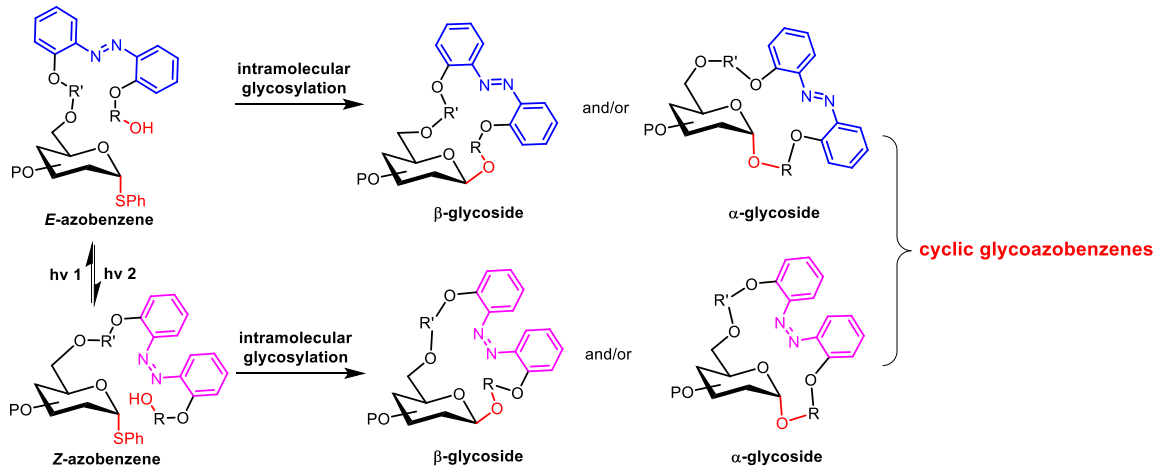

Scheme 24. *Structure of photochromic glycomacrocycles and principle of controlling stereoselectivity of glycosylation with photoswitchable azobenzene linker*

Previously, our group has used the *p,p'*- and *o,o'*-dihydroxy azobenzene as photochromic template to coupling with the glycosyl donor and glycosyl acceptor respectively by using phthalic acid or/and succinic acid as linker to get the glycosyl donor-acceptor pairs (GDAPs).[102] After the intramolecular glycosylation, several photoswitchable glycomacrocycles with excellent α-stereoselectivity have been isolated, with the yield up to 60% (**Figure 17**). Mainly thio-glucopyranosides have been investigated. The *Z*-azobenzene-linked substrates furnished a mixture of α-*E*- and α-*Z*-glycomacrocycles in lower yield.

[103] H. M. Dhammika, S. C. Burdette, *Chem. Soc. Rev*. **2012**, *41*, 1809-1825.

In this thesis, we decided to use the well-developed and versatile CuAAC to link together azobenzene with glycosyl donor and acceptors. Furthermore, triazole is able to complex metal ions, giving us the possibility to investigate the potential coordination properties of the triazole-functionalized glycomacrocycles.[104] As glycosyl acceptor, phenyl thiomannopyranoside is selected to investigate the outcome of the stereselectivity because the β-mannosylation represents a synthetic challenge in chemical glycosylation.[105]

2. Synthesis of photochromic glycomacrocycles containing two sugar units

o,*o*'-Dihydroxyazobenzene is chosen as the photochromic template to construct the new glycosyl donor-acceptor pairs (GDAPs) containing triazole linkers (**Figure 18**) Among the designed GDAPs, compounds **1** and **2** contain a free hydroxyl group at the C-4 position of the glycosyl acceptor; while for compounds **3** and **4**, the free OH is on the C-6. After photoisomerization of *E*-**1**-**4**, the corresponding *Z*-isomers could be obtained so as to investigate their intramolecular glycosylation reaction.

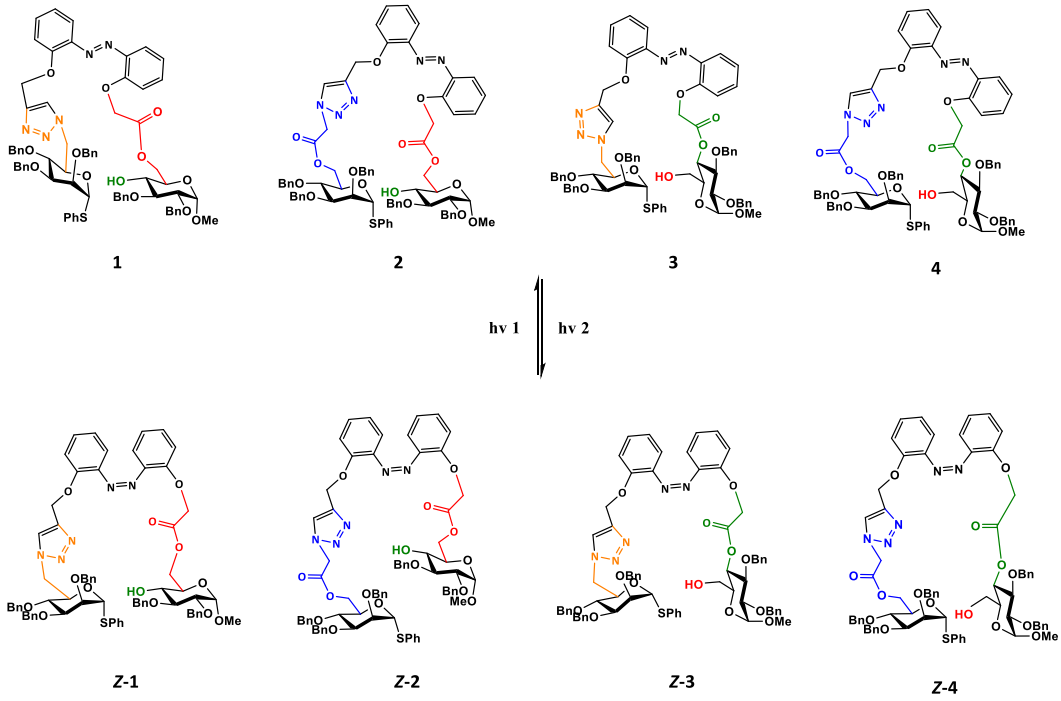

Figure 18. *Structure of new GDAPs*

[104] J. Xie, J. in Carbohydrate Chemistry: Chemical and Biological Approaches, vol. 45 (Eds.: A. P. Rauter, T. K. Lindhorst, Y. Queneau), Royal Society of Chemistry, Cambridge, 2022, pp. 460-498.
[105] Y. Zhu, B. Yu, *Chem. Eur. J.* **2015**, *21*, 8771-8780.

2.1. Retrosynthesis

The retrosynthetic scheme to prepare photochromic glycomacrocycles (PGMs) is shown in the **Scheme 25**. The PGMs could be obtained from the glycosyl donor-acceptor pairs by the intramolecular glycosylation. The GDAPs could be obtained by CuAAC between azido-sugar and azobenzene linked glycosyl acceptor. Azido-sugar could be obtained from the D-mannose, while the azobenzene linked glycosyl acceptor could be obtained from the methyl α-D-glucoside and commercially available *o,o'*-dihydroxy azobenzene.

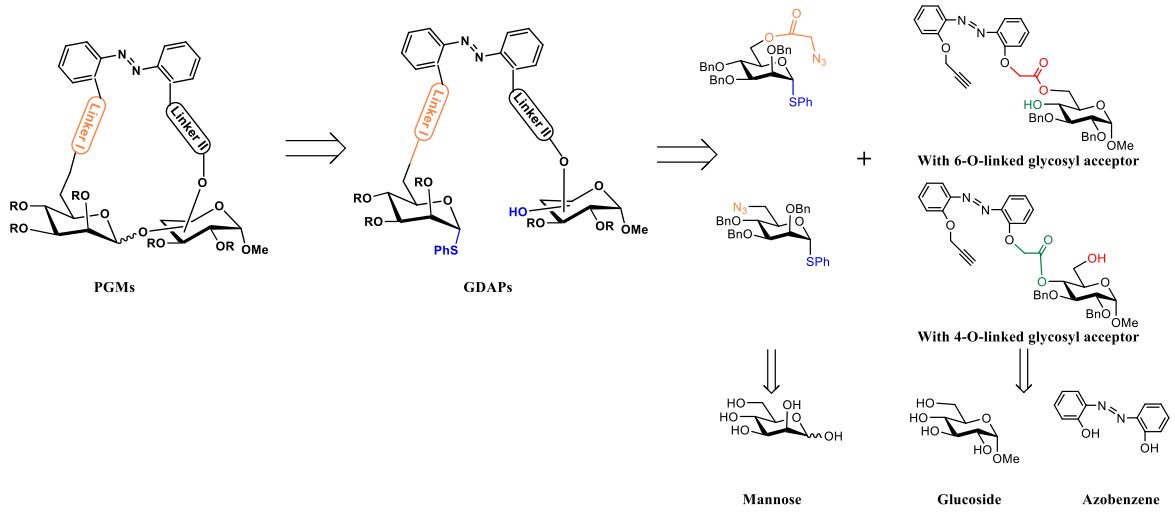

Scheme 25. *Retrosynthesis of the PGMs*

2.2. Preparation of the glycosyl donor-acceptor pairs

The preparation of the phenyl thio-α-D-mannopyranoside **6** commenced with the D-mannose (**Scheme 26**). Acetylation of mannose with Ac_2O catalyzed by $Cu(ClO_4)_2 \cdot 6H_2O$ led to the compound **5** as a mixture of the α/β anomers.[106] Thioglycosylation of **5** with PhSH in the presence of $BF_3.Et_2O$ afforded the 1,2-*trans* anomer **6**α in 63% yield and the 1,2-*cis* anomer **6**β in 5%.[107] Removal of acetyl protecting group in **6**α by using the MeONa in MeOH gave the compound **7** in 99% yield.[108] Compound **7** was then selectively silylated at C-6 position with TBDPSCl and imidazole in THF, leading to **8** in 94% yield.[109] The following benzylation of **8** in dry THF gave a separable mixture of compound **9** in 78% yield and the tetra-*O*-benzylated compound **9a**[110] in 10% yield. Desilylation of **9** in dry THF with TBAF gave the target compound **10** with in 98% yield.

[106] D. Chatterjee, A. P. Rajkamal, S. Yadav, *RSC. Adv*. **2015**, *5*, 29669-29674.
[107] S. Deng, U. Gangadharmath, C-W. T. Chang, *J. Org. Chem.***2006**, *71*, 5179-5185.
[108] M. J. Sofia, R. Kakarla, N. Kogan, R. Dulina, Y. W. Hui, N. T. Hatzenbuhler, D. Liu, A. Chen, T. Wagler, *Bioorg. Med. Chem. Lett.* **1997**, *7*, 2251-2254.
[109] A. Ishiwata, Y. J. Lee, Y. Ito, *Org. Biomol. Chem.* **2010**, *8*, 3596-3608.
[110] M. Heuckendorff, L. T. Poulsen, C. Hedberg, H. H. Jensen, *Org. Biomol. Chem.* **2018**, *16*, 2277-2288.

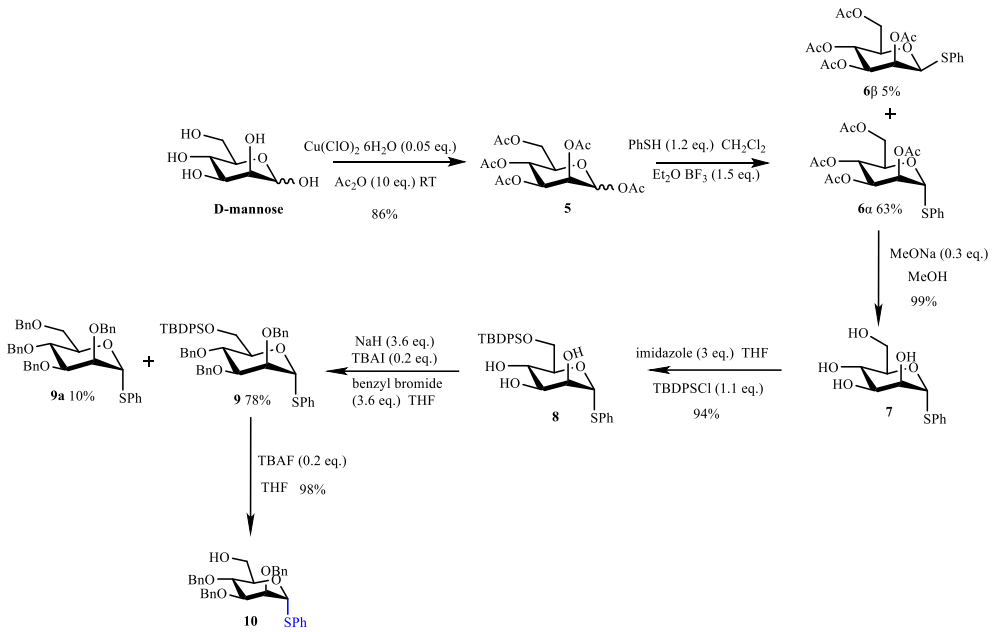

Scheme 26. *Synthesis of functionalized thio-mannopyranoside*

In order to prepare the propargylated azobenzene bearing a carboxylic acid function (**13**) for linking together glycosyl donor and acceptor, *o,o'*-dihydroxy azobenzene was firstly mono-*O*-alkylated with *tert*-butyl bromoacetate to give the compound **11** in 89% yield. The following *O*-propargylation by using cesium carbonate and propargyl bromide in THF gave the compound **12** in 99% yield. The desired ompound **13** was then obtained quantitatively after acidic deptrotection of **12** (**Scheme 27**).

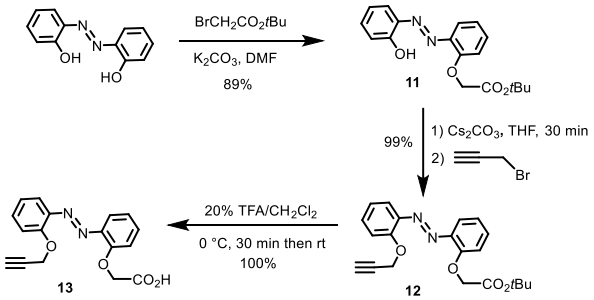

Scheme 27. *Synthesis of functionalized azobenzene*

The two azobenzene-functionalized glycosyl acceptors **15** and **16** were then prepared through esterification of **13** with methyl 2,3-di-*O*-benzyl-α-D-glucopyranoside **14**,[111] affording the desired 6-*O*-esterified compound **15** (41%) and the 4-*O*-esterified compound **16** (15%), along with the 4,6-di-*O*-esterified one **17** (17%) (**Scheme 28**).

[111] M. Matwiejuk, J. Thiem, *Chem. Commun*. **2011**, *47*, 8379-8381.

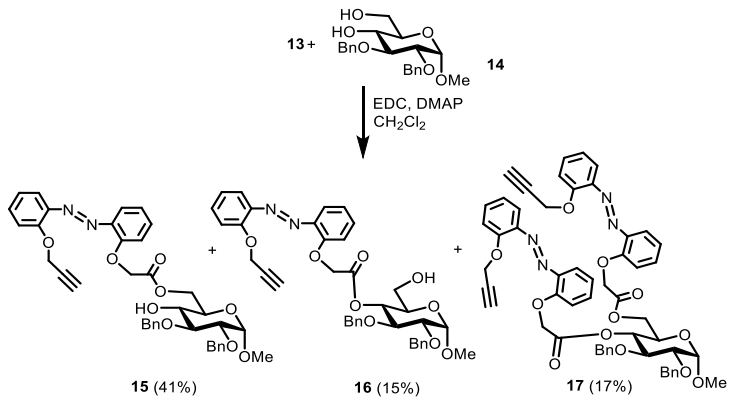

Scheme 28. *Synthesis of azobenzene-linked glycosyl acceptor*

For the synthesis of azido-mannosyl donors, azide function was either directly introduced into the 6-position of phenyl 2,3,4-tri-*O*-benzyl-α-D-thiomannopyranoside **10**,[112] through mesylate intermediate followed by S_N2 reaction with NaN_3, leading to the azido thiomannopyranoside **18** in 86% yield (**Scheme 29**). To study the influence of the linker length on the outcome of intramolecular glycosylation and also prepare larger glycomacrocycles, we have also prepared the compound **19** bearing an azidoacetyl group on the 6-position, through reaction with chloroacetyl chloride or bromoacetyl bromide followed by S_N2 reaction with NaN_3 (**Scheme 29**). CuAAC reaction of **18** with the propargyl derivatives **15** or **16** led respectively to the glycosyl donor-acceptor pairs **1** and **3** in 84 and 86% yield respectively as pure *E*-isomers. In the similar way, CuAAC reaction of **19** with the propargyl derivatives **15** or **16** led respectively to the glycosyl donor-acceptor pairs **2** and **4** in 71 and 84% yields respectively as pure *E*-isomers.

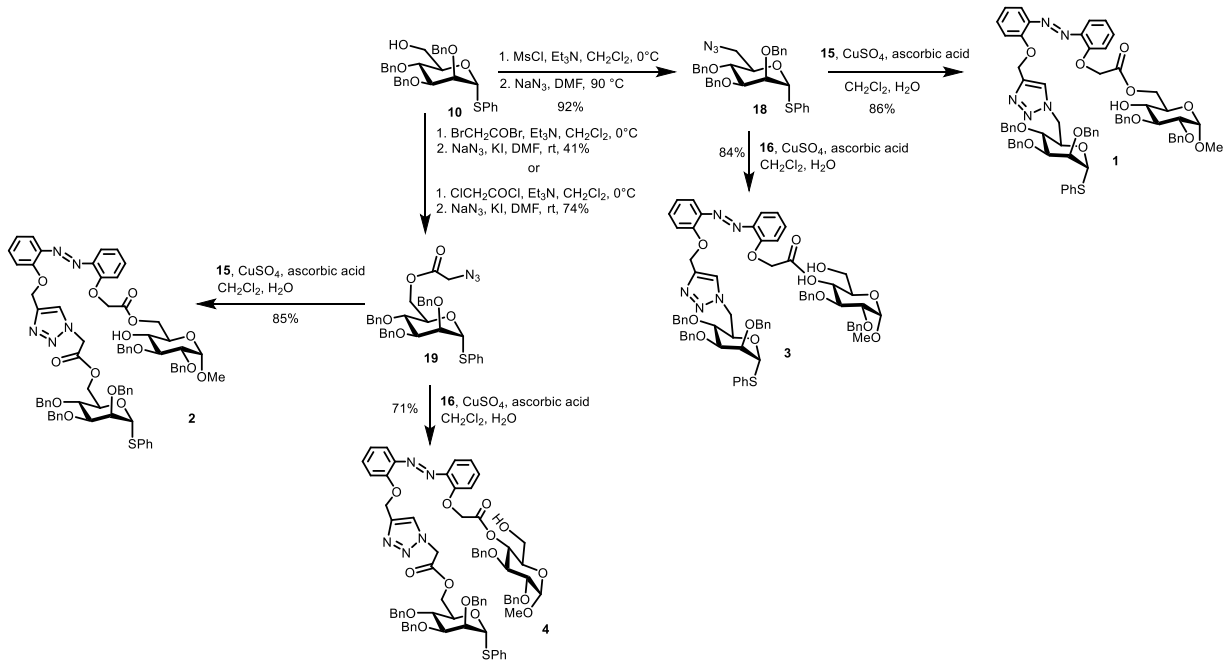

Scheme 29. *Synthesis of GDAPs **1** - **4.***

[112] R. Yadav, S. L. Ben-Arye, B. Subramani, V. Padler-Karavani, R. Kikkeri, *Org. Biomol. Chem.* **2016**, *14*, 10812-10815.

2.3. Intramolecular glycosylation from the *E*-azobenzene substrates

With the *E*-GDAPs **1-4** in hand, we then realized the intramolecular glycosylation by using the NIS and TfOH at -78 °C. To avoid the photoisomerization, the glycosylation was carried out in the dark environment. The reactions were monitored by TLC and it's usually terminated after 3-4h. The structure of the glycomacrocycles was confirmed by ^{1}H and ^{13}C NMR and HRMS. Due to the small coupling constants for both α and β-mannopyranosides ($J_{1,2}$ is often smaller than 2 Hz)[113,114], the anomeric configuration was determined by the coupling constant between C_1 and H_1. Pederson and coworker reported that, for glycopyranoside bearing a $^{1}C_4$ conformation, $J_{C1,H1}$ is near 170 Hz for the α-anomer and about 160 Hz for the β-anomer, with a difference of approximate 10 Hz between two anomers in most cases (**Figure 19**).[115]

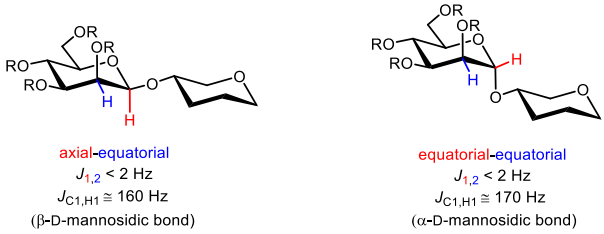

Figure 19. *Coupling constants $J_{1,2}$ and $J_{C1,H1}$ in α- and β-mannopyranosides*

2.3.1. Intramolecular glycosylation of *E*-1

For the glycosyl donor-acceptor pair **1** containing short triazole linker, intramolecular glycosylation was realized by using the NIS and TfOH at -78 °C (**Scheme 30**). The macrocyclization yield and the α-stereoselectivity increased with the increasing reaction concentration (from 5 to 28.6 mM), affording the macrocycle *E*-**20** up to 72% yield as an inseparable mixture of α/β isomers (from 1.8/1 to 4.5/1, entries 1 to 4,

Table 3) A complete α-stereoselectivity was achieved with 0.83 equiv. of TfOH at 40 mM concentration in 50% yield (entry 5). The α- or β-configuration was confirmed by the coupling constant ($J_{C1',H1'}$ = 174.5 Hz, $J_{C1,H1}$ = 167.8 Hz for the α-isomer; and $J_{C1',H1'}$ = 153.5 Hz, $J_{C1,H1}$ = 166.8 Hz for the β-isomer) (**Figure 20**). Structure of the macrocycle *E*-**20**α has also been confirmed by HRMS analysis. During the intramolecular macrocyclization reaction, we have also observed the formation of a mixture of several intermolecular glycosylation products as well as the hydrolyzed glycoside which are more polar than the macrocycle *E*-**20**.

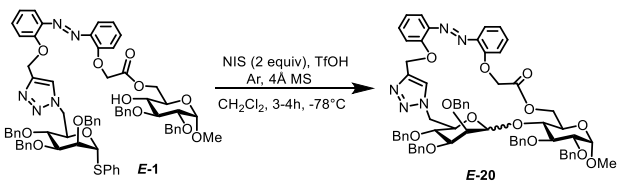

Scheme 30. *Intramolecular glycosylation of E-**1***

[113] R. U. Lemieux, R. K. Kullnig, H. J. Bernstein, W. G. Schneider, *J. Am. Chem. Soc.* **1958**, *80*, 6098-6105.
[114] P.-E. Jansson, L. Kenne, G. Widmalm, *Carbohydr. Res.* **1987**, *168*, 67-77.
[115] K. Bock, C. Pedersen, *J. Chem. Soc. Perkin Trans. 2* **1974**, 293-297.

Table 3. *Reagent and condition screen for the intramolecular glycosylation of E-**1**.*

entry	substrate, concentration	TfOH (equiv.)	isolated product[a]	yield (%)	α:β[b]
1	*E*-**1**, 5 mM	1.5	*E*-**20**	17	1.8:1
2	*E*-**1**, 10 mM	1.5	*E*-**20**	22	3.5 :1
3	*E*-**1**, 20 mM	1.5	*E*-**20**	31	3.8:1
4	*E*-**1**, 28.6 mM	1	*E*-**20**	72	4.5:1
5	*E*-**1**, 40 mM	0.83	*E*-**20**	50	1:0
6	*E*-**1**, 40 mM	1	*E*-**20**	50	5.3:1

[a]Formation of several intermolecular glycosylation products as well as the hydrolyzed thioglycoside has also been observed; [b]The anomeric ratio corresponds to isolated products.

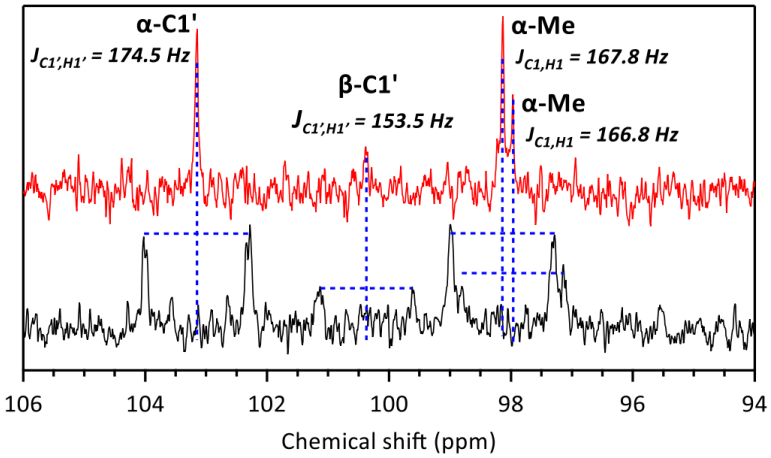

Figure 20. *Partial ^{13}C NMR spectra of the glycomacrocycle E-**20**α,β*

2.3.2. Intramolecular glycosylation of *E*-2

For the glycosyl donor-acceptor pair **2** containing longer triazole linker than **1**, intramolecular glycosylation was successfully only under higher concentration (entry 1 vs entries 2,3, **Table 4**) with the yield up to 70% for *E*-**21**, and a slight *β*-stereoselectivity (α:β = 0.48:1, entry 2) contrary to the α-selectivity from *E*-**1** (**Scheme 31**). No macrocyclization product has been isolated at low concentrations (5 mM, entry 1). Both glycomacrocycles *E*-**21**α and *E*-**21**β can be easily separated by column chromatography in 23 and 47% yields respectively. The coupling constants of the *E*-**21***α* show $J_{C1',H1'}$ = 173.5 Hz and $J_{C1,H1}$ = 173.5 Hz (**Figure 21**), while the isomer *E*-**21**β displayed a small coupling constant for $J_{C1',H1'}$ = 157.3 Hz (**Figure 22**). Structure of the macrocycles *E*-**21***α* and **21***β* have also been confirmed by HRMS analysis.

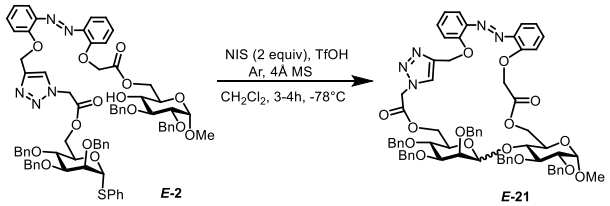

Scheme 31. *Intramolecular glycosylation of E-**2***

Table 4. *Reagent and condition screen for the ntramolecular glycosylation of E-**2**.*

entry	substrate, concentration	TfOH (equiv.)	isolated product[a]	yield (%)	α:β[b]
1	*E*-**2**, 5 mM	1	-	-	-
2	*E*-**2**, 28.6 mM	1	*E*-**21**	70	0.48:1
3	*E*-**2**, 40 mM	0.5	*E*-**21**	55	0.44:1

[a]*Formation of several intermolecular glycosylation products has also been observed;* [b]*The anomeric ratio corresponds to isolated products.*

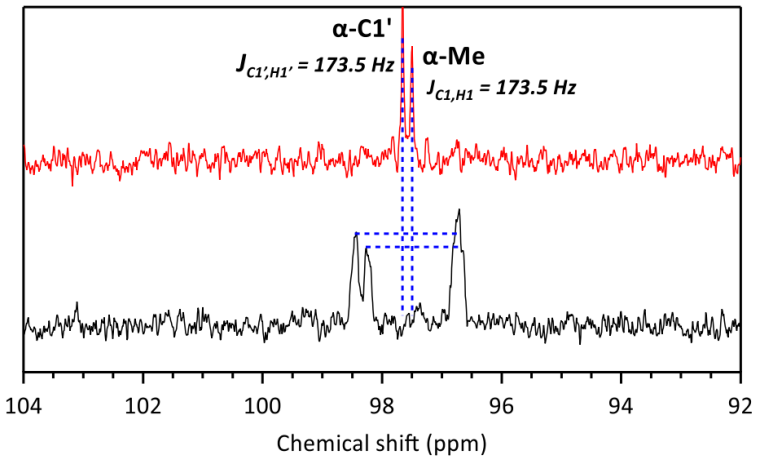

Figure 21. *Partial* ^{13}*C NMR spectra of compound E-**21**α*

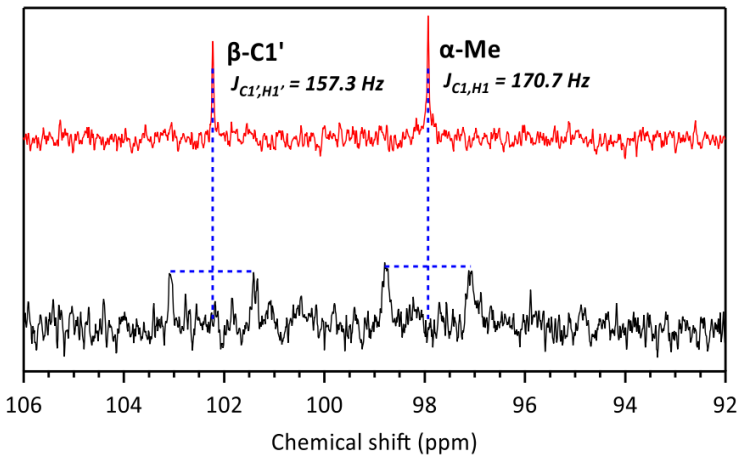

Figure 22. *Partial* ^{13}*C NMR spectra of compound E-**21**β*

2.3.3. Intramolecular glycosylation of *E*-3

For the glycosyl donor-acceptor pair **3** containing the same triazole linker as **1**, and free OH at the C-6 position, intramolecular glycosylation (***Scheme 32***) with NIS and TfOH at -78 °C showed that at lower concentration (5 mM), the reaction led mainly to a mixture of several intermolecular glycosylation products as well as the hydrolyzed glycoside (entry 1, ***Table 5***). However, at higher concentration, the macrocyclization worked with good yields and total *β*-stereoselectivity (entries 2-4, ***Table 5***). The best yield of 78% was obtained at a concentration of 28.6 mM (entry 2). The coupling constants of the *E*-**22***β* show $J_{C1',H1'}$ = 157.3 Hz and $J_{C1,H1}$ = 165.0 Hz (***Figure 23***).

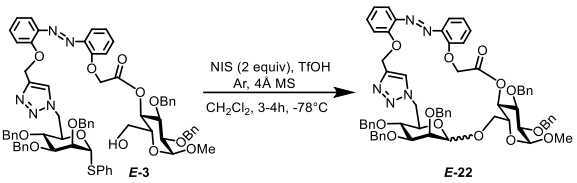

Scheme 32. *Intramolecular glycosylation of E-**3***

Table 5. *Reagent and condition screen for the Intramolecular glycosylation of E-**3**.*

entry	substrate, concentration	TfOH (equiv.)	isolated product[a]	yield (%)	α:β[b]
1	*E*-**3**, 5 mM	1	-	-	-
2	*E*-**3**, 28.6 mM	1	*E*-**22**	78	0:1
3	*E*-**3**, 30 mM	1.5	*E*-**22**	68	0:1
4	*E*-**3**, 40 mM	1	*E*-**22**	57	0:1

[a]Formation of several intermolecular glycosylation products has also been observed; [b]The anomeric ratio corresponds to isolated products.

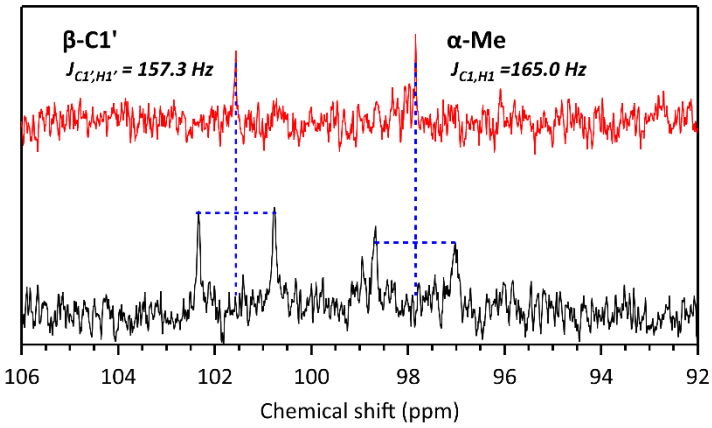

Figure 23. *Partial ^{13}C NMR spectra of compound E-**22**β*

2.3.4. Intramolecular glycosylation of *E*-4

For the glycosyl donor-acceptor pair **4** containing the same triazole linker like **2**, and free OH at the C-6 position, intramolecular glycosylation with NIS (2 equiv.) and TfOH (1 equiv.) at -78°C under the concentration of 28.6 mM furnished the desired glycomacrocycle **23** with a total *β* stereoselectivity (***Scheme 33***). The coupling constants of $J_{C1',H1'}$ = 156.3 Hz and $J_{C1,H1}$ = 167.8 Hz comfirmed the *β*-anomeric configuration for *E*-**23***β* (***Figure 24***).

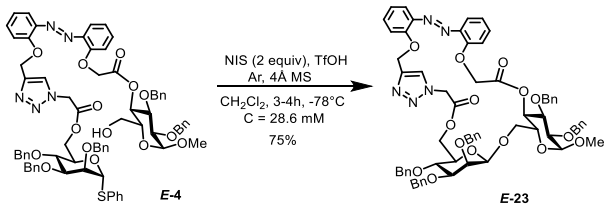

Scheme 33. *Intramolecular glycosylation of E-4*

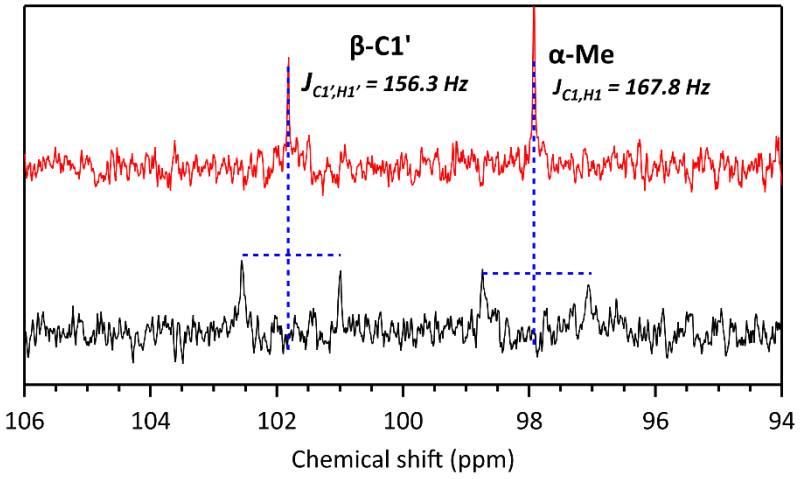

Figure 24. *Partial ^{13}C NMR spectra of compound E-**23β***

2.4. Intramolecular glycosylation from the *Z*-azobenzene substrates

In order to study the influence of the configuration of the photochromic template on the outcome of the intramolecular glycosylation, *E*-GDAPs **1-4** were photoisomerized to the corresponging *Z*-**1-4** under illumination at 365 nm, until the photostationary state (the equilibrium under saturating illumination at specific wavelength) (PSS_{365}). Then, the intramolecular glycosylations with *Z*-GDAPs were carried out in the dark by using NIS and TfOH at -78 °C. (See detail General Procedure H, page **128**)

2.4.1. Intramolecular glycosylation of Z-1

Figure 25 showed the absorption spectrum of *E*-**1** (in black), which after irradiation at 365 nm, led to the corresponding Z-isomer (in red, **Figure 25**). The photoisomerization followed by ^1H NMR gave access to the *Z*:*E* ratio which was estimated to be 93:7 (**Figure 26**). Intramolecular glycosylation of *Z*-**1** by using NIS and TfOH at -78 °C (***Scheme 34***) showed that reaction worked better at lower concentration (5 mM, entry 1, **Table 6**), with 32% of the glycomacrocyle *E*-**20** isolated; while only 4% of *E*-**20** was obtained when the reaction was realized under a concentration of 28.6 mM (entry 2, Table 6). In both conditions, a slight α-stereoselectivity has been observed. The glycosylation from the *Z*-isomer gave lower yield and lower stereoselectivity compared to the *E*-isomer.

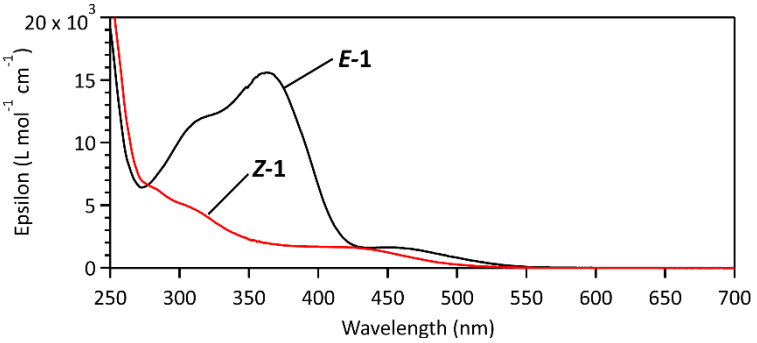

Figure 25. *Absorption spectra of **1** in CH_2Cl_2: E-**1** (black line), PSS_{365} (red line). Irradiation condition at 365 nm: 6.40 mW·cm^{-2}, 600 s.*

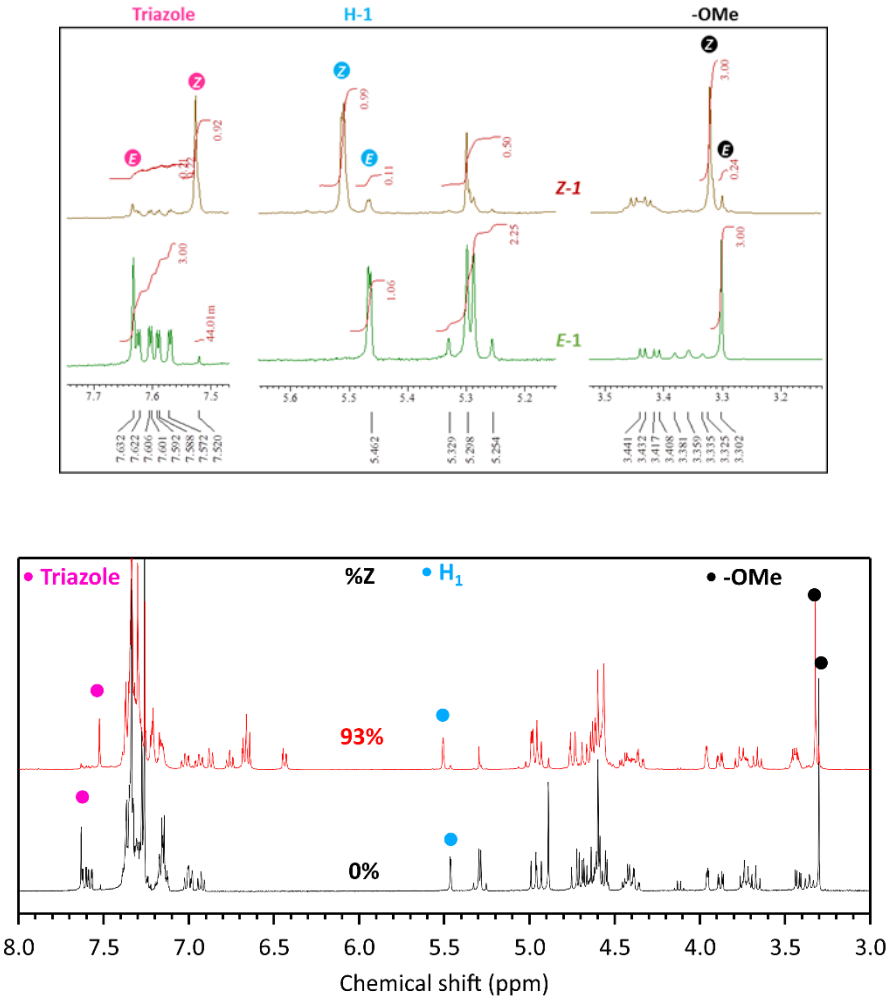

Figure 26. *Partial ^{1}H NMR spectra of E-**1** and PSS_{365} in $CDCl_3$ (E-**1**, black line; PSS_{365}, red line). Top graph: screenshots of the region of interest and the integral values taken for the determination of the photoconversion yields.*

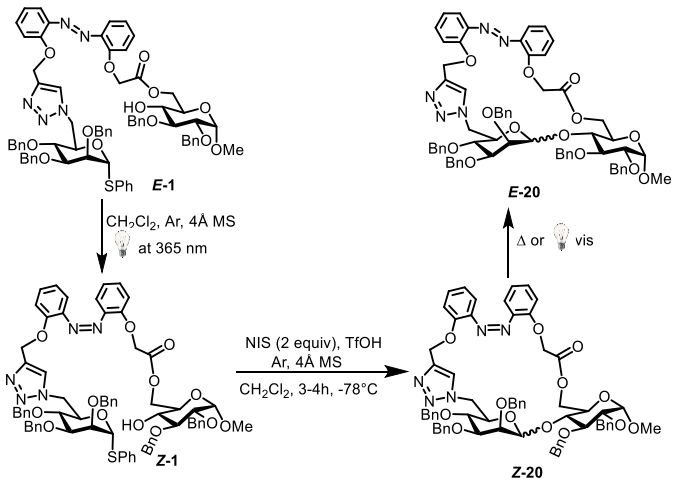

Scheme 34*. Intramolecular glycosylation of Z-**1***

Table 6. Reagent and condition screen for the intramolecular glycosylation of **1**.

entry	substrate, concentration	TfOH (equiv.)	isolated product[a]	yield (%)	α:β[b]
1	*Z*-**1**[c], 5 mM	1.8	*E*-**20**	32	2.7:1
2	*Z*-**1**[c], 28.6 mM	1	*E*-**20**	4	2.3:1
3	*E*-**1**, 5 mM	1.5	*E*-**20**	17	1.8:1
4	*E*-**1**, 28.6 mM	1	*E*-**20**	72	4.5:1

[a]Formation of several intermolecular glycosylation products as well as the hydrolyzed thioglycoside has also been observed; [b]The anomeric ratio corresponds to isolated products; [c]*Z*-enriched mixture obtained at PSS_{365}: 93:7 (*Z*:*E*).

Furthermore, only the *E*-macrocycle **20** has been isolated from *Z*-**1**. Two reasons may explain the isolation of the *E*-macrocycle from the *Z*-substrate: either through the glycosylation of *E*-**1** which could be formed from the *Z*-isomer under the reaction conditions in addition to that present at PSS, or from the isomerization of *Z*-macrocycle **1** after intramolecular glycosylation, during the workup and purification procedure (***Scheme 34***). Comparison of the glycosylation results from both *E* and *Z* isomer under the same concentration (entry 3 vs entry 1: 17% with α:β = 1.8:1 from *E*-**1** vs 32% with α:β = 2.7:1 from *Z*-**1**; entry 4 vs entry 2: 72% with α:β = 4.5:1 from *E*-**1** vs 4% with α:β = 2.3:1 from *Z*-**1**, **Table 6**) would support the hypothesis that the glycosylation of *Z*-**1** occurred before the isomerization of *Z*-**20** to *E*-**20**.

2.4.2. Intramolecular glycosylation of Z-2

Irradiation of the substrate *E*-**2** with 365 nm light led to the Z-**2**, with the *Z*:*E* ratio estimated to be 91:9 at the PSS_{365} (**Figure 27**).

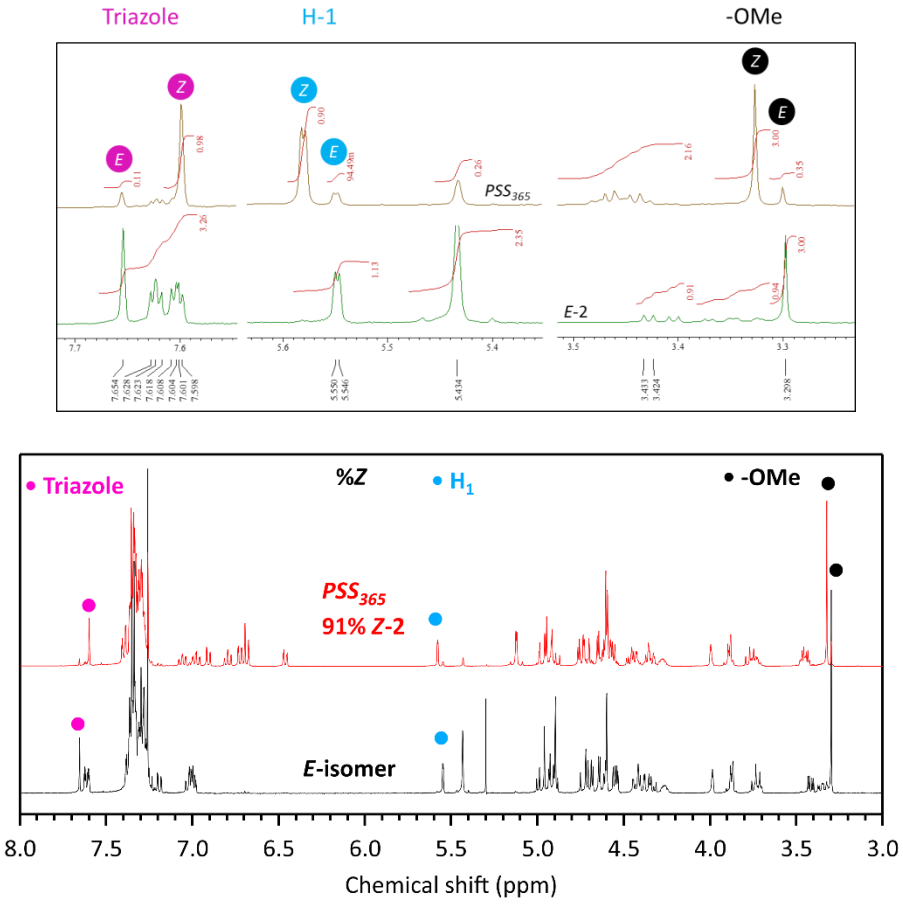

Figure 27. *Partial* ^{1}*H NMR spectra of E-2 and* PSS_{365} *in* $CDCl_3$*. Top graph: screenshots of the region of interest and the integral values taken for the determination of the photoconversion yields.*

Like *Z*-**1**, the macrocyclization of *Z*-**2** was achieved only under 5 mM concentration, furnishing the macrocycle *E*-**21** in 70% yield in favor of the α-isomer (α:β = 1.5:1, entry 1, **Table 7**). Comparison of the glycosylation results from both the *E*- and *Z*-**2** under the same concentration (0 % from *E*-**2** and 70% from *Z*-**2**, entry 3 vs entry 1; 70% from *E*-**2** and 0% from *Z*-**2**, entry 4 vs entry 2, **Table 7**) supported again the hypothesis of the glycosylation of *Z*-**2** occurring before the isomerization of *Z*-**6** to *E*-**6** (***Scheme 35***).

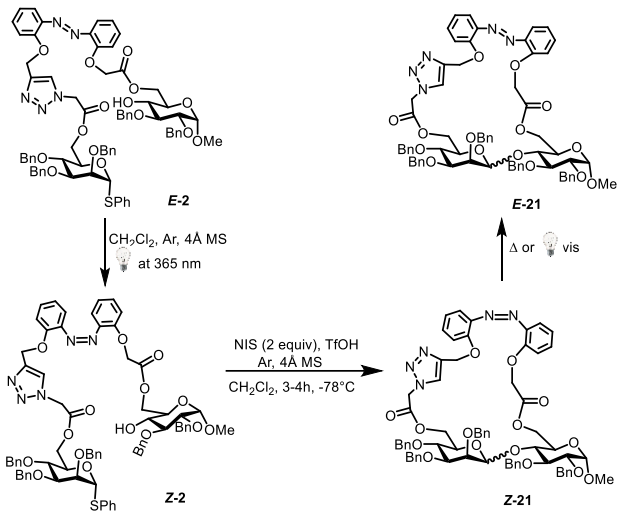

Scheme 35. *Intramolecular glycosylation of Z-**2***

Table 7. Reagent and condition screen for the intramolecular glycosylation of **2**.

entry	substrate, concentration	TfOH (equiv.)	isolated product[a]	yield (%)	α:β[b]
1	*Z*-**2**[c], 5 mM	0.7	*E*-**21**	70	1.5:1
2	*Z*-**2**[c], 28.6 mM	1	-	-	-
3	*E*-**2**, 5 mM	1	-	-	-
4	*E*-**2**, 28.6 mM	1	*E*-**21**	70	0.48:1

[a]Formation of several intermolecular glycosylation products has also been observed; [b]The anomeric ratio corresponds to isolated products; [c]Z-enriched mixture obtained at PSS_{365}: 93:7 (Z:E).

2.4.3. Intramolecular glycosylation of *Z*-3

For the glycosyl donor-acceptor pair **3**, its irradiation at 365 nm led to the *Z*-**3** with the *Z*:*E* ratio estimated to be 90:10 at the PSS_{365} (**Figure 28**). Intramolecular glycosylation with NIS/TfOH at -78°C led however only to un unseparable mixture of intermolecular glycosylation products (***Scheme 36***), whatever the reaction concentration (entries 1, 2, **Table 8**)

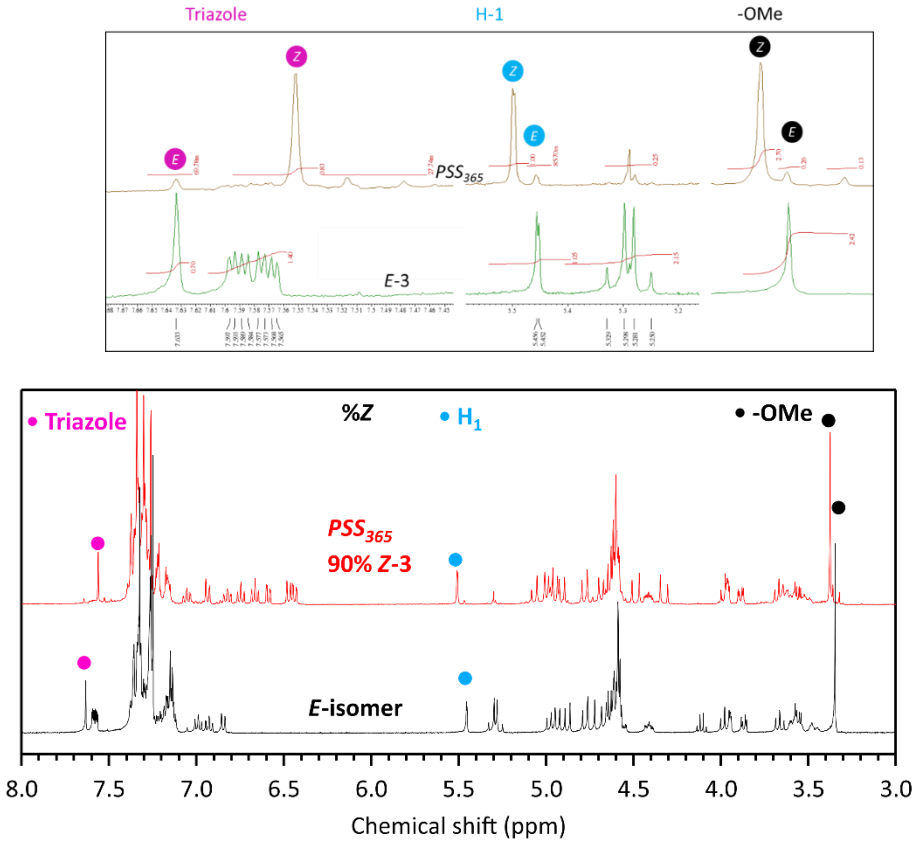

Figure 28. *Partial* ^{1}*H NMR spectra of E-**3** and* PSS_{365} *in* $CDCl_3$*. Top graph: screenshots of the region of interest and the integral values taken for the determination of the photoconversion yields.*

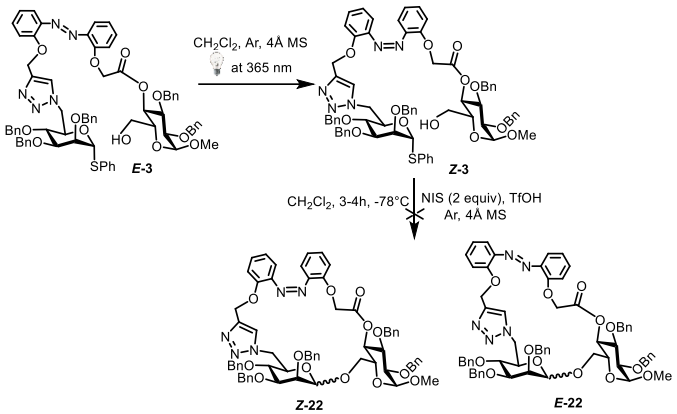

Scheme 36. *Intramolecular glycosylation of Z-**3***

Table 8. *Reagent and condition screen for the intramolecular glycosylation of Z-**3**.*

entry	substrate, concentration	TfOH (equiv.)	isolated product	yield (%)	α:β
1	*Z*-**3**[a], 5 mM	0.4	*E- and Z*-**3**	-	-
2	*Z*-**3**[a], 28.6 mM	0.5	*E- and Z*-**3**	-	-

[a]*Z-enriched mixture obtained at PSS$_{365}$: 90:10 (Z:E).*

2.4.4. Intramolecular glycosylation of *Z*-4

Similarly, the substrate *E*-**4** was photoisomerized at 365 nm to the corresponding *Z*-isomer, with the *Z*:*E* ratio estimated to be 87:13 at the PSS$_{365}$ (**Figure 29**). Intramolecular glycosylation with NIS/TfOH at -78°C failed too, leading to un unseparable mixture of intermolecular glycosylation products (***Scheme 37***).

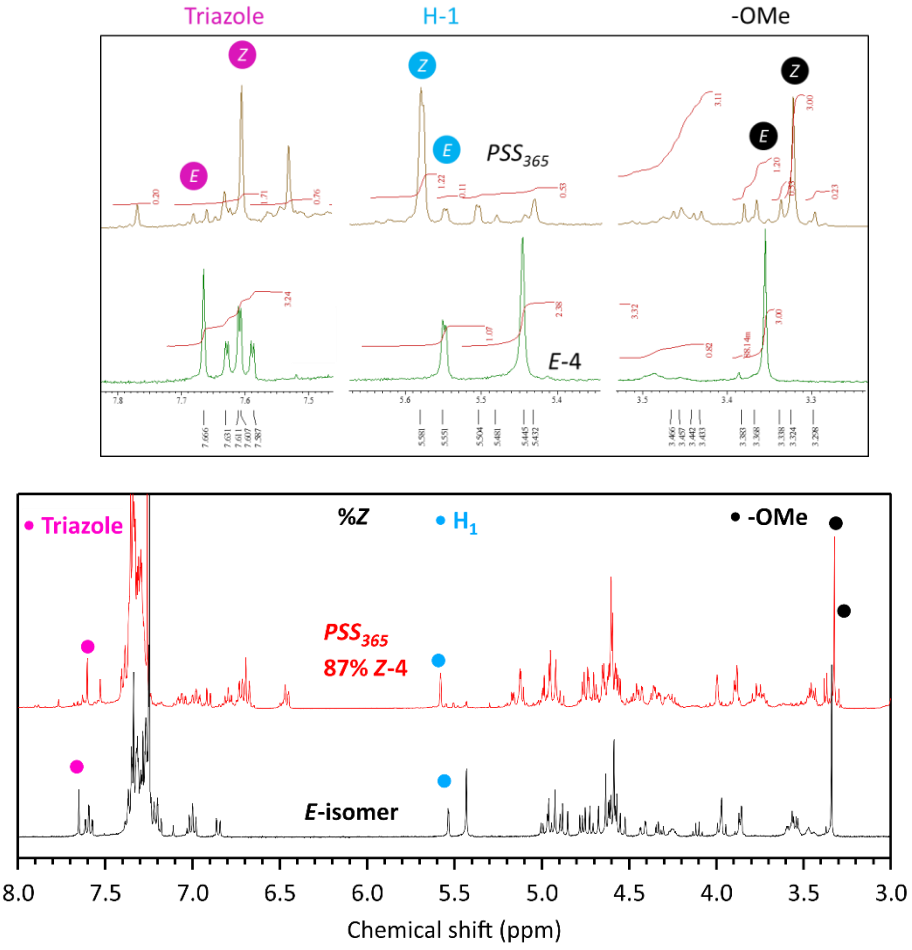

Figure 29. Partial ^{1}H NMR spectra of E-**4** and PSS$_{365}$ in $CDCl_3$. Top graph: screenshots of the region of interest and the integral values taken for the determination of the photoconversion yields.

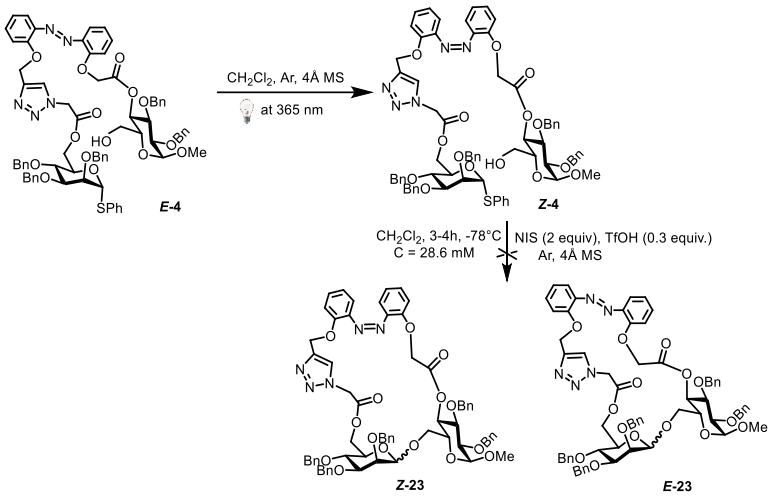

Scheme 37. *Intramolecular glycosylation of Z-**4***

2.5. Mechanistic investigation of intramolecular glycosylation of *Z*-substrate by absorption and NMR

p-Amino substituted methoxyazobenzenes can be protonated on the azo moiety and the corresponding azonium species have been investigated by Woolley and coll. as biologically applicable photoswitching.[116,117] *To further investigate the azobenzene isomerization during the intramolecular glycosylation conditions, we decided to study the influence of TfOH and NIS/TfOH on both* E- *and* Z-***1*** *substrates.* **Figure 30***a showed the absorption spectra evolution of* E-***1*** *with increasing concentration of TfOH which reached a plateau with more than 2.5 equiv. of TfOH in* CH_2Cl_2*. Two red-shifted absorption pics appeared at 396 and 485 nm, showing similar protonation behavior as* ortho-O-*substituted azobenzene derivatives as reported.*[116,117] *Since up to 1.8 equiv. of TfOH has been used to catalyze the intramolecular glycosylation of* Z-***1*** *(*

Table 3, entry 1), we have directly added 2 equiv. of TfOH to *Z*-**1** where the absorption spectra evolved progressively towards *E*-**1**·H^+ species (***Figure 30***b). However, few absorption spectra evolution were observed by introducing NIS (2 equiv.) or TfOH/NIS (2 equiv. each) to a solution of *Z*-**1** (***Figure 30***c). There results confirmed that under glycosylation conditions (NIS/TfOH) at -78°C, back isomerization of *Z*- to *E*-**1** is unlikely.

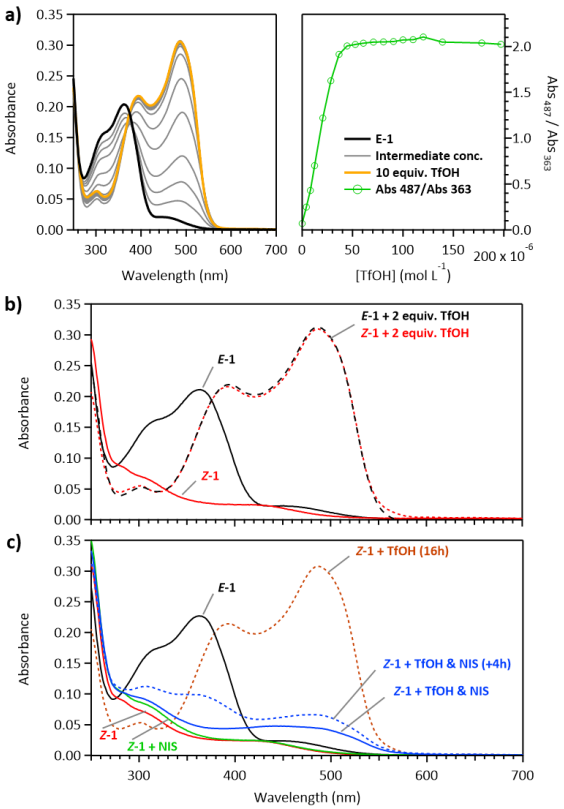

Figure 30. *(a) Absorption spectra of E-**1** (14.8 µM in* CH_2Cl_2*) 30 min after addition of up to 14 equiv. of TfOH at rt; (b) absorption spectra comparison of E- and Z-**1** with or without TfOH; (c) absorption spectra comparison of E-**1** and Z-**1** in the presence of TfOH or NIS or NIS/TfOH (2 equiv. each) at rt. Irradiation conditions at 365 nm: 6.4 mW·cm*$^{-2}$*, 120 s.*

[116] S. Samanta, A. Babalhavaeji, M. Dong, G. A. Woolley, *Angew. Chem. Int. Ed*. **2013**, *52*, 14127-14130.
[117] M. Dong, A. Babalhavaeji, M. J. Hansen, L. Kálmánb, G. A. Woolley, *Chem. Commun*. **2015**, *51*, 12981-12984.

3. Synthesis of photochromic glycomacrocycles containing one sugar unit

The precedent study of intramolecular glycosylation shows that by using triazole-linked *o,o*'-dihydroxyazobenzene photochromic template, an excellent *β*-stereoselectivity can be obtained for the mannosylation with glucosyl acceptor bearing a primary alcohol fonction. To investigate the scope of this method, we decided to use pentaerythritol and 1,2-phenylenedimethanol as glycosyl acceptors to investigate the stereoselectivity of the glycosylation of GDAPs **24** and **25** (**Figure 31**) and to obtain new photoswitchable glycomacrocycles. Use of the isopropylidene-protected pentaerythritol offers the possibility for further functionalization. After photoisomerization of *E*-**24**-**25**, the corresponding *Z*-isomers could be obtained so as to investigate their intramolecular glycosylation reaction.

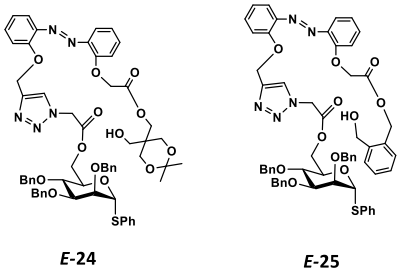

Figure 31. *Structure of new GDAPs* ***24-25***

3.1. Retrosynthesis

The retrosynthetic scheme to prepare photochromic glycomacrocycles (PGMs) is shown in the **Scheme 38**. The GDAPs could be obtained by CuAAC between the previously synthesized azido-sugar **19** and azobenzene linked glycosyl acceptor which could be obtained from 1,2-phenylenedimethanol or (2,2-dimethyl-1,3-dioxane-5,5-diyl) dimethanol and *o,o*'-dihydroxy azobenzene.

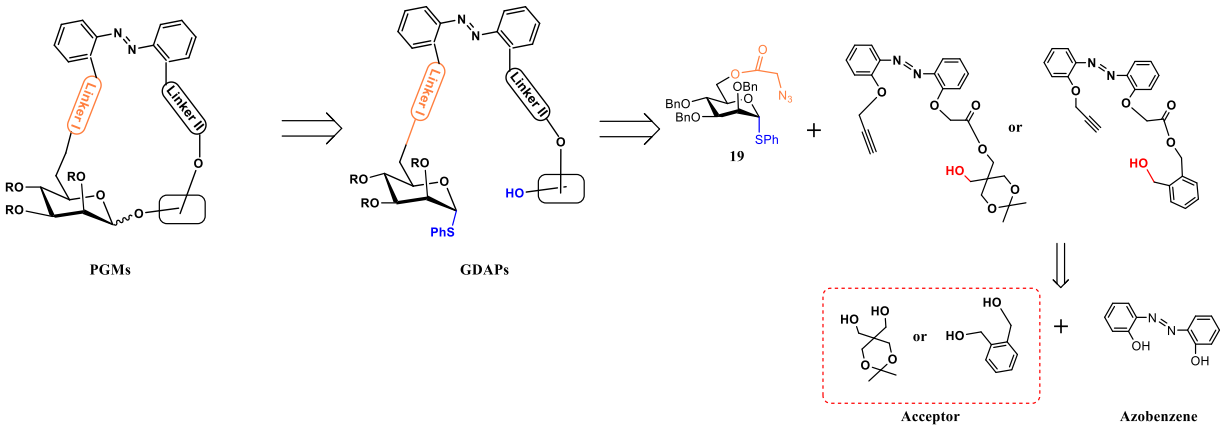

Scheme 38. *Retrosynthesis of new PGMs*

3.2. Preparation of glycosyl donor-acceptor pairs

For the preparation of glycosyl donor-acceptor pair **24**, pentaerythritol was firstly protected as mono-isopropylidene **26** with acetone catalyzed by *p*-TsOH, leading to the compound **26** in 40 % yield and the bis-isopropylidene derivative **26b** in 20 % yield[118] (**Scheme 39**). Esterification of the azobenzene derivative **13** with **26** catalyzed with EDC and DMAP in CH_2Cl_2 afforded the two azobenzene-functionalized glycosyl acceptors **27a** (41%) and **27b** (24%). CuAAC reaction of **19** with **27a** led respectively to the glycosyl donor-acceptor pair **24** in 87% yield as pure *E*-isomer.

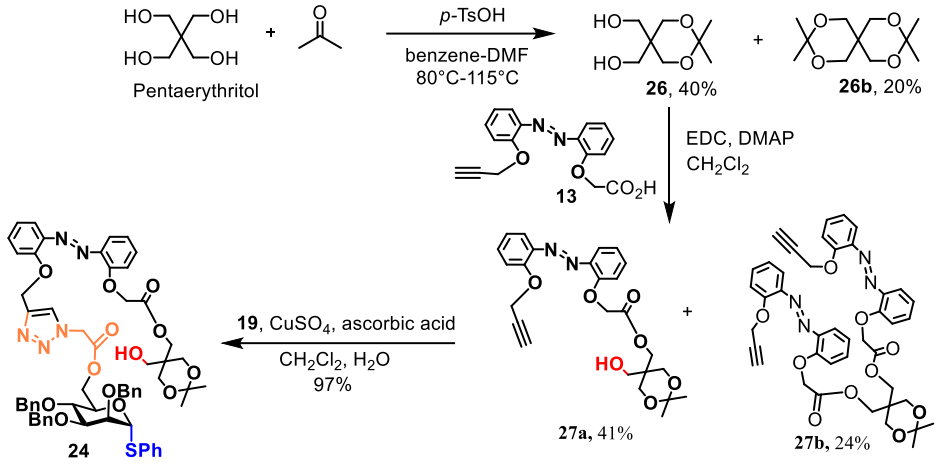

Scheme 39. *Synthesis of GDAP **24**.*

For the preparation of glycosyl donor-acceptor pair **25**, esterification of **13** with 1,2-phenylenedimethanol **28** afforded also the mono- and bis-esterified compounds **29a** (47%) and **29b** (10%) (**Scheme 40**). Subsequent CuAAC reaction of **19** with **29a** led to the glycosyl donor-acceptor pair **25** in 69% yield.

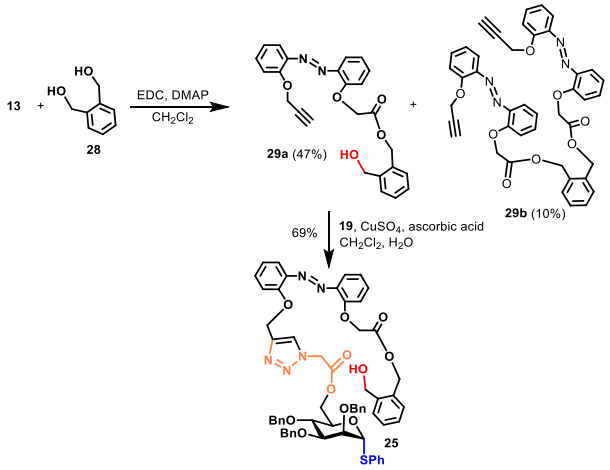

Scheme 40. *Synthesis of GDAP **25**.*

[118] M. C. Murguía, S. E. Vaillard, R. J. Grau, *Synthesis* **2001**, 1093-1097.

3.3. Intramolecular glycosylation from the *E*-azobenzene substrates

With the *E*-GDAPs **24** and **25** in hand, we then realized the intramolecular glycosylation by using the NIS and TfOH at -78 °C. The glycosylation was always carried out in the dark.

3.3.1. Intramolecular glycosylation of *E*-24

Intramolecular glycosylation of **24** under the optimized conditions, that is, NIS (2 equiv.) and TfOH (1 equiv.) at -78 °C under the concentration of 28.6 mM, furnished the glycomacrocycle **30** also with excellent β-stereoselectivity, in 39% yield (**Scheme 41**). The coupling constant of $J_{C1,H1}$ = 153.5 Hz had been observed for *E*-**30β** (**Figure 32**) No intramolecular glycosylation product has been isolated when the reaction was realized at the concentration of 5 mM.

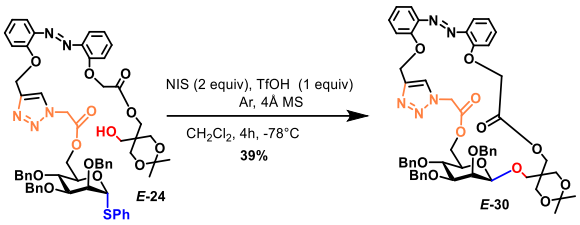

Scheme 41. *Intramolecular glycosylation of E-**24**.*

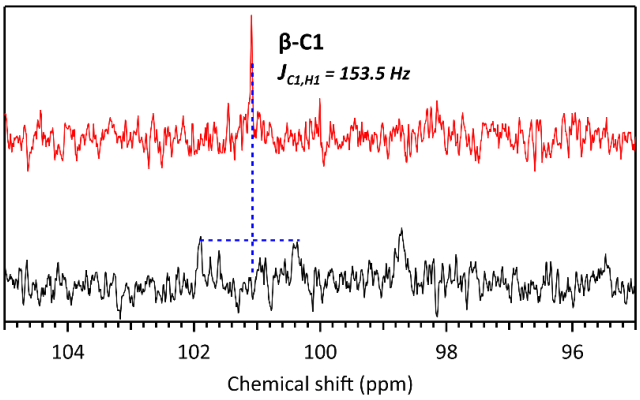

Figure 32. *Partial ^{13}C NMR spectra of compound E-**30β**.*

3.3.2. Intramolecular glycosylation of *E*-25

In the case of glycosyl donor-acceptor pair **25**, intramolecular glycosylation in the presence of NIS (2 equiv.) and TfOH (1 equiv.) at -78 °C under the concentration of 28.6 mM led to the glycomacrocycle **31** in 48% yield with excellent β-stereoselectivity (**Scheme 42**). The coupling constant of $J_{C1,H1}$ = 163.0 Hz had been observed for *E*-**31**β (***Figure 33***).

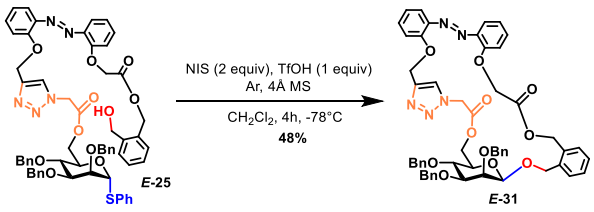

Scheme 42. *Intramolecular glycosylation of E-**25**.*

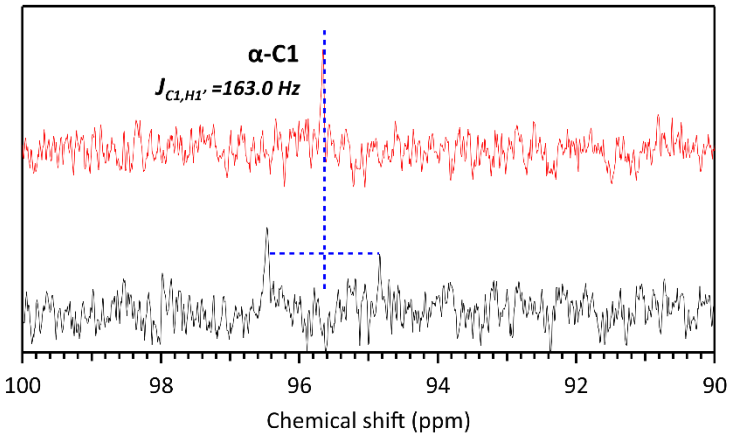

Figure 33. *Partial ^{13}C NMR spectra of compound E-**31**β*

3.4. Intramolecular glycosylation from the *Z*-azobenzene substrates

3.4.1. Intramolecular glycosylation of Z-24

For the glycosyl donor-acceptor pair **24**, its irradiation at 365 nm led to the *Z*-**24** with the *Z*:*E* ratio estimated to be 92:8 at the PSS_{365} (**Figure 34**).

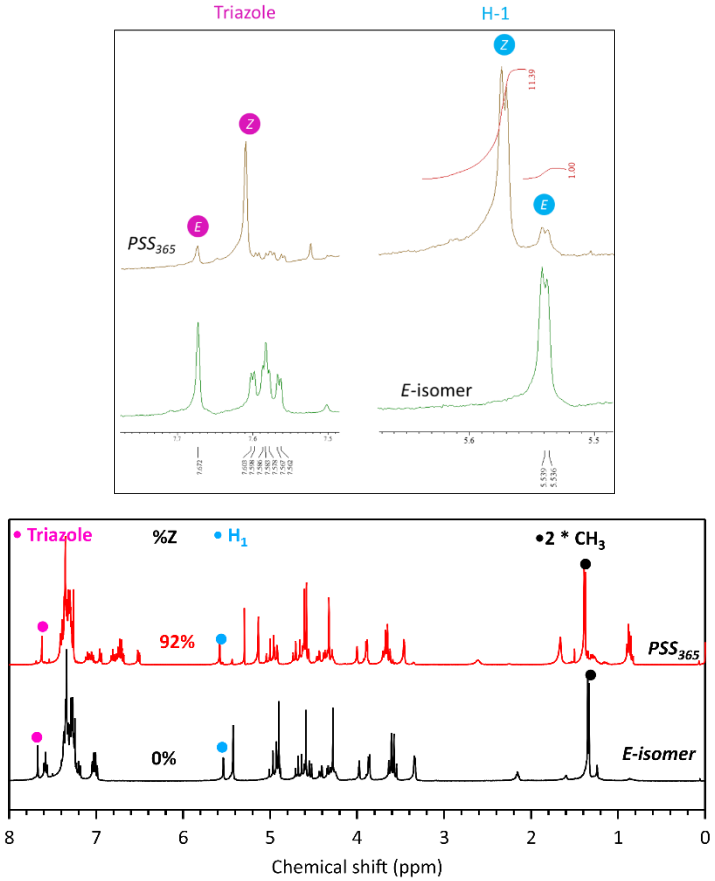

Figure 34. *Partial* ^{1}*H NMR spectra of E-**24** and* PSS_{365} *in* $CDCl_3$*. Top graph: screenshots of the region of interest and the integral values taken for the determination of the photoconversion yields.*

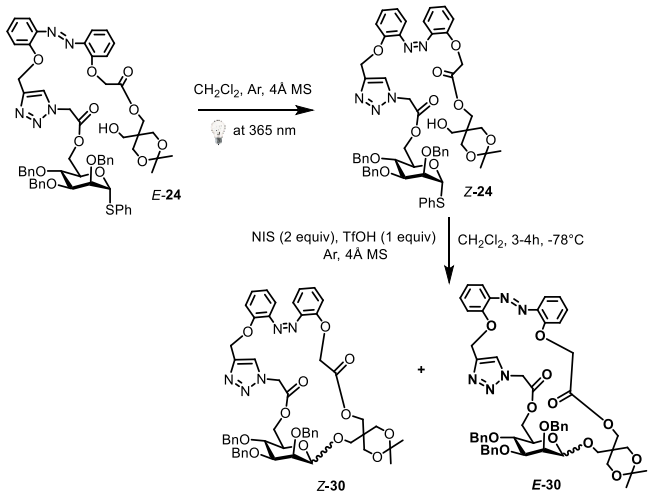

Scheme 43. *Intramolecular glycosylation of Z-**24**.*

Intramolecular glycosylation of *Z*-**24** worked only under 5 mM concentration in the presence of NIS/TfOH at -78°C, leading to the glycomacrocycle **30** as a mixture of *E* and *Z*-isomer in 6.7 % yield (entry 1, **Table 9**). Mixture of intermolecular glycosylations products have been detected on NMR spectra.

Table 9. *Reagent and condition screen for the intramolecular glycosylation of Z-**24**.*

entry	substrate, concentration	isolated product	yield (%)
1	*Z*-**26**, 5 mM	*E and Z*-**30**	6.7
2	*Z*-**26**, 28.6 mM	-	-

3.4.2. Intramolecular glycosylation of *Z*-25

For the glycosyl donor-acceptor pair **25**, its irradiation at 365 nm led to the *Z*-**25** with the *Z*:*E* ratio estimated to be 94:6 at the PSS_{365} (**Figure 35**).

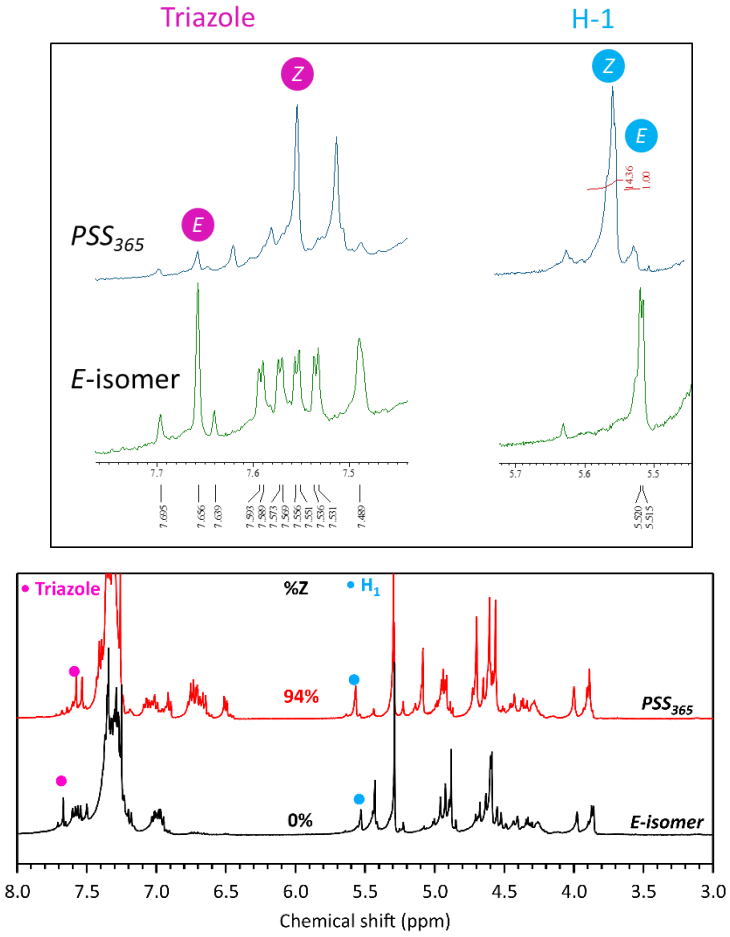

Figure 35. *Partial ^{1}H NMR spectra of E-**25** and PSS_{365} in $CDCl_3$. Top graph: screenshots of the region of interest and the integral values taken for the determination of the photoconversion yields.*

Similar to *Z*-**24**, intramolecular glycosylation of *Z*-**25** with NIS/TfOH at 5 mM concentration led to the glycomacrocycle **31** as a mixture of *E* and *Z*-isomer in very low yield (**Scheme 44**, **Table 10**). No glycomacrocycle has been isolated under 28.6 mM concentration.

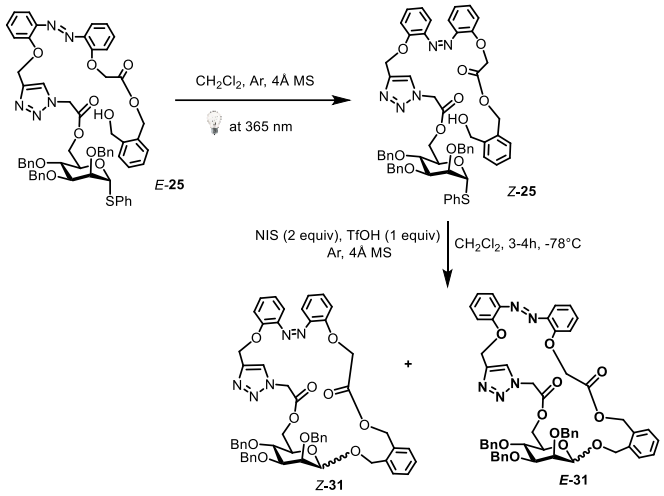

Scheme 44. *Intramolecular glycosylation of Z-**25**.*

Table 10*. Reagent and condition screen for the intramolecular glycosylation of Z-**25**.*

entry	substrate, concentration	isolated product	yield (%)
1	*Z*-**25**, 5 mM	*E and Z*-**31**	7.5
2	*Z*-**25**, 28.6 mM	-	-

4. Conclusions

In summary, through intramolecular glycosylation reaction, we have synthesized seven new azobenzene-based glycomacrocycles containing triazole-linker. The stereoselectivity of the glycosylation is dependent on the linker length, the configuration of the azobenzene template and the reaction concentration.

Starting from *E*-azobenzene glycosyl donor-acceptor pairs with free 4-OH glucosyl acceptors, the 23-membered macrocycle **20** was synthesized with an excellent α-selectivity, while a preferential *1,2-cis*-mannosylation has been achieved with the 26-membered macrocycle **21**. However, the corresponding *Z*-substrates **1** and **2** underwent the intramolecular glycosylation only under more diluted concentration, leading to the *E*-macrocycles with lower yield (for **20**) or inverted β-stereoselectivity (for **21**). Comparison of the glycosylation outcomes with both *E*- and *Z*-substrates as well as the spectroscopic investigation on the stability of *Z*-substrates in the presence of glycosylation promotors NIS/TfOH confirmed that the glycosylation occurred before the isomerization of *Z*- to *E*-macrocycles.

For azobenzene glycosyl donor-acceptor pairs bearing free 6-OH glucosyl acceptors (compounds **3** and **4**), the intramolecular glycosylation worked only with the *E*-substrates, affording 23- and 26-membered macrocycles **22** and **23** in 78% and 75% yield respectively, with excellent *β*-stereoselectivity. This last result is very interesting considering that the β-mannosylation represents still a synthetic challenge in chemical glycosylation.[119]

We have also used pentaerythritol and 1,2-phenylenedimethanol as glycosyl acceptors to realise the intramolecular glycosylation with optimized conditions and obtained the 26-membered macrocycle **30** and the 27-membered macrocycle **31** in 39% and 48% yield respectively, with excellent *β*-stereoselectivity. Reaction from the corresponding the *Z*-substrates led to less than 8% of glycomacrocycles **30** and **31** as a mixture of *Z*- and *E*-isomers.

[119] Y. Zhu, B. Yu, *Chem. Eur. J.* **2015**, *21*, 8771-8780.

Chapter III

Chapter III - PROPERTIES INVESTIGATION OF GLYCOMACROCYCLES

1. Towards new applications of photoswitchable glycomacrocycles (PGM)

As it was presented in the Chapter 1.4 (p35), the recently reported photoswitchable glycomacrocycles showed interesting properties and promising applications. To remember again, Depras *et al*. have reported several photoswitchable glycomacrocycles using *para*-*O*-substituted azobenzene showing a reversible shape switching with an influence on the chiroptical properties, thanks to a chirality transfer from the saccharide to the azobenene moiety.[96,97] In the case of a macrocycle, they have also highlighted the reversible switching of the solubility depending on the wavelength of irradiation (conversion *E/Z*).

Concomitantly, our group has reported a glycomacrocycle with a smaller ring size using *ortho*-*O*-substituted azobenzene demonstrating the multistimuli-responsive behavior capable to form organo-gel. In collaboration with Prof. Y. Kim of the University of Okaïdo, two of our molecules were employed as chiral dopants in liquid crystals and showed a reversible tuning of helical superstructure under light irradiation (Chapter, p38).[100] As part of this thesis, we have also demonstrated the influence of acidic conditions to influence the thermal stability of the *Z-isomer* and the possibility to generate protonated species with a red-shifted absorption (Chapiter II, 2.5, p61).

Jarosz and coworkers have published in 2021 the first photo-glycomacrocycle, using an *ortho*-*O*-substituted azobenzene, including a crown ether in the molecular structure for the cation recognition (**Figure 16** page **39**, and **Figure 53** page **90**).[101] However, to the best of our knowledge, the chiroptical properties associated to the complexation properties were not described.

In this chapter, we will present firstly the photophysical properties and the photoswitching ability of the synthesized PGM, presented in the previous chapter, in comparison of their analoguous GDAP. Also, a particular attention was dedicated to the thermal stability of the *Z-isomers* in different solvents. Obviously, depending on the targeted application, it is sometime more interesting to have a bi-stable or a meta-stable state. As example, we could imagine in the case of the photopharmacology to have a biologicaly active and meta-stable *Z-isomer* capable to return to the *E-isomer* after several hours, while it can be very interesting to have a stable *Z-isomer* with a long half life in the case of a smart material (ex: optical data storage).[120] In the next part of this chapter, we will present secondly the influence of the acidic conditions followed by the chiroptical properties. Finally, it will be presented an on-going work for the exploration of the cation complexation involving the photochemical irradiation and the influence of the pH on the chiroptical properties.

[120] S. Kawata, Y. Kawata, *Chem. Rev.* **2000**, *100*, 1777-1788.

2. Photochemical and photophysical properties of GDAP and PGM

2.1. Experimental considerations

Guided by the conditions of the glycosylation reaction, a particular experimental consideration was about the choice of dichloromethane as solvent, which is not commonly used for photochemistry. To ensure the success of the azobenzene template strategy in glycosylation reactions, some preliminary tests were conducted to characterize the photoswitching ability at different wavelengths in order to determine the best irradiations conditions (time, *E* to *Z* conversion, fatigue resistance). Another key step was the characterization of the thermal stability of *Z-isomers* of both GDAP and PGM, which is a crucial point to ensure the best accuracy in the determination of the yields obtained from the glycosylation reaction. Because we envisioned further applications, then we focused our attention on the acetonitrile which is a common solvent used in the spectroscopic studies and photochemical characterizations. Consequently, in the next sections, we presented only the final results, and the detailed procedures are described in the experimental section (page **107**).

2.2. Photoisomerization of the azobenzene derivatives

In the previous chapter (p54, 56, 58, 59, 66 and 67), through NMR experiments we have briefly presented the capability of GDAP to photo-isomerized upon light irradiation and demonstrated that the photoconversion yield is affected as a function of the molecular structure. Such observation on GDAP showed the reason why all compounds must be characterized and suggests that strong difference is waiting in their cyclic analogous, PGM.

2.2.1. Photoswitching ability

The example below presented the steady-state UV-vis absorption monitoring of a solution of pure *E*-isomer of compounds **20**α, **21**α, **21**β, **22**β and **23**β (**Figure 36**, black line) in CH_3CN. The solution was irradiated successively at different wavelengths after reaching the photostationnary state. An irradiation at 365 nm, corresponding to an excitation in the region of the π-π* band, induces a strong *E* to *Z* photoconversion (red line) observable by a decreasing of the absorption bands circa 310 nm and 360 nm. The comparison of the two spectra (*E* and PSS_{365}) also shows the presence of isosbestic points between 400-450 nm and *circa* 275 nm, and regions where *Z-isomer* has a higher absorption than *E*-isomer. These regions are more favorable to induce the *Z* to *E* photoconversion, and guide us in the choice of the next irradiation wavelengths. An irradiation at 433 nm, corresponding to an excitation in the region of the n-π* band, induces a strong *Z* to *E* photoconversion (blue line) but without a complete photoconversion into the *E*-isomer. The irradiation at 514 nm corresponds to the most red-shifted part of the spectrum. Whatever the lower absorption, this region is particularly appealing to explore for photo-irradiations because it is a less energetic region than UV; which is generally more interesting for biological applications (less invasive). In the case of this compound, this irradiation wavelength favorised the formation of *Z*-isomer with a lower conversion than the irradiation at 365 nm.

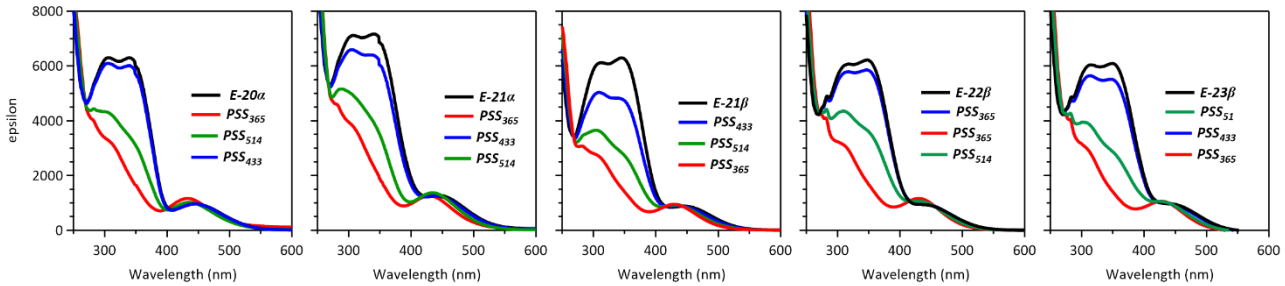

Figure 36: *Determination pf the photostationnary states for* ***PGMs*** *in CH_3CN.*

2.2.2. Photoconversion yields

The **Table 11** below reports the result of this study realized on the different GDAP and PGM in dichloromethane.

Table 11. *Photoconversion yields of GDAP and their respective PGM in CD_2Cl_2 determined by ^1H NMR at 400 MHz.*

GDAP	GDAP-1	GDAP-2		GDAP-3	GDAP-4
PSS_{365} (%Z)	93	91		90	87
PGM	***E*-20α**	***E*-21α**	***E*-21β**	***E*-22β**	***E*-23β**
PSS_{365} (%Z)	89	90	90	90	84
PSS_{433} (%Z)	17	27	29	26	28

After an isomerization at 365 nm, we observed a decrease in the photoconversion yields (***PSS_{365}***), less than 4%, for the PGMs compared to their respective GDAPs, where the lower photoconversion yields are observed for the GDAP-**4** (87%) and its respective PGM ***E-23β*** (84%). These lower photoconversion yields appear as to be a first sign of the rigidity of the PGMs.

After an isomerization at 433 nm, all PGMs show a photoconversion yield between 26% to 29%, except for the compound ***E-20α*** where the percentage of *Z*-isomer was found to be 17%. Regarding the results obtained on the molar absorption coefficient (epsilon), presented in the next section (**Table 12**, page **76**), the epsilon value of compound ***E-20α*** was found to be ≈ 13 100, versus ≈ 6 900 to 8 600 mol L^{-1} cm^{-1} for other PGMs. Similarly, this difference probably indicates a structure-property relationship explaining the difference of flexibility for the PGM ***E-20α***, in addition of a higher planarity of the azobenzene moiety.

2.2.3. Fatigue Resistance

After determining some optimal conditions in terms of time and power of irradiation for the PSS_{365} and PSS_{433}, we realized the fatigue resistance study of all the PGMs in acetonitrile. For both irradiation wavelengths, all PGMs present an excellent photostability after more than 20 irradiation cycles. We present in the **Figure 37** below the evolution absorption bands at 314 nm and 347 nm obtained with the compound ***E-23β***. The figures corresponding to other compounds are presented in experimental section (page **124**).

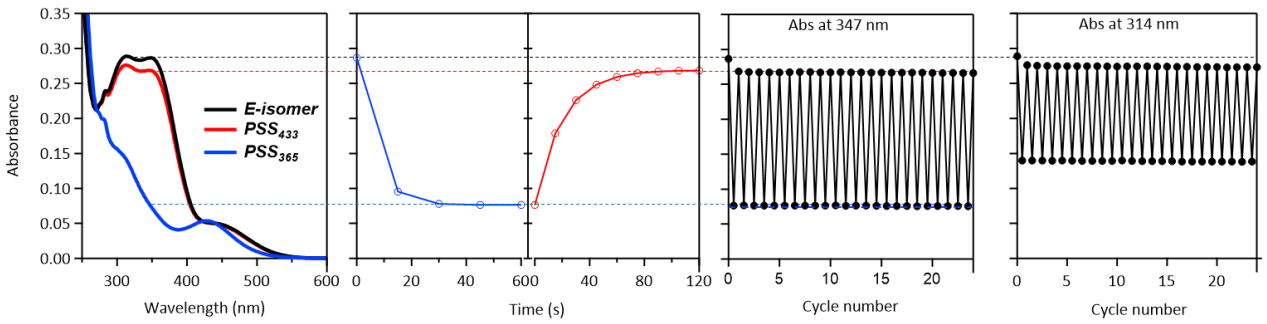

Figure 37: *Fatigue resistance followed by UV-Vis absorption. Absorption spectra (left) and under alternate 365 nm/433 nm irradiation cycles (right) in CH_3CN. Irradiation conditions: PSS_{365}, time = 40 s, power = 6.7 mW cm^{-2}; PSS_{433}, time = 40 s, power = 5.0 mW cm^{-2}.*

2.3. Photophysical Caracterisations

For GDAP **1** and PGMs **20**-**23**, we also measured the molar absorption coefficient (epsilon, ε) of a solution containing only the *E*-isomer (see experimental part for detailed procedures, page **107**). The epsilon values reported in the **Table 12** were calculated from a linear numerical adjustment for both, the maximum of wavelength and the isosbestic point. This last is justified in order to realize further normalization of absorption spectra. Because *E*- and *Z*-isomer have the same epsilon value at the isosbestic point, the normalization at this cross point will ensure the absence of error for a mixture of isomers.

Table 12: Molar absorption coefficients of *E*-GDAP and their respective *E*-PGM in CH_2Cl_2 (left column, white) and CH_3CN (right column, grey) determined by UV-vis absorption spectroscopy.

GDAP	**GDAP *E*-1**		**GDAP *E*-2**		**GDAP *E*-3**		**GDAP *E*-4**	
λ_{max}	363	-	-	-	-	-	-	-
ε (mol L^{-1} cm^{-1})	15 493	-	-	-	-	-	-	-

PGM	***E*-20α**		***E*-21α**		***E*-21β**		***E*-22β**		***E*-23β**	
λ_{max}	348	340	340	339	341	345	348	348	340	349
ε (mol L^{-1} cm^{-1})	13 109	6 244	8 266	8 667	7 436	6 286	8 561	6 885	6 954	4 878
$\lambda_{isosbestic}$	271	269	272	267	272	268	276	271	276	271
ε (mol L^{-1} cm^{-1})	6 826	4 664	6 274	5 404	4 744	3 451	5 631	4 247	5 484	3 347

The **Table 12** shows that only a small variation of the maximum of wavelength was observed whatever the solvent (< 9 nm). However, a possible tendency can be highlighted. As a first approximation, the tendency seems to depend on the anomeric configuration of the glycosidic linkage. More precisely, in the case of PGM-α, the λ_{max} is higher in dichloromethane than in acetonitrile, while for the PGM-β the λ_{max} is lower or equal.

These observations, based only on few examples, can be a starting point for the evidence of the structure-property relationships. Consequently, we decided to plot the comparison of the normalized absorption spectra of *E*-isomers (epsilon scale), which offers another possibility to compare the different PGM to a model compounds as function of the solvent.

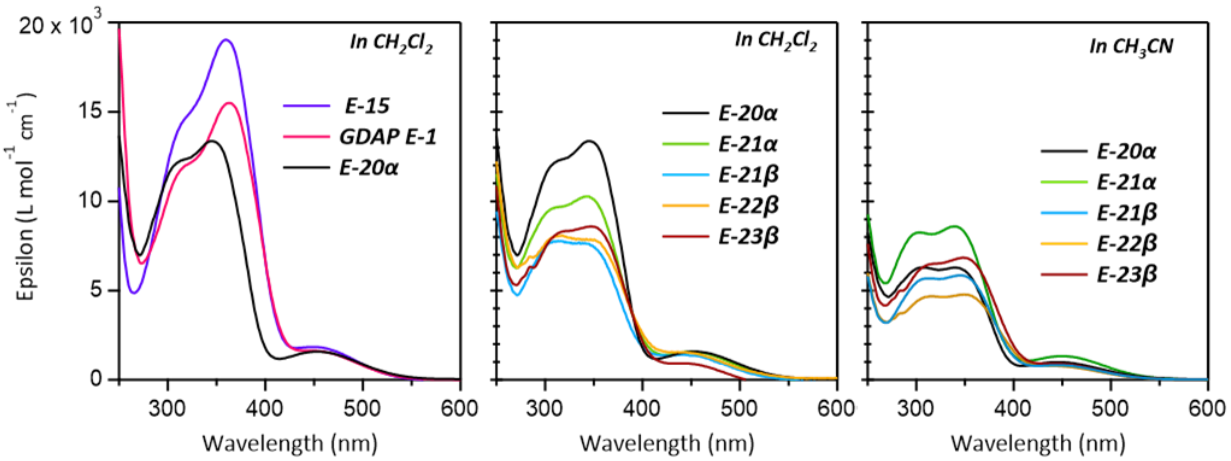

Figure 38: Comparison of the normalized absorption spectra (epsilon scale) in CH_2Cl_2 and CH_3CN.

The left graph of **Figure 38** give a comparison of the normalized absorption spectra in dichloromethane of macrocycle ***E-20α*** with its corresponding GDAP (**GDAP *E*-1**) and the azobenzene-linked glycosyl acceptor *E*-**15** (see structure at p48). This last shows the highest epsilon with a strong difference (≈ 4500 L mol^{-1} cm^{-1}) for the intensity of the bands at 359 nm (19028 L mol^{-1} cm^{-1}) and 315 nm (14422 L mol^{-1} cm^{-1}). Compared to *E*-**15**, the **GDAP *E*-1** presents a higher steric hindrance which can explain the loss in absorbance (15493 L mol^{-1} cm^{-1} at 363 nm and 11949 L mol^{-1} cm^{-1} at 317 nm).

Concerning the comparison with the PGM ***E-20α,*** we observed a weaker absorbance than **GDAP *E*-1** accompanied of a blue shift of the maximum of wavelengths. This observation can be explained by the torsion the *E*-azobenzene, meaning the loss of planarity, which is due to the macrocycle constraints that induce a decrease of the bands intensity. Another proof of this torsion is given by the blue-shift such as in the corresponding *Z*-isomer.

The comparison of PGM in different solvents brings less obvious conclusions. However, as general observation, for all PGMs in acetonitrile, the absorbance *circa* 350 nm is weaker than in dichloromethane. Beyond this observation several hypotheses can be formulated:

- Is there a relationship between the solvent and the constraints in the macrocycle, and showing probable variations in the absorption spectra?
- Is there an impact on the thermal stability of the *Z*-isomers?

The next sections of this chapter are partly dedicated to answer these hypotheses.

2.4. Thermal stability of the *Z*-isomers

The thermal stability of *Z*-isomer, also called half-live ($t_{1/2}$), can be determined through different methods such as NMR or an UV-Vis absorption monitoring as a function of the time. Because the azobenzene is a chromophore, and due to the small amount required, we choose here the UV-Vis absorption monitoring.

In addition, the thermal stability is dependent of the temperature of the system. In other terms, the *Z* to *E* conversion (reaction) is driven by the Arrhenius law. Experimentally, it is possible to calculate the $t_{1/2}$ after a simple kinetic monitoring of the absorbance of the solution at a given temperature (more details are given in experimental section, page **117**). In the case of a compound

with long half-live, where the kinetic experiment is up to 3 consecutive days of acquisition, it is often difficult to obtain a $t_{1/2}$ value with a good accuracy. In such case, it exists two possibilities. The first one consists to realize two independant kinetic measurements at two different temperatures, with a difference of minimum 20°C. From these acquisitions, it is the possible to calculate by extrapolation the half-live at the expected temperature (see **Figure 40**, page **79**). The second case (**Figure 39**), used for solvent with low boiling point or compounds sensitive to the degradation, consists to realize several independent measurements at the same temperature over a long time range (several weeks to months).

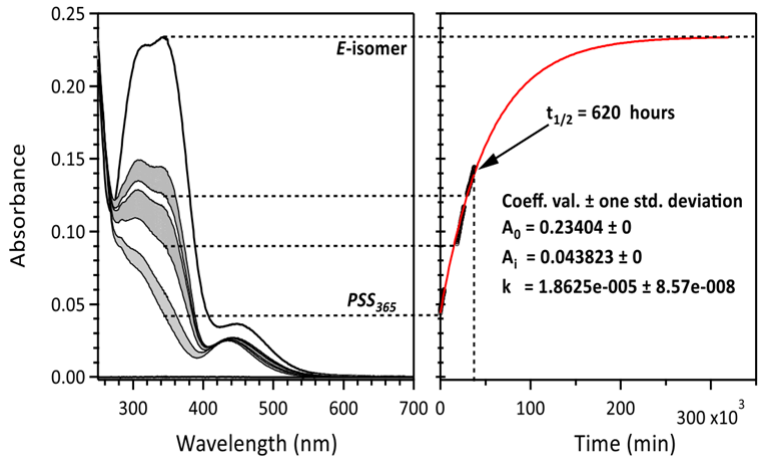

Figure 39: *UV-Vis absorption spectra (left) and thermal return monitoring (right) of* ***Z-20α*** *at 343 nm in CH_2Cl_2 room temperature (≈ 22-25°C). The reported data points are the result of a combination of 3 independent kinetic measurements realized on the same solution from the PSS_{365}: 0 to 3960 min (step = 60 min); 18495 to 26295 min (step = 120 min); 29805 to 37605 min (step = 120 min).*

The **Table 13** reports the comparison of the half-live of PGMs in acetonitrile and dichloromethane. The obtained results in dichloromethane show that the lowest half-live corresponds to the PGM *Z-**21α*** and the highest to *Z*-**20α** with the following sequence *Z*-**21α** < *Z*-**23β** < *Z-**22β*** < *Z-**21β*** < *Z-**20α***.

Table 13: *Thermal returns in dichloromethane (left column, white) and acetonitrile (righ column, grey) of Z-isomers.*

GDAP	**GDAP-1**		**GDAP-2**		**GDAP-3**		**GDAP-4**	
$t_{1/2}$ (days)	9.8	-	-	-	-	-	-	-

PGM	***Z-20α***		***Z-21α***		***Z-21β***		***Z-22β***		***Z-23β***	
$t_{1/2}$ (days)	25.8	50-74	0.5	21-51	10.5	23-45	13.9	19-34	6.9	16-29

Detailed results are presented in experimental section (see section **2.3** page **113** for CH_2Cl_2, and section **2.4** page **117** for CH_3CN).

Less obvious conclusion is possible with the obtained results in acetonitrile. The curve fitting (green color) with free parameters of the experimental data often gave an overestimated value for the absorbance of *E*-isomer at 40°C; while for the determination at 60°C, the fit converged properly whatever the fitting parameters (hold or free). These preliminary results must repeat in order to calculate the values with a better accuracy. However, the calculated half-lives at 20°C in acetonitrile are currently in a time scale from 15 to 75 days while it is from several hours to 10 days in dichloromethane.

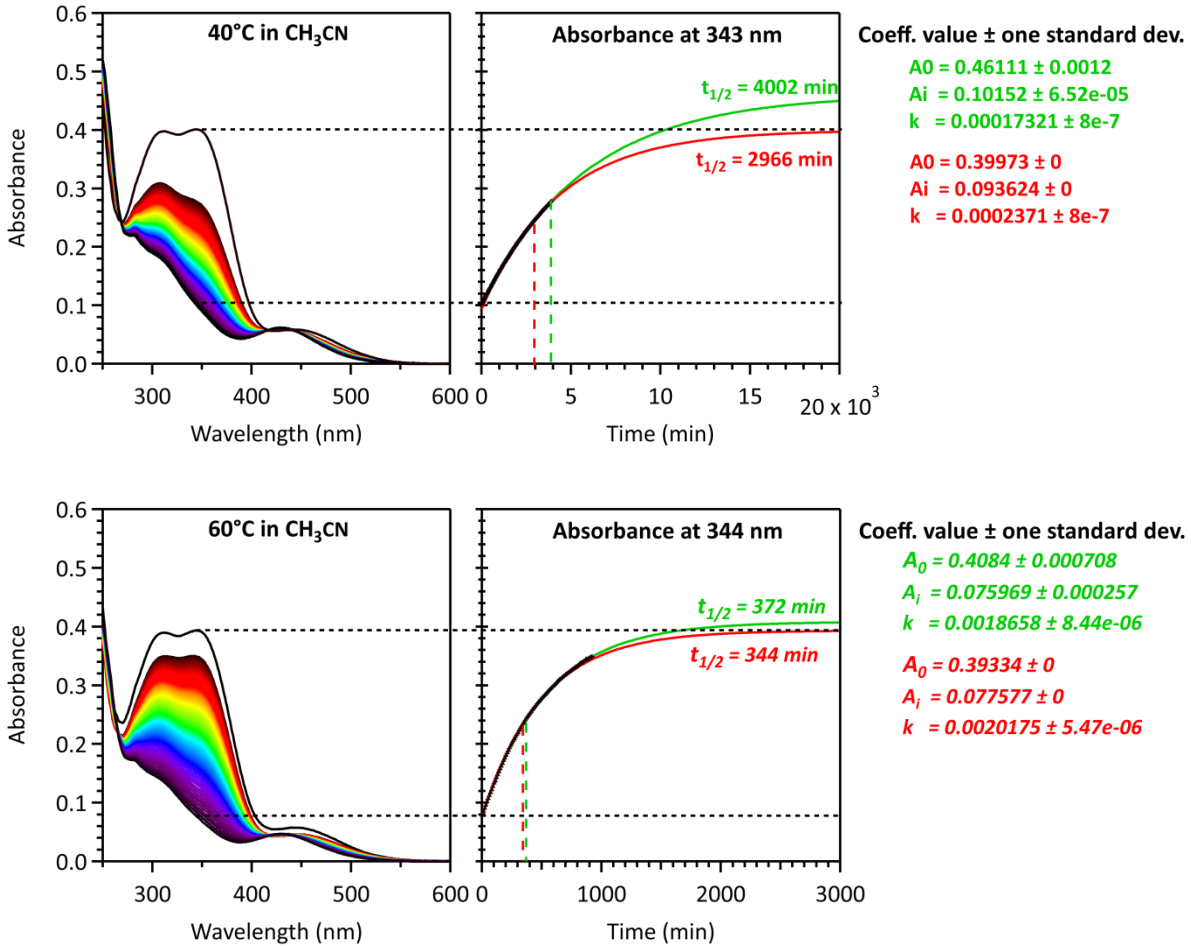

Figure 40: *Comparison of UV-Vis absorption spectra (left) and thermal return monitoring (right) of Z-**21**β in CH_3CN at 40°C (top) and at 60°C (bottom). The reported data points are the result of a single kinetic acquisition realized on the same solution from the PSS_{365}. The curve fittings are plotted in red for hold parameters, and in green for free parameters.*

2.5. Influence of pH on PGM

In the **Chapter II/2.5** (page **62**), we described the influence of TfOH in dichloromethane to investigate the mechanism of the outcome of glycosylation from *Z*-substrate. In the **Figure 30**, we demonstrated that without NIS and in presence of 2 equiv. of TfOH, compound *E*-**1** and *Z*-**1** can be protonated and conducted to the same final absorption spectrum, which corresponds to the *E*-**20α**·H^+ specie (new bands *circa* 380 and 480 nm). A similar behavior was observed on the compound **20α** on which we realized a UV-Vis absorption kinetic monitoring (***Figure 41***) after isomerization to the PSS_{365} followed by addition of 2 equiv. of TfOH. The plot of the absorption at 486 nm as function of the time showed a complete conversion ***E*-20α**·H^+ in less than 1000 minutes, with a half-live of 5.8 h for *Z*-**20α**·H^+, while the $t_{1/2}$ for *Z*-**1** is about 620 h. Consequently, the thermal *Z*→*E* isomerization can be accelerated under acid-catalysis.

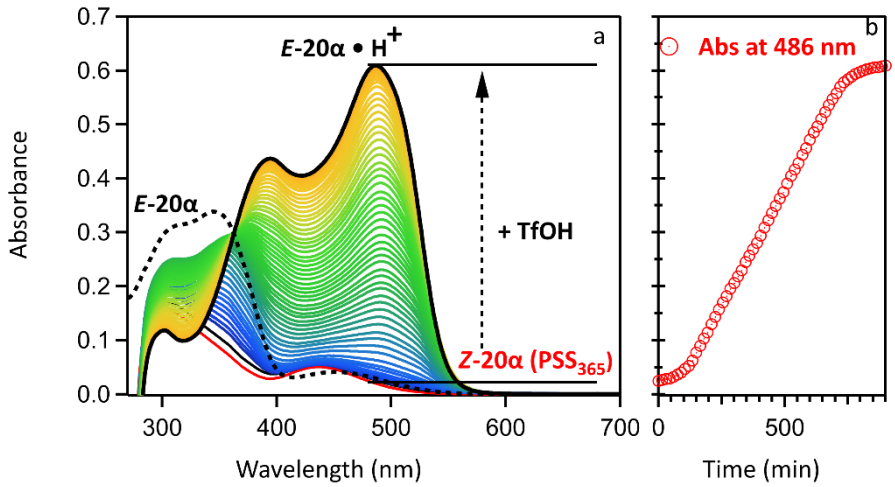

Figure 41: *(a) Absorption of E-**20**α (20 μM in CH_2Cl_2) (black line) 30 min after addition of different concentration of TfOH at rt (2.5 equiv.); (b) absorption spectra evolution of Z-**20**α (red line) after addition of 10 equiv. TfOH in CH_2Cl_2; (c) absorbance at 486 nm as a function of time. Irradiation condition at 365 nm: 6.4 mW·cm^{-2}, 120 s.*

3. Highlighting of chiroptical properties of new PGMs

3.1. Chiroptical properties and chirality transfer behavior

3.1.1. Chiroptical properties: definition and characterization methods

To give a short definition of what is *chiroptical property*, it is an optical property resulting from the interaction of a chiral molecule by the light.

The choice for the characterization method of the chiroptical property depends on the possible photophysical processes involved in the molecule in its environment. The first questioning consists in wondering whether the molecule contains a chromophore, and eventually if it is fluorescent. Thus, it then becomes possible to inform about physical parameters such as the absolute configuration or the helicity of a superstructure (ex: DNA), but also to realize the quantification of analytes like the eniantiomeric purity of a mixture. About the technics commonly used, we met different methods of polarimetry like the measurement of the specific optical rotation, the electronical circular dichroism (ECD) or the circular polarized luminescence employed for the chiral fluorophores (CPL; used for fluorescent compound). The **Figure 42** below illustrates the obtained results from the case of a chiral carbo[6]helicene submitted to these 3 methods using different type of light sources (linearly polarized, circularly polarized, non-polarized).[121]

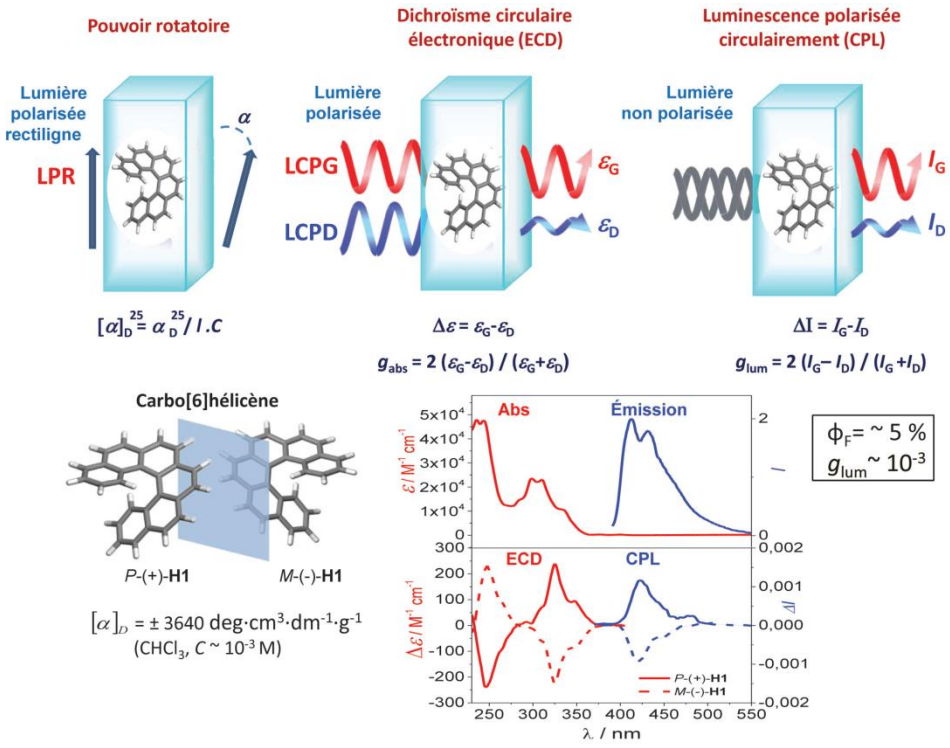

Figure 42: *Illustration of different polarimetry technics to measure chiroptical properties.*[121]

[121] J. Crassous, *L'actualité chimique* **2020**, *449*, 23-30.

3.1.2. Chirality transfer: definition and its extension to azobenzene based PGM

Chirality transfer is the phenomenon whereby an achiral species acquires some of the chiroptical properties of a chiral system.[122] This definition of the chirality transfer applied to the PGM means that the chiral system corresponds to the endo-cyclic sugar unit which transfers its chirality to the achiral endo-cyclic azobenzene unit. Consequently, the azobenzene will appear as to be a chiral entity. Similar to the helicenes, some PGMs are able to form helical structures, with sometimes they look like a Möbius strip. The helicity of the macrocyclic part of PGM can be characterized through the relative orientation of the phenyl ring of the azobenzene moiety. The **Figure 43** below presents the comparison of the helicity in a helicene structure (a) with the 2,2'-azobenzene (b).[123,124] A structure where the helicity is left-oriented will be defined as M, while a right-oriented will be a P. Thanks to the possible *E*/*Z* isomerization of the azobenzene, the level of complexity increases but offers numerous of possibilities for the design and the tuning of chiroptical properties.

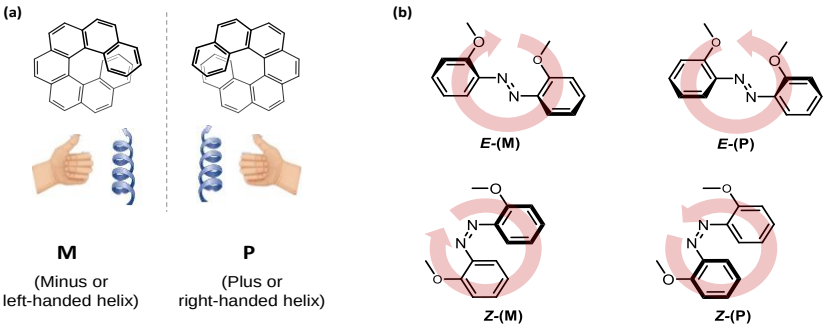

Figure 43: *Representation of helicity in helicene and o,o'-azobenzene structure to define their M and P configurations.*

[122] V. Mujica, *Nature Chem.* **2015**, *7*, 543-544.
[123] G. Haberhaeur, C. Kallweit, *Angew. Chem. Int.Ed.* **2020**, *49*, 2418-2421.
[124] K. Takaishi, M. Kawamoto, K. Tsubaki, T. Furuyama, A. Muranaka, M. Uchiyama, *Chem. Eur. J.* **2011**, *17*, 1778-1782.

3.2. Characterization of the chiroptical properties of new PGM

3.2.1. Influence of solvent on circular dichroism spectra

In order to identify the structure-property relationship between PGMs, we drawn the **Figure 44** below by superimposition of UV-Vis absorption and normalized CD (circular dichroism) spectra for both *E*- and rich *Z-isomers* (PSS_{365}) in a dichloromethane solution.

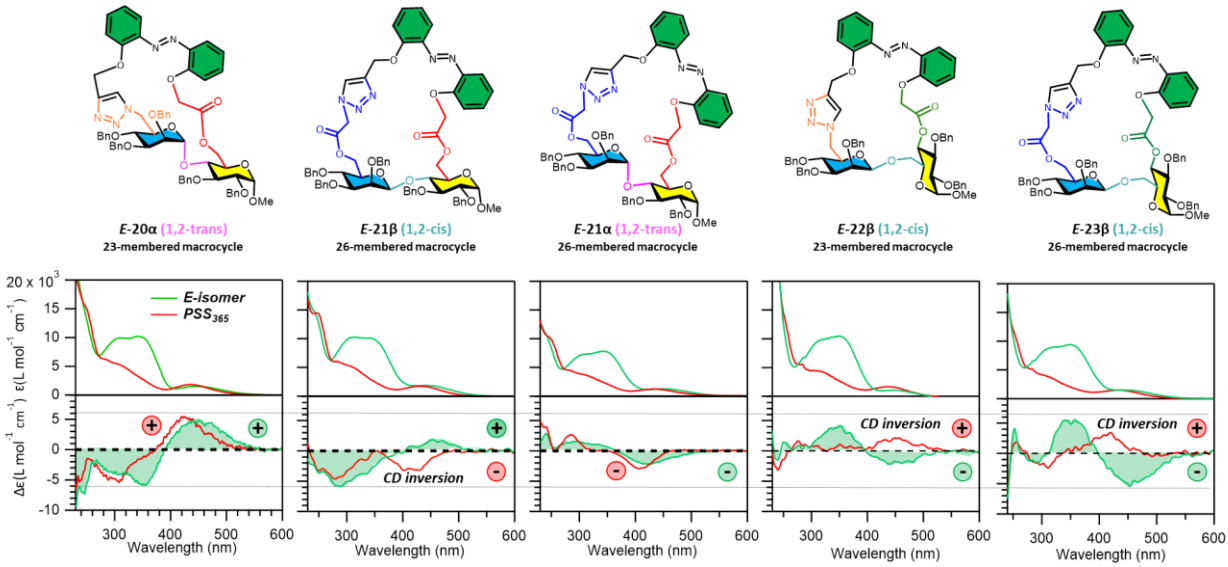

Figure 44: *UV-vis absorption and normalized CD spectra of PGMs in dichloromethane*

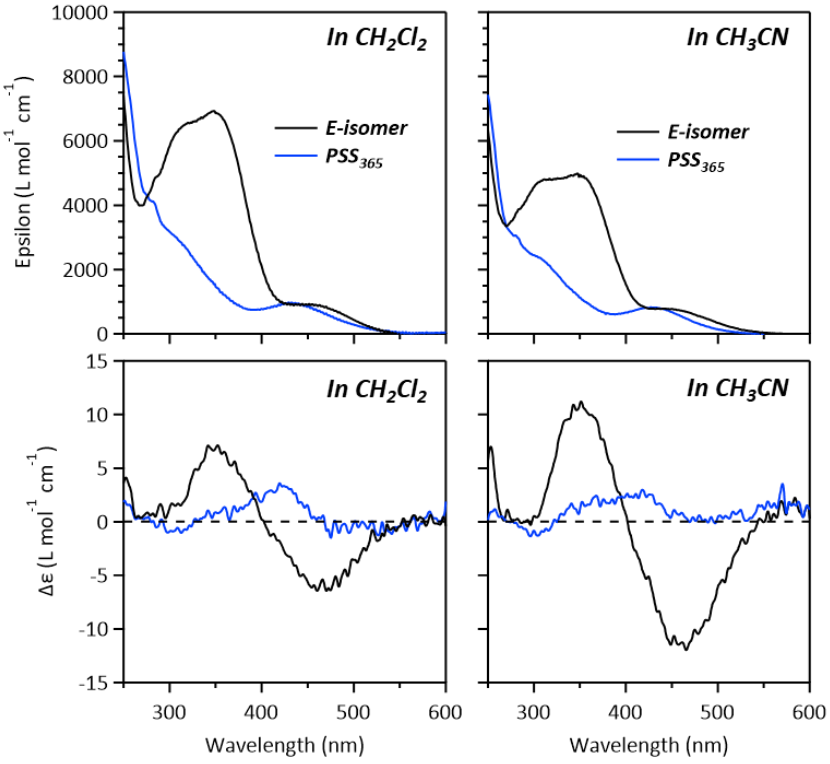

Figure 45: *UV-vis absorption and CD spectra of E-**23β** in dichloromethane and in CH_3CN ($C = 1.68x10^{-5}$ mol L^{-1}).*

For all PGMs, the CD spectra show Cotton effects, before and after irradiation at 365 nm, with maxima located at the same as the UV-Vis absorption ones. Because the free *o,o*'-azobenzene

is not chiral, this observation demonstrates the existence of a chirality transfer from the disaccharide to azobenzene moiety in the PGMs. A careful observation of CD signals highlight that compounds *E-**21α***, *E-**22β*** and *E-**23β*** showed a negative Cotton effect near 450 nm, while *E-**20α*** and *E-**21β*** show a positive one. After *E* to *Z* photoisomerization at 365 nm, we observed a blue-shift of the maxima of wavelengths for all PGMs, and only the **β**-PGMs shown an inversion of CD signal, while the sign (positive or negative) is preserved for **α**-PGMs.

For the *E-**23β***, we also try to measure UV-vis absorption and CD spectra with the same concentration of *E-**23β*** in CH_2Cl_2 and CH_3CN. From the results (**Figure 45**), the CD spectra show that the signal of *E*-**23β** is stronger in acetonitrile than in dichloromethane with the same comcentration, while for *Z*-**23β**, the signal strength is weaker in acetonitrile than that in dichloromethane.

These unexpected results recently drive us to explore more solvents in order to relied solvation parameters and chirality transfer behavior in the PGMs. In the **Figure 46** below we presented the preliminary results (non-normalized) obtained for the compound *E-**23β***. For more readability, we classified the results in 3 independent graphs: non-halogenated solvents, chlorinated solvents and fluorinated alcohol.

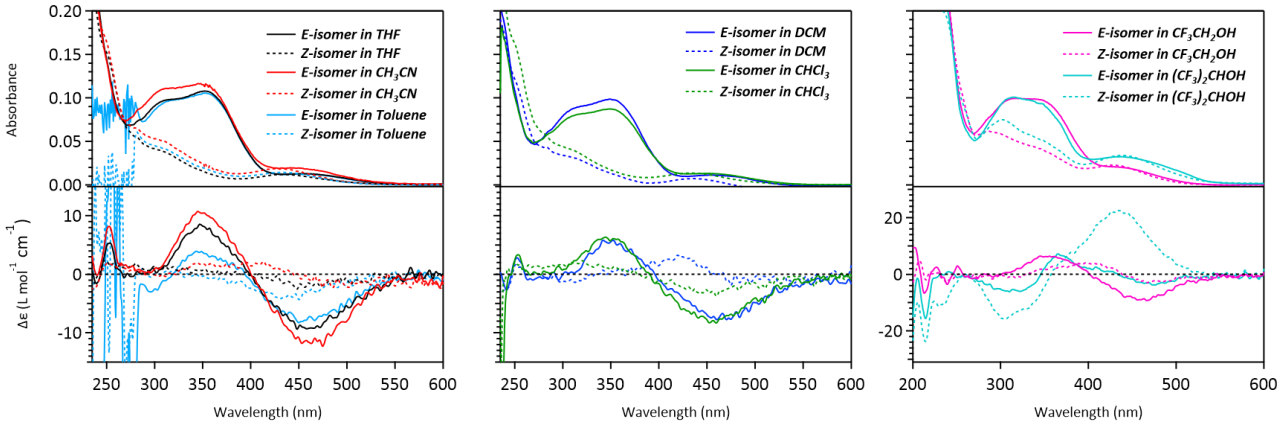

Figure 46: *UV-vis absorption and CD spectra of E-**23β** in different solvents (C = 1.68×10^{-5} mol L^{-1}).*

As first conclusion we observed that all *E*-PGMs show a negative Cotton effect where the stronger intensity corresponds to the acetonitrile, and the weaker to the HFIP (hexafluoroisopropanol). After *E* to *Z* photo-isomerization at 365 nm, inversion of CD signals was observed for acetonitrile, dichloromethane and HFIP, in the positive order of the increasing intensity. The qualitative effect on CD signals is summarized in the **Table 14** below.

Table 14: *Qualitative effect of the solvent on the Cotton effect for solution of E- and rich Z-isomer.*

Solvent	**Non-halogenated**			**Chlorinated**		**Fluorinated alcohol**	
	PhMe	**THF**	**MeCN**	**CH_2Cl_2**	**$CHCl_3$**	**TFE**	**HFIP**
PGM *E-23β***	Strong -	Strong -	Strong -	Strong -	Strong -	Weak -	Weak -
PSS_{365}	Weak -	Weak -	Weak +	Weak +	Weak -	Weak -	Strong +

In addition of these results, a careful observation of the bands in the region of 310 to 360 nm on the UV-Vis absorption spectra of *E*-isomer shows an inversion between the two maxima of π-π* bands in HFIP. In presence of fluorinated alcohol, the band intensity *circa* 350 nm diminishes relatively to the one *circa* 315 nm. Also, some differences can be observed in the spectral shape after *E* to *Z* photo-isomerization.

To explain these results, we can refer to the section **3.2.3** of this chapter (page **86**) where we present independently some results concerning the influence of TfOH on chiroptical properties. We show in this section a reversion of the CD signal after addition of TfOH which induces the protonation of the azobenzene moiety. Similarly, the results obtained with the fluorinated alcohol can be explained by their acidic behavior due to the strong electronegativity of the trifluoromethyl group(s). Consequently, this property offers the possibility to form hydrogen bonding and some complexes, and confers to these molecules a high polarity and a high solvation force. It is also well known that TFE is commonly used as co-solvent in the NMR studies of proteins, which influences strongly the tridimensional structure of proteins.[125, 126]

This recent works on with the fluorinated alcohols looks promising for our future developments and questioned about the amount required to influence the photoconversion yields or the stability of *Z*-isomer.

3.2.2. Comparison of optical activities

The analysis of the **Table 15** shows that all ***E*-GDAPs** have a positive value of specific rotation. However, strong changes are observable for PGMs before and after photoisomerization at 365 nm. Similar to the results previously presented, for all derivatives the sign for the specific rotation before and after irradiation is the same as for the Cotton effect measure by CD. We also observed an inversion of the sign for all the β-derivatives after illumination while it still preserved for *α*-PGMs. This observation seems to highlight a possible dependency of the specific rotation to the wavelength. Further experiments must be realized to confirm the hypothesis an optical rotatory dispersion (ORD) or a circular birefringence phenomenon.

Table 15: *Optical activities in dichloromethane of E-isomer of GDAPs and PGMs, and at the PSS_{365} for PGMs. $[\alpha]_D^{25}$ measured at C = 5 mg mL^{-1}, rt.*

Specific rotation					
GDAP	**GDAP-*E*1**	**GDAP- *E*2**		**GDAP- *E*3**	**GDAP- *E*4**
***E*-isomer**	+46.3	+70.9		+41.9	+129.1
PGM	***E-20α***	***E-21α***	***E-21β***	***E-22β***	***E-23β***
***E*-isomer**	+563.32	-99.6	+72.76	-162.84	-126
PSS_{365}	+427.97	-16.8	-117.84	+210.15	+54.9
Sign of Cotton effect from CD signals for PGMs					
***E*-isomer**	+	-	+	-	-
PSS_{365}	+	-	-	+	+

[125] I. Colomer, A. E. R. Chamberlain, M. B. Haughey, T. J. Donohoe, *Nat. Chem. Rev*. **2017**, *1*, 0088 (1-12).
[126] V. Pozhydaiev, M. Power, V. Gandon, J. Moran, D. Lebœuf, *Chem. Commun*. **2020**, *56*, 11548-11564.

3.2.3. Influence of TfOH on chiroptical properties

We selected the compound *E-**23β*** as candidate to realize preliminary tests to evaluate the influence of acidic species, the TfOH, on chiroptical properties. The **Figure 47** below shows that before addition of TfOH, the CD bands of *E-**23β*** located at 472 nm and 352 nm correspond respectively to a negative and a positive Cotton effect. After a successive addition of a solution of TfOH in dichloromethane (0 to 1.2 equiv.), we observed a decrease in the intensity of the two bands and the appearance of a new red-shifted band *circa* 493 nm with positive Cotton effect accompanied by an isosbestic point at 400 nm. This new band, corresponding to the nitrogen atom protonation of the azobenzene moiety, suggests an inversion on the helicity in the macrocyclic ring.

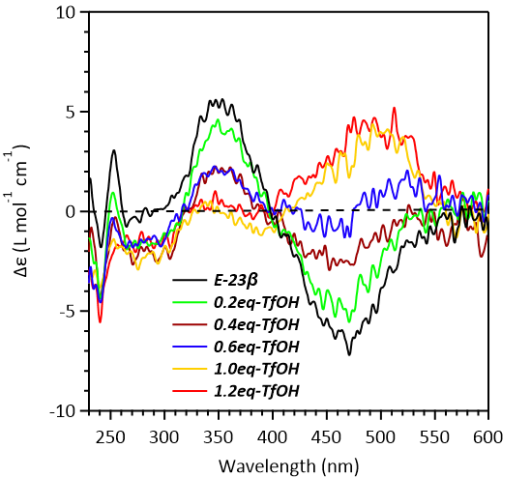

Figure 47: *Evolution of the CD spectra of E-**23β** in dichloromethane as function of the number of equiv. of TfOH* (C = 1.68×10^{-5} mol·L^{-1}).

To go further this promising preliminary characterization, we then decided to evaluate the possibility to recover the initial signal in both acetonitrile and dichloromethane. Firstly, the **Figure 48** shows that the inversion of Cotton effect also occurs in acetonitrile with a higher influence of the *"acidochromism*" than in dichloromethane ($\Delta\lambda_{max}$ = 35 nm in CH_2Cl_2 vs 50 nm in CH_3CN). In addition, the difference in amplitude shows a higher absolute value for the acetonitrile (-12 to +8 for CH_3CN *vs* -8 to +4 in CH_2Cl_2).

Secondly, after addition of an excess of trimethylamine in the solution, we observed the complete recovery of the initial CD signal (red spectrum).

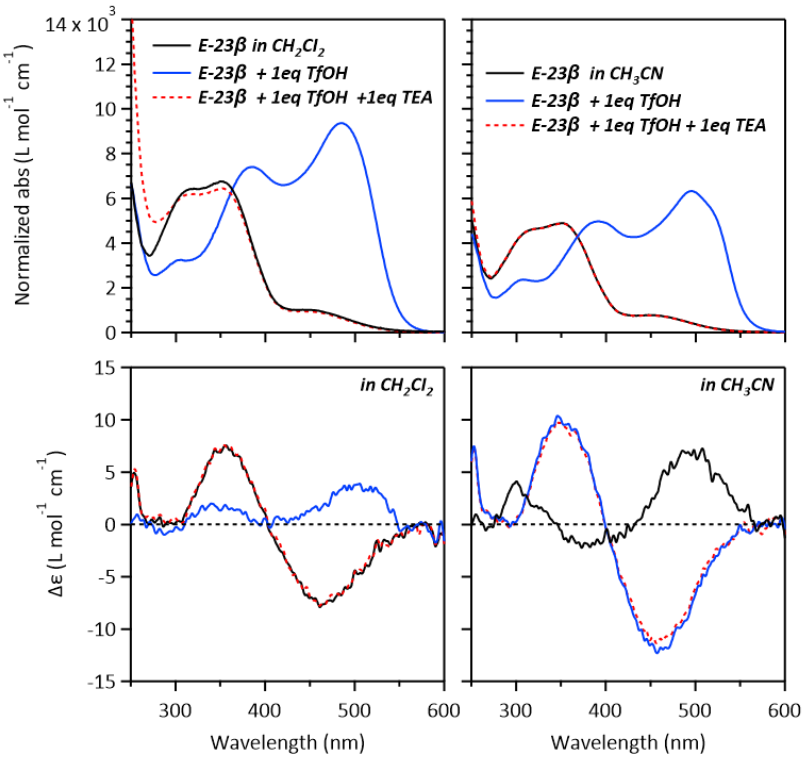

Figure 48: *Normalized UV-vis absorption and CD spectra of E-**23β**, [E-**23β**+1.0 equiv. TfOH] and the [E-**23**β+1.0 equiv. TfOH]+1.0 equiv. TEA in CH_2Cl_2 or CH_3CN (C = 1.68×10^{-5} mol·L^{-1}).*

These preliminary results need further investigations for a complete study of properties and the performances of the system. As suggestion of additional experiments, we propose to conduct the addition of TfOH in a solution realized in HFIP where we previously observed a positive Cotton effect of *E*-isomer. In such conditions, does the CD signal will reverse?

Also, the photoswitching ability could be tested at different PSS in different conditions (TfOH vs neutralized), similarly to the previously presented results in the different sections. These results could inform about the possible helicity inversion on the protonated *Z*-isomer.

4. Influence of ion complexation on the chiroptical properties of a PGM

4.1. A rapid overview from the recent literature

Molecular photoswitches, implied photochromic units, are widely described in the scientific literature.[127] Inside this impotant category of molecules, we can meet some photoswitchable cation chemosensors, [128] cyclometalated complexes, [129, 130] etc. Because we focus our interest on macrocyclic compounds containing azobenzene as photoswitchable unit, an examination of the litterature highlight also the importance of this class of molecules, where the sugar-based macrocyclic azobenzene compounds represent only few examples since their first publication in 2017. In this section, we would like to put forward our strategy consisting to valorize our new sugar-based macrocyclic azobenzene derivatives, the PGM, in cation complexation and the influence on their chiroptical properties which is underexplored to date.

A bibliographic research through Web of Knowledge database and focussed on the keywords association of "complexation"-and-"azobenzene" furnish 369 publications for the period 1982-2022 (research date: 1st july 2022). The chart below (**Figure 49**) also demonstrates the growing interest for the field.

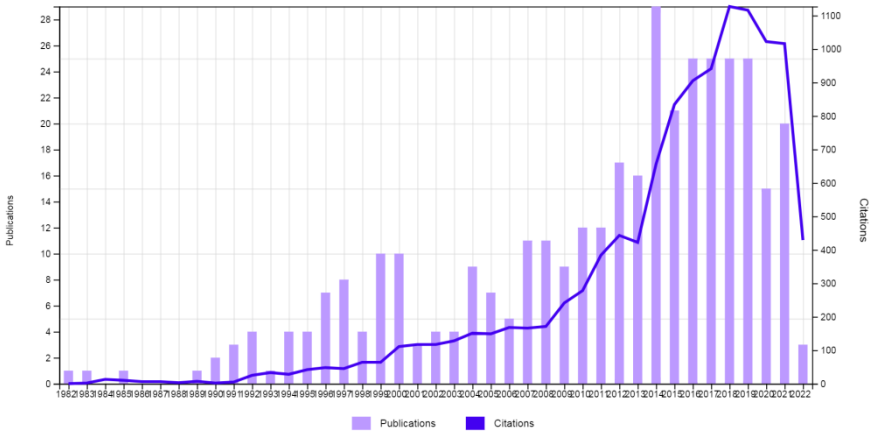

Figure 49: *Chronological evolution of the publications (purple bar) and citations (blue line) containing the keywords association "complexation"-and-"azobenzene".*

Another chart (**Figure 50**), obtained from the keywords association "chiroptical"-and-"azobenzene" furnishs 202 publications as result. The number of publications reaches a plateau since the year 2006 but the citations number shows a regain of interest since 2016, probably due to the Nobel price awarded for the molecular machines which included the molecular photoswitches developped by B. L. Feringa and his collaborators (*Chiroptical molecular switches*).[131]

[127] M. Natali, S. Giordani, *Chem. Soc. Rev.* **2012**, *41*, 4010-4029.
[128] C. Yue, C. Liao, Z. Yang, F. Hu, *Curr. Org. Chem.* **2018**, *22*, 1458-1467.
[129] J. Pérez-Miqueo, A. Altube, E. García-Lecina, A. Tron, N. D. McClenaghanc, Z. Freixa, *Dalton Trans.* **2016**, *45*, 13726-13741
[130] E. Wagner-Wysiecka, N. Łukasik, J.-F. Biernat, E. Luboch, *J. Inclusion Phenomena Macrocyclic Chem.* **2018**, *90*, 189-257.
[131] B. L. Feringa, R. A. van Delden, N. Koumura, E. M. Geertsema, *Chem. Rev.* **2000**, *100*, 1789-1816.

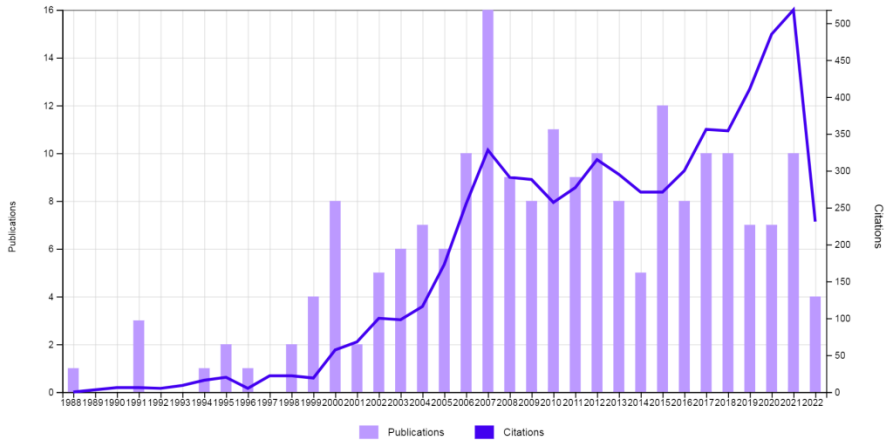

Figure 50: Chronological evolution of the publications (purple bar) and citations (blue line) containing the keywords association "chiroptical"-and-"azobenzene".

In 2021, an example of a chiral macrocycle containing an azobenzene has been reported as a phase transfer catalyst (PTC).[132] In this article, the aim is oriented on the impact of the modification of the crown ether shape induced by the *E*/*Z* photoisomerization of the azobenzene. The *Z*-isomer appears as the active form of the catalyst and promoted the enantioselective alkylation of the glycine Schiff base to obtain chiral amino acids compounds (**Figure 51**).

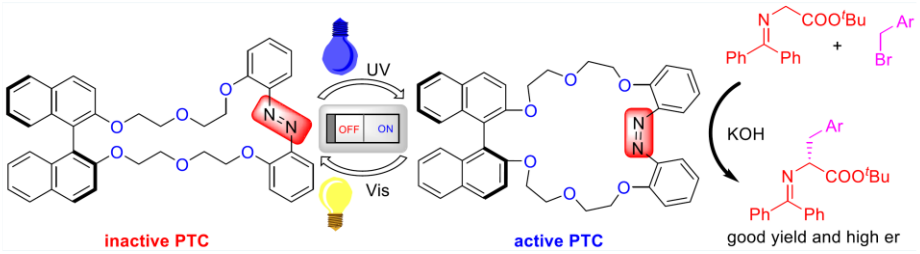

Figure 51 : Simplified representation of the mechanism of the photoresponsive phase transfer catalyst published by M. Kondo *et al.*[132]

Recently, a second example of an asymmetric chiral azobenzene was published by Japanese groups and claimed the photomodulation of cation-binding modes in catalytic asymmetric aminal synthesis (**Figure 52**).[133]

Despite that this article does not deal with a macrocyclic structure, however it illustrates the possibilities of photoswitching applications using the cation complexation and the impact of an *E*/*Z* photoisomerization of azobenzene. The *E*-isomer which does not chelate the ion is less active for the enantioselective Mannich-type reaction of α-amidosulfone. After photoisomerisation, the ion (K^+ or Cs^+) is chelated by oxygen atoms and form the active catalyst.

[132] M. Kondo, K. Nakamura, C. G. Krishnan, S. Takizawa, T. Abe, H. Sasai, *ACS Catal.* **2021**, *11*, 1863-1867.
[133] C. G. Krishnan, M. Kondo, K. Nakamura, H. Sasai, S. Takizawa, *Org. Lett.* **2022**, *24*, 2670-2674.

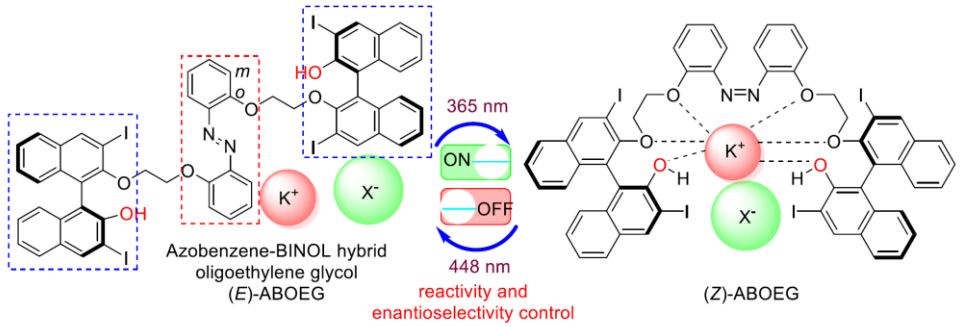

Figure 52 : *Simplified representation of the mechanism of the photoresponsive catalyst for the enantioselective Mannich-type reaction of α-amidosulfone.*[133]

S. Jarosz *and coll.* have also published recently the synthesis of a photoswitchable glycomacrocycle through a Cs_2CO_3-templated macrocyclization *via* an *O*-alkylation, and proposed a mechanism where the azobenzene is implicated in the metal coordination. To go further in the understanding, by UV-Vis absorption they realized, for both *E*- and *Z*-isomer, the determination of the association constant with different alkali metal triflates (Li^+, Na^+, K^+, Cs^+). They found the highest K_{cis}/K_{trans} for the Cs^+ in acetonitrile.[101]

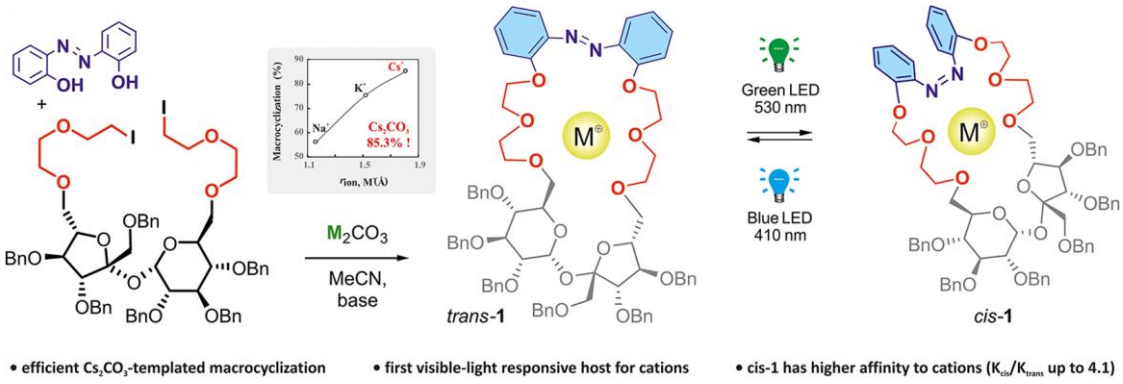

Figure 53 : *Photoswitchable glycomacrocycle developed by S. Jarosz and coll.*[101]

4.2. Screening of cations complexation with PGM 23β

4.2.1. Experimental considerations

For the complexation studies, we chose as first candidate the compound ***E*-23β** for its strong inversion of CD signal in CH_3CN. In addition, acetonitrile is a commonly used solvent for the cation complexation studies and is easier than dichloromethane to carry out such type of experiments.

For the preliminary tests of selectivity (**Figure 54**) we choose transition metal and a lanthanide due to the large cavity of the ring size of the macrocycle and its contained heteroelements (O and N).

Based on the experience in the group, we realized the selectivity test by addition of 50 equiv. of a metal ion solution to the ligand. Such amount is generally enough to form rapidly a complex with a significant impact on UV-Vis absorption spectra.

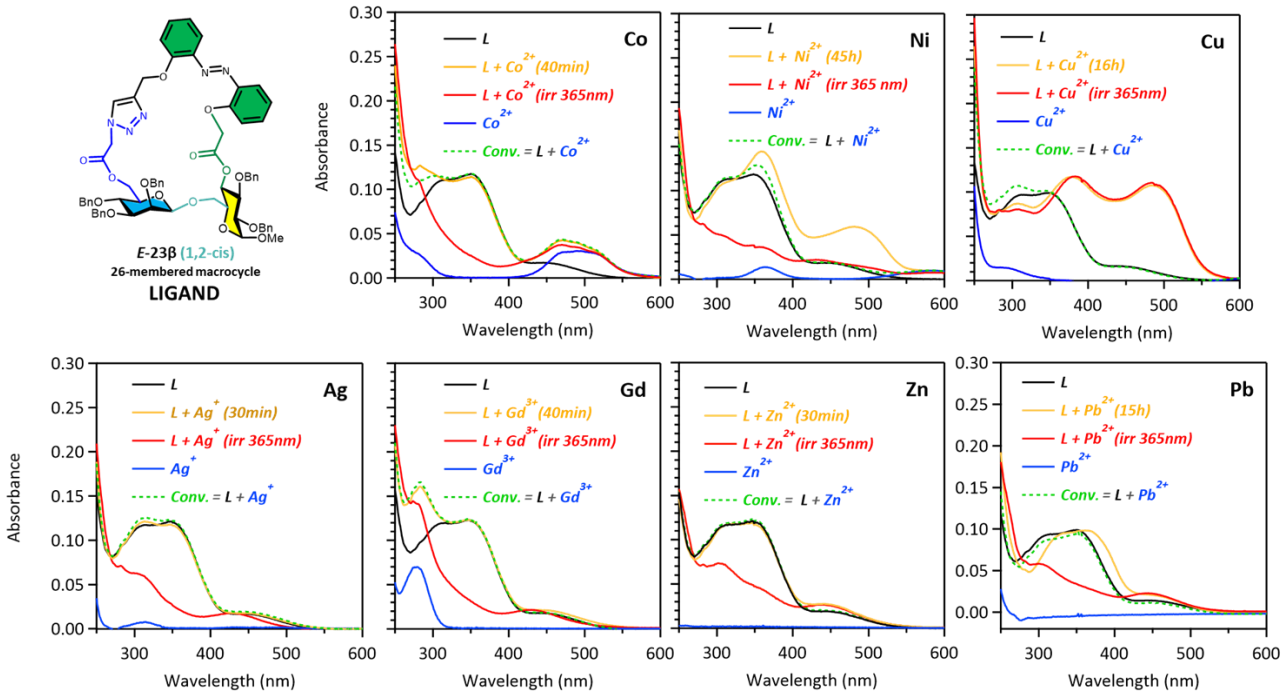

Figure 54: *UV-Vis absorption spectra of the ligand **E-23β** (**L**, **black spectrum**) in presence of 50 equiv. of cation in CH_3CN before (**orange spectrum**) and after irradiation at 365 nm (**red spectrum**), the solution with 50 equiv. of free metal cation (**blue spectrum**), and the convolved spectrum of ligand with the solution of free metal cation (**Conv.**, **green spectrum**).*

The **Figure 54** presents the absorption spectra in acetonitrile of the ligand ***E*-23β** (**black line**) and after addition of 50 equiv. of cation to the solution (**orange line**). Because some cations form colored species in solution, we also measured for each cation a solution containing 50 equiv. of cation without the ligand at the same final concentration (**blue line**). After that, it was possible to plot the calculated spectrum (**dash green line**) corresponding to the sum of the spectrum of the ligand alone in solution with the 50 equiv. of cation alone in solution. In absence of complexation, the calculated spectrum and the experimental spectrum must be superimposed. In case of complexation, we expect significant differences in the absorption bands with a possible presence of isosbestic points. The photoswitchability was also tested on the solution of ligand containing 50 equiv. of cation (**red line**).

4.2.2. Influence of cation on *E*-23β ligand

As results, we observed for the Ag^+, Gd^{3+} and Zn^{2+} cations there is no significant difference between the calculated spectra (**dash green**) and *E*-isomer in presence of 50 equiv. of cation, which indicate the absence of complexation with the ligand in these conditions.

For Ni^{2+} and Cu^{2+}, we observed an important increase of the absorption bands for the spectrum corresponding to the addition of 50 equiv. of cation (**orange**) and the formation of new bands in the visible region (and NIR for Cu) indicating the possible formation of colored complexes.

Concerning the Co^{2+} and the Pb^{2+} cations, they correspond to intermediate cases with only weak changes. In case of addition of Co^{2+} a weak increase of the absorbance below 300 nm is observable. For Pb^{2+}, we observed a red-shift of the absorption bands *circa* 350 nm while *circa* 460

nm we observe only an increase of the absorption without spectral shift. These results indicate a probable weak complexation with the *E*-isomer ligand.

During the screening tests, we observed in these conditions some fluctuations in the absorption spectra indicating a possible influence of the complexation time. To verify this hypothesis, we monitored by absorption kinetic measurement the evolution after addition of 50 equiv. of cation (Co, Ni, Cu, Pb). After that, we reported in the graphs an indicative time where no more significant change was observed in the absorbance evolution. The longer observed time periods correspond to the Cu^{2+} and Ni^{2+} with 16h and 42h, respectively.

4.2.3. Influence of light irradiation before and after addition of cations

For all tested cations, photoswitching is possible after addition of cation to the *E*-isomer solution (**Figure 54**). By comparison with the free *Z*-ligand (rich *Z* form at PSS_{365}), we observed for some cations important differences in the absorption spectra, which indicates probably that the complexation still exists with the *Z*-isomer. In addition, we observed that after irradiation, some cations seem accelerating the thermal return process and returned to the initial state corresponding to the [*E*-isomer·M]$^{2+}$ species.

These observations questioned us about the faculty of the macrocycle to form a complex before or after irradiation and its stability against light irraidation. We consequently adopt another point of view by looking at the sequence order (**Scheme 45**): "*metal addition, then light irradiation*" (Sequence 1, **Figure 54**) or "*light irradiation, then metal addition*" (Sequence 2, **Figure 55**). The scheme presented below is a simplified representation and does not exclude the possible formation of multiple complexes.

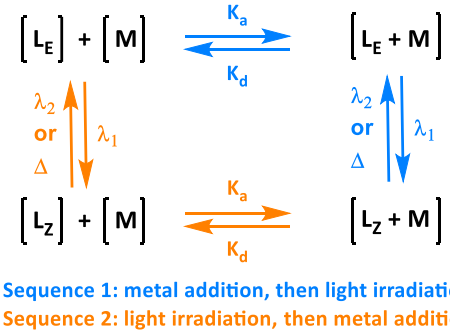

Scheme 45 : *Complexation sequence combined light irradiation.*

Our complementary experiments realized using the second sequence (**Figure 55**), where the *E*-ligand was firstly isomerized into the corresponding *Z*-ligand, followed by the addition of 50 equiv. of M^{2+}. We also observed similar behavior in results from the kinetic experiments. In comparison of the thermal return determined for the *Z*-**23β** which was estimated to be 16 to 29 days (**Table 13**) in acetonitrile, the observed time are arround 15h for Cu^{2+}, Ni^{2+} and Pb^{2+}, 72h for Co^{2+} and seems to have no effect on Ag^{+}, Gd^{3+} and Zn^{2+}. For Ag^{+} and Gd^{3+}, the changes in the absorption bands correspond to the colored complexe of the salt in solution.

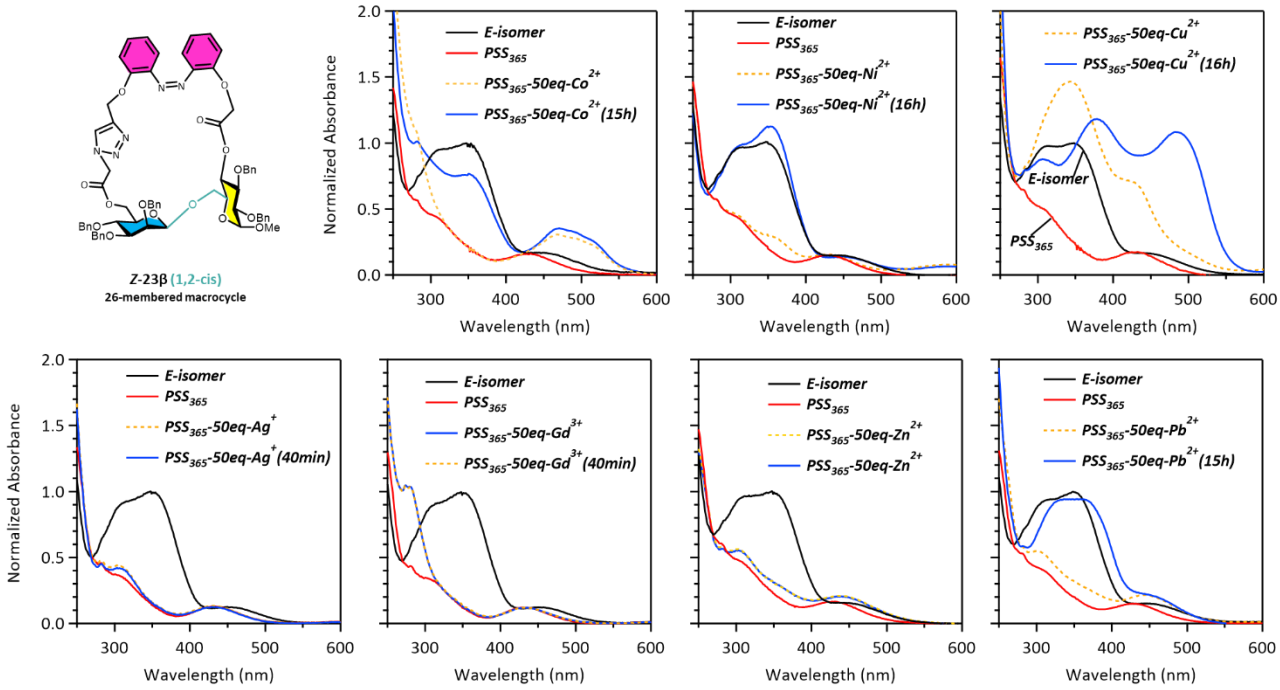

Figure 55: *absorption spectra in CH_3CN of **E-23β**, and **Z-23β** before (**PSS_{365}**) and after addition of cation (**PSS_{365}-50eq M^{2+}**).*

4.3. Impact of cation concentration on the thermal stability of *Z-23β*

Considering the results presented in the previous section, we decided to evaluate the influence of the concentration in cation on the thermal stability of the *Z*-isomer. In this section, we present the preliminary results obtained with different concentrations of Co^{2+} cation (**Figure 56**).

Experimentaly, we freshly prepared 3 solutions of *E*-isomer complexes [*E*-isomer·Co]$^{2+}$ with different concentrations of cation (5, 20, 50 equiv.), and we verified its formation by a UV-vis absorption kinetic monitoring. Then, a photoisomerization at 365 nm was realized on the solution to form the major complex [*Z*-isomer·Co]$^{2+}$. After that, the evolution of the composition was again monitored by UV-Vis absorption.

After acquisition, we plotted as function of the time the absorbance at 353 nm, where there is no absorption of colored complexe in solution. In presence of 5 equiv. of cation, the calculated half-live was found to be 332.3 h while it decreases to 12.3 h and 6.8 h, after addition of 20 and 50 equiv. respectively. The tendency describes a non-linear profile behavior.

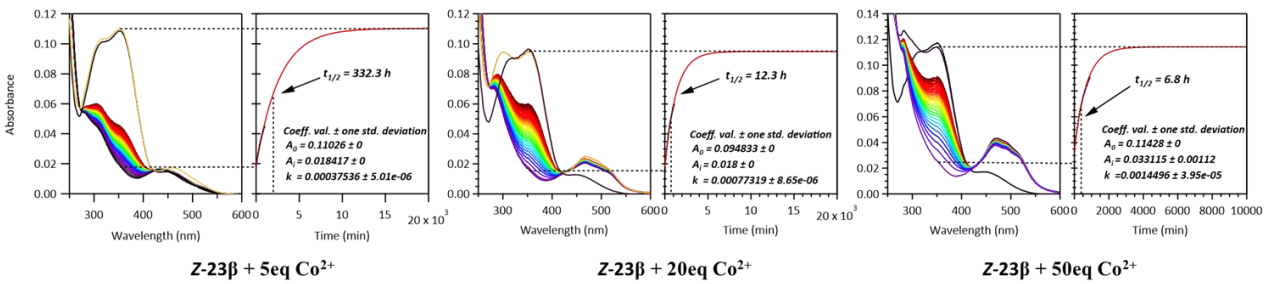

Figure 56: *Time-dependent absorption profiles of Z-**23β** (PSS_{365}) + 5, 20 and 50 equiv. at rt*

4.4. Influence of cations on photoswitching and chrioptical properties of *E-23β*

A comparison by superimposition of the spectra highlights interesting properties of the impact of the nature of the metal ion on the CD signal which is not observable in absorption (***Figure 57***).

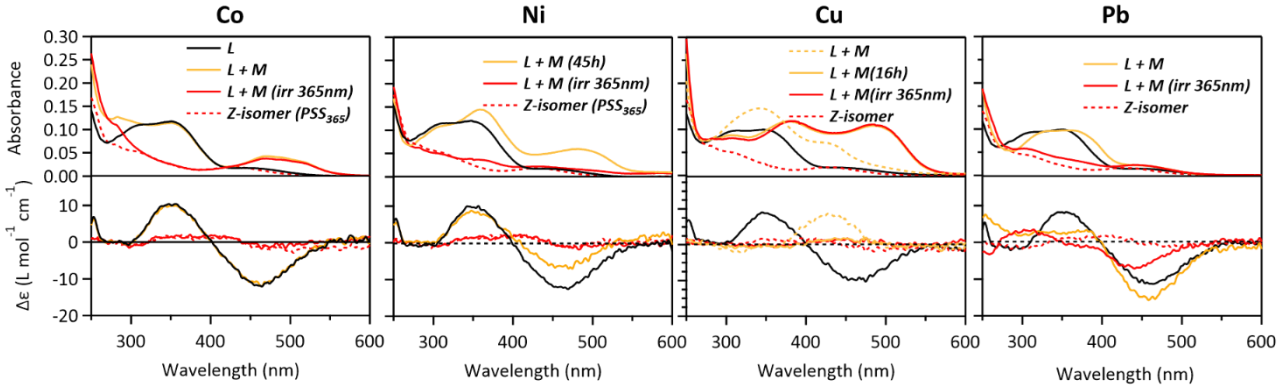

Figure 57: *UV-Vis absorption (top graph) and CD (bottom graph) spectra of Ligand* ***E-23β*** *before (**L**, **black spectrum**) and after irration at 365 nm (**red dash spectrum**). **L+M** (dash or full line **orange spectrum**): solution after addition of 50 equiv. of cation M; **L+M** (**red spectrum**): solution after addition of 50 equiv. of cation M followed by an irradiation at 365 nm.*

As a first observation on CD spectra, addition of metal to the solution of *E*-isomer shows that, complexation with Co^{2+} has no significant influences on the band located at 470 nm (overlap of spectra **L** with **L+M**). Only small changes have been observed for the Ni^{2+} (decrease of intensity of **L+M** spectrum) and Pb^{2+} (increase of intensity), while for the Cu^{2+} the CD signal becomes positive (dash line **L+M** spectrum). However, the CD signal become flat after several hours (full line **L+M** spectrum), showing a loss of the helicity in the macrocycle. Concerning the band at 330 nm, we can observe for Cu^{2+} and Pb^{2+} a decreasing of the intensity without any inversion of CD signals. After irradiation at 365 nm, the intensitiy of both CD bands diminish drastically for all cations (**red spectrum**). Also, the overlap of the CD spectra of the isomerised solution with the free *Z*-isomer (dash line **red spectrum**) shows similar behaviors in terms of loss of helicity in the macrocycle. In case of Pb^{2+}, we only observed a decrease of the intensity in addition of a blue-shift of the band *circa* 450 nm.

As a second observation, the superimposition of the CD spectra shows the presence of an isosbestic point located at 390 nm which is not observable on the UV-vis absorption spectra (**Figure 58**). Because the CD signals inform on the helicity type, this observation drives us to formulate the hypothesis that the nature of the cation can probably influence the geometry of the macrocycle with a possible inversion of the helicity.

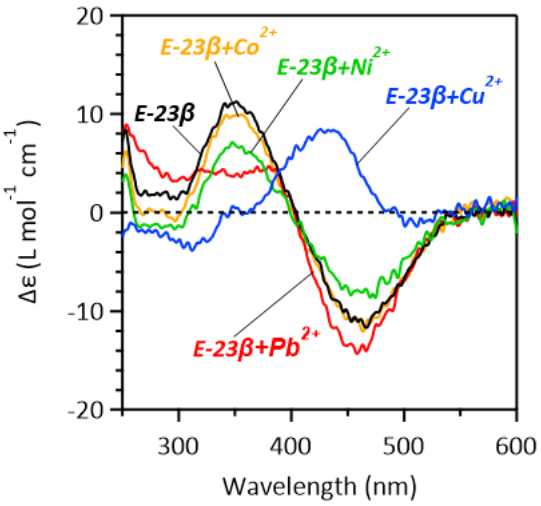

Figure 58: *Superimposition of the CD signals of E-isomer with and without 50 equiv. of different cations.*

To go further, we then decided to test the photoswitching ability and the fatigue resistance of the macrocycle in presence of the different cations.

The irradiation cycle was performed after stabilization of addition of 50 equiv. of cation to the *E*-isomer solution. The **Figure 59** shows the results in presence of Ni^{2+} cation in acetonitrile and demonstrates the excellent photostability after 10 alternate irradiation cycles at 365 nm and 433 nm. Complementary experiments in presence of other studied metals show also an excellent photostability without noticeable photodegradation (the results are not presented in this manuscript).

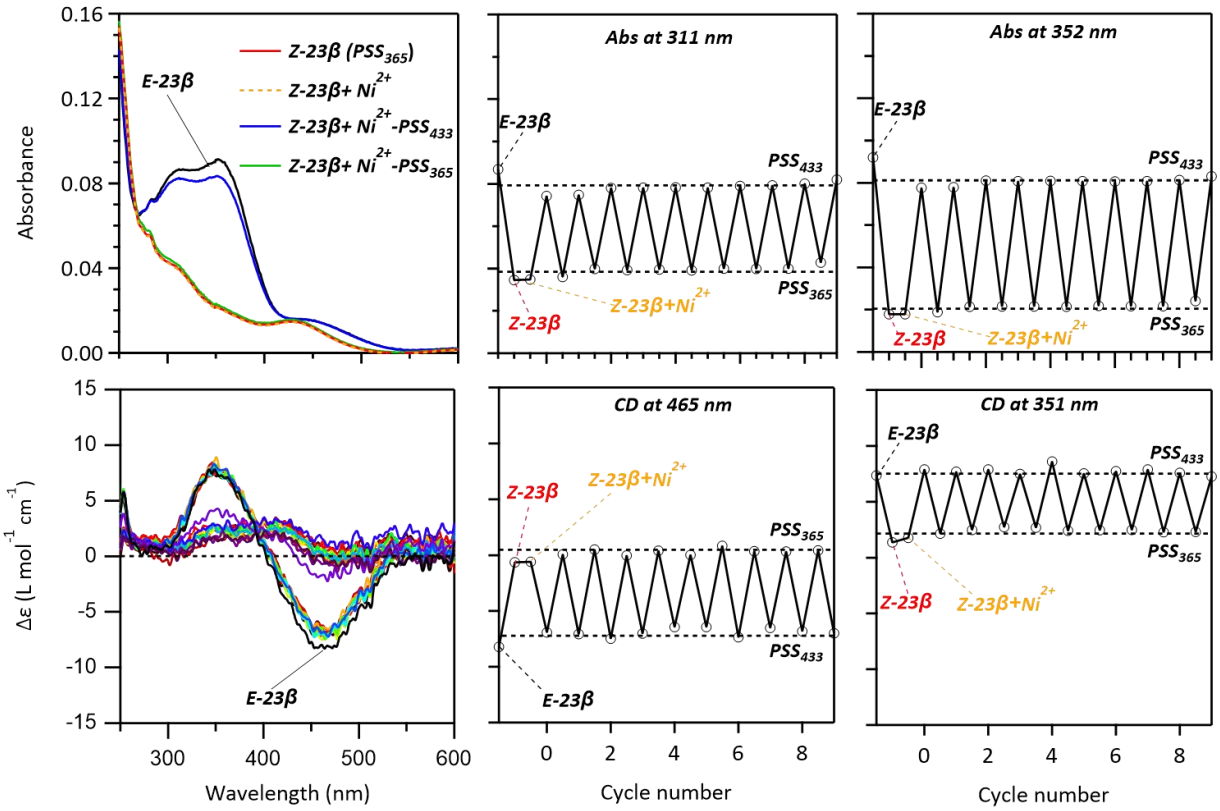

Figure 59: *Fatigue resistance of compound* ***23β*** *monitored by UV-Vis absorption (top graphs) and CD (bottom graphs) in CH_3CN. Irradiation conditions: PSS_{365}, time = 60 s, power = 6.7 mW cm^{-2}; PSS_{433}, time = 60 s, power = 5.0 mW cm^{-2}.*

5. Conclusion and perspectives

Through this chapter we firstly presented photochemical and photophysical properties of GDAPs and PGMs (epsilon, half-live of *Z*-isomers, effect of pH, photoconversion yields, and fatigue resistance). We demonstrated that photophysical and photochemical parameters can also be sensitive to solvent (dichloromethane vs acetonitrile).

To go further, we also explore the chiroptical properties and demonstrated the chiralitry transfer behavior in all PGM thanks to the observation of Cotton effects before and after irradiation at 365 nm. The careful observation of CD signals highlights that compounds ***E-21α***, ***E-22β*** and ***E-23β*** showed a negative Cotton effect, while ***E-20α*** and ***E-21β*** show a positive one. After *E* to *Z* photoisomerization at 365 nm, we observed a blue-shift of the maxima of wavelengths for all PGMs, and only the **β-PGMs** shown an inversion of CD signal, while the sign (positive or negative) is preserved for **α-PGMs**.

In addition, we also observed a possible correlation between the specific rotation and the CD signals, where the sign is kept at the observed wavelength. Further experiments should help in the possibility of an existing ORD (optical rotatory dispersion).

Unexpected promising results were also obtained on chiroptical properties thanks to the use of fluorinated alcohol such as HFIP. The use of this type of alcohol induces an inversion of the Cotton effect with enhancement of the CD signal intensity.

More particularly with the chosen compound ***E*-23α**, we then decided to explore the cation complexation behavior on chiroptical properties. The preliminary results show that Ni, Cu, Pb and Co cations are promising. These metals influence the thermal return of *Z* to *E* isomerization, and also the photoswitching ability. UV-Vis absorption and circular dichroism spectra are strongly affected by the presence of these metals, and particularly in presence of Cu, an inversion of the Cotton effect (negative to positive) has been observed.

As future developments, we can envision new experiments linking the pH dependency to cation complexation to explore the possibility of gated photochromism.

In addition, molecular modeling, such as DFT and TD-DFT, can help in the characterization of our new PGMs. Particularly, geometry optimization combined to TD-DFT results will give information about the *P* and *M* geometries and their theoretical absorption and ECD spectra. Also, cavity size and shape of *E* and *Z* isomers can be regarded for a better understanding of the cation complexation binding.

GENERAL CONCLUSION

The objectif of this thesis is to synthesize new photoswitchable glycomacrocycles and investigate their photophysical, chiroptical and complexation properties.

The first part of the work is focused on the synthesis of photoswitchable glycomacrocycles throught intramolecular glycosylation approach with azobenzene as photochromic template, and investigation of the influence of light illumination on the stereoselectivity of intramolecular glycosylation. We have decided to use the well-developed and versatile CuAAC to link together azobenzene with glycosyl donor and acceptors. As glycosyl acceptor, phenyl thiomannopyranoside is selected to investigate the outcome of the stereselectivity because the β-mannosylation represents a synthetic challenge in chemical glycosylation. *o,o*'-Dihydroxyazobenzene is chosen as the photochromic template to construct the glycosyl donor-azobenzene-acceptor pairs (GDAPs). Four GDAPs (**1**-**4**) contain a free hydroxyl group at the C-4 or C-6 position of the glucosyl acceptor have been synthesized. Starting from *E*-azobenzene glycosyl donor-acceptor pairs with free 4-OH group as glycosyl donors (**1** and **2**), the 23-membered macrocycle **20** was synthesized with an excellent α-selectivity, while a preferential *1,2-cis*-mannosylation has been achieved with the 26-membered glycomacrocycle **21**. However, the corresponding *Z*-substrates **1** and **2** underwent the intramolecular glycosylation only under more diluted concentration, leading to the *E*-macrocycles with lower yield (for **20**) or inverted β-stereoselectivity (for **21**) (**Figure 60**).

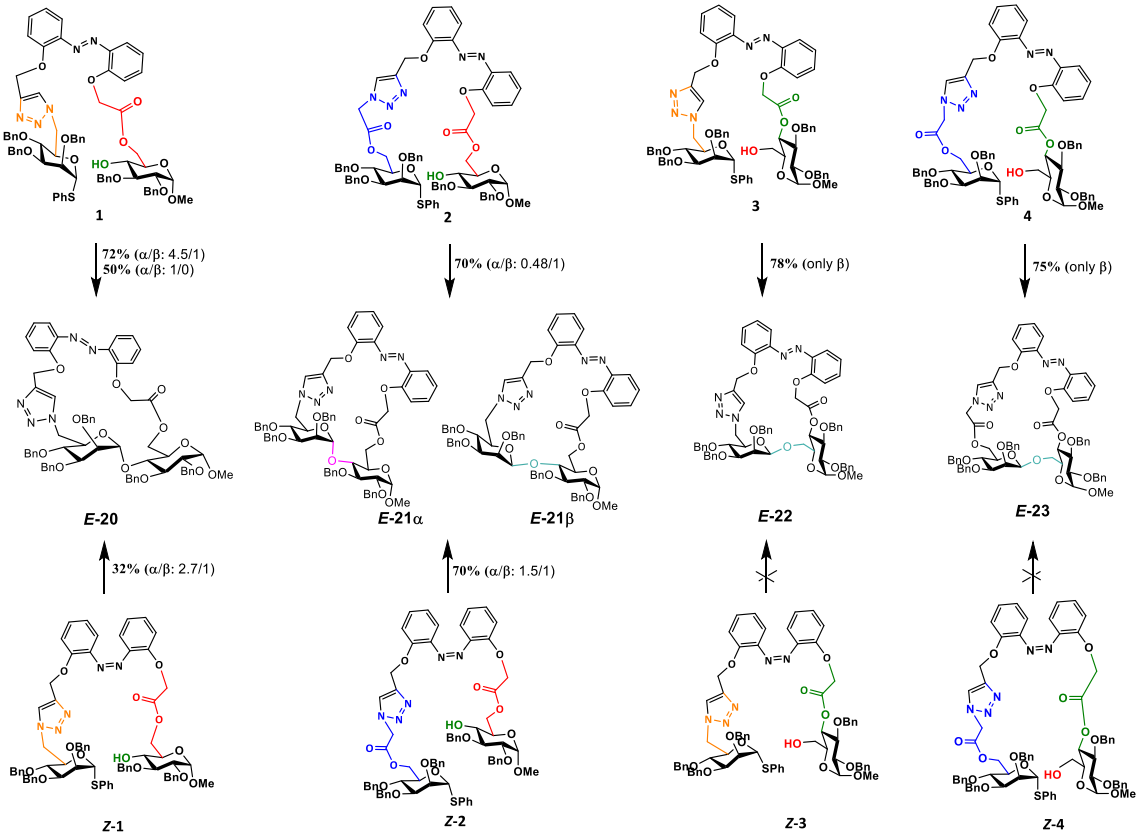

Figure 60. *Summary of results of intramolecular glycosylation from GDAPs* ***1-4****.*

To understand the formation of *E*-macrocycles from the corresponding *Z*-substrates, we have compared the glycosylation outcomes obtained from both *E*- and *Z*-substrates, and investigated by UV-vis spectroscopy the stability of *Z*-substrates in the presence of glycosylation promotors NIS/TfOH. These results confirmed that the glycosylation occurred before the isomerization of *Z*- to *E*-macrocycles. For azobenzene glycosyl donor-acceptor pairs bearing free 6-OH group (compounds **3** and **4**), the intramolecular glycosylation worked only with the *E*-substrates, affording 23- and 26-membered macrocycles **22** respectively, with excellent *β*-stereoselectivity. In summary, the stereoselectivity of the glycosylation is dependent on the linker length, the configuration of the azobenzene template and the reaction concentration.

To investigate the scope of stereoselective 1,2-*cis* mannosylation with primary alcohol, we decided to use pentaerythritol and 1,2-phenylenedimethanol as glycosyl acceptors (**Figure 61**). By employing optimized glycosylation conditions, we have obtained the 26-membered macrocycle **30** and the 27-membered macrocycle **31** in 39% and 48% yield respectively, with excellent *β*-stereoselectivity. Reaction from the corresponding the *Z*-substrates led to less than 8% of glycomacrocycles **30** and **31** as a mixture of *Z*- and *E*-isomers.

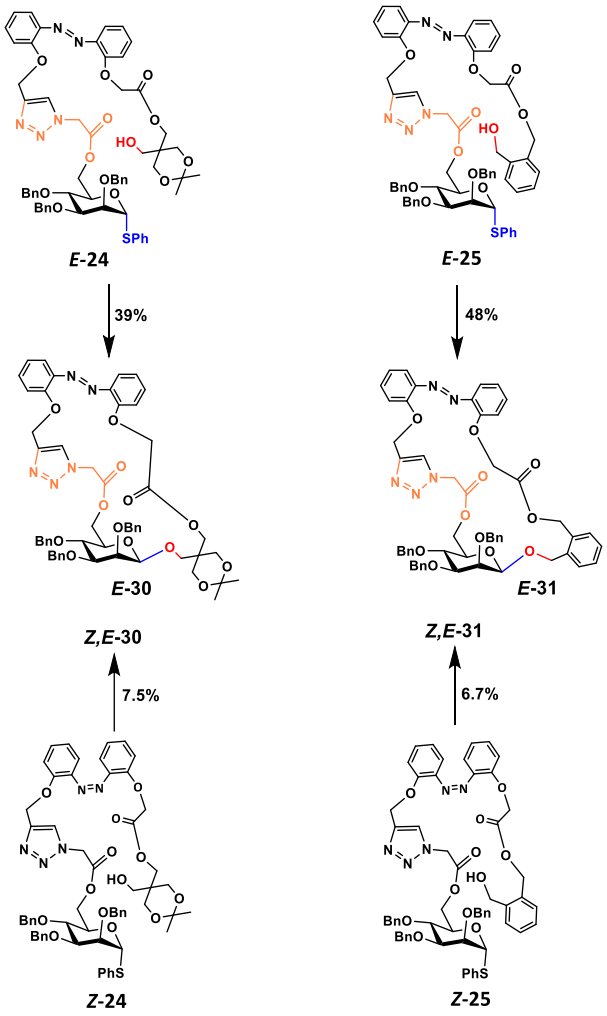

Figure 61. *Summary of results of intramolecular glycosylation from GDAPs **24-25**.*

In the second part of this thesis, we have investigated the photophysical, chiroptical properties of glycomacrocycles **20α**, **21α**, **21β**, **22β** and **23β**, and studed the influence of TfOH on the $E \leftrightarrow Z$ isomerization. The synthesized macrocycles exhibit very similar $n \rightarrow \pi^*$ and $\pi \rightarrow \pi^*$ transition bands in the absorption spectra. The $E \leftrightarrow Z$ isomerization of these macrocycles can be realized by exposing to 365 nm and 433 nm light, with high photoconvertion yield of Z/E = 89/11, 90/10, 90/10, 90/10 and 84/16 for **20**α, **21**α, **21**β, **22β** and **23β** at PSS_{365}, and E/Z = 83/17, 73/27, 71/29, 74/26, 72/28 for **20α**, **21α**, **21β**, **22β** and **23β** at PSS_{433} respectively for the back reaction under visible illumination. These glycomacrocycles also display high fatigue resistance. Besides, the half-lives of the *Z*-macrocycles are estimated to be 630 h, 12 h, 253 h, 334 h and 166 h at room temperature for **20**α, **21**α, **21β**, **22β** and **23β** respectively. Investigation of influence of protonation on the photochromic glycomacrocycles has been realized on the macrocycle *E*-**20**α, showing that addition of 2 equiv. of TfOH led to a red-shift of the absorption (λ_{max} at 396 and 485 nm). For the *Z*-**20**α, addition of 10 equiv. of TfOH converted it slowly into the *E*-**20α**·H^+ species, with a half-life of *Z*-**20**α·H^+ estimated to be 5.8 h (compared to 620 h for *Z*-**20α**). Consequently, the thermal $Z \rightarrow E$ isomerization can be accelerated under acid-catalysis.

Chirality transfer from the disaccharide to the azobenzene part was observed in all the macrocycles, The ***E*-21α**, **22β** and **23β** showed a negative Cotton effect near 450 nm, while ***E*-20α** and ***E*-21β** show a positive one. Inversion of CD signals for all β-GMs after ***E*** → ***Z*** photoisomerization has also been observed, and only the **β-PGM** shown an inversion of CD signal, while the sign (positive or negative) is preserved for **α-PGM**.

Unexpected results were being also obtained. Firstly, on chiroptical properties we observed the strong inversion of the Cotton effect in presence fluorinated alcohols. Secondly, correlation between the CD signals and the measured specific rotations demonstrates a possible optical rotatory dispersion effect.

With the macrocycle ***E*-23β**, we explored the possibility of complexation and screened several cations: Ag^+, Gd^{3+}, Ni^{2+}, Cu^{2+}, Zn^{2+}, Pb^{2+} and Co^{2+}. Our first results in acetonitrile show that Ni^{2+}, Cu^{2+}, Pb^{2+} and Co^{2+} look promising to modulate the chiroptical properties (inversion od Cotton effect). In addition, with the same cations, we observe an acceleration of the rate for the thermal back isomerization ($Z \rightarrow E$).

Experimental section

EXPERIMENTAL SECTION

1. General experimental details and apparatus

General solvents and reagents are used without further purification. The reactions carried out under anhydrous conditions are performed under argon in glassware previously dried in an oven. Tetrahydrofuran (THF), dimethylformamide (DMF), acetonitrile (MeCN) and toluene are previously dried by using a solvent purificator MBRAUN SPS-800. The dichloromethane (DCM) and acetone are previously dried over molecular sieves 4 Å, the methanol is previously dried over molecular sieves 3 Å. Reactions were monitored by TLC on Silica Gel 60F-254 plates with detection by UV (254 nm or 365 nm) or by spraying with 10% H_2SO_4 in EtOH and heating about 30 s at 400-600 °C.

Column chromatography purifications: Column chromatography purifications were performed on silica gel or with a CombiFlash® Rf+ purifier using RediSep® RF or RF Gold normal phase silica columns (with UV detection at 254 and 350 nm for all azobenzene-derivatives).

NMR spectrometry: NMR spectra were recorded by using the JEOL ECS-400 spectrometer. Irradiation frequencies of ^{1}H and ^{13}C were respectively 399.78 MHz and 100.53 MHz. The chemical shift was reported in delta (δ) parts per million (ppm) by using a reference the residual solvent signal or tetramethylsilane (TMS). The coupling constants (*J*) are given in Hertz (Hz). The followed abbreviations used are: single (s), doublet (d), triplet (t), quadruplet (q), septuplet (seven), massive (m), wide (br). The assignment was achieved by the help of 1D sequence for ^{1}H, ^{13}C, DEPT, and 2D sequences such as gCoSy and gHMQC. UDEFT sequence was used preferentially for a low concentrated sample or for molecules containing ^{13}C atoms with long relaxation delay. The mention Cq indicates the quaternary carbons. The numbering of the different atoms does not necessarily follow the nomenclature rules recommended by the IUPAC and is only used for the assignment of NMR spectra.

HRMS spectrometry: HRMS (ESI) spectrum was recorded on a Q-TOF mass spectrometer by the "Fédération de Recherche" ICOA/CBM (FR2708) platform.

Specific optical rotation measurments - $[\alpha]_D$: Optical rotation $[\alpha]_D$ was measured using a JASCO P-2000 polarimeter at 589 nm (Na light source) where no absorption occurred for all compounds, by using an 1.8 mm of aperture (S). The reported value corresponds to the average value from the acquisition of 3 iterations of 5 seconds (D.I.T.). The blank (solvent) was previously measured and automatically subtracted for each sample. A cylindrical glass cell of 100 mm path length has been used for solution measurements (model CG3-100; 5×100 mm).

The specific rotation $[\alpha]_D^T$ is based on the equation $[\alpha]_D^T = (100\times\alpha)/(l\times c)$ where $[\alpha]_D^T$ is in (deg×mL)/(g×dm), the concentration c is in mg.ml-1, and the path length l in dm.

Melting points were measured with a Köfler bench previously calibrated using the usual standard references.

UV-Vis spectroscopy: Absorption spectra were recorded on a Cary-100, or Cary-4000 or Cary-5000 spectrophotometer from Agilent Technologies. A Hellma® quartz cell of 10 mm path length has been used for solution measurements.

Photochromic reactions: Photochromic reactions were induced *in situ* by a continuous irradiation Hg/Xe lamp (Hamamatsu, LC6- or LC8-Lightningcure, 200 W) equipped with narrow band interference filters of appropriate wavelengths Semrock Hg01-364-25 for λ_{irr} = 365 nm; Semrock FF01-433/24-25 for λ_{irr} = 433 nm. The incident lamp power was measured by means of an Ophir PD300-UV photodiode. NIR contribution (P_{LP}) has been measured and subtracted from the total value using Schott long pass filters LP-545 and LP-495 nm, respectively for irradiations at 365 nm and 433 nm that is let through the Semrock filter (P_{Total}), and considering a 90% transmittance: $P_{\lambda irr} = P_{Total} - (10/9 \times P_{LP})$.

Photoconversion yields: The photoconversion yields were measured from a solution of compound in deuterated solvent and monitored by 1H NMR and UV-visible absorption, after successive irradiations at 365 nm (or 433 nm) in the case of the PSS. The *E:Z* ratios were determined by integration of characteristic band of each isomer.

CD spectroscopy: Circular dichroism spectra for solutions were performed on a Jobin Yvon CD 6 spectropolarimeter with a spectral bandwidth of 1 nm, a response time of 1 s and a scan rate of 60 nm/min. The final spectrum is obtained after the means of 2 scans subtracted from the blank (solvent) and smoothed with a binomial algorithm (smoothing = 16). A quartz cell of 10 mm path length has been used for solution measurement.

Data processing: Data processing was realized with the help of Microsoft® Excel® and Igor Pro from WaveMetrics, Inc (versions 7 to 9).

2. Photophysical characterizations

2.1. General procedure for the determination the molar absorption coefficient (ε)

A mother solution of compound was freshly prepared in dichloromethane in a precise concentration. From the mother solution, a series of 7 to 12 daughter solutions were prepared with a concentration range from 10 µM to 150 µM, and their absorbance was measured independently by UV-Vis absorption at room temperature. To ensure the reproducibility and evaluate the accuracy of the measurements, each recorded spectrum was divided by its concentration in order to obtain the corresponding normalized spectrum; only the overlapped normalized spectra are used for the determination of the molar absorption coefficient. Then, the absorption was taken at the maximum of wavelength and at the isosbestic point of each original spectrum to calculate the molar absorption coefficients by a linear regression fitting using the least squares method and with a forcing to pass through the origin of coordinates. The isosbestic point was determined after photoisomerization at 365 nm. The molar extinction coefficient determined the isosbestic point was then used for the further normalizations which let us avoid the consideration E/Z proportion in the solution.

The molar absorption coefficient is calculated according to the BEER-LAMBERT law,

$$A(\lambda) = \varepsilon(\lambda).l.C$$

with

$A(\lambda)$, represents the absorbance at the wavelength λ

$\varepsilon(\lambda)$, represents the molar absorption coefficient at the wavelength λ, in mol.L^{-1}.cm^{-1}

l, the distance of the trajectory in the media, in cm

C, the concentration of the substrate in mol·L^{-1}

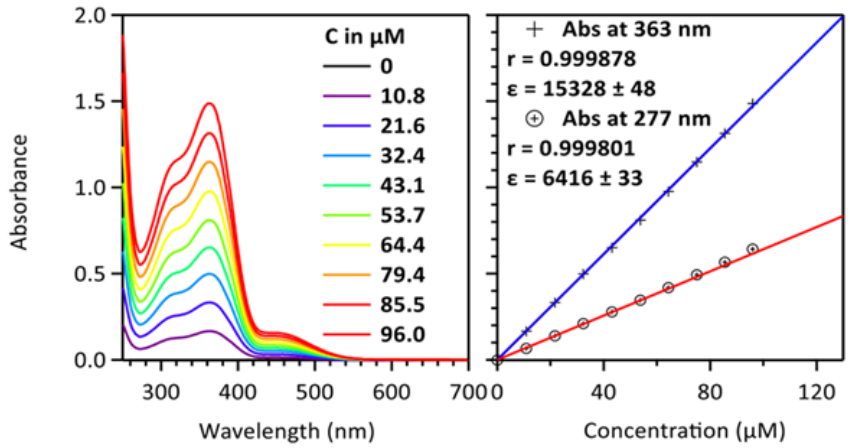

Figure 62. *UV-Vis absorption spectra of GDAP E-**1** measured in CH_2Cl_2 for the daughter solutions (left) and evolution of the absorbance (right) as function of the concentration at the maximum of wavelength (363 nm) and at the isosbestic point for the photoconversion (277 nm). Mother solution: 6.7 mg dissolved in 1000 µL of CH_2Cl_2 (C = 0.0054 mol ·L-1).*

Determination of epsilon of E-20α in CH_2Cl_2

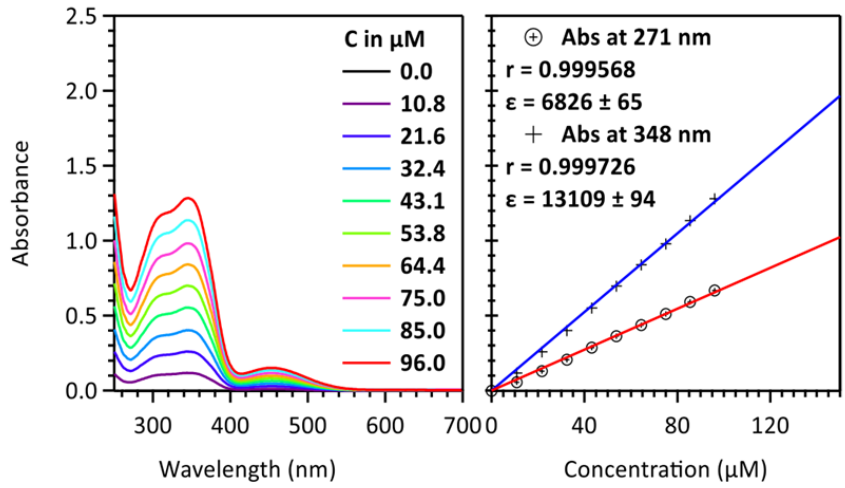

Figure 63. *UV-Vis absorption spectra of E-**20**α measured in CH_2Cl_2 for the daughter solutions (left) and evolution of the absorbance (right) as function of the concentration at the maximum of wavelength (348 nm) and at the isosbestic point (271 nm). Mother solution: 6.1 mg dissolved in 1000 µL of CH_2Cl_2 (C = 0.0054 mol L^{-1}).*

Determination of epsilon of E-21α in CH_2Cl_2

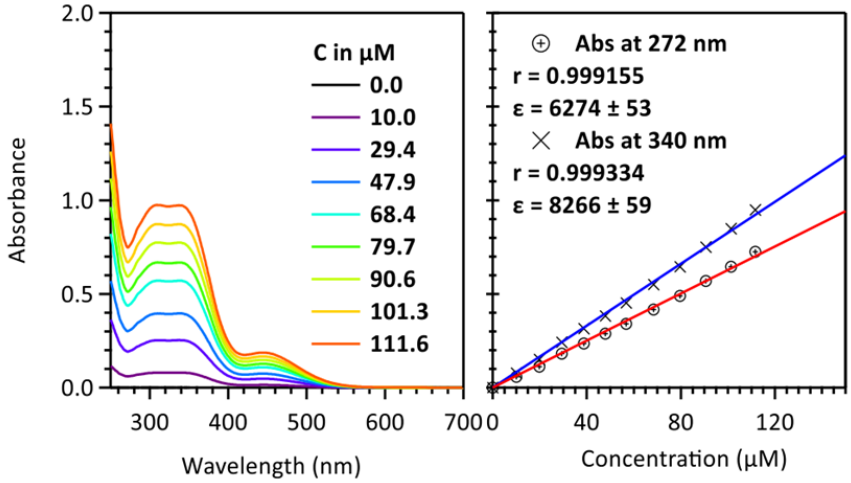

Figure 64. *UV-Vis absorption spectra of E-**21**α measured in CH_2Cl_2 for the daughter solutions (left) and evolution of the absorbance (right) as function of the concentration at the maximum of wavelength (340 nm) and at the isosbestic point (272 nm). Mother solution: 1.2 mg dissolved in 1200 µL of CH_2Cl_2 (C = 0.0008 mol L^{-1}).*

Determination of epsilon of E-21β in CH_2Cl_2

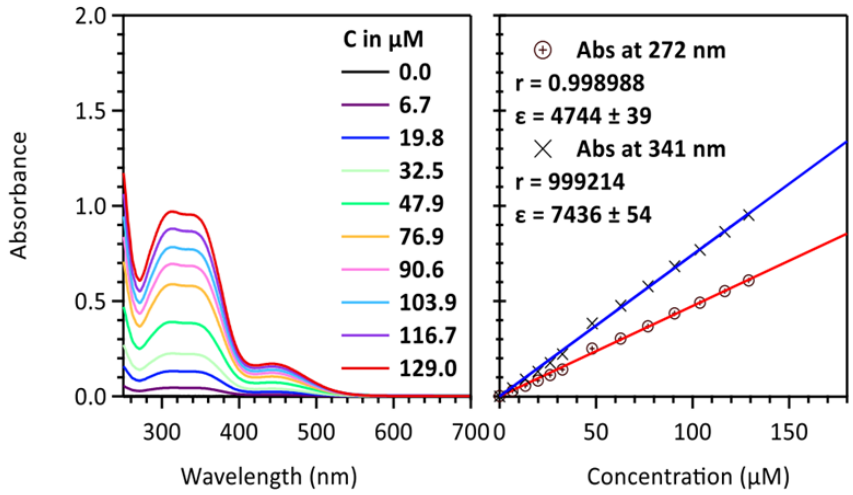

Figure 65. *UV-Vis absorption spectra of E-**21**β measured in CH_2Cl_2 for the daughter solutions (left) and evolution of the absorbance (right) as function of the concentration at the maximum of wavelength (341 nm) and at the isosbestic point (272 nm). Mother solution: 1.4 mg dissolved in 1400 µL of CH_2Cl_2 (C = 0.0008 mol L^{-1}).*

Determination of epsilon of E-22β in CH_2Cl_2

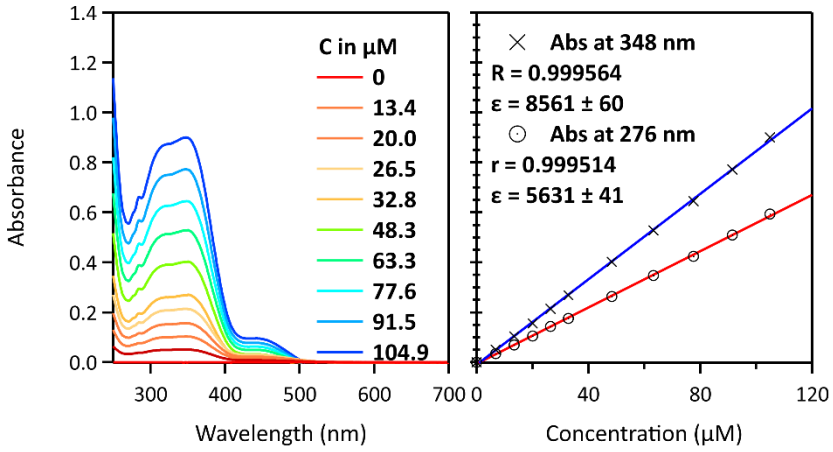

Figure 66. *UV-Vis absorption spectra of E-**22**β measured in CH_2Cl_2 for the daughter solutions (left) and evolution of the absorbance (right) as function of the concentration at the maximum of wavelength (348 nm) and at the isosbestic point (276 nm). Mother solution: 2.4 mg dissolved in 2500 µL of CH_2Cl_2 (C = 0.0009 mol L^{-1}).*

Determination of epsilon of E-23β in CH_2Cl_2

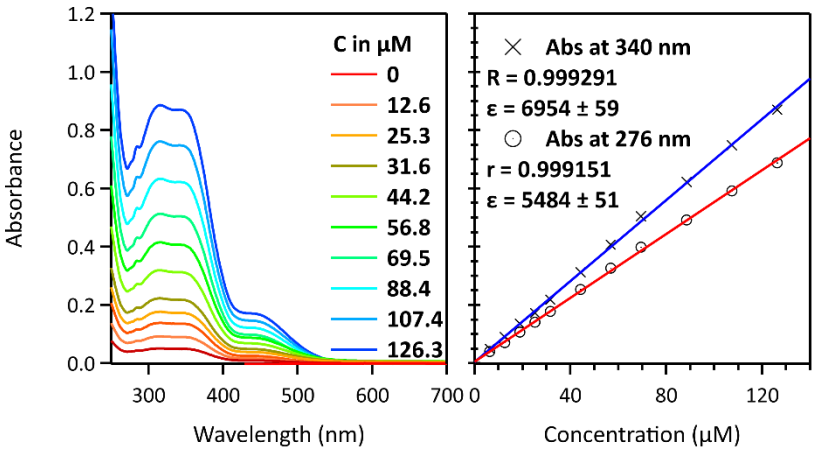

Figure 67. *UV-Vis absorption spectra of* ***E-23β*** *measured in CH_2Cl_2 for the daughter solutions (left) and evolution of the absorbance (right) as function of the concentration at the maximum of wavelength (340 nm) and at the isosbestic point (276 nm). Mother solution: 1.4 mg dissolved in 1500 µL of CH_2Cl_2 (C = 0.0008 mol L^{-1}).*

Determination of epsilon of E-20α in CH_3CN

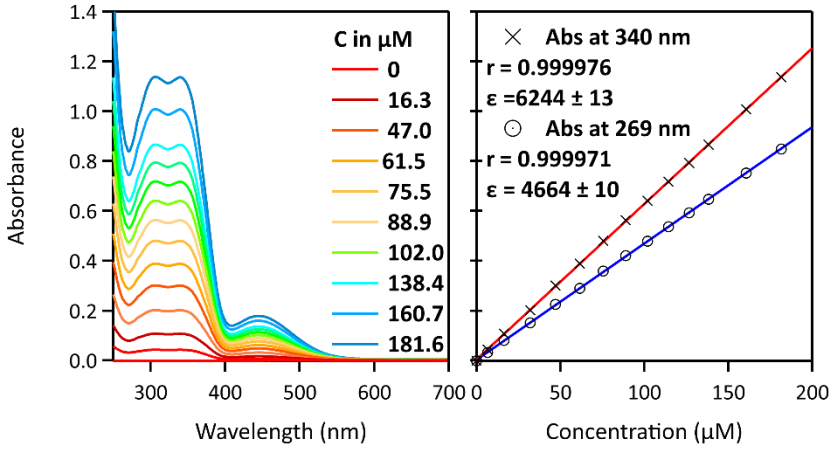

Figure 68. *UV-Vis absorption spectra of E-**20**α measured in CH_3CN for the daughter solutions (left) and evolution of the absorbance (right) as function of the concentration at the maximum of wavelength (340 nm) and at the isosbestic point (269 nm). Mother solution: 2.24 mg dissolved in 2400 µL of CH_3CN (C = 0.0008 mol L^{-1}).*

Determination of epsilon of E-21β in CH_3CN

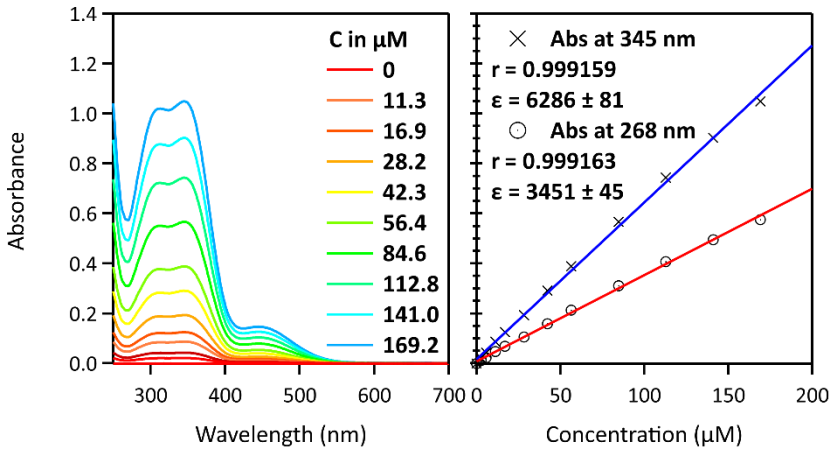

Figure 69. *UV-Vis absorption spectra of E-**21β** measured in CH_3CN for the daughter solutions (left) and evolution of the absorbance (right) as function of the concentration at the maximum of wavelength (345 nm) and at the isosbestic point (268 nm). Mother solution: 1.00 mg dissolved in 1200 µL of CH_3CN (C = 0.0007 mol L^{-1}).*

Determination of epsilon of E-21α in CH_3CN

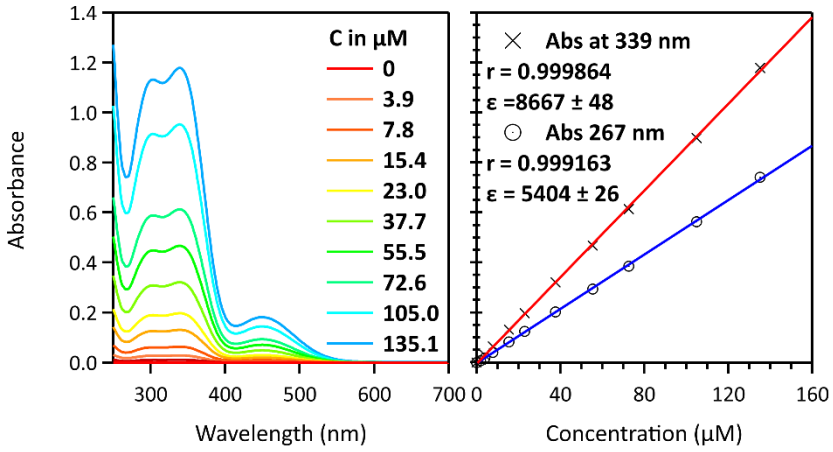

Figure 70. *UV-Vis absorption spectra of E-**21α** measured in CH_3CN for the daughter solutions (left) and evolution of the absorbance (right) as function of the concentration at the maximum of wavelength (339 nm) and at the isosbestic point (267 nm). Mother solution: 1.39 mg dissolved in 1200 µL of CH_3CN (C = 0.0010 mol L^{-1}).*

Determination of epsilon of E-22β in CH_3CN

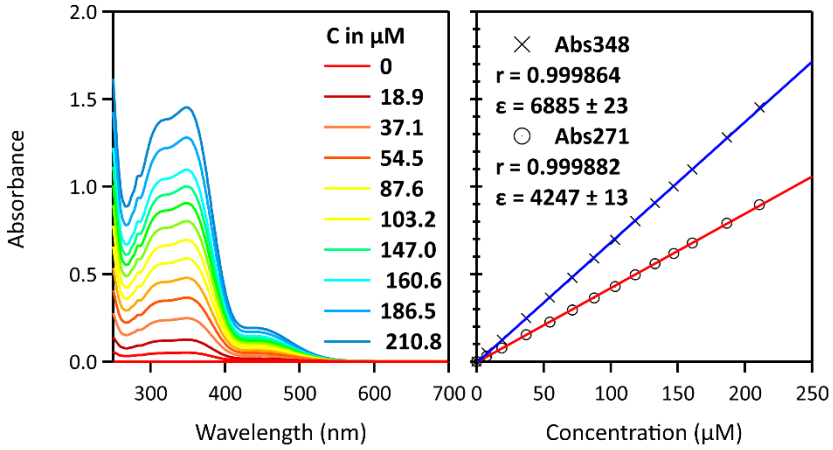

Figure 71. *UV-Vis absorption spectra of* ***E-22β*** *measured in CH_3CN for the daughter solutions (left) and evolution of the absorbance (right) as function of the concentration at the maximum of wavelength (345 nm) and at the isosbestic point (268 nm) (C = 0.0010 mol L^{-1}).*

Determination of epsilon of E-23β in CH_3CN

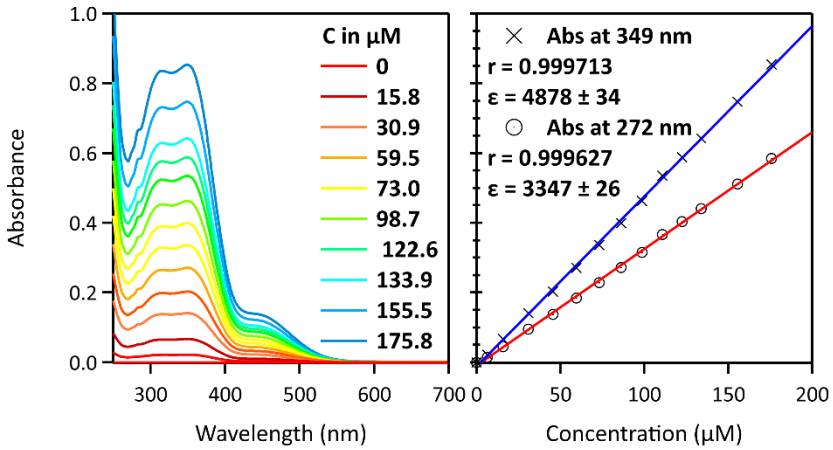

Figure 72. *UV-Vis absorption spectra of E-**23**β measured in CH_3CN for the daughter solutions (left) and evolution of the absorbance (right) as function of the concentration at the maximum of wavelength (349 nm) and at the isosbestic point (272 nm). Mother solution: 1.14 mg dissolved in 1200 µL of CH_3CN (C = 0.0008 mol L^{-1}).*

2.2. Procedure for titration by TfOH

To a solution of compound in dichloromethane, was added sequentially a solution of TfOH. For each addition, the evolution of the reaction was monitored by UV-Vis absorption to follow the acido-basic reaction kinetic. After reaching the equilibrium state, where no more significant changes appeared in the absorption spectra (maximum 30 to 60 minutes), the next addition was then realized. Only the last spectrum of each series of spectra was taken for the preparation of the figure. This titration method, which induces a variation of volume after each addition, was chosen in order to prevent the possible degradation of the compound in presence of a large amount of acid, which can induce the cleavage of the ester bonds. It is to be noticed that usually, the preference is oriented for the preparation of a stock solution containing both the TfOH, and the photochromic glycomacrocycles at the same concentration used for the titration (concentration in cuvette) in order to prevent the dilution effect due to the variation of volume. Consequently, due to the important variation of volume after each addition of TfOH solution, the evolution of the absorbance was monitored by plotting the ratio E•H^+/E-isomer corresponding to the maximum of absorption of the involved species in solution.

2.3. Determination of half-lifes of *Z*-isomers (1)

General procedure for the determination of the half-life of Z-isomers at room temperature

For the glycosyl azobenzenes with long half-life (more than several days), the thermal *Z*→*E* isomerization was tracked by measuring UV-Vis absorption spectra at a given temperature (temperature = 22°C to 25°C). The obtained time-dependent absorption profile, taking ***Z-20α*** as an example (black dot, right Fig.), was fitted with the following first order rate equation (red line):

$$Abs(t) = A_o - (A_o - A_i)e^{-kt}$$

with

A_o, the absorption of original E-isomer (hold parameter)

A_i, the absorption at the PSS_{365} (hold or free parameter)

k, the rate constant of thermal isomerization at the given temperature

t, the time in minutes or hours

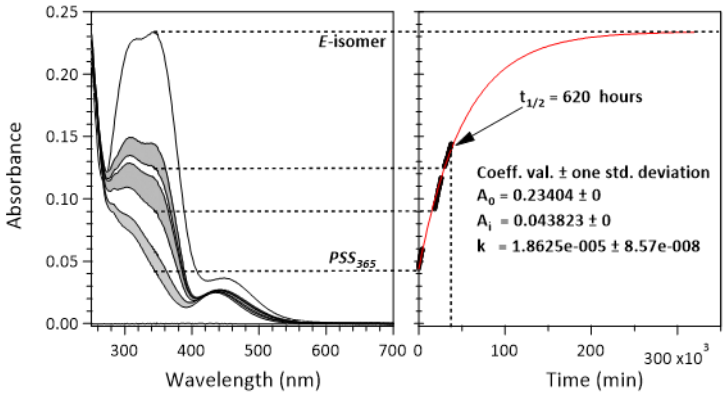

Figure 73. *UV-Vis absorption spectra (left) and thermal return monitoring (right) of Z-**20**α at 343 nm in CH_2Cl_2 room temperature (≈ 22-25°C). The reported data points are the result of a combination of 3 independent kinetic measurements realized on the same solution from the PSS_{365}: 0 to 3960 min (step = 60 min); 18495 to 26295 min (step = 120 min); 29805 to 37605 min (step = 120 min).*

After fitting (red curve), the rate constant at 25°C (T = 298 K) was obtained from the fitting parameters:

$$k_{298} = 1.86 \times 10^{-5}\, min^{-1}$$

The half-life of ***Z-20α*** at room temperature was then calculated:

$$t_{1/2} = \frac{\ln(2)}{k_T}$$

$$t_{1/2} = 37\ 216 \text{ min} \cong 620 \text{ hours}$$

Similarly, the half-life of *Z-**21α**, Z-**21β**, Z-**22β*** and *Z-**23β*** were estimated by this method.

Determination of the half-life of Z-21α in CH_2Cl_2

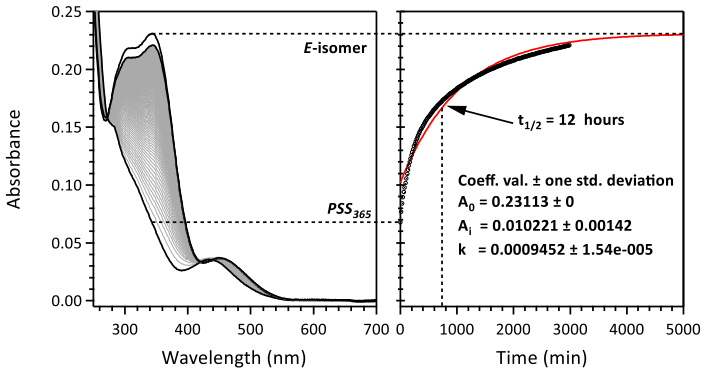

Figure 74. *UV-Vis absorption spectra (left) and thermal return monitoring (right) of Z-**21**α at 343 nm in CH_2Cl_2 room temperature (≈ 22-25°C). The reported data points are the result of a single kinetic measurement realized on a solution from the PSS_{365}: 0 to 2985 min (step = 15 min).*

Determination of the half-life of Z-21β in CH_2Cl_2

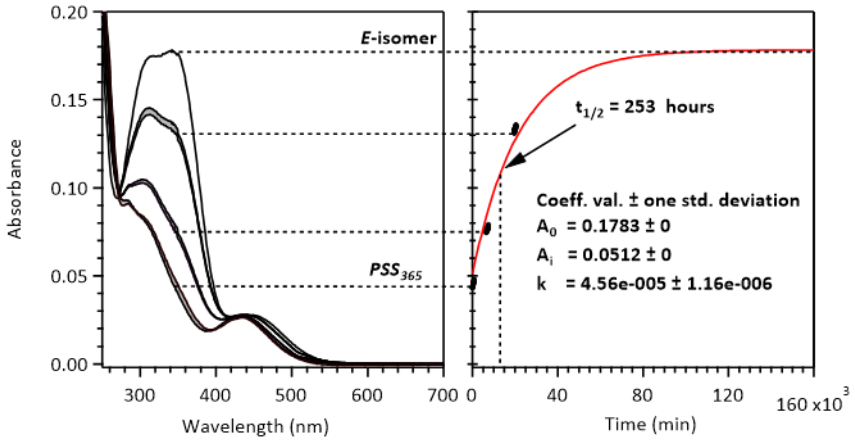

Figure 75. *UV-Vis absorption spectra (left) and thermal return monitoring (right) of **Z-21β** at 342 nm in CH_2Cl_2 room temperature (≈ 22-25°C). The reported data points are the result of a combination of 3 independent kinetic measurements realized on the same solution from the PSS_{365}: 0 to 780 min (step = 30 min); 5370 to 6330 min (step = 30 min); 19527 to 21267 min (step = 60 min).*

Determination of the half-life of Z-22β in CH_2Cl_2

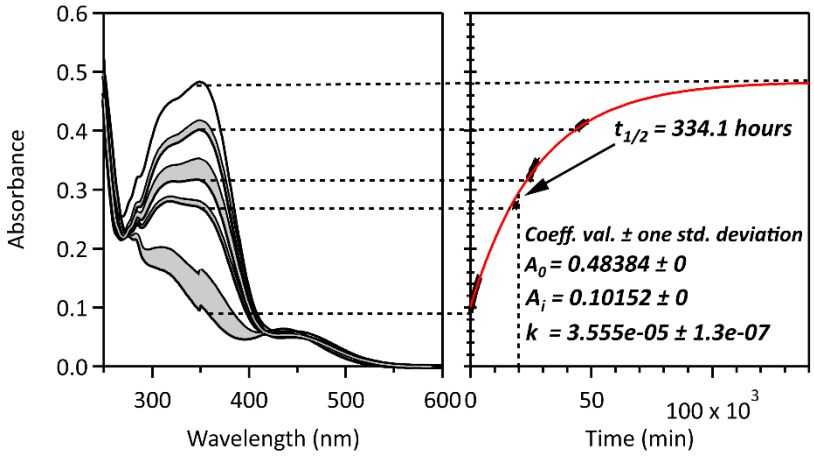

Figure 76. *UV-Vis absorption spectra (left) and thermal return monitoring (right) of* ***Z-22β*** *at 342 nm in CH_2Cl_2 room temperature (≈ 22-25°C). The reported data points are the result of a combination of 4 independent kinetic measurements realized on the same solution from the PSS_{365}: 0 to 3720 min (step = 60 min); 18120 to 19020 min (step = 30 min); 23880 to 27600 min (step = 60 min); 44040 to 47760 min (step = 60 min).*

Determination of the half-life of Z-23β in CH_2Cl_2

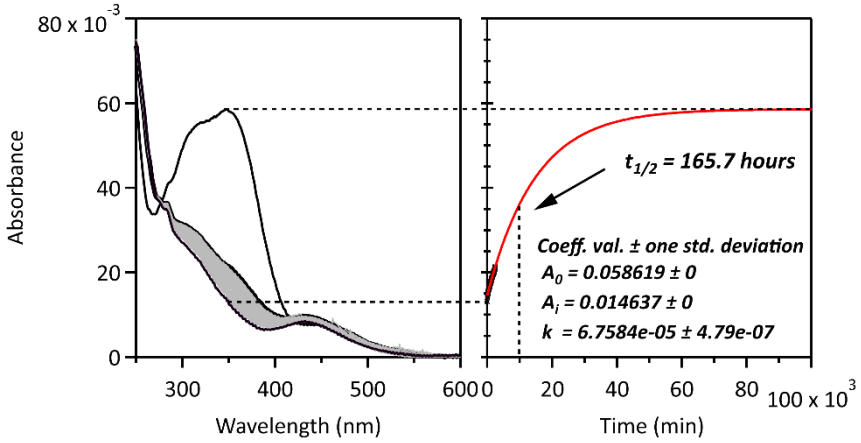

Figure 77. *UV-Vis absorption spectra (left) and thermal return monitoring (right) of* ***Z-23β*** *at 342 nm in CH_2Cl_2 room temperature (≈ 22-25°C). The reported data points are the result of a combination of 1 independent kinetic measurements realized on the same solution from the PSS_{365}: 0 to 2490 min (step = 00 min).*

Molecule mumber	***Z-20α***	***Z-21α***	***Z-21β***	***Z-22β***	***Z-23β***
$t_{1/2}$	620.0h	12.0h	253.0h	334.1h	165.7h

2.4. Determination of the half-life of *Z*-isomers (2)

General procedure for the determination of the half-life of Z-isomers at 2 temperatures

For the glycosyl azobenzenes with long half-life (more than several days), the thermal Z→E isomerization was tracked by measuring UV absorption spectra at 40 °C and 60 °C, respectively. The obtained time-dependent absorption profiles, taking *Z*-**20**α as an example (black spots, **Figure 78**), were fitted following first order rate equation:

$$Abs(t) = A_o - (A_o - A_i)e^{-kt}$$

with

A_0, the absorption of original *E*-form

A_i , the absorption of PSS_{365}

k, the rate constant of thermal isomerization

t, the time in minutes

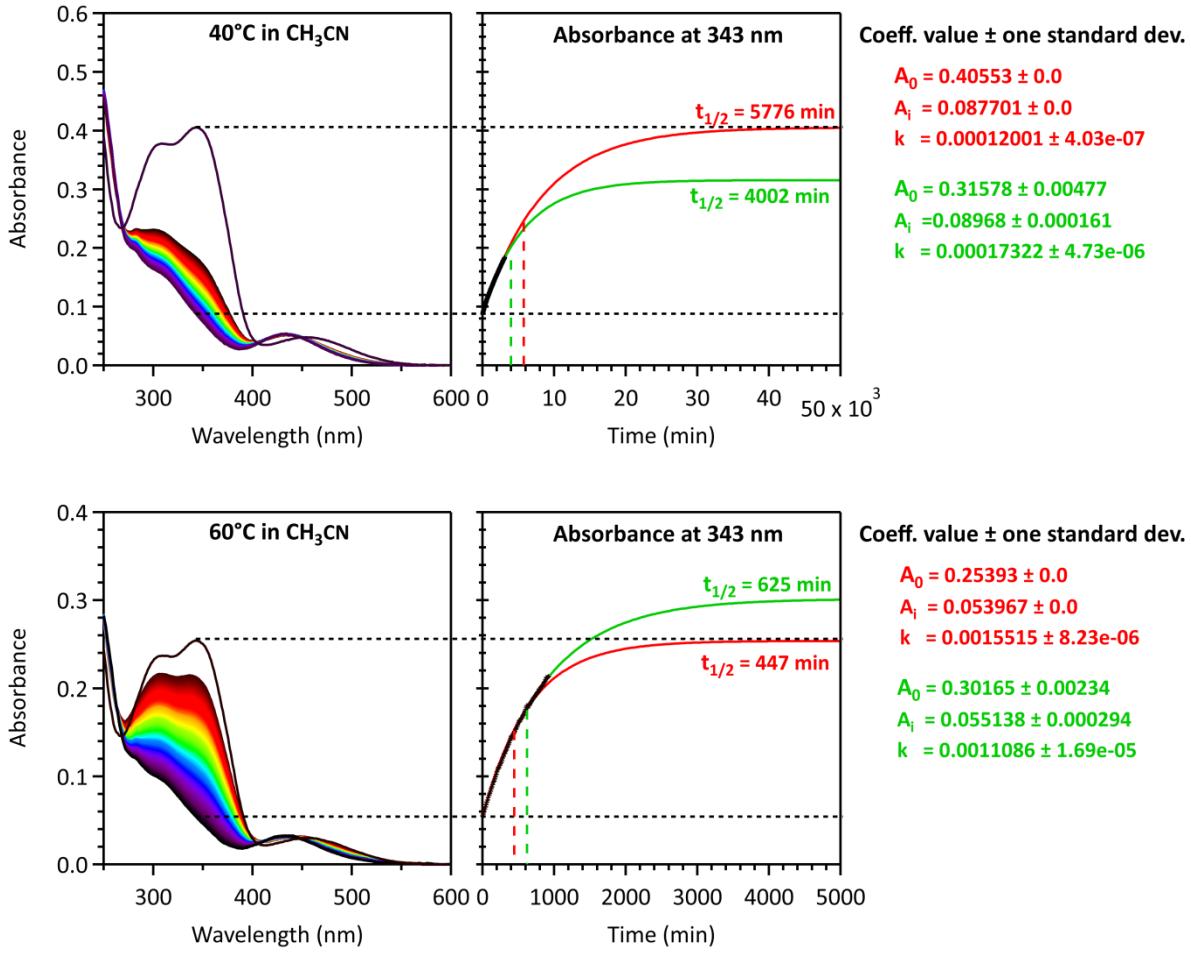

Figure 78 : *Time-dependent absorption profiles of Z-**20**α (PSS_{365}) at 40 °C (above) and 60 °C (below) in MeCN.*

After fitting (red curve, **Figure 78**), the rate constants at 40 °C (T_1 = 313 K) and 60 °C (T_2 = 333 K) were obtained:

$$k_1 = 1.7322 \times 10^{-4}\ min^{-1};\ k_2 = 1.109 \times 10^{-3}\ min^{-1}$$

According to the Arrhenius law, the relationship between rate constant and temperature is:

$$k = Fe^{-\frac{E_a}{RT}}$$

with,

F, the pre-exponential factor

E_a, the activation energy in J.mol^{-1}

R, the constant of perfect gasses in J.K^{-1}.mol^{-1}

Consequently, F and E_a can be figured out based on the two *k*/T combination. Considering the variation E_a as independent of the temperature, the activation energy of the system can be determined using the following equation:

$$E_a = \ln\left(\frac{k_1}{k_2}\right) R \frac{T_1 T_2}{T_1 - T_2}, \text{ with } T_1 < T_2$$

The pre-exponential factor is then calculated from the values obtained for T_1 or T_2 using the following equation:

$$F = k_1 e^{\frac{Ea}{RT_1}}$$

Consequently, in the case of Z-20α, $F = 3.93 \times 10^{14}\ and\ E_a = 1.11 \times 10^5\ J \cdot mol^{-1}$

Therefore, the rate constant k_T at room temperature (T = 293 K) should be $6.55 \times 10^{-6}\ min^{-1}$. The half-life of *Z-**20**α* at room temperature should be:

$$t_{1/2} = \frac{\ln(2)}{k_T} = \frac{\ln(2)}{k_1 e^{\frac{\ln\left(\frac{k_1}{k_2}\right) R \frac{T_1 T_2}{T_1 - T_2}}{RT_1}} \times e^{-\frac{\ln\left(\frac{k_1}{k_2}\right) R \frac{T_1 T_2}{T_1 - T_2}}{293.15\ R}}}$$

$$t_{1/2} = 105\,879 \text{ min} = 73 \text{ days}$$

Similarly, the half-life of *Z*-**22** and *Z*-**23** were estimated by this method.

Determination of the half-life of Z-20α in CH_3CN

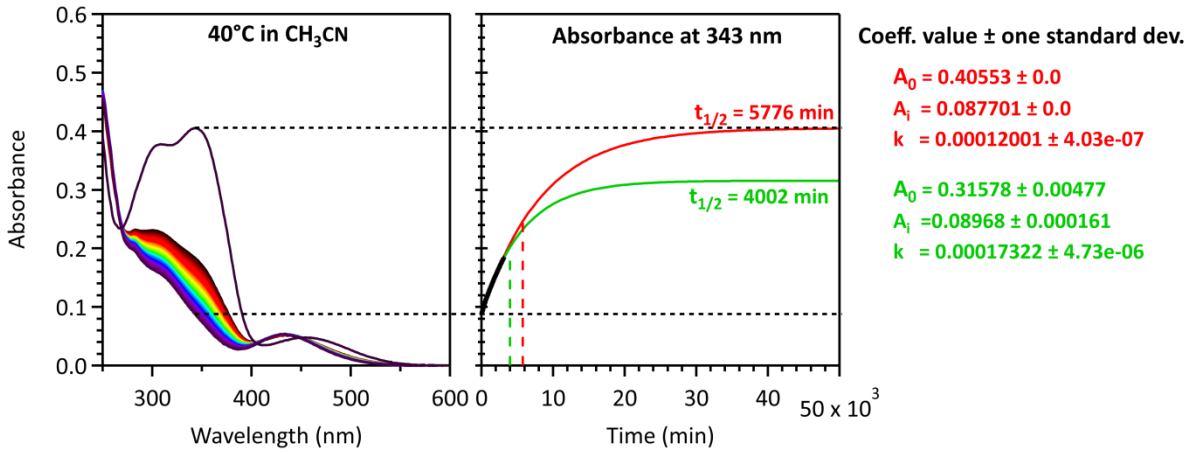

Figure 79. *UV-Vis absorption spectra (left) and thermal return monitoring (right) of Z-**20**α at 343 nm in CH_3CN at 40°C. The reported data points are the result of a single kinetic acquisition realized on the same solution from the PSS_{365}: 0 to 3090 min (step = 30 min).*

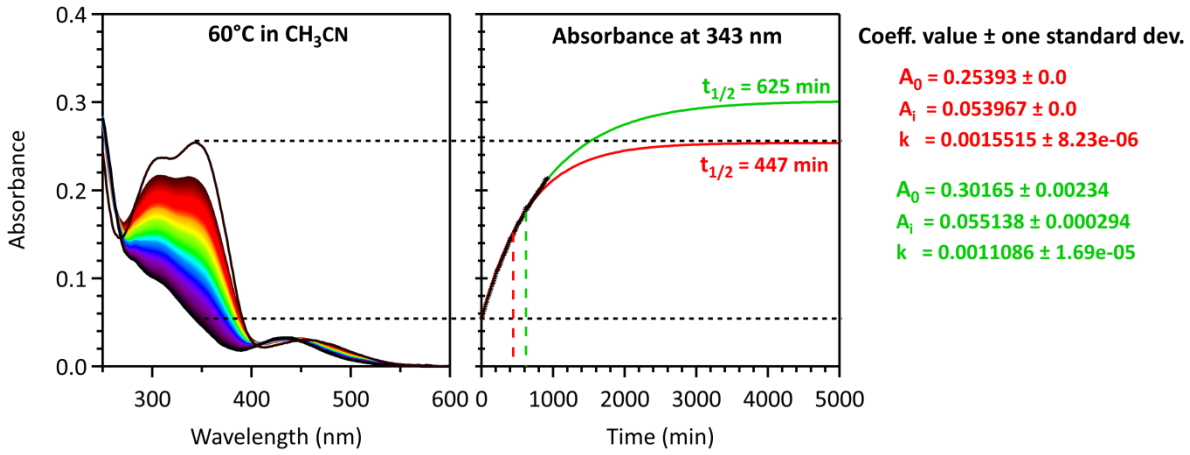

Figure 80. *UV-Vis absorption spectra (left) and thermal return monitoring (right) of Z-**20**α at 343 nm in CH_3CN at 60°C. The reported data points are the result of a single kinetic acquisition realized on the same solution from the PSS_{365}: 0 to 920 min (step = 10 min).*

Determination of the half-life of Z-21β in CH_3CN

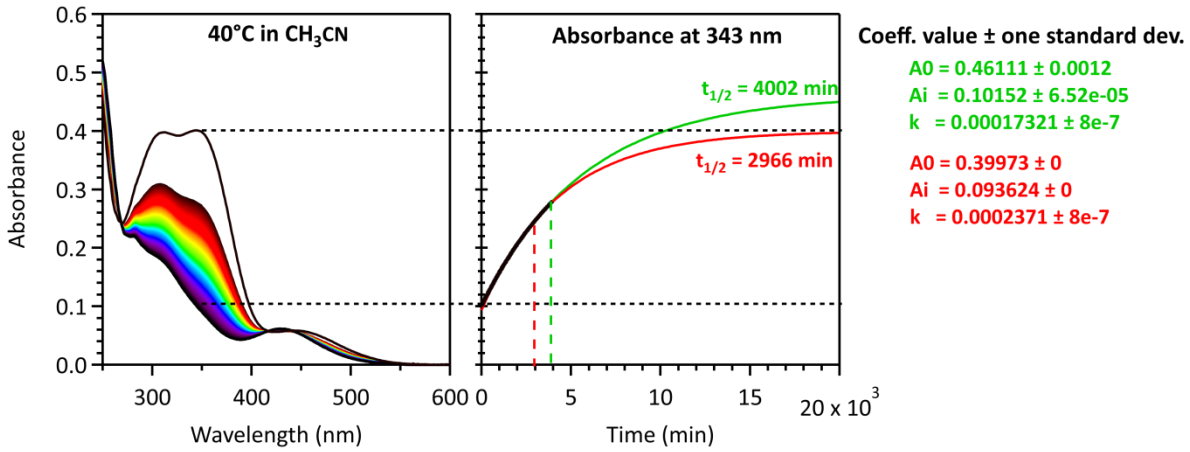

Figure 81 *UV-Vis absorption spectra (left) and thermal return monitoring (right) of Z-**21β** at 343 nm in CH_3CN at 40°C. The reported data points are the result of a single kinetic acquisition realized on the same solution from the PSS_{365}: 0 to 3900 min (step = 30 min).*

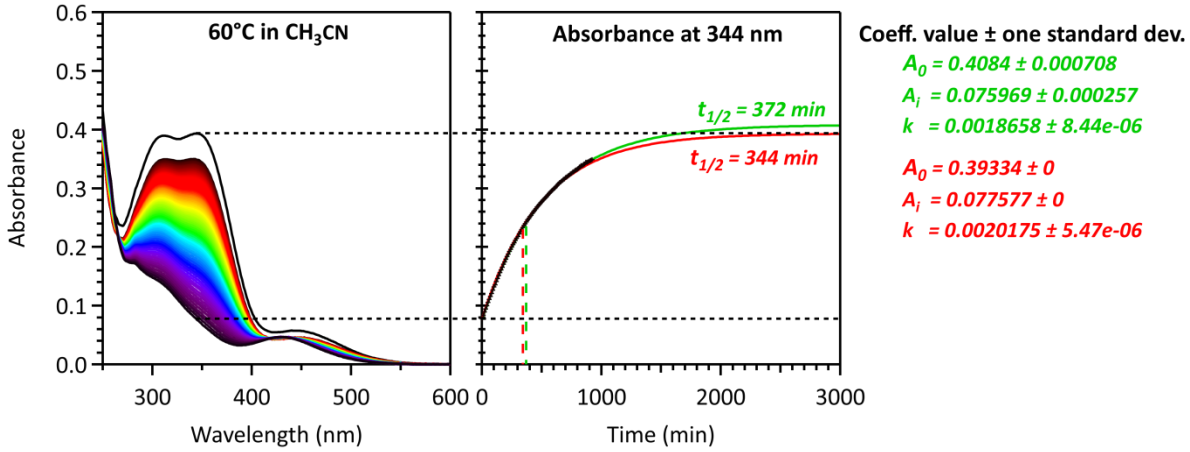

Figure 82. *UV-Vis absorption spectra (left) and thermal return monitoring (right) of Z-**21β** at 344 nm in CH_3CN at 40°C. The reported data points are the result of a single kinetic acquisition realized on the same solution from the PSS_{365}: 0 to 920 min (step = 10 min).*

Determination of the half-life of Z-21α in CH_3CN

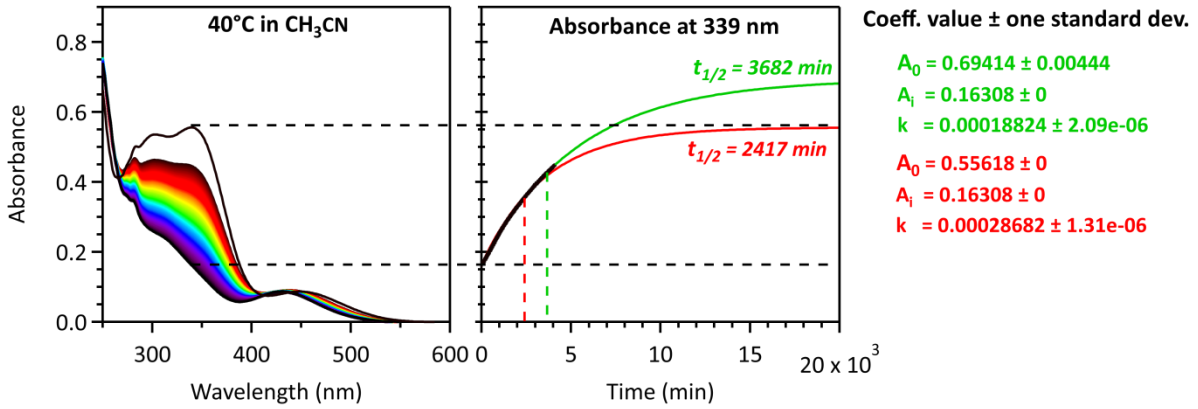

Figure 83. *UV-Vis absorption spectra (left) and thermal return monitoring (right) of Z-**21**α at 339 nm in CH_3CN at 40°C. The reported data points are the result of a single kinetic acquisition realized on the same solution from the PSS_{365}: 0 to 4050 min (step = 30 min).*

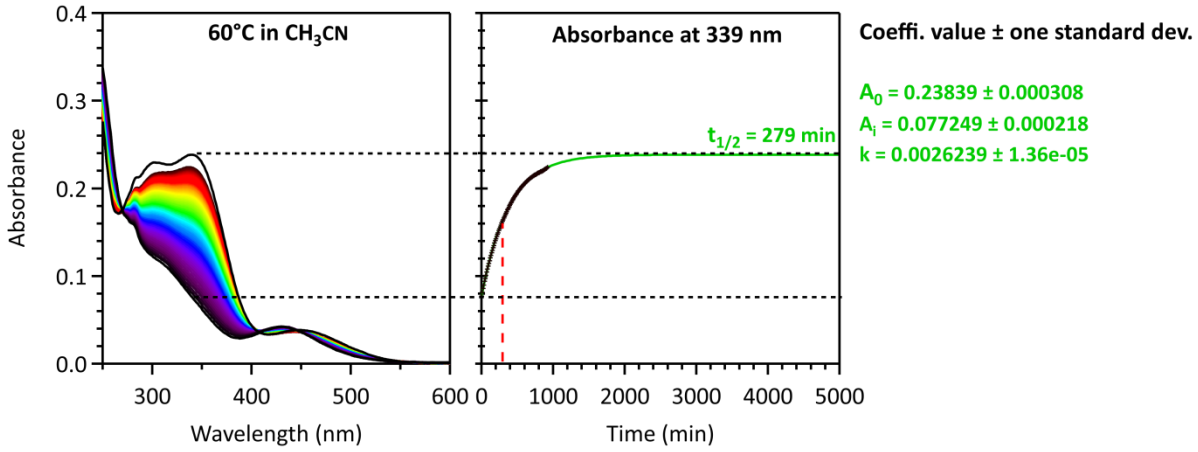

Figure 84. *UV-Vis absorption spectra (left) and thermal return monitoring (right) of Z-**21**α at 339 nm in CH_3CN at 60°C. The reported data points are the result of a single kinetic acquisition realized on the same solution from the PSS_{365}: 0 to 920 min (step = 10 min).*

Determination of the half-life of Z-22β in CH_3CN

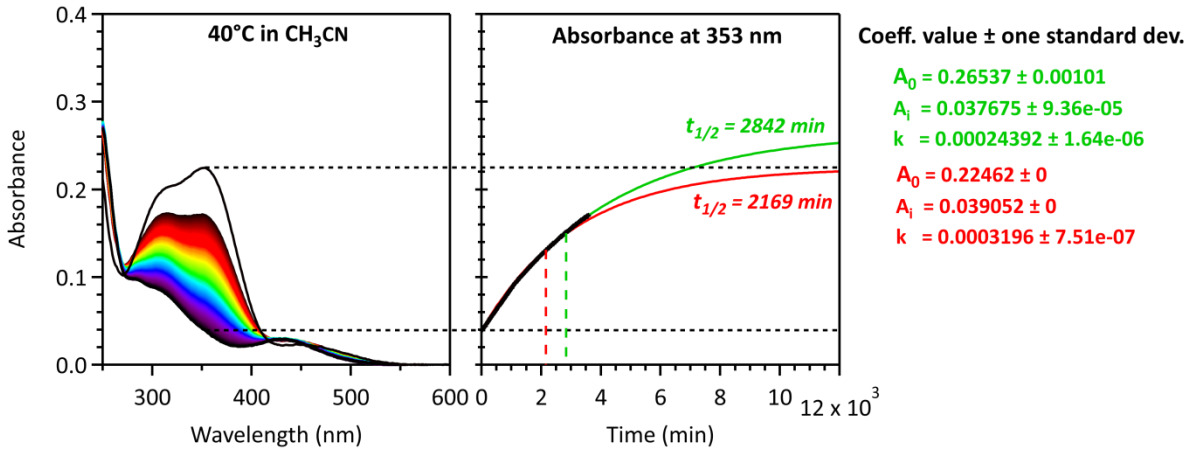

Figure 85. *UV-Vis absorption spectra (left) and thermal return monitoring (right) of Z-**22β** at 353 nm in CH_3CN at 40°C. The reported data points are the result of a single kinetic acquisition realized on the same solution from the PSS_{365}: 0 to 3590 min (step = 10 min).*

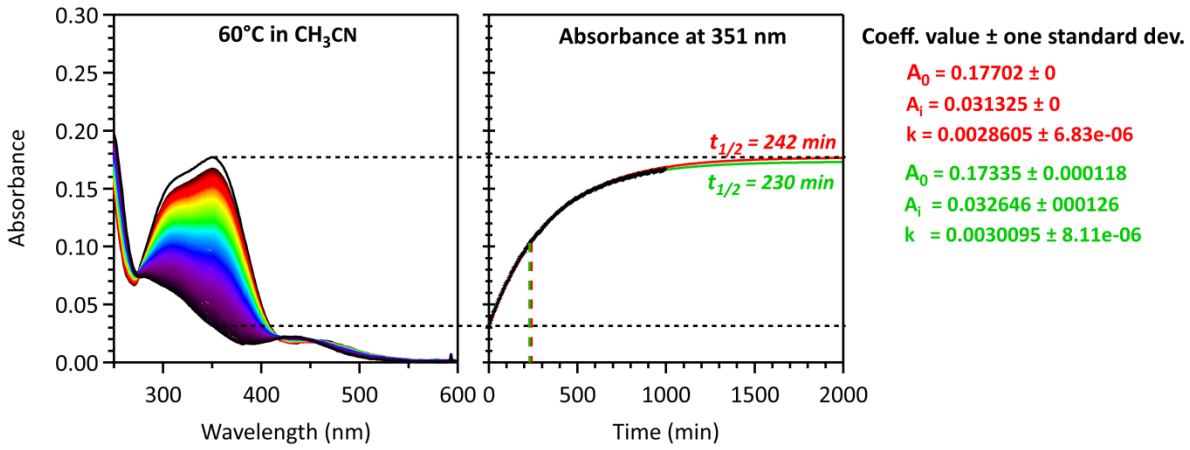

Figure 86. *UV-Vis absorption spectra (left) and thermal return monitoring (right) of Z-**22β** at 351 nm in CH_3CN at 60°C. The reported data points are the result of a single kinetic acquisition realized on the same solution from the PSS_{365}: 0 to 995 min (step = 5 min).*

Determination of the half-life of Z-23β in CH_3CN

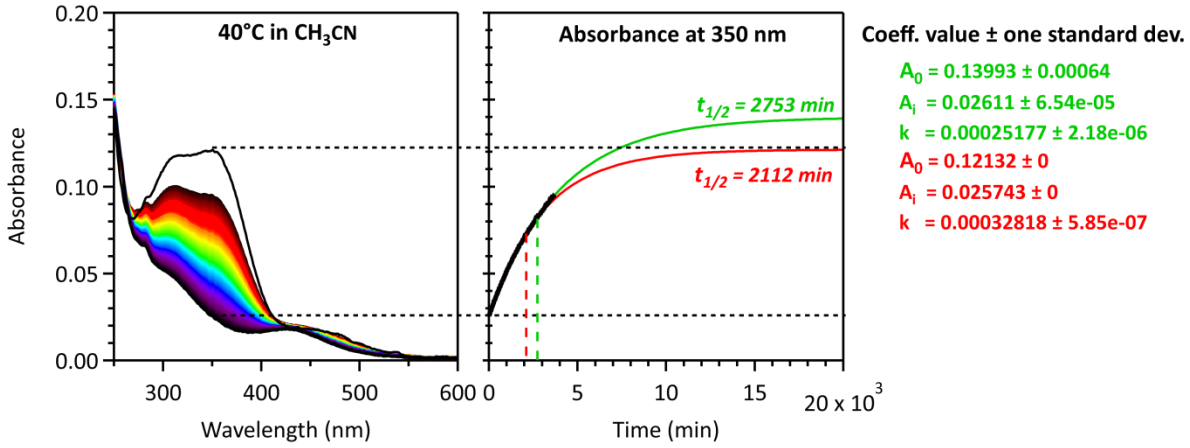

Figure 87. *UV-Vis absorption spectra (left) and thermal return monitoring (right) of Z-**23**β at 350 nm in CH_3CN at 60°C. The reported data points are the result of a single kinetic acquisition realized on the same solution from the PSS_{365}: 0 to 3650 min (step = 10 min).*

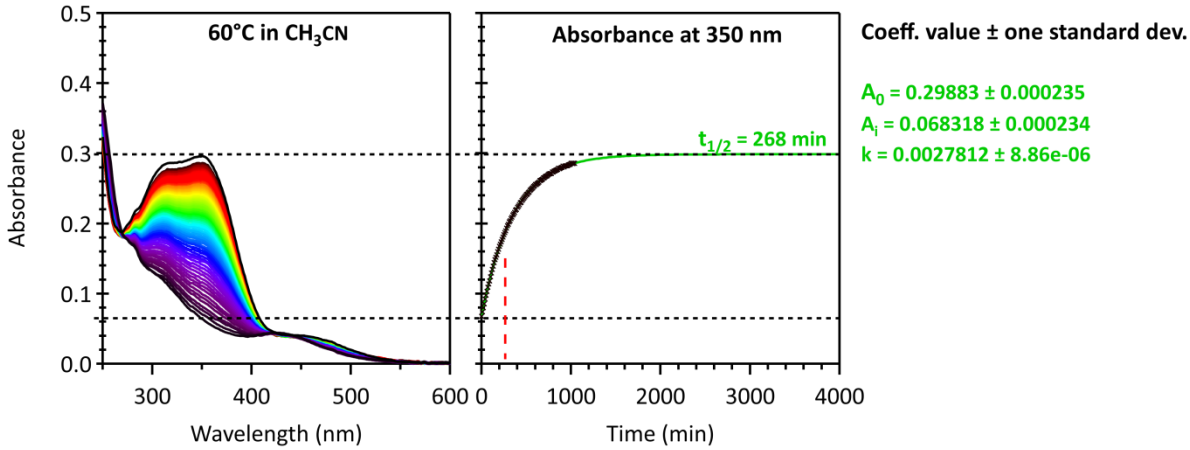

Figure 88. *UV-Vis absorption spectra (left) and thermal return monitoring (right) of Z-**23**β at 350 nm in CH_3CN at 60°C. The reported data points are the result of a single kinetic acquisition realized on the same solution from the PSS_{365}: 0 to 1040 min (step = 10 min).*

2.5. Fatigue resistance measurements

General procedure for the fatigue resistance measurements

Starting from a solution of compound containing 100% of the E-isomer, the solution was irradiated sequentially at 365 nm and at 435 nm. The absorbance was measured before and after each illumination realized with constant optical length distance. The sequence, which constitutes a cycle, was repeated for a minimum of 25 times.

Fatigue resistance of the glycomacrocycle E-20α

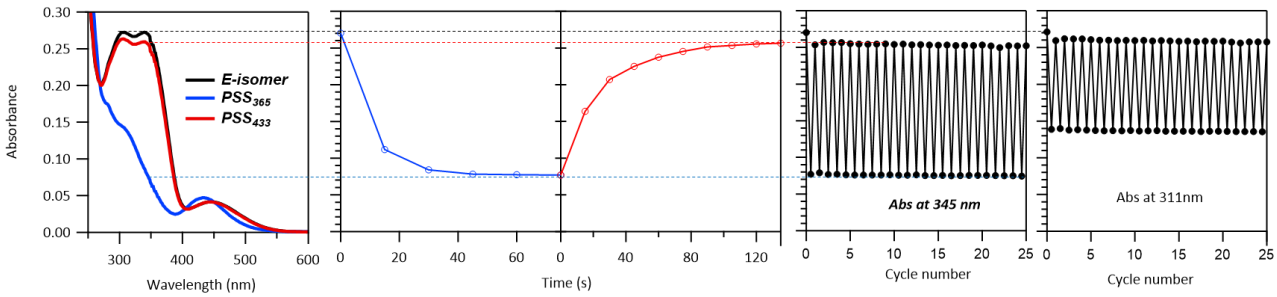

Figure 89: *Fatigue resistance followed by the absorption band at 311nm (left) and 345 nm (right) under alternate 365 nm/433 nm irradiation cycles in CH_3CN. Irradiation conditions: 60 s at P_{365} = 6.74 mW cm^{-2} and 60 s at P_{433} = 4.99 mW cm^{-2}.*

Fatigue resistance of the glycomacrocycle E-21α

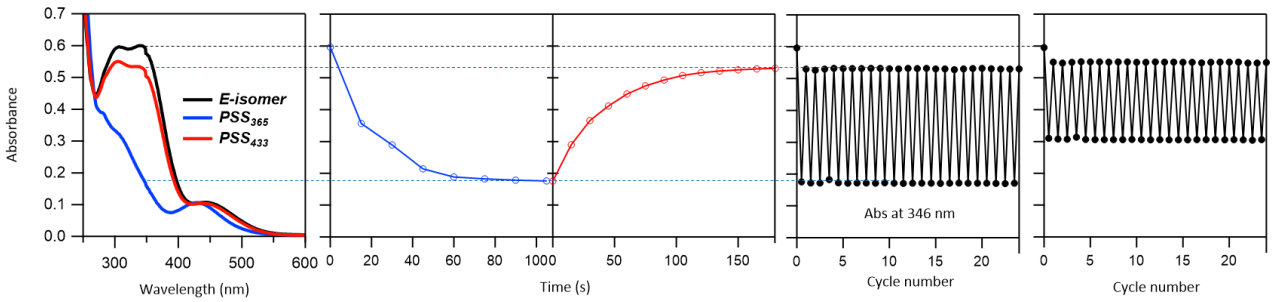

Figure 90: *Fatigue resistance followed by the absorption band at 311 nm (left) and 346 nm (right) under alternate 365 nm/433 nm irradiation cycles in CH_3CN. Irradiation conditions: 60 s at P_{365} = 6.74 mW cm^{-2} and 60 s at P_{433} = 4.99 mW cm^{-2}.*

Fatigue resistance of the glycomacrocycle E-21β

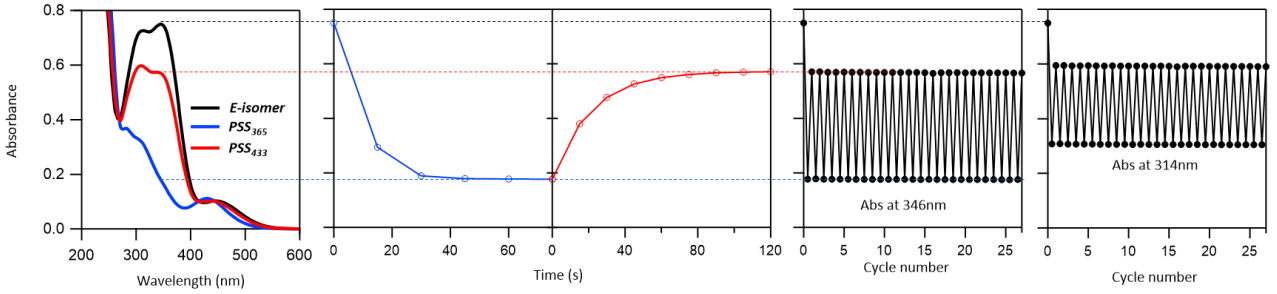

Figure 91: *Fatigue resistance followed by the absorption band at 314 nm (left) and 346 nm (right) under alternate 365 nm/433 nm irradiation cycles in CH_3CN. Irradiation conditions: 50 s at P_{365} = 6.74 mW cm^{-2} and 50 s at P_{433} = 4.99 mW cm^{-2}.*

Fatigue resistance of the glycomacrocycle E-22β

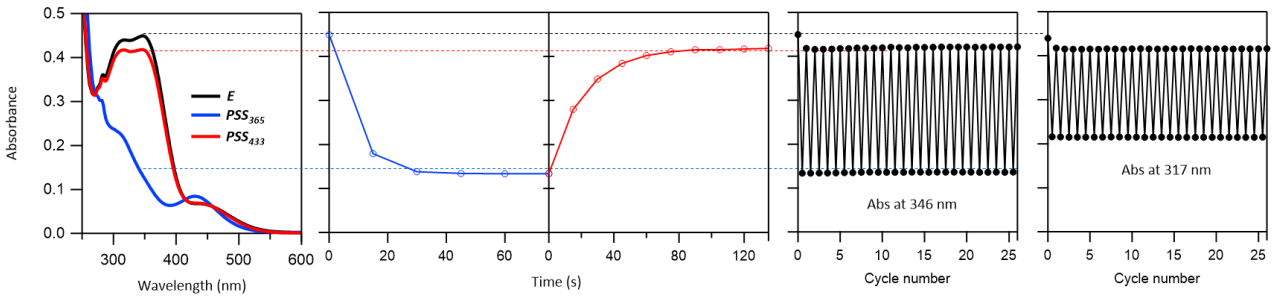

Figure 92: *Fatigue resistance followed by the absorption band at 317nm (left) and 346 nm (right) under alternate 365 nm/433 nm irradiation cycles in CH_3CN. Irradiation conditions: 40 s at P_{365} = 6.74 mW cm^{-2} and 40 s at P_{433} = 4.99 mW cm^{-2}.*

Fatigue resistance of the glycomacrocycle E-23β

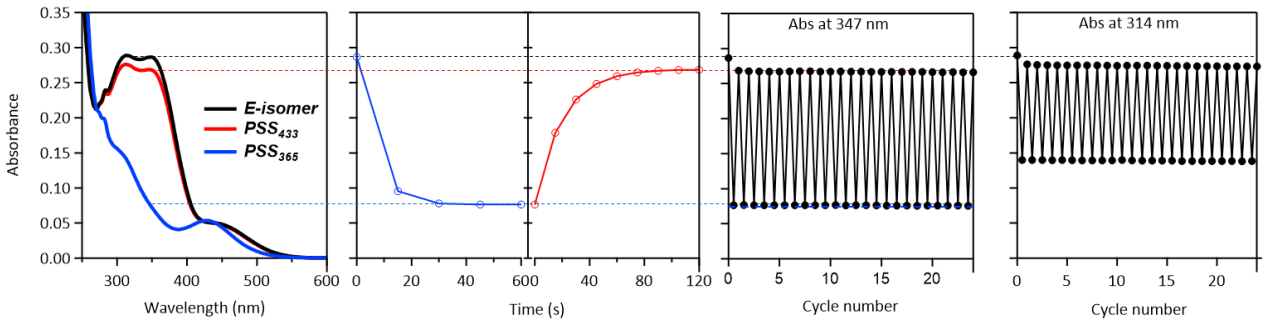

Figure 93: *UV-Vis absorption spectra (left) and fatigue resistance (right) in CH_3CN. Irradiation conditions: PSS_{365}, time = 40 s, power = 6.7 mW cm^{-2}; PSS_{433}, time = 40 s, power = 5.0 mW cm^{-2}.*

2.6. Photoconversion yields

General procedure for the determination of the photoconversion yields by absorption and 1H NMR

A freshly prepared solution of *E*-azobenzene derivative was prepared in $CDCl_3$ and taking into account the maximum absorbance limit of the spectrophotometer ($Abs_{lim} < 4$). The deuterated solution is monitored by absorption and ^1H NMR before and after irradiation. More precisely, the absorbance was firstly recorded, and a small amount of the solution was taken for the ^1H NMR monitoring. The sequence was then repeated after irradiation of the solution to the photostationary state (PSS). The ^1H NMR spectra were recorded with a relaxation delay of 2 s, and 256 or 512 scans.

Then, the corresponding photoconversion yield (CY) was calculated, after integration of the pic areas, according to the following equation,

$$CY_i = \frac{A_E}{A_E + A_Z}$$

With,

CY_i represents the conversion yield for a given state (i) of the solution,

A_E represents the area taken under the pic of *E*-isomer,

A_Z represents the area taken under the pic of *Z*-isomer.

3. General procedure of synthesis

General procedure A: Acetylation with $Cu(ClO_4)_2 \cdot 6H_2O$

To a solution of saccharide (133.3 mmol, 1.0 eq) and Ac_2O (10.0 eq) was added slowly $Cu(ClO_4)_2 \cdot 6H_2O$ (0.05 eq). The reaction was monitored by TLC until the sugar was consumed completely (about 2h). The reaction mixture was treated with saturated aq. $NaHCO_3$ and extracted with EA. The organic phase was washed with water and brine, then dried over $MgSO_4$ and concentrated to get the acetylated compound.

General procedure B: Thioglycosylation with $BF_3 \cdot Et_2O$

To a solution of per-acetylated saccharide (25.4 mmol, 1.0 eq) and PhSH (2.0 eq) in CH_2Cl_2 (~ 6.5 mL per mmol) was added slowly $Et_2O \cdot BF_3$ (1.5 eq) at 0 °C. The reaction was monitored by TLC until the starting material was consumed completely, then diluted with CH_2Cl_2, washed with 1M HCl, saturated aq. $NaHCO_3$ and brine, dried over $MgSO_4$ and concentrated. The residue was purified with CombiFlash R_f to give the corresponding thioglycoside.

General procedure C: Zemplen deacetylation with MeONa

To a solution of acetylated glycoside (4.5 mmol, 1.0 eq) in dry MeOH under Ar was added MeONa (solution in MeOH, 0.3 eq). Under stirring at rt, the reaction was monitored by TLC until the starting material was consumed completely. The reaction mixture was then neutralized with H^+ resin to pH 6, and the mixture was filtered and concentrated to afford the deacetylated compound.

General procedure D: Benzylation with benzyl bromide

A solution of glycoside (6.5 mmol, 1.0 eq) in THF (~2 mL per mmol) was added to a stirred suspension of sodium hydride (60%, 1.5 eq) and TBAI (0.2 eq) in THF (15 mL) at 0°C. After 15 min, benzyl bromide (3.6 eq) was added and stirring was continued at rt. The reaction was monitored by TLC until the starting material was consumed completely. The mixture was then diluted with CH_2Cl_2 and washed successively with saturated aqueous NH_4Cl and brine, dried over $MgSO_4$ and evaporated to dryness. The residue was purified by CombiFlash R_f.

General procedure E: Esterification of azobenzene-linked glycosyl acceptor

A solution of EDC (1.0 eq) and DMAP (0.1 eq) in dry CH_2Cl_2 (~2 mL/mmol) was added dropwise to a solution of an azobenzene linker (1.9 mmol, 1.0 eq) and glycosyl acceptor (1.0 equiv.) in dry CH_2Cl_2 (~50 mL/mmol) at 0 °C. The solution was stirred (0 °C to rt) until the reaction was finished as indicated by TLC. The reaction mixture was diluted with CH_2Cl_2 and washed with water (3 times). The organic layer was separated, dried over $MgSO_4$, and concentrated. The residue was purified by CombiFlash R_f.

General procedure F: CuAAC (Click reaction)

To a mixture of the azido-compound (0.4 mmol, 1.0 eq) and alkynyl-compound (1.0 eq) in CH_2Cl_2/H_2O (4 mL/1 mL), were added $CuSO_45H_2O$ (0.5 eq) and ascorbic acid or Na ascorbate (1.0 eq). The solution was stirred at rt for 16h until the reaction was finished as indicated by TLC. The solution was diluted with CH_2Cl_2, and the organic layer was washed with brine (3 times), dried over $MgSO_4$, concentrated and purified with CombiFlash R_f.

General procedure G: Intramolecular glycosylation of E-azobenzene-linked glycosyl donor-acceptor pairs

A mixture of glycosyl donor-acceptor pair (0.04 mmol, 1.0 eq) and freshly dried 4Å molecular sieves (50 mg per 0.01mmol) in dry CH_2Cl_2 was stirred under Argon for 6h at rt. To this solution cooled to -78 °C, was added NIS (2.0 eq) and TfOH (0.5 to 2 eq). The solution was kept stirring at -78 °C for 3-4h until the reaction was finished as indicated by TLC. The solution was diluted with CH_2Cl_2, then filtered. The organic layer was washed with 20% aq. $Na_2S_2O_3$ and water (3 times), dried over $MgSO_4$, concentrated and purified with CombiFlash R_f.

General procedure H: Intramolecular glycosylation of Z-azobenzene-linked glycosyl donor-acceptor pairs

A mixture of glycosyl donor-acceptor pair (0.04 mmol, 1.0 eq) and freshly dried 4Å molecular sieves (50 mg per 0.01mmol) in dry CH_2Cl_2 was stirred under Argon for 6h at rt. Then the solution was irradiated with 365 nm light until it's absorption didn't change (until the PSS state). To this solution cooled to -78 °C, was added NIS (2.0 eq) and TfOH (0.5 to 2 eq). The solution was kept stirring at -78 °C for 3-4h until the reaction was finished as indicated by TLC. The solution was diluted with CH_2Cl_2, then filtered. The organic layer was washed with 20% aq. $Na_2S_2O_3$ and water (3 times), dried over $MgSO_4$, concentrated under vacuum at r.t. and purified with CombiFlash R_f to give the desired compound.

4. Detailed synthetic procedures

D-Mannose pentaacetate (5)[134]

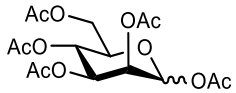

$C_{16}H_{22}O_{11}$
Mw: 390.12 g/mol

To a solution of D-mannose (24.0 g, 133.3 mmol) and Ac_2O (136 g, 1.3 mol) was added $Cu(ClO_4)_2$ $6H_2O$ (2.48 g, 6.64 mmol) according to the general procedure **A**. The target compound was isolated as a colorless oil (49.79 g, 86 %).

^{1}H NMR (400 MHz, $CDCl_3$) (α/β = 9/1): δ 6.02 (d, *J* = 1.2 Hz, 0.9H, H_1α), 5.80 (d, *J* = 0.8 Hz, 0.1H, H_1β), 5.42 (dd, *J* = 0.8, 3.2 Hz, 0.1H, H_2β), 5.32-5.25 (m, 1.9H, H_4α+β, H_2α), 5.20-5.19 (m, 0.9H, H_3α), 4.27-4.20 (m, 1H, H_6), 4.05-3.97 (m, 2.1H, $H_{6'}$+H_5+H_3β), 3.76-3.72 (m, 0.1H, H_5β), 2.28, 2.15, 2.12, 2.11, 2.04, 2.03, 1.99, 1.95 (8×s, 24H, H_{OAc}α+β).

^{13}C NMR (100 MHz, CD_3OD): δ 170.8, 170.4, 170.2, 170.0, 169.9, 169.7, 169.7, 168.5, 168.2 (C=O); 90.7, 90.5 (C_1); 73.4, 70.8, 70.7, 68.8, 68.4, 68.2, 65.6, 65.5 (CH); 62.20, 62.16 (C_6); 21.2, 21.01, 20.92, 20.9, 20.8, 20.7, 20.6 (CH_3).

Rf = 0.75 (PE/EA = 1/1)

[134] D. Chatterjee, A. Paul, Rajkamal, S. Yadav, *RSC Adv*. **2015**, *5*, 29669-29674.

Phenyl 2,3,4,6-*tetra*-*O*-acetyl-1-thio-α-D-mannopyranoside (6*α*) and phenyl 2,3,4,6-*tetra*-*O*-acetyl-1-thio-β-D-mannopyranoside (6β)[1,135,136]

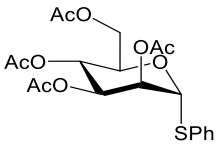

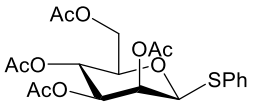

$C_{20}H_{24}O_9S$
Mw: 440.11g/mol

To a solution of **5** (9.93 g, 25.4 mmol) and PhSH (3.36 g, 30.32 mmol) in CH_2Cl_2 (50 mL), was added slowly $Et_2O.BF_3$ (4.79 mL, 38.15 mmol) at 0 °C. After 20 min at 0°C, the reaction mixture was stirred at rt for 18 h according to the general procedure **B**, affording 6.7 g (63 %) of **6α** as a colorless oil and 0.56 g (5 %) of **6β** as a white solid.

Compound **6α:**

^{1}H NMR (400 MHz, $CDCl_3$): δ 7.48-7.44 (m, 2H, H_{Ph}), 7.32-7.20 (m, 3H, H_{Ph}), 5.49-5.45 (m, 2H, H_1+H_3), 5.35-5.28 (m, 2H, H_2+H_4), 4.55-4.51 (m, 1H, H_5), 4.31 (dd, *J* = 2.0, 12.4 Hz, 1H, H_6), 4.11 (dd, *J* = 2.8, 12.4 Hz, 1H, $H_{6'}$), 2.16, 2.08, 2.06, 2.02 (4×s, 12H, H_{OAc}).

^{13}C NMR (100 MHz, $CDCl_3$): δ 170.6, 170.0, 169.9, 169.8, 132.7 (C_q); 132.1, 129.3, 128.2 (CH_{Ph}); 85.7 (C_1), 70.9 (C_3), 69.6 (C_5), 69.4 (C_2), 66.4 (C_4), 62.5 (C_6), 20.9, 20.80, 20.78, 20.7 (CH).

R_f = 0.58 (PE/EA = 2/1)

Compound **6β:**

^{1}H NMR (400 MHz, $CDCl_3$): δ 7.52-7.50 (m, 2H, H_{Ph}), 7.31-7.28 (m, 3H, H_{Ph}), 5.65 (dd, *J* = 3.6, 1.6 Hz, 1H, H_2), 5.27 (t, *J* = 10.0 Hz, 1H, H_4), 5.04 (dd, *J* = 10.0, 3.2 Hz, 1H, H_3), 4.91 (d, *J* = 0.8 Hz, 1H, H_1), 4.28 (dd, *J* = 12.0, 6.8 Hz, H_6), 4.16 (dd, *J* = 12.4, 2.0 Hz, 1H, $H_{6'}$), 3.72-3.67 (m, 1H, H_5), 2.20, 2.08, 2.03, 1.98 (4×s, 12H, H_{OAc}).

^{13}C NMR (100 MHz, $CDCl_3$): δ 170.7, 170.3, 170.2, 169.8, 133.3 (C_q); 132.1, 129.2, 128.3 (CH_{Ph}); 85.7 (C_1), 76.6 (C_5), 71.9 (C_3), 70.7 (C_2), 65.9 (C_4), 62.9 (C_6), 20.9, 20.8, 20.73, 20.68 (CH_3).

R_f = 0.57 (PE/EA = 2/1)

[135] P. Blom, B. Ruttens, S. V. Hoof, I. Hubrecht, J. V. der Eycken, *J. Org. Chem*. **2005**, *70*, 10109-10112.
[136] S. Deng, U. Gangadharmath, C-W. T. Chang, *J. Org. Chem*. **2006**, *71*, 5179-5185.

Phenyl 1-thio-α-D-mannopyranoside (7)[137]

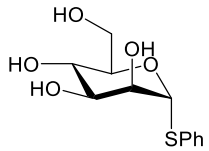

$C_{12}H_{16}O_5S$
Mw: 272.32g/mol

To a solution of **6α** (2.0 g, 4.54 mmol) in dry MeOH under Ar, was added MeONa (1 M in MeOH). After stirring 3h at rt, compound **7** (1.21 g, 98 %) was isolated as a white solid according to the general procedure **C**.

^{1}H NMR (400 MHz, CD_3OD): δ 7.54-7.51 (m, 2H, H_{Ph}), 7.30-7.24 (m, 3H, H_{Ph}), 5.42 (d, *J* = 1.2 Hz, 1H, H_1), 4.08-4.07 (m, 1H, OCH), 4.05-4.01 (m, 1H, OCH), 3.80-3.66 (m, 4H, 4xOCH).

^{13}C NMR (100 MHz, CD_3OD): δ 135.9 (C_q), 132.9, 130.1, 128.5 (CH_{Ph}); 90.5 (C_1), 75.7, 73.8, 73.2, 68.7 (CH); 62.6 (C_6).

Phenyl 6-*O*-*tert*butyldiphenylsilyl-1-thio-α-D-mannopyranoside (8)[138]

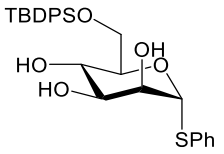

$C_{28}H_{34}O_5SSi$
Mw: 510.72g/mol

A solution of phenyl 1-thio-*α*-D-mannopyranoside **7** (757.4 mg, 2.78 mmol) and imidazole (568.0 mg, 8.34 mmol) in THF (15 mL) was treated with TBDPSCl (795 µL, 3.06 mmol) at 0 °C. After 24 h, saturated aqueous NH_4Cl was added and the mixture was extracted with CH_2Cl_2. The organic layer was washed with brine, dried over $MgSO_4$ and concentrated. The residue was purified by CombiFlash® Rf+ (CH_2Cl_2/MeOH = 9/1) to give the title compound **8** (801.2 mg, 89%) as a white foam.

^{1}H NMR (400 MHz, CD_3COCD_3): δ 7.73-7.70 (m, 4H, H_{Ph}), 7.57-7.55 (m, 2H, H_{Ph}), 7.43-7.33 (m, 6H, H_{Ph}), 7.23-7.19 (m, 3H, H_{Ph}), 5.55 (d, *J* = 0.8 Hz, 1H, H_1), 4.31 (d, *J* = 4.4 Hz, 1H, OH), 4.22-4.17 (m, 2H, OH + H_5), 4.14-4.12 (m, 1H, H_2), 4.08 (d, *J* = 6.4 Hz, 1H, OH), 4.04 (dd, *J* = 10.4, 2.4 Hz, 1H, H_6), 3.92 (dd, *J* = 10.8, 6.4 Hz, 1H, $H_{6'}$), 3.80 (td, *J* = 9.2, 5.2 Hz, 1H, H_4), 3.69 (td, *J* = 9.2, 6.4, 3.2 Hz, 1H, H_3), 1.00 (s, 9H, C*H*$_3$).

^{13}C NMR (100 MHz, CD_3COCD_3): δ 136.5, 136.3, 136.2, 134.6, 134.2 (C_q); 131.9, 130.4, 129.8, 128.5, 127.8 (CH_{Ph}), 89.7 (C_1), 75.7 (C_5), 73.3, 73.2 ($C_{2,3}$), 68.6 (C_4), 64.8 (C_6), 27.2 (CH_3), 19.8 (C_q).

R_f = 0.25 (PE/EA=1/1)

[137] M. J. Sofia, R. Kakarla, N. Kogan, R. Dulina, Y. W. Hui, N. T. Hatzenbuhler, D. Liu, A. Chen, T. Wagler, *Bioorg. Med. Chem. Lett.* **1997**, *7*, 2251-2254.
[138] A. Ishiwata, Y. J. Lee, Y. Ito, *Org. Biomol. Chem*. **2010**, *8*, 3596-3608.

Phenyl 2,3,4-tri-*O*-benzyl-6-*O*-*tert*butyldiphenylsilyl-1-thio-α-D-mannopyranoside (9)[139]

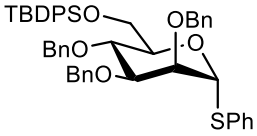

$C_{49}H_{52}O_5SSi$
Mw: 781.10 g/mol

A solution of **8** (3.32 g, 6.5 mmol) in THF (45 mL) was added to a stirred suspension of sodium hydride (60%, 936 mg, 23.4 mmol) and TBAI (480 mg, 1.3 mmol) in THF (15 mL) at 0°C. After 15 min, benzyl bromide (2.78 mL, 23.4 mmol) was added and stirring was continued at room temperature for 20 h. According to the general procedure **D**, compound **9** (3.94 g, 78 %, colorless oil) and 403 mg (10 %) of phenyl 2,3,4,6-*tetra*-*O*-benzyl-1-thio-α-D-mannopyranoside (**19**) (403 mg, 10%, colorless oil) were isolated after purification by CombiFlash® Rf+ (PE/EA = 8/2).

Compound 9:

^{1}H NMR (400 MHz, $CDCl_3$): δ 7.74-7.67 (m, 4H, H_{Ph}), 7.40-7.03 (m, 26H, H_{Ph}), 5.60 (d, *J* = 1.2 Hz, 1H, H_1), 4.94 (d, *J* = 10.8 Hz, 1H, OCH_{Ph}), 4.70-4.65 (m, 5H, 5xOCH_{Ph}), 4.19-4.15 (m, 2H, 2xOCH), 4.05-4.00 (m, 2H, 2xOCH), 3.91-3.84 (m, 2H, 2xOCH), 1.03 (s, 9H, H_{tBu})

^{13}C NMR (100 MHz, $CDCl_3$): δ 138.6, 138.4, 138.2 (C_q), 136.1, 135.7 (CH_{Ph}), 135.2 (C_q), 134.9, 134.0, 133.3, 131.0, 129.6, 129.0, 128.6, 128.5, 128.1, 128.0, 127.84, 127.76, 127.72, 127.6, 127.1 (CH_{Ph}), 85.7 (C_1), 80.4 (C_3), 76.9 (C_2), 75.5 (CH_2Ph), 74.8, 74.1 ($C_{4,5}$); 72.3, 72.1 (CH_2Ph); 63.1 (C_6), 26.9 (CH_3), 19.4 (C_q).

R_f = 0.56 (PE/EA = 8/1)

Compound **9a**:

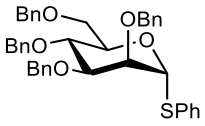

$C_{40}H_{40}O_5S$
Mw: 632.82 g/mol

^{1}H NMR (400 MHz, $CDCl_3$): δ 7.45-7.19 (m, 25H, H_{Ph}), 5.61 (d, *J* = 1.6 Hz, 1H, H_1), 4.90 (d, *J* = 10.4 Hz, 1H, OCH_{Ph}), 4.75-4.47 (m, 7H, 7xOCH_{Ph}), 4.30-4.26 (m, 1H, H_5), 4.07 (t, *J* = 1.6 Hz, 1H), 4.98-400 (m, 1H), 3.88-3.83 (m, 2H, 2xOCH), 3.75 (dd, *J* = 1.6, 10.8 Hz, 1H, OCH).

Phenyl 2,3,4-tri-*O*-benzyl-1-thio-α-D-mannopyranoside (10)[139]

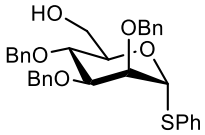

$C_{33}H_{34}O_5S$
Mw: 542.69 g/mol

A 1 M solution of TBAF (1.212 g, 3.8 mmol) in THF (10 mL) was added dropwise to a solution of **9** (1.5 g, 1.92 mmol) in THF (10 mL) at rt. After 12 h, the mixture was treated with saturated aqueous NH_4Cl solution and then extracted with CH_2Cl_2. The organic layer was dried over $MgSO_4$ and concentrated. The residue was purified by CombiFlash® Rf+ (PE/EA = 8/2) to give the title compound **10** (1.02 g, 98%) as a colorless oil.

[139] M. Heuckendorff, L. T. Poulsen, C. Hedberg, H. H. Jensen, *Org. Biomol. Chem*. **2018**, *16*, 2277-2288.

^{1}H NMR (400 MHz, $CDCl_3$): δ 7.37-7.27 (m, 20H, H_{Ph}), 5.52 (d, *J* = 2.0 Hz, 1H, H_1), 4.97 (d, *J* = 10.8 Hz, 1H, OCH_{Ph}), 4.68-4.62 (m, 5H, 5xOCH_{Ph}), 4.14-4.10 (m, 1H, H_5), 4.00 (t, *J* = 9.6 Hz, 1H, H_4), 3.90 (dd, *J* = 3.2, 9.2 Hz, 1H, H_3), 3.83-3.73 (m, 3H, $H_{2,6,6'}$).
^{13}C NMR (100 MHz, $CDCl_3$): δ 138.4, 138.2, 137.9, 134.0 (C_q), 131.9, 129.2, 128.6, 128.2, 128.1, 127.96, 127.90, 127.8 (CH), 86.1 (C_1), 80.2 (C_3), 76.5 (C_2), 75.4 (CH_2Ph), 74.9 (C_4), 73.3 (C_5), 72.5, 72.4 (CH_2Ph), 62.3 (C_6).
R_f = 0.10 (PE/EA = 5/1)

***tert*-Butyl (*E*)-2-(2-((2-hydroxyphenyl) diazenyl) phenoxy) acetate (11)**

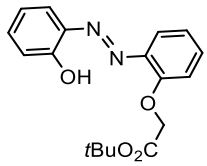

$C_{18}H_{20}N_2O_4$
Mw: 328.14g/mol

To a mixture of 2,2-dihydroxyazobenzene (1.00 g, 4.68 mmol) and K_2CO_3 (1.29 g, 9.36 mmol) in dry DMF (50 mL), was added $BrCH_2CO_2tBu$ (681 µL, 4.68 mmol) at 60 °C in an oil bath for 4h. After the completion of this reaction, it was poured into a mixture of EtOAc/H_2O (30/90 mL), and the organic phase was washed with sat NH_4Cl (3x20 mL), water (3x20 mL), brine (3x20 mL), dried over $MgSO_4$ and concentrated. The residue was purified with CombiFlash® Rf+ with Petroleum ether/EtOAc (7/3) as eluent to give **11** as a red solid (1.37 g, 89 %).

^{1}H NMR (400 MHz, $CDCl_3$): δ 7.94 (dd, *J* = 1.6, 8.0 Hz, 1H, H_{Ph}), 7.46 (dd, *J* = 2.0, 8.4 Hz, 1H, H_{Ph}), 7.33-7.29 (m, 1H, H_{Ph}), 7.09-7.01 (m, 3H, H_{Ph}), 6.82 (dd, *J* = 1.2, 8.4 Hz, 1H, H_{Ph}), 4.71 (s, 2H, OCH_2CO), 1.50 (s, 9H, *t*Bu).

^{13}C NMR (400 MHz, $CDCl_3$): δ 167.4 (CO), 154.7, 153.1, 139.4, 138.2 (Cq), 133.0, 132.9, 132.5, 121.8, 119.6, 118.5, 116.4, 113.2 (CH_{Ph}), 82.8 (C_q), 66.3 (OCH_2), 28.1 (CH_3).

R_f = 0.72 (PE/EA = 7/1)

mp: 171°C

HRMS (ESI) m/z: Calcd for $C_{18}H_{21}N_2O_4$ $[M+H]^+$: 329.1501, Found: 329.1496; Calcd for $C_{18}H_{20}N_2NaO_4$ $[M+Na]^+$: 351.1321, Found: 351.1315.

***tert*-Butyl (*E*)-2-(2-((2-(prop-2-yn-1-yloxy) phenyl) diazenyl) phenoxy) acetate (12)**

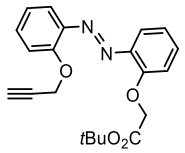

$C_{21}H_{22}N_2O_4$
Mw: 366.16 g/mol

To a solution of **11** (1.37 g, 4.18 mmol) in dry THF (40 mL) was added Cs_2CO_3 (2.72 g, 8.35 mmol). The mixture was stirred at rt for 30 min, then propargyl bromide (812 µL, 8.35 mmol) was added. After 6 hours' reaction, the mixture was neutralized to the pH 7 with HCl (1 M), then extracted with EtOAc. The organic phase was washed with brine, dried over $MgSO_4$, and concentrated to give the target compound as a red solid (1.51 g, 99 %).

^{1}H NMR (400 MHz, $CDCl_3$): δ 7.70-7.67 (m, 2H, H_{Ph}), 7.44-7.37 (m, 2H, H_{Ph}), 7.24 (dd, *J* = 1.6, 8.4 Hz, 1H, H_{Ph}), 7.09-6.99 (m, 3H, H_{Ph}), 4.94 (d, *J* = 2.0 Hz, 2H, OCH_2), 4.78 (s, 2H, OCH_2), 2.55 (t, *J* = 2.0 Hz, 1H, CH≡), 1.47 (s, 9H, *t*Bu).

^{13}C NMR (100 MHz, $CDCl_3$): δ 168.0 (CO), 155.8, 155.2, 143.6, 143.2 (C_q), 132.2, 132.1, 122.3, 122.1, 117.8, 117.7, 115.9, 115.6 (C_{Ph}), 82.4 (Cq), 76.1 (CH), 67.8 (OCH_2), 60.5, 57.9 (OCH_2); 28.1 (CH_3).

R_f = 0.59 (PE/EA = 7/1).

mp:154°C.

HRMS (ESI) m/z: Calcd for $C_{21}H_{23}N_2O_4[M+H]^{+:}$ 367.1658, Found: 367.1654; Calcd for $C_{21}H_{22}N_2NaO_4$ $[M+Na]^+$: 389.1477, Found: 389.1471.

***(E)*-2-(2-((2-(Prop-2-yn-1-yloxy) phenyl) diazenyl) phenoxy) acetic acid (13)**

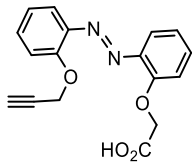

$C_{17}H_{14}N_2O_4$
Mw: 310.10 g/mol

Compound **12** (580.5 mg, 1.59 mmol) was dissolved in a solution (30 mL) of CH_2Cl_2 containing 20 % TFA at 0 °C. The reaction was stirred at 0 °C for 30 min, then at rt for 25 h. After evaporation, the residue was dissolved in EtOAc (20 mL), washed with water (3x20 mL), then concentrated to afford **13** as a red solid (490.8 mg, 100 %).

^{1}H NMR (400 MHz, $CDCl_3$): δ 7.82 (dd, *J* = 1.6, 8.0 Hz, 1H, H_{Ph}), 7.61 (dd, *J* = 2.0, 8.4 Hz, 1H, H_{Ph}), 7.52-7.47 (m, 2H, H_{Ph}), 7.28-7.26 (m, 2H, H_{Ph}), 7.17 (dd, *J* = 1.2, 8.4 Hz, 1H, H_{Ph}), 7.14-7.10 (m, 1H, H_{Ph}), 4.94 (d, *J* = 2.0 Hz, 2H, OCH_2), 4.86 (s, 2H, OCH_2), 2.56 (t, *J* = 2.4 Hz, 1H, CH≡).

^{13}C NMR (100 MHz, $CDCl_3$): δ 170.1 (CO), 155.0, 154.0, 143.2, 142.7 (C_q), 133.3, 133.0, 124.5, 122.2, 118.4, 118.0, 115.0 (CH_{Ph}), 78.2 (C≡CH), 76.5 (C≡CH), 70.0, 57.2 (OCH_2).

R_f = 0.59 (PE/EA =7/1).

mp: 152°C.

HRMS (ESI) m/z: Calcd for $C_{17}H_{15}N_2O_4[M+H]^+$: 311.1032, Found: 311.1028; Calcd for $C_{17}H_{14}N_2NaO_4$ [M+Na]+: 333.0851, Found: 333.0846.

Methyl 2,3-di-*O*-benzyl-6-*O*-[(E)-(2-(2-(prop-2-yn-1-yloxy)phenyl) diazenyl)phenoxy)]acetyl-α-D-glucopyranoside (15)

Methyl 2,3-di-*O*-benzyl-4-*O*-[(*E*)-(2-(2-(prop-2-yn-1-yloxy) phenyl)diazenyl)phenoxy)]acetyl-α-D-glucopyranoside (16)

Methyl 2,3-di-*O*-benzyl-4,6-di-*O*-[2-((*E*)-(2-(prop-2-yn-1-yloxy)phenyl)diazenyl)phenoxy]acetyl-α-D-glucopyranoside (17)

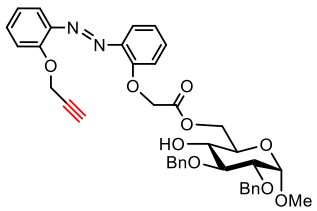

15

$C_{38}H_{38}N_2O_9$
Mw: 666.73 g/mol

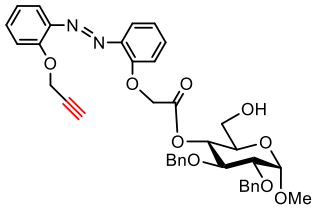

16

$C_{38}H_{38}N_2O_9$
Mw: 666.73 g/mol

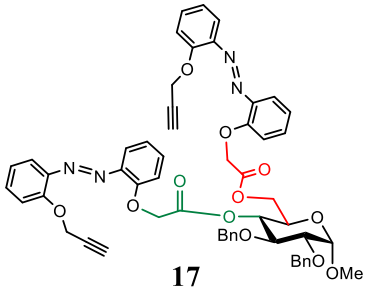

17

$C_{55}H_{50}N_4O_{12}$
Mw: 959.02 g/mol

To a solution of **13** (590 mg, 1.9 mmol) and methyl 2,3-di-*O*-benzyl-α-D-glucopyranoside **14**[111] (714 mg, 1.9 mmol) in anhydrous CH_2Cl_2 was added a solution of the EDC (582 mg, 3.0 mmol) and DMAP (24 mg, 0.19 mmol) in dry CH_2Cl_2 at 0°C. The solution was stirring (0 °C to rt) for 14h. according to the general procedure **E**. The residue was purified by flash chromatography (CH_2Cl_2/EtOAc = 8/2) to afford **15** (540 mg, 41 %), **16** (195 mg, 15 %) and **17** (154 mg, 17 %) as red solids.

Compound **15**:

^{1}H NMR (400 MHz, $CDCl_3$): δ 7.65 (dd, *J* = 2.0, 8.0 Hz, 2H, H_{Ph}), 7.35-7.26 (m, 13H, H_{Ph}), 7.06-7.00 (m, 3H, H_{Ph}), 4.98 (d, *J* = 11.6 Hz, 1H, OCH_{Ph}), 4.93-4.92 (m, 4H, 2×OCH_2), 4.74 (d, *J* = 12.4 Hz, 1H, OCH_{Ph}), 4.69 (d, *J* = 11.6 Hz, 1H, OCH_{Ph}), 4.63 (d, *J* = 12.0 Hz, 1H, OCH_{Ph}), 4.54 (d, *J* = 3.6 Hz, 1H, H_1), 4.44 (dd, *J* = 12.0, 4.8 Hz, 1H, H_6), 4.38 (dd, *J* = 12.4, 2.8 Hz, 1H, $H_{6'}$), 3.76-3.72 (m, 2H, H_5+H_3), 3.41 (dd, *J* = 9.2, 3.2 Hz, 1H, H_2), 3.36-3.34 (m, 1H, H_4), 3.30 (m, 3H, OMe), 2.54 (t, *J* = 2.1 Hz, 1H, C≡CH), 2.29 (d, *J* = 2.4 Hz, 1H, OH).

^{13}C NMR (100 MHz, $CDCl_3$): δ 169.1 (CO), 155.5, 155.1, 143.4, 143.3, 138.7, 138.0 (C_q); 132.2, 132.1, 128.7, 128.6, 128.0, 122.5, 122.2, 117.9, 117.7, 116.0, 115.8 (CH_{Ph}); 98.2 (C_1), 81.1, 79.6 (CH); 77.5 (C≡CH), 76.2 (C_q), 75.4, 73.2 (OCH_2Ph); 69.8, 68.9 (CH); 67.5, 63.9, 57.8 (OCH_2); 55.3 (OCH_3).

R_f = 0.77 (PE/EA = 5/5)

$[\alpha]_D$: +51.7 (c = 0.25, CH_2Cl_2)

mp: 82°C

HRMS (ESI) m/z: Calcd for $C_{38}H_{39}N_2O_9$ $[M+H]^+$: 667.2656, Found: 667.2650.

Compound **16**:

^{1}H NMR (400 MHz, $CDCl_3$): δ 7.67-7.61 (m, 2H, H_{Ph}), 7.45-7.41 (m, 1H, H_{Ph}), 7.34-7.26 (m, 12H, H_{Ph}), 7.09-7.04 (m, 2H, H_{Ph}), 6.88 (dd, *J* = 8.4, 0.8 Hz, 1H, H_{Ph}), 4.99 (t, *J* = 9.6 Hz, 1H, H_3), 4.94-4.93 (m, 2H, OCH_2C≡CH), 4.89 (d, *J* = 12.0 Hz, 1H, OCH_{Ph}), 4.80-4.75 (m, 2H, OCH), 4.66-4.63 (m, 2H, 2×OCH_{Ph}), 4.61-4.59 (m, 2H, H_1+ OCH), 3.99 (t, *J* = 9.6 Hz, 1H, H_4), 3.63-3.55 (m, 3H, $H_{2,6,6'}$), 3.51-3.46 (m, 1H, H_5), 3.37 (s, 3H, OCH_3), 2.54 (t, *J* = 2.0 Hz, 1H, C≡CH), 2.31-2.32 (m, 1H, OH).

^{13}C NMR (100 MHz, $CDCl_3$): δ 169.2 (CO), 155.3, 155.1, 143.4, 143.3, 138.6, 137.8 (C_q), 132.3, 132.2, 128.6, 128.5, 128.2, 127.8, 122.2, 117.9, 117.6, 115.8, 115.7 (CH_{Ph}); 98.2 (C_1), 79.5, 78.7, 77.3 (CH); 76.2 (C_q), 75.5, 73.6 (OCH_2), 71.4, 69.3 (CH); 67.3, 61.1, 57.7 (OCH_2); 55.5 (OCH_3).
R_f = 0.36 (PE/EA = 5/5)
$[\alpha]_D$: +49.9 (c = 0.5, CH_2Cl_2)
mp: 78°C
HRMS (ESI) m/z: Calcd for $C_{38}H_{39}N_2O_9$ $[M+H]^+$: 667.2656, Found: 667.2650.

Compound **17**:

^{1}H NMR (400 MHz, $CDCl_3$): δ 7.67-7.62 (m, 4H, H_{Ph}), 7.43-7.39 (m, 2H, H_{Ph}), 7.34-7.18 (m, 15H, H_{Ph}), 7.07-6.96 (m, 4H, H_{Ph}), 6.84 (d, *J* = 8.4 Hz, 1H, H_{Ph}), 5.10 (t, *J* = 9.6 Hz, 1H, H_4), 4.94-4.86 (m, 7H), 4.79-4.72 (m, 2H), 4.63-4.57 (m, 3H), 4.55 (d, 1H, *J* = 3.2 Hz, H_1), 4.28 (dd, *J* = 12.4, 5.2 Hz, 1H, H_6), 4.14-4.10 (m, 1H, $H_{6'}$), 3.93 (t, *J* = 9.2 Hz, 1H, H_3), 3.88-3.84 (m, 1H, H_5), (dd, *J* = 9.6, 3.2 Hz, 1H, H_2), 3.31 (s, 3H, OCH_3), 2.54-2.52 (m, 2H, 2xC≡CH).
^{13}C NMR (100 MHz, $CDCl_3$): δ 169.1, 162.6, 155.5, 155.1 143.4, 143.2, 138.7, 138.0 (C_q), 132.2, 132.1, 128.6, 128.5, 128.1, 128.0, 128.0, 127.9, 127.7, 122.4, 122.2 117.8, 117.7, 115.9, 115.7 (CH_{Ph}); 98.1 (C_1), 81.2, 79.5 (CH); 78.6 (C_q); 76.2, 75.4, 73.2 (OCH_2); 69.9, 69.0 (OCH); 67.4, 64.0, 57.7 (OCH_2); 55.3 (OCH_3).
R_f = 0.88 (PE/EA = 5/5)
$[\alpha]_D$: +101.9 (c = 0.5, CH_2Cl_2)
mp: 74°C;
HRMS (ESI) m/z: Calcd for $C_{55}H_{51}N_4O_{12}$ $[M+H]^+$: 959.3503, Found: 959.3490; Calcd for $C_{55}H_{51}N_4NaO_{12}$ $[M+Na]^+$: 981.3323, Found: 981.3317.

Phenyl 6-azide-2,3,4-tri-*O*-benzyl-6-deoxy-1-thio-α-D-mannopyranoside (18)[140]

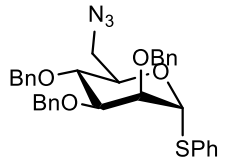

$C_{33}H_{33}N_3O_4S$
Mw: 567.70 g/mol

To the solution of **10** (1.12 g, 2.06 mmol) and Et_3N (580 µL, 4.1 mmol) in CH_2Cl_2 (18 mL) was added MsCl (260 µL, 3.3 mmol) at 0 °C. The solution was stirring for 20h at rt before addition of methanol (280 µL). The solution was concentrated, then dissolved in 30 mL EtOAc, washed with water (30 mL), saturated aqueous $NaHCO_3$ (2×20 mL) and brine (2×20 mL), then dried over $MgSO_4$ and concentrated to an oil which was used directly without purification. To the crude product dissolved in 25 mL of DMF, was added NaN_3 (805 mg, 12.38 mmol). The reaction was heated at 90 °C for 20h, and then cooled down to rt and diluted with 30 mL water, causing the formation of a white precipitate. The solution was extracted with ether (3×20 mL) and the combined organic layers were washed with brine (30 mL), dried over $MgSO_4$ and concentrated. Purification by CombiFlash® Rf+ (PE/EA = 9/1) afforded **18** (1.2 g, 92 %) as a colorless oil.

^{1}H NMR (400MHz, $CDCl_3$): δ 7.41-7.28 (m, 20H, H_{Ph}), 5.55 (d, *J* = 1.6 Hz, 1H, H_1), 4.97 (d, *J* = 10.8 Hz, 1H, OCH), 4.72 (d, *J* = 12.4 Hz, 1H, OCH), 4.66 (d, *J* = 12.8 Hz, 1H, OCH), 4.61 (d, *J* = 11.2 Hz, 1H, OCH), 4.60 (s, 2H, OCH_2), 4.23 (ddd, *J* = 2.8, 5.6, 9.2 Hz, 1H, H_5), 4.01 (dd, *J* = 2.0, 3.2 Hz, 1H, H_2), 3.96 (t, *J* = 9.2 Hz, 1H, H4), 3.85 (dd, *J* = 8.8, 3.2 Hz, 1H, H_3), 3.48 (dd, *J* = 2.8, 13.2 Hz, 1H, H_6), 3.43 (dd, *J* = 5.6, 13.2 Hz, 1H, $H_{6'}$).

^{13}C NMR (100 MHz, $CDCl_3$): δ 138.2, 138.0, 137.8, 134.1 (C_q), 131.5, 129.2, 128.5, 128.5, 128.1, 128.0, 127.9, 127.6 (CH_{Ph}); 85.7 (C_1), 80.1 (C_3), 76.1 (C_2), 75.5 (C_4), 75.5 (CH_2-Ph), 72.6 (C_5), 72.1 (CH_2-Ph), 51.5 (C_6).

R_f = 0.84 (PE/EA = 6/1)

$[\alpha]_D$: +46.8 (c = 1.0, CH_2Cl_2)

HRMS (ESI) m/z: Calcd for $C_{33}H_{35}O_5S$ $[M+H]^+$: 543.2205, Found: 543.2201

[140] L. Yan, D. Kahne, *J. Am. Chem. Soc*. **1996**, *118*, 9239-9248.

Phenyl 6-*O*-azidoacetyl-2,3,4-tri-*O*-benzyl-1-thio-α-D-mannopyranoside (19)

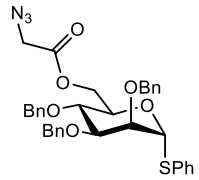

$C_{35}H_{35}N_3O_6S$
Mw: 625.74 g/mol

To a solution of **10** (201.8 mg, 0.372 mmol) and Et_3N (205 µL, 1.475 mmol) in CH_2Cl_2 (15 mL) at 0 °C, was added chloroacetyl chloride (60 µL, 0.738 mmol). The mixture was stirred for 2h at 0°C and at rt overnight. After evaporation of the solvent, the residue was dissolved in EtOAc (20 mL). The organic layer was washed with saturated aqueous $NaHCO_3$ (3x10 mL) and brine (3x10 mL), then dried over $MgSO_4$ and concentrated under vacuum to give the crude product, which was used without purification in the next step. To a solution of crude 6-*O*-chloroacetyl mannopyranoside in acetone (10 mL), were added NaN_3 (121 mg, 1.86 mmol) and KI (12 mg, 0.074 mmol). After stirring for 24h at room temperature, the mixture was evaporated. The residue was dissolved in EtOAc (20 mL), washed with saturated aqueous $NaHCO_3$ (3 x 10 mL) and brine (3 x 10 mL), then dried over $MgSO_4$ and concentrated under vacuum to give the crude product which was purified by column chromatography (PE/EA = 9:1) to afford the target compound **19** (150 mg, 64%) as a white solid.

^{1}H NMR (400 MHz, $CDCl_3$): δ 7.37-7.24 (m, 20H, H_{Ph}), 5.54 (d, *J* = 2.0 Hz, 1H, H_1), 4.94 (d, *J* = 11.2 Hz, 1H, OCH), 4.69 (d, *J* = 12.4 Hz, 1H, OCH), 4.64-4.58 (m, 4H, 4xOCH), 4.40-4.39 (m, 2H, H_6, $H_{6'}$), 4.30-4.25 (m, 1H, H_5), 4.00-3.99 (m, 1H, H_2), 3.93 (t, *J* = 9.2 Hz, 1H, H_4), 3.87 (dd, *J* = 9.2, 2.8 Hz, 1H, H_3), 3.74 (d, *J* = 16.8 Hz, 1H, CHN_3), 3.67 (d, *J* = 16.8 Hz, 1H, CHN_3).

^{13}C NMR (100 MHz, $CDCl_3$): δ 168.2 (CO), 138.1, 138.0, 137.8 (C_q); 131.5, 129.1, 128.6, 128.5, 128.3, 128.0, 127.9, 127.6 (CH_{Ph}); 85.5 (C_1), 80.2 (C_3), 75.9 (C_2), 75.3 (CH_2-Ph), 74.2 (C_4), 72.1 (CH_2-Ph), 70.7 (C_5), 64.6 (C_6), 50.1 (CH_2N_3).

R_f = 0.53 (PE/EA = 6/1)

$[\alpha]_D$: +101.9 (c = 0.5, CH_2Cl_2)

mp: 88°C

HRMS (ESI) m/z: Calcd for $C_{35}H_{36}N_3O_6S$ $[M+H]^+$: 626.2325, Found: 626.2319.

Glycosyl donor-acceptor pair *E*-1

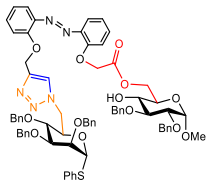

$C_{71}H_{71}N_5O_{13}S$
Mw: 1234.43 g/mol

To a solution of **18** (291 mg, 0.51 mmol) and **15** (342 mg, 0.51 mmol) in CH_2Cl_2/H_2O (4/1, 10.5 mL), were added $CuSO_4.5H_2O$ (130 mg, 0.5 mmol) and ascorbic acid (182 mg, 1.02 mmol) according to the general procedure **F**. The residue was purified by flash chromatography (PE/EA = 5/5) to afford ***E*-1** (543 mg, 86 %) as a red solid.

^{1}H NMR (400 MHz, $CDCl_3$): δ 7.63 (s, 1H, CH-triazole), 7.59 (dd, *J* = 7.6, 2.4 Hz, 1H, H_{Ph}), 7.56 (dd, *J* = 8.0, 1.6 Hz, 1H, H_{Ph}), 7.37-7.26 (m, 27 H, H_{Ph}), 7.16-7.13 (m, 6H, H_{Ph}), 7.01-6.96 (m, 2H, H_{Ph}), 6.93-6.90 (m, 1H, H_{Ph}), 5.47 (d, *J* = 1.6 Hz, 1H, $H_{1'}$), 5.32 (d, *J* = 12.4 Hz, 1H, OCH_{Ph}), 5.26 (d, *J* = 12.4 Hz, 1H, OCH_{Ph}), 4.97 (d, *J* = 11.2 Hz, 1H, OCH_{Ph}), 4.94 (d, *J* = 10.8 Hz, 1H, OCH_{Ph}), 4.89 (s, 2H, OCH_2 Ph), 4.76-4.53 (m, 10H, 10×OCH), 4.54 (d, *J* = 4.0 Hz, 1H, H_1), 4.44-4.36 (m, 3H, 3xOCH), 3.96-3.95 (m, 1H, $H_{2'}$), 3.88 (dd, *J* = 9.2, 3.2 Hz, 1H, OCH), 3.76-3.70 (m, 2H, 2xOCH), 3.66 (t, *J* = 9.2 Hz, 1H, OCH), 3.41 (dd, *J* = 9.6, 3.6 Hz, 1H, H_2), 3.41-3.33 (m, 1H, OCH), 3.30 (m, 3H, OCH_3).

^{13}C NMR (100 MHz, $CDCl_3$): δ 169.1 (CO), 155.9, 155.5, 144.0, 143.3, 138.7, 138.0, 138.0, 137.8, 137.6 (C_q); 133.1, 132.4, 132.0, 131.8, 129.2, 128.7, 128.6, 128.5, 128.3, 128.1, 128.0, 127.9, 127.8 (CH); 124.5 (CHtriazole), 122.5, 121.7, 117.7, 116.2, 115.5 (CH); 98.2 (C_1), 85.8 ($C_{1'}$), 81.1, 80.1 (CH); 79.5 (C_2), 75.9 ($C_{2'}$),; 75.5, 75.3 (OCH_2Ph); 75.0 (CH), 73.2, 72.2, 72.1 (OCH_2Ph); 71.5, 69.9, 69.0 (CH); 67.5, 64.1, 63.9 (OCH_2); 55.4 (OCH_3), 50.9 (OCH_2).

Rf = 0.35 (PE/EA = 5/5)

$[\alpha]_D$: +46.3 (c = 0.5, CH_2Cl_2)

mp: 76°C

HRMS (ESI) m/z: Calcd for $C_{71}H_{72}N_5O_{13}S$ $[M+H]^+$: 1234.4847, Found: 1234.4842.

Glycosyl donor-acceptor pair *Z*-1 at PSS_{365}

^{1}H NMR (400 MHz, $CDCl_3$): δ 7.51 (s, 1H), 7.37-7.12 (m, 29 H, H_{Ph}), 7.02-6.98 (m, 1H), 6.94-6.90 (m, 1H), 6.85 (d, *J* = 8.0 Hz, 1H), 6.76-6.72 (m, 1H), 6.67-6.62 (m, 4H), 6.42 (dd, *J* = 8.8, 1.6 Hz, 1H), 5.49 (d, *J* = 2.0 Hz, 1H), 4.97-4.91 (m, 4H), 4.75-4.55 (m, 14H), 4.43 (dd, *J* = 12.0, 4.4 Hz, 1H), 4.40-4.37 (m, 1H), 4.32 (dd, *J* = 12.0, 2.4 Hz, 1H), 3.94-3.93 (m, 1H), 3.87 (dd, *J* = 9.2, 2.4 Hz, 1H), 3.77-3.70 (m, 2H), 3.64 (t, *J* = 9.6 Hz, 1H), 3.44-3.40 (m, 2H), 3.30 (s, 3H, OCH_3).

^{13}C NMR (100 MHz, $CDCl_3$): δ 168.7, 148.6, 148.2, 144.5, 138.9, 138.1, 137.9, 137.7, 133.2, 131.9, 131.8 (C_q); 129.3, 128.6, 128.4, 128.2, 128.0, 127.9 (CH); 124.8, 121.5, 121.1, 119.4, 118.9, 113.5 (CH); 98.3, 85.7, 81.3, 80.1, 79.6, 75.9 (CH); 75.6, 75.4 (CH_2); 75.1 (CH), 73.3, 72.3, 72.2 (CH_2); 71.5, 69.8, 69.2 (CH); 65.9, 64.1, 62.6 (CH_2); 55.5 (OCH_3), 51.0 (NCH_2).

R = 0.2 (PE/EA = 5/5)

Glycosyl donor-acceptor pair *E*-2

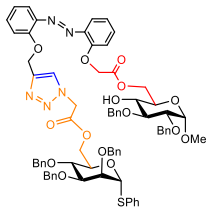

$C_{73}H_{73}N_5O_{15}S$
Mw: 1292.47 g/mol

To a solution of **19** (254 mg, 0.4 mmol) and **15** (268 mg, 0.4 mmol) in CH_2Cl_2/H_2O (4/1, 12.5 mL), were added $CuSO_4$.$5H_2O$ (50 mg, 0.2 mmol) and ascorbic acid (71 mg, 0.4 mmol) according to the general procedure **F**. The residue was purified by flash chromatography (PE/EA = 5/5) to get the product ***E*-2** (448 mg, 85 %) as a red solid.

^{1}H NMR (400 MHz, $CDCl_3$): δ 7.65 (s, 1H, CH-triazole), 7.64-7.60 (m, 2H, H_{Ph}), 7.39-7.26 (m, 33H, H_{Ph}), 7.02-6.99 (m, 3H, H_{Ph}), 5.55 (d, *J* = 1.6 Hz, 1H, $H_{1'}$), 5.43 (s, 2H, OCH_2) 4.99-4.90 (m, 7H, 5×OCH_{Ph}+OCH_2), 4.75-4.60 (m, 8H, 6×OCHPh+OCH_2), 4.55 (d, *J* = 3.6 Hz, 1H, H_1), 4.54 (d, *J* = 10.8 Hz, 1H, OCH_{Ph}), 4.42-4.31 (m, 4H, 4×OCH), 4.28-4.25 (m, 1H), 3.99-3.97 (broad s, 1H, $H_{2'}$), 3.88-3.87 (m, 2H), 3.76-3.70 (m, 2H), 3.41 (dd, *J* = 9.6, 3.6 Hz, 1H, H_2), 3.38-3.32 (m, 1H), 3.30 (s, 3H, OCH_3), 2.42 (d, *J* = 3.2 Hz, 1H, OH).

^{13}C NMR (100 MHz, $CDCl_3$): δ 169.2, 165.9 (CO); 155.6, 155.4, 144.7, 143.4, 143.3, 133.9 (C_q); 132.4, 132.0, 131.4, 129.2, 128.7, 128.6, 128.2, 128.1, 128.0, 127.9, 127.7 (CH); 124.5 ($CH_{triazole}$), 122.5, 121.9, 118.0, 117.9, 116.1, 115.7 (CH); 98.2 (C_1), 85.4 ($C_{1'}$), 81.2, 80.2 (CH); 79.5 (C_2), 75.9 ($C_{2'}$), 75.5, 75.2 (OCH_2Ph); 74.1 (CH), 73.2, 72.2, 72.1 (OCH_2Ph); 70.7, 69.9, 69.0 (CH); 67.5, 64.9, 64.0, 63.9 (OCH_2); 55.3 (OCH_3), 50.6 (CH_2N).

R_f = 0.28 (PE/EA = 5/5)

$[\alpha]_D$: +70.9 (c = 0.5, CH_2Cl_2)

mp: 78°C

HRMS (ESI) m/z: Calcd for $C_{73}H_{74}N_5O_{15}S$ $[M+H]^+$: 1292.4902, Found: 1292.4897.

Glycosyl donor-acceptor pair *Z*-2 at PSS_{365}

^{1}H NMR (400 MHz, $CDCl_3$): δ 7.60 (s, 1H), 7.41-7.25 (m, H), 7.08-7.04 (m, 1H), 6.98 (td, *J* = 8.0, 1.6 Hz, 1H), 6.90 (d, *J* = 8.8 Hz, 1H), 6.80 (t, *J* = 7.6 Hz, 1H), 6.72 (dd, *J* = 8.0, 1.6 Hz, 1H), 6.69 (d, *J* = 7.6 Hz, 2H), 6.46 (dd, *J* = 7.6, 1.6 Hz, 1H), 5.58 (d, *J* = 1.6 Hz, 1H), 5.14 (d, *J* = 15.6 Hz, 1H), 5.10 (d, *J* = 15.6 Hz, 1H), 4.99-4.87 (m, 5H), 4.77-4.55 (m, 11H), 4.47-4.42 (m, 2H), 4.73-4.32 (m, 2H), 4.28-4.25 (m, 1H), 4.00-3.99 (m, 1H), 3.92-3.87 (m, 2H), 3.79-3.73 (m, 2H), 3.47-3.43 (m, 2H), 3.32 (s, 3H, OCH_3), 2.95 (d, *J* = 4.0 Hz, 1H).

^{13}C NMR (100 MHz, $CDCl_3$): δ 168.8, 166.1, 148.9, 147.9, 144.5, 144.4, 144.3, 138.9, 138.2, 138.1, 138.0, 137.9, 133.9 (Cq); 131.4, 129.3, 128.6, 128.2, 128.1, 127.9, 127.3, 124.7, 121.6, 121.2, 119.8, 118.8, 113.8, 113.5, 98.3, 85.4, 81.3, 80.2, 79.5, 77.3 (CH); 75.9, 75.5 (CH_2); 74.1 (CH), 73.3, 72.2, 72.1 (CH_2); 70.7, 69.7, 69.1 (CH); 66.0, 65.0, 63.9, 62.6 (CH_2); 55.5 (OCH_3), 50.6 (CH_2N).

Rf = 0.15 (PE/EA = 5/5)

Glycosyl donor-acceptor pair *E*-3

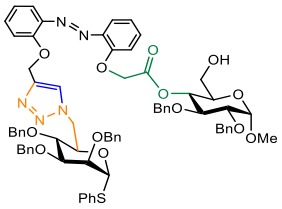

$C_{71}H_{71}N_5O_{13}S$
Mw: 1234.43 g/mol

To a solution of **18** (230 mg, 0.4 mmol) and **16** (270 mg, 0.4 mmol) in CH_2Cl_2/H_2O (8/2 mL), were added $CuSO_4{\cdot}5H_2O$ (51 mg, 0.2 mmol) and ascorbic acid (71 mg, 0.4 mmol) according to the general procedure **F**. The residue was purified by CombiFlash® Rf+ (PE/EA = 5/5) to get the desired product (420 mg, 84 %) as a red solid.

^{1}H NMR (400 MHz, $CDCl_3$): δ 7.64 (s, 1H, CH-triazole), 7.60-7.58 (m, 2H, H_{Ph}), 7.39-7.26 (m, 27H, H_{Ph}), 7.22-7.12 (m, 6H, H_{Ph}), 7.00 (td, *J* = 8.4, 1.2 Hz, 1H, H_{Ph}), 6.94 (td, *J* = 7.8, 1.2 Hz, 1H, H_{Ph}), 6.85 (dd, *J* = 8.0, 1.2 Hz, 1H, H_{Ph}), 5.46 (d, *J* = 1.6 Hz, 1H, $H_{1'}$), 5.32 (d, *J* = 12.4 Hz, 1H), 5.26 (d, *J* = 12.4 Hz, 1H), 5.01-4.87 (m, 2H), 4.80-4.55 (m, 14H), 4.45-4.40 (m, 1H), 4.00 (d, *J* = 12.4 Hz, 1H), 3.96-3.95 (m, 1H), 3.88 (dd, *J* = 9.6, 3.2 Hz, 1H), 3.68 (t, *J* = 9.6 Hz, 1H), 3.61-3.54 (m, 3H), 3.50-3.46 (m, 1H), 3.36 (s, 3H, OCH_3), 2.35-2.31 (m, 1H, OH).

^{13}C NMR (100 MHz, $CDCl_3$): δ 169.3 (CO), 156.1, 155.4, 144.1, 143.2, 138.6, 138.1, 137.9, 137.7 (C_q); 133.2, 132.6, 132.1, 131.9, 128.6, 128.5, 128.3, 128.0, 127.9, 127.8 (CH); 124.5 ($CH_{triazole}$), 122.6, 121.7, 117.7, 117.5, 115.9, 115.6 (CH); 98.3 (C_1), 85.9 ($C_{1'}$), 80.1, 79.6, 78.8, 75.9 (CH); 75.5, 75.4 (OCH_2Ph); 75.1 (CH), 73.6, 72.3, 72.2 (OCH_2Ph); 71.6, 71.5, 69.4 (CH); 67.3, 64.1, 61.2 (OCH_2); 55.6 (OCH_3), 51.0 ($C_{6'}$).

R_f = 0.35 (PE/EA = 5/5)

$[\alpha]_D$: +41.9 (*c* = 0.5, CH_2Cl_2)

mp: 82°C

HRMS (ESI) m/z: Calcd for $C_{71}H_{72}N_5O_{15}S$ $[M+H]^+$: 1234.4847, Found: 1234.4842.

Glycosyl donor-acceptor pair *Z*-3 at PSS_{365}

Rf = 0.22 (PE/EA = 5/5)

Glycosyl donor-acceptor pair *E*-4

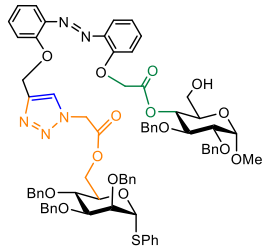

$C_{73}H_{73}N_5O_{15}S$
Mw: 1292.47 g/mol

To a solution of **19** (206 mg, 0.33 mmol) and **16** (219 mg, 0.33 mmol) in CH_2Cl_2/H_2O (7/1.4 mL), were added $CuSO_4{\cdot}5H_2O$ (41 mg, 0.16 mmol) and ascorbic acid (182 mg, 1.02 mmol) according to the general procedure **F**. The residue was purified by CombiFlash® Rf+ (PE/EA = 5/5) to get the desired product (301 mg, 71 %) as a red solid.

^{1}H NMR (400 MHz, $CDCl_3$): δ 7.67 (s, 1H, CH-triazole), 7.63-7.61 (m, 3H, H_{Ph}), 7.35-7.18 (m, 32H, H_{Ph}), 7.03-7.00 (m, 2H, H_{Ph}), 6.86 (d, *J* = 9.2 Hz, 1H, H_{Ph}), 5.55 (s, 1H, $H_{1'}$), 5.45 (s, 2H, OCH_2), 5.02-4.91 (m, 4H, NCH, 3xOCH), 4.88 (d, *J* = 12.0 Hz, 1H, NCH), 4.79 (d, *J* = 12.0 Hz, 1H, OCH), 4.79-4.69 (m, 2H), 4.65-4.58 (m, 7H, 4xOCH, OCH_2, H_1), 4.55 (d, *J* = 11.6 Hz, 1H, OCH), 4.43 (dd, *J* = 11.6, 2.0 Hz, 1H), 4.35 (dd, *J* = 11.6, 1.2 Hz, 1H), 4.36-4.32 (m, 1H), 4.28-4.24 (m, 1H), 4.01-3.96 (m, 2H), 3.88-3.87 (m, 2H), 3.61-3.55 (m, 3H), 3.48-3.46 (m, 1H), 3.32 (s, 3H, OCH_3), 2.36-2.33 (m, 1H, OH).

^{13}C NMR (100 MHz, $CDCl_3$): δ 169.2, 165.9 (CO); 155.8, 155.3, 144.7, 143.4, 143.3, 137.9, 137.9, 137.8, 137.7 (C_q); 133.9, 132.5, 132.1, 131.5, 129.2, 128.6, 128.3, 128.2, 128.1, 127.9, 127.8, 127.8, 127.7, 124.6, 122.7, 121.8, 117.9, 115.9, 115.7 (CH); 98.2 (C_1), 85.4 ($C_{1'}$), 80.2, 79.6, 78.7, 75.9 (CH); 75.5, 75.2 (OCH_2Ph); 74.1 (CH), 73.6, 72.2, 72.1 (OCH_2Ph); 71.4, 70.7, 69.3 (CH); 67.3, 65.0, 64.0, 61.1 (OCH_2); 55.5 (OCH_3), 50.6 (OCH_2).

R_f = 0.28 (PE/EA=5/5)

$[\alpha]_D$: +129.1 (*c* = 0.5, CH_2Cl_2)

mp: 79°C

HRMS (ESI) m/z: Calcd for $C_{73}H_{74}N_5O_{15}S$ $[M+H]^+$: 1292.4902, Found: 1292.4897.

Glycosyl donor-acceptor pair *Z*-4 at PSS_{365}

Rf = 0.20 (PE/EA = 5/5)

Glycomacrocycle *E*-20*α*

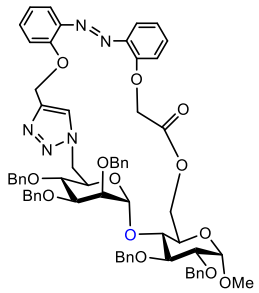

$C_{65}H_{65}N_5O_{13}$
Mw: 1123.46 g/mol

A mixture of glycosyl donor-acceptor pair ***E*-1** (50 mg, 0.04 mmol) in CH_2Cl_2 (1.0 mL) was treated with 4Å molecular sieve, NIS (18 mg, 0.08 mmol) and TfOH (1.8 µL, 0.02 mmol) according to the general procedure **G**. The residue was purified by CombiFlash® Rf+ (PE/EA 7/3 - 5/5) to give the desired macrocycle ***E*-20*α*** (23 mg, 50 %) as a red solid.

^{1}H NMR (400 MHz, $CDCl_3$): δ 7.82 (s, 1H, CH-triazole), 7.64-7.63 (m, 2H, H_{Ph}), 7.33-7.26 (m, 25H, H_{Ph}), 7.17-7.10 (m, 3H, H_{Ph}), 6.92-6.88 (m, 3H, H_{Ph}), 5.35 (d, *J* = 12.0 Hz, 1H, OCH), 5.14-5.11 (m, 2H, 2xOCH), 4.95-4.87 (m, 6H), 4.73 (d, *J* = 12.0 Hz, 1H, OCH_{Ph}), 4.67 (d, *J* = 3.6 Hz, 1H, H_1), 4.66 (d, *J* = 12.0 Hz, 1H, OCH_{Ph}), 4.57-4.42 (m, 6H, $H_{1'}$ + 5xOCH), 4.19-4.14 (m, 2H), 3.84-3.70 (m, 4H), 3.63-3.48 (m, 4H), 3.42 (m, 3H, OCH_3).

^{13}C NMR (100 MHz, $CDCl_3$): δ 169.3 (C=O); 154.2, 151.4, 143.9, 143.8, 143.2, 138.7, 138.6, 138.2, 137.6 (C_q); 131.8, 131.5, 128.7, 128.5, 128.4, 128.3, 128.1, 127.7, 122.3, 121.7, 119.4, 115.3, 115.0 (CH); 103.1 ($C_{1'}$); 98.1 (C_1); 80.7, 80.4, 79.7, 79.2, 76.1 (CH); 75.5, 75.2, 75.1 (OCH_2Ph); 75.0, 73.6 (CH); 73.2, 72.3 (OCH_2Ph); 71.8 (CH); 70.6 (OCH_2Ph), 67.8 (CH), 66.7, 64.7(O**C**H_2); 63.8 (C_6); 55.8 (OCH_3); 48.9 ($C_{6'}$).

R_f = 0.67 (PE/EA=5/5)

$[\alpha]_D$: +563.32 (*c* = 0.5, CH_2Cl_2)

mp: 102°C;

HRMS (ESI) m/z: Calcd for $C_{65}H_{66}N_5O_{13}[M+H]^+$: 1124.4657, Found: 1124.4652.

Glycomacrocycle *Z*-20*α* at PSS_{365}

^{1}H NMR (400 MHz, $CDCl_3$): δ 7.40-7.14 (m, 26H), 7.02-6.99 (m, 2H), 6.91-6.78 (m, 4H), 6.68 (dd, *J* = 8.0, 2.0 Hz, 1H), 5.16 (d, *J* = 12.8 Hz, 1H), 5.10 (d, *J* = 11.6 Hz, 1H), 5.01 (d, *J* = 13.2 Hz, 1H), 4.97 (d, *J* = 10.8 Hz, 1H), 4.88-4.85 (m, 2H), 4.67-4.56 (m, 6H), 4.53 (d, 1H, *J* = 2.8 Hz, 1H), 4.52-4.44 (m, 3H), 4.35 (d, *J* = 12.4 Hz, 1H), 4.16 (dd, *J* = 12.0, 1.6 Hz, 1H), 4.02 (d, *J* = 12.0 Hz, 1H), 3.96 (dd, *J* = 9.6, 2.8 Hz, 1H), 3.93-3.90 (m, 1H), 3.88 (d, *J* = 2.4 Hz, 1H), 3.85 (d, *J* = 9.6 Hz, 1H), 3.76-3.60 (m, 3H), 3.54-3.48 (m, 2H), 3.42-3.39 (m, 3H), 3.35 (s, 3H, OMe).

^{13}C NMR (100 MHz, $CDCl_3$): δ 168.4, 152.5, 149.2, 146.8, 144.2, 144.1, 143.3, 138.7, 138.2, 137.8 (C_q); 130.0, 129.3, 129.0, 128.7, 128.6, 128.2, 127.9, 127.8, 127.4, 127.0 (CH); 124.5 ($CH_{triazole}$), 121.8, 120.8, 120.4, 113.6 (CH); 102.9 ($C_{1'}$), 98.0 (C_1), 80.6, 80.4, 80.0, 79.3, 77.2, 76.4 (CH); 75.3, 75.2 (CH_2); 75.1, 74.8 (CH); 73.3, 72.8 (CH_2); 72.1 (CH), 72.0, 70.7 (CH_2); 67.9 (CH), 67.3 (CH_2), 64.1, 63.4 (CH_2); 55.7 (OMe), 50.1 (CH_2N).

R_f = 0.34 (PE/EA = 5/5)

$[\alpha]_D$: +427.97 (*c* = 0.5, CH_2Cl_2)

Glycomacrocycles *E*-21α and *E*-21β

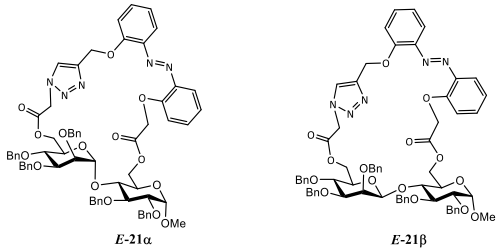

$C_{67}H_{67}N_5O_{15}$
Mw: 1182.29 g/mol

A mixture of glycosyl donor-acceptor pair ***E*-2** (50 mg, 0.039 mmol) in CH_2Cl_2 (1.0 mL) was treated with 4Å molecular sieve, NIS (18 mg, 0.08 mmol) and TfOH (3.8 µL, 0.04 mmol) according to the general procedure ***G***. The residue was purified by CombiFlash® Rf+ (PE/EA 7/3 - 5/5) to give the desired macrocycle *E*-**21**α (11 mg, 23 %) and *E*-**21**β (22 mg, 47 %) as red solids.

Glycomacrocycle *E*-21α

^{1}H NMR (400 MHz, $CDCl_3$): δ 7.80 (s, 1H, CH-triazole), 7.50 (dd, *J* = 7.6, 1.2 Hz, 1H, H_{Ph}), 7.46 (dd, J = 8.0, 1.6 Hz, 1H, H_{Ph}), 7.32-7.22 (m, 26H, H_{Ph}), 7.17-7.13 (m, 2H, H_{Ph}), 7.08 (t, J = 8.0 Hz, 1H, H_{Ph}), 6.98 (t, *J* = 7.6 Hz, 1H, H_{Ph}), 6.81 (d, *J* = 8.0 Hz, 1H, H_{Ph}), 5.35 (s, 2H, OCH_2), 5.23-5.13 (m, 3H, 2xNCH, OCH), 5.06 (d, *J* = 1.2 Hz, 1H, $H_{1'}$), 4.93-4.78 (m, 3H), 4.72 (d, *J* = 13.4 Hz, 1H), 4.64-4.59 (m, 3H, H_1+2×OCH), 4.56-4.46 (m, 3H), 4.40-4.36 (m, 2H), 4.26 (d, *J* = 10.8 Hz, 1H, OCH), 4.11 (d, *J* = 11.2 Hz, 1H, OCH), 4.01 (dd, *J* = 11.6, 8.8 Hz, 1H), 3.91-3.82 (m, 5H), 3.76-3.75 (m, 1H, $H_{2'}$), 3.68-3.59 (m, 1H), 3.56 (dd, *J* = 9.6, 3.6 Hz, 1H, H_2), 3.42 (m, 3H, OCH_3).

^{13}C NMR (100 MHz, $CDCl_3$): δ 169.1, 166.6 (CO); 153.9, 151.0, 145.1, 144.8, 143.2, 138.7, 138.4, 138.2, 137.7, 132.1 (Cq); 131.0, 128.7, 128.6, 128.3, 128.0, 127.8, 126.8 (CH); 124.8 ($CH_{triazole}$), 123.4, 122.1, 122.0, 118.5, 116.4, 113.0 (CH); 102.3 ($C_{1'}$); 98.0 (C_1); 80.9, 79.9, 79.5, 77.3 (CH); 76.2 ($C_{2'}$), 75.5, 75.4 (OCH_2); 74.7 (CH), 73.3, 73.1, 72.1 (OCH_2); 71.8, 67.7 (CH); 65.8, 65.1, 65.0, 64.9 (OCH_2); 55.7 (OCH_3), 50.6 (NCH_2).

Rf = 0.22 (PE/EA = 5/5)

$[\alpha]_D$: -99.6 (c = 0.5, CH_2Cl_2)

mp: 94 °C

HRMS (ESI) m/z: Calcd for $C_{67}H_{68}N_5O_{15}$ $[M+H]^+$: 1182.4712, Found: 1182.4706.

Glycomacrocycle *Z*-**21**α at PSS_{365}

^{1}H NMR (400 MHz, $CDCl_3$): δ 7.81 (s, 1H, CH), 7.29-6.92 (m, 29H), 6.87 (d, *J* = 8.4 Hz, 1H), 6.74 (dd, *J* = 8.0, 0.8 Hz, 1H), 6.58 (td, *J* = 8.0, 0.8 Hz, 1H), 6.73 (dd, *J* = 8.0, 1.6 Hz, 1H), 5.13-5.04 (m, 3H), 4.95 (d, *J* = 9.6 Hz, 1H), 4.90-4.84 (m, 2H), 4.63-4.45 (m, 11H), 4.37-4.35 (m, 1H), 4.22-4.03 (m, 2H), 4.09-4.03 (m, 2H), 3.83 (dd, *J* = 8.8, 2.4 Hz, 1H), 3.80-3.67 (m, 4H), 3.64-3.62 (m, 1H), 3.56-3.51 (m, 1H), 3.41 (dd, *J* = 9.6, 3.6 Hz, 1H), 3.28 (s, 3H, OMe).

^{13}C NMR (100 MHz, $CDCl_3$): δ 169.4, 166.7, 150.9, 145.1, 144.3, 143.6, 143.5, 138.9, 138.5, 138.3, 137.9, 137.8 (Cq); 129.6, 128.7, 128.6, 128.5, 128.3, 128.1, 127.9, 127.8, 127.4, 126.7 (CH); 124.7 ($CH_{triazole}$), 122.7, 121.4, 121.3, 119.2, 118.5, 115.8, 113.7 (CH); 102.0 ($C_{1'}$), 97.8 (C_1), 80.9, 79.9, 79.7, 79.4, 76.1 (CH); 75.3, 75.2 (CH_2); 74.8 (CH), 73.3, 72.8, 72.1 (CH_2); 71.7, 67.8 (CH); 67.1, 65.4, 65.0, 63.7 (CH_2); 55.6 (OMe), 50.9 (CH_2N).

Rf = 0.20 (PE/EA = 5/5)

$[\alpha]_D$: -16.8 (c = 0.5, CH_2Cl_2)

Glycomacrocycle *E*-21β

^{1}H NMR (400 MHz, $CDCl_3$): δ 7.80 (s, 1H, CH-triazole), 7.47-7.43 (m, 2H, H_{Ph}), 7.33-7.17 (m, 26H, H_{Ph}), 7.12-7.10 (m, 2H, H_{Ph}), 7.05-6.97 (m, 3H, H_{Ph}), 5.46 (d, *J* = 13.2 Hz, 1H, OCHPh), 5.41 (d, *J* = 13.2 Hz, 1H, OCHPh), 5.04-4.96 (m, 2H, 2xOCH), 4.86 (d, *J* = 11.6 Hz, 1H, OCH), 4.83 (d, *J* = 11.6 Hz, 1H, NCH), 4.81 (d, *J* = 10.0 Hz, 1H, OCH), 4.75-4.68 (m, 2H, 2xOCH), 4.65-4.53 (m, 5H, H_1+ NCH+3xOCH), 4.42 (d, *J* = 12.0 Hz, 1H, OCH), 4.35 (d, *J* = 11.6 Hz, 1H, OCH), 4.25 (s, 1H, $H_{1'}$), 4.15 (dd, *J* = 11.9, 4.6 Hz, 1H, OCH), 3.98-3.80 (m, 5H, 5xOCH), 3.84-3.69 (m, 2H), 3.49 (dd, *J* = 8.8, 3.6 Hz, 1H), 3.27 (s, 3H, OMe), 3.18 (dd, *J* = 8.8, 2.0 Hz, 1H), 3.15-3.11 (m, 1H).
^{13}C NMR (100 MHz, $CDCl_3$): δ 169.3, 166.2 (C=O); 154.1, 152.9, 144.7, 144.4, 144.3, 139.0, 138.6, 138.0, 137.9, 137.8 (Cq); 131.7, 131.5, 128.6, 128.4, 128.3, 128.2, 127.9, 127.7, 127.6 (CH); 125.3 ($CH_{triazole}$), 122.7, 122.2, 120.8, 119.4, 116.8, 116.6 (CH); 97.6 (C1); 97.5 ($C_{1'}$); 82.6, 81.0, 77.1, 75.3 (CH); 75.1, 74.7 (OCH_2); 74.4 (CH), 74.0, 73.3 (OCH_2); 73.2, 73.1 (CH); 71.4, 67.6 (OCH_2); 67.5 (CH), 64.6 (OCH_2), 64.3, 63.7 (C_6+$C_{6'}$); 55.3 (OCH_3); 50.3 (OCH_2).
Rf = 0.51 (PE/EA = 5/5)
$[\alpha]_D$: +72.76 (c = 0.5, CH_2Cl_2)
mp: 100°C
HRMS (ESI) m/z: Calcd for $C_{67}H_{68}N_5O_{15}$ $[M+H]^+$: 1182.4712, Found: 1182.4706.

Glycomacrocycle *Z*-21β

^{1}H NMR (400 MHz, $CDCl_3$): δ 7.84 (s, 1H, CH-triazole), 7.38-7.12 (m, 27H), 7.01 (d, *J* = 8.4 Hz, 1H), 6.91-6.84 (m, 2H), 6.80 (dd, *J* = 8.4, 0.8 Hz, 1H), 6.63 (td, *J* = 8.0, 1.6 Hz, 1H), 6.41 (dd, *J* = 8.0, 1.6 Hz, 1H), 5.16 (d, *J* = 12.0 Hz, 1H), 5.03 (d, *J* = 12.0 Hz, 1H), 5.01 (d, *J* = 10.8 Hz, 1H), 4.92 (d, *J* = 8.8 Hz, 1H), 4.89 (d, *J* = 3.2 Hz, 1H), 4.83 (d, *J* = 12.0 Hz, 1H), 4.76-4.73 (m, 2H), 4.70 (s, 2H), 4.66 (d, *J* = 12.4 Hz, 1H), 4.56-4.47 (m, 9H), 3.88-3.69 (m, 6H), 3.58-3.52 (m, 2H), 3.36 (s, 3H, OMe), 3.28-3.25 (m, 2H).
^{13}C NMR (100 MHz, $CDCl_3$): δ 168.6, 165.8, 150.3, 146.9, 144.2, 144.1, 144.0, 139.2, 138.9, 138.2, 138.0 (C_q); 129.1, 129.0, 128.6, 128.4, 128.2, 127.9, 127.7, 127.4, 126.8 (CH) ; 125.2 ($CH_{triazole}$), 121.9, 121.4, 120.6, 118.1, 114.9, 113.6 (CH) ; 100.2 ($C_{1'}$), 97.8 (C_1), 83.1, 79.8, 78.5, 77.5, 75.9, 75.6 (CH); 75.3, 74.1, 73.2 (CH_2); 72.6 (CH), 72.1 (CH_2), 68.0 (CH), 66.7, 65.5, 64.1, 63.4 (CH_2); 55.5 (OMe), 50.6 (CH_2N).
Rf = 0.35 (PE/EA = 5/5)
$[\alpha]_D$: -117.8 (c = 0.5, CH_2Cl_2)

Glycomacrocycle *E*-22β

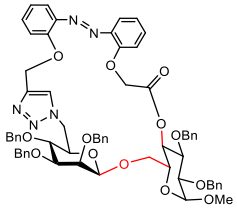

$C_{65}H_{65}N_5O_{13}$
Mw: 1123.46 g/mol

A mixture of glycosyl donor-acceptor pair ***E*-3** (50 mg, 0.04 mmol) in CH_2Cl_2 (1.0 mL) was treated with 4Å molecular sieve, NIS (18 mg, 0.08 mmol) and TfOH (3.8 µL, 0.04 mmol) according to the general procedure **G**. The residue was purified by CombiFlash® Rf+ (PE/EA 7/3 - 5/5) to give the desired macrocycle ***E*-22β** (36 mg, 78 %) as a red solid.

^{1}H NMR (400 MHz, $CDCl_3$): δ 7.62 (s, 1H, CH-triazole), 7.49 (dd, *J* = 8.0, 1.2 Hz, 1H, H_{Ph}), 7.39-7.26 (m, 29H, H_{Ph}), 7.06-6.94 (m, 3H, H_{Ph}), 5.58 (d, *J* = 13.2 Hz, 1H, OCH), 5.39 (d, *J* = 12.8 Hz, 1H, OCH), 4.95 (d, *J* = 11.0 Hz, 1H, OCH), 4.93 (d, *J* = 12.0 Hz, 1H, OCH), 4.90-4.60 (m, 10H), 4.51 (d, *J* = 3.2 Hz, 1H, H_1), 4.46 (d, *J* = 12.0 Hz, 1H, OCH), 4.36 (d, *J* = 12.0 Hz, 1H, OCH), 4.22 (dd, *J* = 13.6, 8.8 Hz, 1H), 3.90 (t, *J* = 9.6 Hz, 1H, H_3), 3.82-3.81 (m, 2H, $H_{1'}$+CH), 3.66 (t, *J* = 9.2 Hz, 1H, $H_{3'}$), 3.54-3.52 (m, 2H), 3.49 (dd, *J* = 9.6, 3.6 Hz, 1H, H_2), 3.33 (dd, *J* = 8.8, 2.4 Hz, 1H, $H_{2'}$), 3.32-3.34 (m, 1H), 3.29 (s, 3H, OCH_3), 2.85 (dd, *J* = 10.8, 5.2 Hz, 1H).

^{13}C NMR (100 MHz, $CDCl_3$): δ 167.8, 154.5, 154.0, 144.7, 144.0, 143.9, 138.7, 138.5, 137.9 (C_q); 132.3, 131.8, 128.7, 128.6, 128.3, 128.2, 127.9, 123.9, 122.7, 121.9, 120.5, 119.3, 117.1 (CH); 101.6 ($C_{1'}$), 97.9 (C_1), 81.8, 79.8, 79.0, 77.4 (CH); 75.4, 75.2 (OCH_2); 74.5, 73.8 (CH); 73.7, 71.4 (OCH_2); 71.0, 68.2 (CH); 68.1, 67.7, 64.7 (OCH_2); 55.4 (OCH_3), 50.9 ($C_{6'}$).

R_f = 0.53 (PE/EA = 5/5)

$[\alpha]_D$: -162.84 (*c* = 0.5, CH_2Cl_2)

mp: 98°C

HRMS (ESI) m/z: Calcd for $C_{65}H_{66}N_5O_{13}[M+H]^+$: 1124.4657, Found: 1124.4652.

Glycomacrocycle *Z*-22β

^{1}H NMR (400 MHz, $CDCl_3$): δ 8.09-8.08 (m, 1H), 7.41-7.04 (m, 27H), 6.94-6.91 (m, 2H), 6.68-6.58 (m, 3H), 6.37 (dd, *J* = 9.2, 1.6 Hz, 1H), 5.42 (d, *J* = 13.6 Hz, 1H), 5.00-4.89 (m, 3H), 4.83-4.77 (m, 2H), 4.68-4.57 (m, 6H), 4.56 (d, 1H, *J* = 3.6 Hz, 1H), 4.51-4.40 (m, 3H), 4.01 (t, *J* = 9.6 Hz, 1H), 3.96 (d, *J* = 3.2 Hz, 1H), 3.93-3.80 (m, 3H), 3.71 (t, *J* = 9.6 Hz, 1H), 3.54-3.42 (m, 3H), 3.41 (s, 3H, OMe), 3.39-3.38 (m, 1H), 3.34-3.32 (m, 1H), 3.14-3.09 (m, 1H).

^{13}C NMR (100 MHz, $CDCl_3$): δ 168.8, 144.4, 144.2, 143.8, 142.2, 138.6, 138.5, 137.8 (C_q); 130.0, 129.4, 128.8, 128.7, 128.6, 128.4, 128.1, 128.0, 127.9, 127.7 (CH); 124.9, 124.6, 120.9, 117.5, 117.1, 113.9, 112.8 (CH); 102.2 ($C_{1'}$), 97.8 (C_1), 81.9, 79.8, 78.4 (CH); 75.7, 75.3 (OCH_2); 75.1, 75.0 (CH); 74.5 (OCH_2), 74.2 (CH), 73.7 (OCH_2), 72.4 (CH), 71.6, 70.1 (OCH_2); 68.8 (CH), 65.5, 61.6 (OCH_2); 55.4 (OMe), 51.2 (CH_2N).

R_f = 0.38 (PE/EA = 5/5)

$[\alpha]_D$: +210.15 (*c* = 0.5, CH_2Cl_2)

Glycomacrocycle *E*-23β

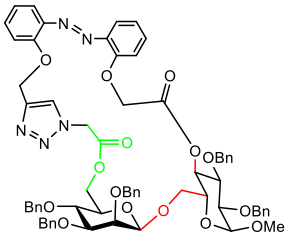

$C_{67}H_{67}N_5O_{15}$
Mw: 1182.29 g/mol

A mixture of glycosyl donor-acceptor pair ***E*-4** (52 mg, 0.04 mmol) in CH_2Cl_2 (1.0 mL) was treated with 4Å molecular sieve, NIS (18 mg, 0.08 mmol) and TfOH (3.8 µL, 0.04 mmol) according to the general procedure **G**. The residue was purified by CombiFlash® Rf+ (PE/EA 7/3 - 5/5) to give the desired macrocycle ***E*-23β** (30 mg, 63 %) as a red solid.

^{1}H NMR (400 MHz, $CDCl_3$): δ 7.66 (s, 1H, CH-triazole), 7.51 (dd, *J* = 8.0, 1.6 Hz, 1H, H_{Ph}), 7.47 (dd, *J* = 7.6, 1.6 Hz, 1H, H_{Ph}), 7.38-7.14 (m, 28H, H_{Ph}), 7.05-6.97 (m, 3H, H_{Ph}), 5.46 (d, *J* = 12.8 Hz, 1H, NCH), 5.42 (d, *J* = 12.8 Hz, 1H, NCH), 5.01 (s, 2H, OCH_2), 4.91-4.84 (m, 5H), 4.76 (d, *J* = 12.0 Hz, 1H, OCH), 4.72 (d, *J* = 12.4 Hz, 1H, OCH), 4.63-4.62 (m, 2H), 4.60-4.58 (m, 2H, H_1+OCH), 4.55-4.47 (m, 3H), 4.42-4.36 (m, 2H), 4.10 (dd, *J* = 11.2, 3.2 Hz, 1H), 3.92-3.86 (m, 2H, $H_{1'}$+OCH), 3.77 (dd, *J* = 11.2, 2.0 Hz, 1H), 3.77 (t, *J* = 11.0 Hz, 1H), 3.76-3.59 (m, 1H), 3.49 (dd, *J* = 9.6, 3.6 Hz, 1H, H_2), 3.39-3.35 (m, 1H, $H_{2'}$), 3.33 (s, 3H, OCH_3), 3.30-3.22 (m, 1H), 3.08 (dd, *J* = 10.8, 6.0 Hz, 1H).

^{13}C NMR (100 MHz, $CDCl_3$): δ 168.4, 165.8 (CO); 154.9, 154.1, 144.8, 144.3, 143.7, 138.7, 138.1, 137.9 (C_q); 132.3, 132.2, 128.7, 128.6, 128.5, 128.3, 127.9, 124.5, 122.9, 122.3, 120.0, 118.2, 116.6 (CH); 101.9 ($C_{1'}$); 98.0 (C_1); 81.8, 79.7, 78.9 (CH); 75.5, 75.2 (OCH_2); 74.5 (CH), 74.4 (OCH_2), 73.8 (CH); 73.7 (OCH_2), 73.0, 71.5 (CH); 71.2, 68.8, 68.7 (OCH_2); 68.4 (CH), 65.6, 64.8 (OCH_2); 55.5 (OCH_3); 50.9 (CH_2N).

R_f = 0.26 (PE/EA = 5/5)

$[\alpha]_D$: -126 (*c* = 0.5, CH_2Cl_2)

mp: 96°C

HRMS (ESI) m/z: Calcd for $C_{67}H_{68}N_5O_{15}$ $[M+H]^+$: 1182.4712, Found: 1182.4706.

(2,2-Dimethyl-1,3-dioxane-5,5-diyl) dimethanol (26)[141]

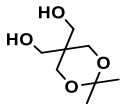

$C_8H_{16}O_4$
Mw: 176.2120 g/mol

To a solution of pentaerythritol (2g, 14.65 mmol) in benzene-DMF (16/24 mL) was added *p*TsOH (30 mg, 5% w/w relative to the acetone) at rt. The well-stirred dispersion was warmed to 80°C until complete dissolution, and the acetone (5 mL) was added dropwise while the reaction mixture was heated to 115 °C. The H_2O formed during the reaction was removed by reactive distillation and collected in the Dean-Stark trap. The reaction was stopped when there was no further increase in the collected H_2O. After cooling, the reaction mixture was poured into H_2O (30 mL), neutralized with K_2CO_3 and extracted with CH_2Cl_2 (3*30 mL). The organic layer was dried over $MgSO_4$, the residue was purified with CombiFlash (PE/EA, 7/3-5/5) to give the desired monoacetal **26** (1.04 g, 40%) and the diacetal derivative (3,3,9,9-tetramethyl-2,4,8,10-tetraoxaspiro [5.5] undecane, **26b**) (0.63 g, 20%). NMR data were in agreement with the literature.[141]

[141] M. C. Murguía, S. E. Vaillard, R. J. Grau, *Synthesis*, **2001**, 1093-1097.

(5-(Hydroxymethyl)-2,2-dimethyl-1,3-dioxan-5-yl)methyl-(*E*)-2-(2-((2-(prop-2-yn-1-yloxy)phenyl) diazenyl)phenoxy)acetate (27a)

(2,2-dimethyl-1,3-dioxane-5,5-diyl)bis (methylene)bis(2-(2-((*E*)-(2-(prop-2-yn-1-yloxy)phenyl)diazenyl)phenoxy)acetate (27b)

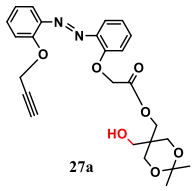

27a

$C_{25}H_{28}N_2O_7$
Mw: 468.51 g/mol

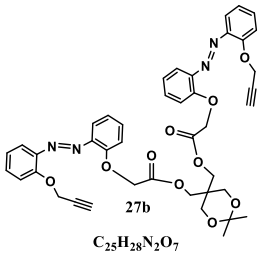

27b

$C_{25}H_{28}N_2O_7$
Mw: 468.51 g/mol

To the solution of compounds **13** (630 mg, 2.03 mmol) and **26** (349.4 mg, 2.03 mmol) in CH_2Cl_2 was added a solution of the EDC (389.4 mg, 2.03 mmol) and DMAP (26.4 mg, 0.20 mmol) in dry CH_2Cl_2 at 0°C according to the general procedure **E**. The residue was purified by flash chromatography (DCM/EA = 8/2) to afford **27a** (203 mg, 41 %) and **27b** (106 mg, 24 %) as red solids.

Compound **27a**:

^{1}H NMR (400 MHz, $CDCl_3$): δ 7.66 (dd, *J* = 8.0, 2.0 Hz, 1H, H_{Ph}), 7.63 (dd, *J* = 8.0, 1.6 Hz, 1H, H_{Ph}), 7.47-7.39 (m, 2H, H_{Ph}), 7.26-7.24 (m, 1H, H_{Ph}), 7.10-7.07 (m, 2H, H_{Ph}), 7.03 (d, *J* = 8.0 Hz, 1H, H_{Ph}), 4.95-4.94 (m, 4H), 3.65 (d, *J* = 12.0 Hz, 1H, OCH), 3.61 (d, *J* = 12.0 Hz, 1H, OCH), 3.40 (s, 2H, CH_2), 2.56 (t, *J* = 2.4 Hz, 1H, CH≡), 1.38 (s, 3H, CH_3), 1.36 (s, 3H, CH_3).

^{13}C NMR (100 MHz, $CDCl_3$): δ 169.6 (C=O); 155.3, 155.2, 144.4, 143.4 (C_q); 132.4, 132.3, 122.6, 122.3, 118.1, 117.7, 115.8, 115.6 (CH); 98.6 (C_q), 78.6 (C≡), 76.3 (CH≡), 67.5, 64.5, 64.4, 62.0, 57.8 (CH_2); 39.0 (C_q), 24.8, 22.7 (CH_3).

R_f = 0.42 (PE/EA = 5/5)

$[\alpha]_D$: -0.7 (*c* = 0.5, CH_3CN)

mp: 77°C

HRMS (ESI) m/z: Calcd for $C_{25}H_{28}N_4O_7$ $[M+H]^+$: 469.1975, Found: 469.1970.

Compound **27b**:

^{1}H NMR (400 MHz, $CDCl_3$): δ 7.65 (dd, *J* = 7.6, 2.0 Hz, 2H, H_{Ph}), 7.63 (dd, *J* = 8.0, 1.6 Hz, 1H, H_{Ph}), 7.45-7.35 (m, 4H, H_{Ph}), 7.23 (d, *J* = 8.0 Hz, 2H, H_{Ph}), 7.08-7.00 (m, 4H, H_{Ph}), 6.98 (d, *J* = 7.2 Hz, 2H, H_{Ph}), 4.94-4.89 (m, 8H), 4.12 (s, 4H, 2xCH_2), 3.57 (s, 4H, 2xCH_2), 2.55 (t, *J* = 2.4 Hz, 2H, 2xCH≡), 1.26 (s, 6H, 2xCH_3).

^{13}C NMR (100 MHz, $CDCl_3$): δ 168.8 (C=O); 155.4, 155.2, 143.5, 143.2 (C_q); 132.2, 122.6, 122.3, 118.0, 117.7, 115.9, 115.5 (CH); 98.8 (C_q), 78.7 (C≡), 76.3 (CH≡), 67.3, 63.9, 62.0, 57.8 (CH_2); 37.4 (C_q), 23.6 (CH_3).

R_f = 0.29 (PE/EA = 5/5);

$[\alpha]_D$: -6.5 (*c* = 0.5, CH_3CN)

mp: 84°C

HRMS (ESI) m/z: Calcd for $C_{42}H_{41}N_4O_{10}$ $[M+H]^+$: 761.2823, Found: 761.2819.

Glycosyl donor-acceptor pair 24

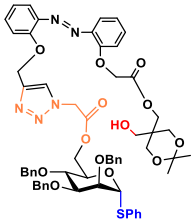

$C_{60}H_{63}N_5O_{13}S$
Mw: 1094.25 g/mol

To a solution of **19** (200 mg, 0.427 mmol) and **27a** (267.2 mg, 0.427 mmol) in CH_2Cl_2/H_2O (4/1, 12.5 mL), were added $CuSO_4 \cdot 5H_2O$ (53.3 mg, 0.213 mmol) and ascorbic acid (75.2 mg, 0.427 mmol according to the general procedure **F**. The residue was purified by flash chromatography (PE/EA = 5/5) to get the product **24** (417 mg, 87%) as a red solid.

^{1}H NMR (400 MHz, $CDCl_3$): δ 7.62 (s, 1H, CH-triazole), 7.54-7.50 (m, 2H, H_{Ph}), 7.34-7.19 (m, 22H, H_{Ph}), 7.13 (dd, *J* = 8.8, 0.8 Hz, 1H, H_{Ph}), 7.00-6.92 (m, 3H, H_{Ph}), 5.48 (d, *J* = 1.6 Hz, 1H, H_1), 5.37 (s, 2H, CH_2), 4.96-4.83 (m, 3H), 4.84 (s, 2H, CH_2), 4.64 (d, *J* = 12.4 Hz, 1H), 4.56 (d, *J* = 12.4 Hz, 1H), 4.55-4.53 (m, 3H), 4.48 (d, *J* = 11.2 Hz, 1H), 4.36 (dd, *J* = 11.2, 2.4 Hz, 1H, H_6), 4.36 (dd, *J* = 11.6, 5.6 Hz, 1H, $H_{6'}$), 4.22 (s, 2H, CH_2), 4.20-4.18 (m, 1H, H_5), 3.92 (t, *J* = 2.0 Hz, 1H, H_2), 3.81-3.80 (m, 2H, $H_{3,4}$), 3.56 (d, *J* = 12.4 Hz, 2H, 2xCH), 3.50 (d, *J* = 12.4 Hz, 2H, 2xCH), 3.28 (s, 2H, CH_2), 2.16 (s large, 1H, OH), 1.29 (s, 3H, CH_3), 1.28 (s, 3H, CH_3).

^{13}C NMR (100 MHz, $CDCl_3$): δ 169.6, 166.0 (CO); 155.6, 155.2, 144.7, 143.5, 143.4, 138.0, 137.9, 137.7, 133.9 (C_q); 132.6, 132.2, 131.4, 129.3, 128.6, 128.3, 128.1, 128.0, 127.8 (CH); 124.7 (CH-triazole), 122.6, 122.0, 118.2, 118.1, 115.8, 115.7 (CH); 98.6 (C_q), 85.4 (C_1), 80.2 (CH), 75.9 (C_2), 75.2 (CH_2), 74.1 (CH), 72.2, 72.1 (CH_2); 70.6 (C_5); 67.5 (CH_2), 65.0 (C_6), 64.5, 64.0, 62.4, 61.9, 50.6 (CH_2), 38.9 (C_q), 25.0, 22.4 (CH_3).

R_f = 0.58 (PE/EA = 3/7)

$[\alpha]_D$: +16.3 (*c* = 0.5, CH_3CN)

mp: 92°C

HRMS (ESI) m/z: Calcd for $C_{60}H_{64}N_5O_{13}S$ $[M+H]^+$: 1094.4221, Found: 1094.4229.

***Z*-24 at PSS$_{365}$**

^{1}H NMR (400 MHz, $CDCl_3$): δ 7.63 (s, 1H, CH-triazole), 7.42-7.27 (m, 20H, H_{Ph}), 7.10 (td, *J* = 8.4, 2.0 Hz, 1H, H_{Ph}), 7.06 (td, *J* = 8.0, 1.2 Hz, 1H, H_{Ph}), 6.95 (d, *J* = 8.0 Hz, 1H, H_{Ph}), 6.83-6.68 (m, 4H, H_{Ph}), 6.51 (dd, *J* = 8.0, 1.6 Hz, 1H, H_{Ph}), 5.58 (d, *J* = 1.6 Hz, 1H, H_1), 5.30 (s, 2H, OCH_2), 5.02 (d, *J* = 18.0 Hz, 1H, NCH), 4.94 (d, *J* = 18.0 Hz, 1H, NCH), 4.93 (d, *J* = 9.2 Hz, 1H, OCH), 4.72 (d, *J* = 13.4 Hz, 1H, OCH), 4.65 (d, *J* = 13.4 Hz, 1H, OCH), 4.61-4.56 (m, 5H, OCH, 2xOCH_2), 4.45 (dd, *J* = 12.0, 1.6 Hz, 1H, H_6), 4.36 (dd, *J* = 12.0, 5.6 Hz, 1H, $H_{6'}$), 4.32 (s, 2H, OCH_2), 4.27-4.29 (m, 1H, H_5), 4.01-3.99 (m, 1H, H_2), 3.90-3.88 (m, 2H, $H_{3,4}$), 3.69 (d, *J* = 12.0 Hz, 2H, 2xOCH), 3.64 (d, *J* = 12.0 Hz, 2H, 2xOCH), 3.46 (s, 2H, OCH_2), 2.61 (s large, 1H, OH), 1.39 (s, 3H, CH_3), 1.39 (s, 3H, CH_3).

^{13}C NMR (100 MHz, $CDCl_3$): δ 169.2, 166.1, 148.3, 148.0, 144.4, 144.3, 138.0, 137.9, 137.8, 134.0 (C_q); 131.5, 129.3, 128.9, 128.7, 128.4, 128.1, 128.0, 127.8 (CH); 124.8 ($CH_{triazole}$), 121.7, 121.2, 119.8, 119.2, 113.8, 113.4 (CH); 98.6 (C_q), 85.4 (C_1), 80.1 (C_2), 75.9 (CH); 75.3 (C_6), 75.2 (CH), 72.3, 72.2 (CH_2); 70.7 (C_5), 66.1, 65.1, 64.3, 62.6, 62.5, 62.4, 61.8 (CH_2); 50.7 (NCH_2), 39.0 (C_q), 25.4, 22.2 (CH_3).

R_f = 0.45 (PE/EA = 3/7)

$[\alpha]_D$: +30.6 (*c* = 0.5, CH_3CN)

2-(Hydroxymethyl) benzyl (*E*)-2-(2-((2-(prop-2-yn-1-yloxy) phenyl) diazenyl) phenoxy) acetate (29a)
1,2-phenylenebis (methylene) bis(2-(2-((*E*)-(2-(prop-2-yn-1-yloxy) phenyl) diazenyl) phenoxy) acetate (29b)

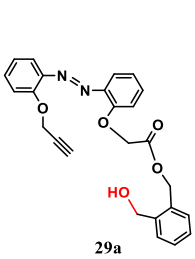

29a

$C_{25}H_{22}N_2O_5$
Mw: 430.46 g/mol

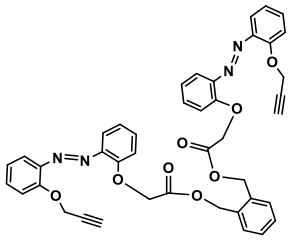

29b

$C_{42}H_{34}N_4O_8$
Mw: 722.75 g/mol

To the solution of compound **13** (299.7mg, 0.97 mmol) and 1,2-phenylenedimethanol **28** (133.7 mg, 0.97 mmol) in CH_2Cl_2 was added a solution of the EDC (185.5 mg, 0.97 mmol) and DMAP (12.5 mg, 0.10 mmol) in dry CH_2Cl_2 at 0°C according to the general procedure **E**. The residue was purified by flash chromatography (DCM/EA = 8/2) to afford **29a** (196 mg, 47 %) and **29b** (34 mg, 10 %) as red solids.

Compound **29a**:

^{1}H NMR (400 MHz, $CDCl_3$): δ 7.64 (dd, *J* = 8.4, 2.0 Hz, 1H, H_{Ph}), 7.59 (dd, *J* = 8.0, 2.0 Hz, 1H, H_{Ph}), 7.43-7.21 (m, 7H, H_{Ph}), 7.07-6.96 (m, 3H, H_{Ph}), 5.32 (s, 2H, OCH_2), 4.91 (d, *J* = 2.8 Hz, 2H, $OCH_2CH{\equiv}$), 4.89 (s, 2H, OCH_2), 4.64 (d, *J* = 5.2 Hz, 2H, CH_2OH), 2.53 (t, *J* = 2.4 Hz, 1H, CH≡), 2.13-2.11 (m, 1H, OH).

^{13}C NMR (100 MHz, $CDCl_3$): δ 168.9, 155.4, 155.2, 143.5, 143.4, 139.6, 133.1 (C_q); 132.3, 132.2, 130.1, 129.3, 129.0, 128.2, 122.7, 122.3, 118.0, 117.8, 116.0, 115.8 (CH_{Ph}); 78.6 (C_q), 76.3 (CH), 67.9, 65.0, 62.9, 57.8 (OCH_2).

R_f = 0.39 (PE/EA = 5/5)

$[\alpha]_D$: -2.9 (*c* = 0.5, CH_3CN)

mp: 62°C

HRMS (ESI) m/z: Calcd for $C_{25}H_{23}N_2O_5$ $[M+H]^+$: 431.1607, Found: 431.1608.

Compound **29b**:

^{1}H NMR (400 MHz, $CDCl_3$): δ 7.66 (dd, *J* = 8.0, 1.6 Hz, 2H, H_{Ph}), 7.61 (dd, *J* = 8.0, 1.6 Hz, 2H, H_{Ph}), 7.43-7.21 (m, 10H, H_{Ph}), 7.07-7.00 (m, 4H, H_{Ph}), 6.95 (d, *J* = 8.0 Hz, 2H, H_{Ph}), 5.26 (s, 4H, 2xOCH_2), 4.93 (d, *J* = 2.4 Hz, 4H, 2x$OCH_2CH{\equiv}$), 4.89 (s, 4H, 2xOCH_2), 2.54 (t, *J* = 2.4 Hz, 1H, CH≡).

^{13}C NMR (100 MHz, $CDCl_3$): δ 168.8, 155.5, 155.2, 143.5, 143.3, 134.0, 133.1 (C_q); 132.2, 130.2, 129.1, 122.5, 122.2, 117.9 117.7, 115.9, 115.8 (CH_{Ph}); 78.7 (C_q), 76.3 (CH≡), 67.6, 64.4, 57.8 (OCH_2).

Rf = 0.61 (PE/EA = 5/5)

$[\alpha]_D$: -1.7 (*c* = 0.5, CH_3CN)

mp: 64°C

HRMS (ESI) m/z: Calcd for $C_{42}H_{41}N_4O_{10}$ $[M+H]^+$: 723.2455, Found: 723.2452.

Glycosyl donor-acceptor pair 25

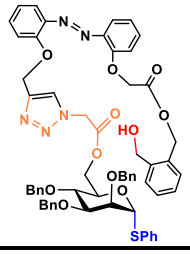

$C_{60}H_{57}N_5O_{11}S$
MW: 1056.20 g/mol

To a solution of **19** (171.6 mg, 0.27 mmol) and **29a** (118 mg, 0.27 mmol) in CH_2Cl_2/H_2O (4/1, 6.25 mL) were added $CuSO_4 \cdot 5H_2O$ (34.3 mg, 0.14 mmol) and ascorbic acid (48 mg, 0.27 mmol) according to the general procedure **F**. The residue was purified by flash chromatography (PE/EA = 5/5) to get the product **25** (201 mg, 69 %) as a red solid.

^{1}H NMR (400 MHz, $CDCl_3$): δ 7.68 (s, 1H, CH-triazole), 7.61 (dd, *J* = 8.0, 1.6 Hz, 1H, H_{Ph}), 7.57 (dd, *J* = 8.0, 1.6 Hz, 1H, H_{Ph}), 7.51 (s, 1H), 7.40-7.17 (m, 25H, H_{Ph}), 7.03-6.95 (m, 4H, H_{Ph}), 5.55 (d, *J* = 1.6 Hz, 1H, H_1), 5.44-5.42 (m, 2H, OCH_2), 5.28 (s, 2H, OCH_2), 4.97-4.86 (m, 5H, $OCH+NCH_2$), 4.69-4.59 (m, 6H, $3xOCH_2$), 4.55 (d, *J* = 10.8 Hz, 1H, OCH), 4.43 (dd, *J* = 11.6, 1.6 Hz, 1H, H_6), 4.34 (dd, *J* = 11.6, 5.6 Hz, 1H, $H_{6'}$), 4.29-4.25 (m, 1H), 4.01-3.99 (m, 1H), 3.90-3.86 (m, 2H).

^{13}C NMR (100 MHz, $CDCl_3$): δ 168.8, 166.0 (CO); 155.6, 155.3, 144.7, 143.3, 143.2, 139.7, 138.0, 137.9, 137.7, 133.9 (C_q); 133.0, 132.5, 132.1, 131.4, 129.6, 129.3, 129.1, 128.6, 128.5, 128.3, 128.1, 128.0, 127.7 (CH); 124.7 (CH-triazole), 122.6, 121.9, 118.1, 118.0, 116.0, 115.7 (CH); 85.4 (C_1), 80.1, 75.9 (CH); 75.4 (CH_2), 74.1 (CH), 72.2, 72.1 (CH_2); 70.6 (CH), 67.7, 64.9, 64.8, 63.9, 62.6 (CH_2); 50.6 (NCH_2).

R_f = 0.55 (PE/EA = 3/7)

$[\alpha]_D$: +48.9 (*c* = 0.5, CH_3CN)

mp: 60°C

HRMS (ESI) m/z: Calcd for $C_{60}H_{58}N_5O_{11}S$ $[M+H]^+$: 1056.3854, Found: 1056.3847.

***Z*-25 at PSS$_{365}$**

^{1}H NMR (400 MHz, $CDCl_3$): δ 7.58 (s, 1H, CH-triazole), 7.43-7.24 (m, 24H, H_{Ph}), 7.09-7.05 (m, 1H, H_{Ph}), 7.03-6.99 (m, 1H, H_{Ph}), 6.90 (d, *J* = 8.0 Hz, 1H, H_{Ph}), 6.77-6.65 (m, 4H, H_{Ph}), 6.50 (dd, *J* = 7.6, 1.2 Hz, 1H, H_{Ph}), 5.57 (s, 1H, H_1), 5.30 (s, 2H, OCH_2), 5.09 (s, 2H, OCH_2), 4.95-4.92 (m, 3H), 4.72-4.56 (m, 9H), 4.45-4.25 (m, 3H), 4.00 (s, 1H), 3.91-3.89 (m, 2H), 2.59 (broad s, 1H, OH).

^{13}C NMR (100 MHz, $CDCl_3$): δ 168.6, 144.3, 138.0 (C_q); 131.5, 130.1, 129.3, 128.6, 128.3, 128.1, 128.0, 127.8 (CH); 124.7 ($CH_{triazole}$), 121.5, 121.1, 119.8, 119.1, 113.4, 113.3 (CH); 85.4 (C_1), 80.2, 75.9 (CH); 75.2 (CH_2), 74.1 (CH), 72.2, 72.1 (CH_2); 70.7 (CH), 66.1, 65.0, 62.7, 62.6, (CH_2); 50.6 (NCH_2).

R_f = 0.48 (PE/EA = 3/7)

$[\alpha]_D$: +54.6 (*c* = 0.5, CH_3CN)

Glycomacrocycle *E-30*

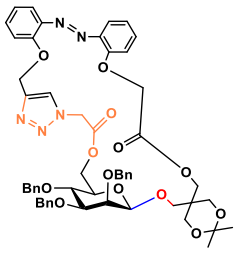

$C_{54}H_{57}N_5O_{13}$
MW:984.0720

A mixture of glycosyl donor-acceptor pair **24** (87 mg, 0.08 mmol) in CH_2Cl_2 (2.8 mL) was treated with 4Å molecular sieve, NIS (35 mg, 0.16 mmol) and TfOH (7 µL, 0.08 mmol) according to the general procedure **G**. The residue was purified by CombiFlash® Rf+ (PE/EA 7/3 - 5/5) to give the desired macrocycle ***E*-30** (29 mg, 39 %) as a red solid.

^{1}H NMR (400 MHz, $CDCl_3$): 7.78 (s, 1H, CH-triazole), 7.48-7.46 (m, 2H, H_{Ph}), 7.38-7.16 (m, 17H, H_{Ph}), 7.01-6.93 (m, 4H, H_{Ph}), 5.46-5.39 (m, 2H, OCH_2), 5.08-4.98 (m, 2H, NCH_2), 4.95-4.86 (m, 3H), 4.78 (d, *J* = 12.4 Hz, 1H), 4.66 (d, *J* = 12.4 Hz, 1H), 4.57-4.54 (m, 2H), 4.47 (d, *J* = 12.0 Hz, 1H), 4.41 (dd, *J* = 12.0, 2.4 Hz, 1H), 4.19-4.10 (m, 3H), 3.82 (s, 1H, H_1), 3.73-3.68 (m, 2H), 3.62 (s, 2H, CH_2), 3.51-3.42 (m, 3H), 3.38 (dd, *J* = 9.6, 2.8 Hz, 1H), 3.24-3.19 (m, 1H, H_5), 3.10 (d, *J* = 9.6 Hz, 1H), 1.35 (s, 3H, CH_3), 1.29 (s, 3H, CH_3).

^{13}C NMR (100 MHz, $CDCl_3$): δ 169.1, 165.9 (CO); 154.7, 154.0, 144.6, 144.1, 143.8, 138.4, 137.9, 137.7 (C_q); 132.2, 131.9, 128.7, 128.4, 128.3, 128.2, 128.1, 128.0, 127.8, 127.7, 127.6 (CH); 124.7 (CH-triazole), 122.3, 122.0, 120.0, 118.7, 115.6, 114.6 (CH); 101.1 (C_1), 98.8 (C_q), 81.8 (CH); 79.5, 74.5 (CH), 74.2 (CH_2); 73.8, 73.0 (CH); 71.5, 68.6, 66.9, 65.3, 64.6, 64.1, 63.1, 61.5 (CH_2); 50.9 (NCH_2), 37.9 (C_q), 23.9, 23.6 (CH_3).

R_f = 0.52 (PE/EA = 5/5)

$[\alpha]_D$: -326.4 (*c* = 0.25, CH_3CN)

mp: 77°C

HRMS (ESI) m/z: Calcd for $C_{54}H_{58}N_5O_{13}$ $[M+H]^+$: 984.4031, Found: 984.4027

Glycomacrocycle *E*-31

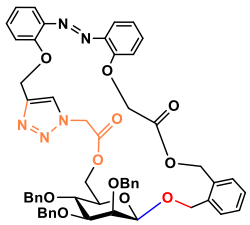

$C_{54}H_{51}N_5O_{11}$
MW:946.0260

A mixture of glycosyl donor-acceptor pair **25** (42.2 mg, 0.04 mmol) in CH_2Cl_2 (1.4 mL) was treated with 4Å molecular sieve, NIS (17.9 mg, 0.08 mmol) and TfOH (3.5 µL, 0.04 mmol) according to the general procedure **G**. The residue was purified by CombiFlash® Rf+ (PE/EA 7/3 - 5/5) to give the desired macrocycle ***E*-31** (18.2 mg, 48 %) as a red solid.

^{1}H NMR (400 MHz, $CDCl_3$): δ 7.70 (s, 1H, CH-triazole), 7.59-7.54 (m, 2H, H_{Ph}), 7.50 (s, 4H, H_{Ph}), 7.36-7.23 (m, 17H, H_{Ph}), 7.02-6.95 (m, 4H, H_{Ph}), 5.44-5.41 (m, 2H, OCH_2), 5.28 (s, 2H, OCH_2), 5.05-4.91 (m, 2H, NCH_2), 4.88-4.84 (m, 2H), 4.59-4.48 (m, 8H), 4.40-4.37 (m, 1H), 4.31-4.30 (m, 1H), 4.25-4.19 (m, 2H), 4.13-4.08 (m, 2H), 3.89-3.85 (m, 1H).

^{13}C NMR (100 MHz, $CDCl_3$): δ 168.9, 165.9 (CO); 155.5, 155.3, 144.8, 144.7, 144.6, 144.5, 144.4, 144.2, 143.4, 141.4, 140.3, 139.7, 137.9, 137.8, 137.4, 133.0 (C_q), 132.5, 132.2, 131.8, 130.0, 129.5, 129.2, 128.9, 128.6, 128.5, 128.3, 128.2, 128.1, 128.0, 127.7 (CH); 124.5 (CH-triazole), 122.6, 122.0, 121.6, 118.2, 118.1, 116.0, 115.8 (CH); 95.7 (C_1); 79.5, 75.4 (CH), 75.3 (CH_2); 73.1 (CH); 72.7, 72.3 (CH_2); 71.3 (CH); 67.8, 64.9, 64.1, 62.7, 53.6 (CH_2); 50.9 (NCH_2).

R_f = 0.41 (PE/EA = 3/7)

$[\alpha]_D$: -10.1 (*c* = 0.25, CH_3CN)

mp: 83°C

HRMS (ESI) m/z: Calcd for $C_{54}H_{51}N_5O_{11}$ $[M+H]^+$: 946.3663. Found: 946.3654

REFERENCES

1. C. R. Bertozzi, L. L. Kiessling, *Science* **2001**, *291*, 2357-2364.

2. V. Ajit, C. Richard, E. Jeffrey, F. Hudson, H. Gerald, M. Jamey, Essentials of glycobiology, *Cold Spring Harb. Lab. Press N. Y.* **2009**.

3. L. K. Mydock, A. V. Demchenko, *Org. Biomol. Chem*. **2010**, *8*, 497-510.

4. D. Crich, *Acc. Chem. Res.* **2010**, *43*, 1144-1153.

5. T. G. Frihed, M. Bols, C. M. Pedersen, *Chem. Rev*. **2015**, *115*, 4963-1153.

6. X. G. Jia, A. V. Demchenko, *Beilstein J. Org. Chem*. **2017**, *13*, 2028-2048.

7. L. Bohé, D. Crich, *Comptes Rendus Chim*. **2011**, *14*, 3-16.

8. L. Bohé, D. Crich, *Carbohydr. Res*. **2015**, *403*, 48-59.

9. P. O. Adero, H. Amarasekara, P. Wen, L. Bohe, D. Crich, *Chem. Rev*. **2018**, *118*, 8242-8284.

10. R. A. Mensink, T. J. Boltje, *Chem. Eur. J.* **2017**, *23*, 17637-17653.

11. S. C. Ranade, A. V. Demchenko, *J. Carbohydr. Chem.* **2013**, *32*, 1-43.

12. J. Guo, X.-S. Ye, *Molecules* **2010**, *15*, 7235-7265.

13. H. Paulsen, *Angew. Chem. Int. Ed. Engl*. **1982**, *21*, 155-173.

14. H. Paulsen, *Chem. Soc. Rev*. **1984**, *13*, 15-45.

15. K. C. Nicolaou, R. E. Dolle, D. P. Papahatjis, *J. Am. Chem. Soc*. **1984**, *106*, 4189-4192.

16. T. Matsumoto, H. Maeta, K. Suzuki, G. Tsuchihashi, *Tetrahedron Lett.* **1988**, *29*, 3567-3570.

17. R. R. Schmidt, J. Michel, *Angew. Chem. Int. Ed. Engl*. **1980**, *19*, 731-732.

18. R. R. Schmidt, *Angew. Chem. Int. Ed. Engl.* **1986**, *25*, 212-235.

19. K. C. Nicolaou, S. P. Seitz, D. P. Papahatjis, *J. Am. Chem. Soc*. **1983**, *105*, 2430-2434.

20. J. D. C. Codée, R.E. J. N. Litjens, L. J. Bos, H. S. Overkleefta, G. A. Marel, *Chem. Soc. Rev.* **2005**, *34*, 769-782.

21. L. F. Tietze, P. Fischer, H. J. Guder, *Tetrahedron Lett.* **1982**, *23*, 4661-4664.

22. D. Kahne, S. Walker, Y. Cheng, D. V. Engen, *J. Am. Chem. Soc*. **1989**, *111*, 6881-6882.

23. D. Crich, S. Sun, *J. Am. Chem. Soc*. **1998**, *120*, 435-436.

24. B. A. Garcia, J. L. Poole, D. Y. Gin, *J. Am. Chem. Soc*. **1997**, *119*, 7597-7598.

25. H. Paulsen, *Chem. Soc. Rev*. **1984**, *13*, 15-45.

26. K. C. Nicolaou, R. E. Dolle, D. P. Papahatjis, *J. Am. Chem. Soc*. **1984**, *106*, 4189-4192.

27. T. Matsumoto, H. Maeta, K. Suzuki, G. Tsuchihashi, *Tetrahedron Lett.* **1988**, *29*, 3567-3570.

28. G. Bati, J.-X. He, K. B. Pal, X.-W. Liu, *Chem. Soc. Rev*. **2019**, *48*, 4006-4018.

29. P. Sinaÿ, *Pure Appl. Chem.* **1978**, *50*, 1437-1452.

30. S. Vorm, T. Hansen, J. Hengst, H. S. Overkleeft, J. D. C. Codée, *Chem. Soc. Rev.* **2019**, *48*, 4688-4706.

31. X. G. Jia, A. V. Demchenko, Beilstein *J. Org. Chem*. **2017**, *13*, 2028-2048.

32. S. Kusumoto, M. Imoto, T. Ogiku, T. Shiba, *Bull. Chem. Soc. Jpn*. **1986**, *59*, 1419-1423.

33. S. Valverde, A. M. Gómez, A. Hernández, B. Herradón, J. C. López, *J. Chem. Soc., Chem. Commun*. **1995**, 2005-2006.

34. H. Yamada, K. Imamura, T. Takahashi, *Tetrahedron Lett*. **1997**, *38*, 391-394.

35. G. Lemanski, T. Ziegler, *Tetrahedron* **2000**, *56*, 579.

36. R. Lau, G. Schüle, U. Schwanaberg, T. Ziegler, *Liebigs Ann*. **1995**, 1745-1754.

37. G. Lemanski, T. Ziegler, *Helv. Chim. Acta*. **2000**, *83*, 2655-2675.
38. M. Wakao, K. Fukase, S. Kusumoto, *Synlett* **1999**, 1911-1914.
39. T. Ziegler, R. Lau, *Tetrahedron Lett.* **1995**, *36*, 1417-1420.
40. G. Lemanski, T. Ziegler, *Tetrahedron* **2000**, *56*, 563-579.
41. G. Lemanski, T. Ziegler, *Helv. Chim. Acta.* **2000**, *83*, 2655-2675.
42. M. Müller, U. Huchel, A. Geyer, R. R. Schmidt, *J. Org. Chem*. **1999**, *64*, 6190-6201.
43. D. R. Greenwell, A. F. Ibnouzaki, S. L. Warriner, *Angew. Chem., Int. Ed.* **2002**, *41*, 1215-1218.
44. E. A. Villar, D. Beglov, S. Chennamadhavuni, J. A. Porco, Jr., D. Kozakov, S. Vajda, A. Whitty, *Nat. Chem. Biol*. **2014**, *10*, 723-731.
45. J. Xie, N. Bogliotti, *Chem. Rev.* **2014**, *114*, 7678-7739.
46. T. Fujioka, Y. H. Kashiwada, K. Okabe, K. H. B. Lee, *Med. Chem. Lett.* **1996**, *6*, 2807-2810.
47. A. Fürstner, M. Albert, J. Mlynarski, M. Matheu, E. DeClercq, *J. Am. Chem. Soc*. **2003**, *125*, 13132-13142.
48. D. P. Larson, C. H. Heathcock, *J. Org. Chem*. **1996,** *61*, 5208-5209
49. D. P. Larson, C. H. Heathcock, *J. Org. Chem.* **1997**, *62*, 8406-8418.
50. S.-F. Lu, Q. O'yang, Z.-W. Guo, B. Yu, Y.-Z. Hui, *Angew. Chem., Int. Ed*. **1997**, *36*, 2344-2346.
51. S.-F. Lu, Q. O'yang, Z.-W. Guo, B. Yu, Y.-Z. Hui, *J. Org. Chem*. **1997**, *62*, 8400-8405.
52. S.-H. Son, N. Yanagiya, J. Furukawa, N. Sakairi, *Synlett* **2009**, *18*, 2957-2960.
53. M. Brito-Arias, R. Pereda-Miranda, C. H. Heathcock, *J. Org. Chem*. **2004**, *69*, 4567-4570.
54. R. R. Bukownik, C. S. Wilcox, *J. Org. Chem.* **1988**, *53*, 463-471.
55. C. S. Wilcox, M. D. Cowart, *Carbohydr. Res*. **1987**, *171*, 141-160.
56. S. Penadés, J. M. Coterón, *J. Chem.* Soc., *Chem. Commun*. **1992**, *9*, 683-684.
57. J. M. Coterón, C. Vicent, C. Bosso, S. Penadés, *J. Am. Chem. Soc*. **1993**, *115*, 10066-10076.
58. J. Jiménez-Barbero, E. Junquera, M. Martín-Pastor, S. Sharma, C. Vicent, S. Penadés, *J. Am. Chem. Soc.* **1995**, *117*, 11198-11204.
59. A. Dondoni, X. Hu, A. Marra, H. D. Banks, *Tetrahedron Lett*. **2001**, *42*, 3295-3298.
60. H. C. Kolb, M. G. Finn, K. B. Sharpless, *Angew. Chem., Int. Ed*. **2001**, *40*, 2004-2021.
61. M. Meldal, C. W. Tornøe, *Chem. Rev*. **2008**, *8*, 3295-3298.
62. H. Struthers, T. L. Mindt, R. Schibli, *Dalton Trans*. **2010**, *39*, 675-696.
63. S. G. Agalave, S. R. Maujan, V. S. Pore, *Chem. Asian J.* **2011**, *6*, 2696-2718.
64. K. D. Bodine, D. Y. Gin, M. S. Gin, *J. Am. Chem. Soc*. **2004**, *126*, 1638-1639.
65. J. F. Billing, U. J. Nilsson, *J. Org. Chem.* **2005**, *70*, 4847-4850.
66. A. Allam, L. Dupont, J.-B. Behr, R. Plantier-Royon, *Eur. J. Org. Chem*. **2012**, *4*, 817-823.
67. S. Muthana, H. Yu, H. Cao, J. Cheng, X. Chen, *J. Org. Chem*. **2009**, *74*, 2928-2936.
68. R. Leyden, P. Murphy, *Synlett* **2009**, *12*, 1949-1950.
69. M. Irie, *Chem. Rev*. **2000**, *100*, 1683-1684.
70. H. Dürr, H. Bouas-Laurent, Photochromism: *Molecules and Systems, Elsevier*, **2003**.
71. W. Szymański, J. M. Beierle, H. A. V. Kistemaker, W. A. Velema, B. L. Feringa, *Chem. Rev*. **2013**, *113*, 6114-6178.
72. S. Kawata, Y. Kawata, *Chem. Rev*. **2000**, *100*, 1777-1788.
73. T. Ozawa, H. Yoshimura, S. B. Kim, *Anal. Chem*. **2013**, *85*, 590-609.
74. R. Gostl, A. Senf, S. Hecht, *Chem. Soc. Rev*. **2014**, *43*, 1982-1996.

75. M. M. Lerch, M. J. Hansen, G. M. van Dam, W. Szymanski, B. L. Feringa, *Angew. Chem. Int. Ed*. **2016**, *55*, 10978-10999.

76. D. H. Qu, Q. C. Wang, Q. W. Zhang, X. Ma, H. Tian, *Chem. Rev*. **2015**, *115*, 7543-7588.

77. Demselben, *Ann. Pharm*. **1834**, *12*, 311-314.

78. G. S. Hartley, *Nature* **1937**, *140*, 281-281.

79. A. A. Beharry, G. A. Woolley, *Chem. Soc. Rev.* **2011**, *40*, 4422-4437.

80. H. Rau, *Photoreact. Org. Thin Films*, **2002**, 3-47

81. H. Rau, E. Lueddecke, *J. Am. Chem. Soc*., **1982**, *104*, 1616-1620.

82. R. Turansky, M. Konopka, N. L. Doltsinis, I. Stich, D. Marx, *Phys. Chem. Chem. Phys.*, **2010**, *12*, 13922-13932.

83. J. Henzl, M. Mehlhorn, H. Gawronski, K.-H. Rieder, K. Morgenstern, *Angew. Chem., Int. Ed.*, **2006**, *45*, 603-606.

84. X. Tong, M. Pelletier, A. Lasia, Y. Zhao, *Angew. Chem., Int.Ed.*, **2008**, *47*, 3596-3599.

85. E. Fischer, *J. Am. Chem. Soc*. **1960**, *82*, 3249-3252.

86. H. M. Bandara, S. C. Burdette, *Chem. Soc. Rev*. **2012**, *41*, 1809-1825.

87. A. A. Beharry, G. A. Woolley, *Chem. Soc. Rev*. **2011**, *40*, 4422-4437.

88. M. Quick, A. L. Dobryakov, M. Gerecke, C. Richter, F. Berndt, I. N. Ioffe, S. A. Kovalenko, *J. Phys. Chem. B* **2014**, *118*, 8756-8771.

89. C. J. Otolski, A. M. Raj, V. Ramamurthy, C. G. Elles, *Chem. Sci*. **2020**, ***11***, 9513-9523.

90. E. Merino, M. Ribagorda, *Beilstein J. Org. Chem*. **2012**, *8*, 1071-1090.

91. J. Calbo, A. R. Thawani, R. S. Gibson, A. J. White, M. J. Fuchter, *Beilstein J. Org. Chem*. **2019**, *15*, 2753-2764.

92. F. A. Jerca, V. V. Jerca, R. Hoogenboom, *Nat. Rev. Chem*. **2022**, *6*, 51-69.

93. N. L. Mutter, J. Volaric, W. Szymanski, B. L. Feringa, G. Maglia, *J. Am. Chem. Soc*. **2019**, *141*, 14356-14363.

94. S. K. Rastogi, H. E. Anderson, J. Lamas, S. Barret, T. Cantu, S. Zauscher, W. J. Brittain, T. Betancourt, *ACS Appl. Mater. Interfaces* **2018**, *10*, 30071-30080.

95. C. Yao, P. Wang, X. Li, X. Hu, J. Hou, L. Wang, F. Zhang, *Adv. Mater*. **2016**, *28*, 9341-9348.

96. G. Despras, J. Hain, S. Jaeschke, *Chem. Eur. J.* **2017**, *23*, 10838-10847.

97. J. Hain, G. Despras, *Chem. Commun*. **2018**, *54*, 8563-8566.

98. C. Lin, S. Maisonneuve R. Métivier, J. Xie, Chem. Eur. J. **2017**, 23, 14996-15001.

99. C. Lin, S. Maisonneuve, C. Theulier, J. Xie, *Eur. J. Org. Chem*. **2019**, 1770-1777.

100. Y. Kim, N. Mafy, S. Maisonneuve, C. Lin, N. Tamaoki, J. Xie, *ACS Appl. Mater. Interfaces*, **2020**, *12*, 52146-52155.

101. P. S. Owska, K, Dąbrowa, S. Jarosz, *Org. Lett*. **2021**, *23*, 2687-2692.

102. C. Lin, J. Jiao, S. Maisonneuve, J. Malletroit, J. Xie, *Chem. Commun*. **2020**, *56*, 3261-3264.

103. H. M. Dhammika, S. C. Burdette, *Chem. Soc. Rev*. **2012**, *41*, 1809-1825.

104. J. Xie, J. in Carbohydrate Chemistry: Chemical and Biological Approaches, vol. 45 (Eds.: A. P. Rauter, T. K. Lindhorst, Y. Queneau), Royal Society of Chemistry, Cambridge, 2022, pp. 460-498.

105. Y. Zhu, B. Yu, *Chem. Eur. J.* **2015**, *21*, 8771-8780.

106. D. Chatterjee, A. P. Rajkamal, S. Yadav, *RSC. Adv*. **2015**, *5*, 29669-29674.

107. S. Deng, U. Gangadharmath, C-W. T. Chang, *J. Org. Chem.***2006**, *71*, 5179-5185.

108. M. J. Sofia, R. Kakarla, N. Kogan, R. Dulina, Y. W. Hui, N. T. Hatzenbuhler, D. Liu, A. Chen, T. Wagler, *Bioorg. Med. Chem. Lett.* **1997**, *7*, 2251-2254.

109. A. Ishiwata, Y. J. Lee, Y. Ito, *Org. Biomol. Chem.* **2010**, *8*, 3596-3608.

110. M. Heuckendorff, L. T. Poulsen, C. Hedberg, H. H. Jensen, *Org. Biomol. Chem.* **2018**, *16*, 2277-2288.

111. M. Matwiejuk, J. Thiem, *Chem. Commun*. **2011**, *47*, 8379-8381.

112. R. Yadav, S. L. Ben-Arye, B. Subramani, V. Padler-Karavani, R. Kikkeri, *Org. Biomol. Chem.* **2016**, *14*, 10812-10815.

113. R. U. Lemieux, R. K. Kullnig, H. J. Bernstein, W. G. Schneider, *J. Am. Chem. Soc.* **1958**, *80*, 6098-6105.

114. P.-E. Jansson, L. Kenne, G. Widmalm, *Carbohydr. Res.* **1987**, *168*, 67-77.

115. K. Bock, C. Pedersen, *J. Chem. Soc. Perkin Trans. 2* **1974**, 293-297.

116. S. Samanta, A. Babalhavaeji, M. Dong, G. A. Woolley, *Angew. Chem. Int. Ed*. **2013**, *52*, 14127-14130.

117. M. Dong, A. Babalhavaeji, M. J. Hansen, L. Kálmánb, G. A. Woolley, *Chem. Commun*. **2015**, *51*, 12981-12984.

118. M. C. Murguía, S. E. Vaillard, R. J. Grau, *Synthesis* **2001**, 1093-1097.

119. Y. Zhu, B. Yu, *Chem. Eur. J.* **2015**, *21*, 8771-8780.

120. S. Kawata, Y. Kawata, Chemical reviews, 2000, 100(5), 1777-1788.

121. J. Crassous, *L'actualité chimique* **2020**, *449*, 23-30.

122. V. Mujica, *Nature Chem*. **2015**, *7*, 543-544.

123. G. Haberhaeur, C. Kallweit, *Angew. Chem. Int.Ed.* **2020**, *49*, 2418-2421.

124. K. Takaishi, M. Kawamoto, K. Tsubaki, T. Furuyama, A. Muranaka, M. Uchiyama, *Chemistry–A European Journal*, **2011**, *17*(6), 1778-1782.

127. M. Natali, S. Giordani, *Chem. Soc. Rev.* **2012**, *41*, 4010-4029.

128. C. Yue, C. Liao, Z. Yang, F. Hu, *Current Organic Chemistry* **2018**, *22*, 1458-1467.

129. J. Pérez-Miqueo, A. Altube, E. García-Lecina, A. Tron, N. D. McClenaghanc, Z. Freixa, *Dalton Trans.* **2016**, *45*, 13726–13741.

130. E. Wagner Wysiecka, N. Łukasik, J.-F. Biernat, E. Luboch, *Journal of Inclusion Phenomena and Macrocyclic Chemistry* **2018**, *90*, 189-257.

131. B. L. Feringa, R. A. van Delden, N. Koumura, E. M. Geertsema, *Chemical Reviews*, **2000**, *100*(5), 1789-1816.

132. M. Kondo, K. Nakamura, C. G. Krishnan, S. Takizawa, T. Abe, H. Sasai, *ACS Catal.* **2021**, *11*, 1863-1867.

133. C. G. Krishnan, M. Kondo, K. Nakamura, H. Sasai, S. Takizawa; *Org. Lett.* **2022**, *24*, 2670-2674.

134. D. Chatterjee, A. Paul, Rajkamal, S. Yadav, *RSC Adv*. **2015**, *5*, 29669-29674.

135. P. Blom, B. Ruttens, S. V. Hoof, I. Hubrecht, J. V. der Eycken, *J. Org. Chem*. **2005**, *70*, 10109-10112.

136. S. Deng, U. Gangadharmath, C-W. T. Chang, *J. Org. Chem*. **2006**, *71*, 5179-5185.

137. M. J. Sofia, R. Kakarla, N. Kogan, R. Dulina, Y. W. Hui, N. T. Hatzenbuhler, D. Liu, A. Chen, T. Wagler, *Bioorg. Med. Chem. Lett.* **1997**, *7*, 2251-2254.

138. A. Ishiwata, Y. J. Lee, Y. Ito, *Org. Biomol. Chem*. **2010**, *8*, 3596-3608.

140. M. Heuckendorff, L. T. Poulsen, C. Hedberg, H. H. Jensen, *Org. Biomol. Chem*. **2018**,*16*,2277-2288.

141. L. Yan, D. Kahne, *J. Am. Chem. Soc*. **1996**, *118*, 9239-9248.

141. M. C. Murguía, S. E. Vaillard, R. J. Grau, *Synthesis*, **2001**, 1093-1097.

PUBLICATIONS AND COMMUNICATIONS

Publications

1. 'Stereoselective synthesis and properties of glycoazobenzene macrocycles through intramolecular glycosylation'
   Lin, C.; Jiao, J.; Maisonneuve, S.; Mallétroit, J.; Xie, J. *Chem. Commun*. **2020**, *56*, 3261-3264.
2. 'Synthesis and Azobenzene Isomerization Investigation of Photoswitchable Glycomacrocycles'
   Jiao, J.; Maisonneuve, S.; Xie, J. *J. Org. Chem*. **2022**, *87*, 8534-8543.

Oral communications

1. Photochromic glycomacrocycles: synthesis, characterization and light-controlled stereoselective glycosylation investigation
   Jiao, J.; Maisonneuve, S.; Xie, J. *2ème Journée des Doctorants PPSM*, Mercredi 26 juin **2019**, cachan, France
2. Synthesis, photochromic and chiroptical properties of photoswitchable glycomacrocycles
   Jiao, J.; Maisonneuve, S.; Kim, Y.; Xie, J. *5th Nanosynergetics Workshop*, 13th Nov. **2020**, Online.
3. Photochromic glycomacrocycles: synthesis, characterization and light-controlled stereoselective glycosylation investigation
   Jiao, J.; Maisonneuve, S.; Kim, Y.; Xie, J. *Seminary of PPSM*, 6th April **2021**, Online.
4. Photochromic glycomacrocycles: synthesis, characterization and light-controlled stereoselective glycosylation investigation
   Jiao, J.; Maisonneuve, S.; Xie, J. *JED2022*, 24th May **2022**, oral presentation, Gif-sur-Yvette, France.

Communications by poster

1. Photochromic template for light-controlled stereoselective glycosylation: stereoselectivity and properties of photoswitchable glycomacrocycles
   Jiao, J.; Maisonneuve, S.; Xie, J. *9th International Symposium On Photochromism* (*ISOP2019*), 23-27 September **2019**, Institut Pasteur, Paris, France.
2. Photochromic glycomacrocycles: synthesis, characterization and light-controlled stereoselective glycosylation investigation
   Jiao, J.; Maisonneuve, S.; Xie, J. *Journées de Chimie Organique* **2019** (*JCO2019*), 29-31, October 2019, École polytechnique, Palaiseau, France. Gif-sur-Yvette, France.

université PARIS-SACLAY

ÉCOLE DOCTORALE
Sciences Chimiques : Molécules, Matériaux, Instrumentation et Biosystèmes (2MIB)

Titre : Glycomacrocycles photocommutables : synthèse, caractérisation et étude de la stéréosélectivité de glycosylation contrôlée par la lumièreumière

Mots clés : azobenzène, glucides, glycosylation, macrocycle, photochrome.

Résumé : Les molécules photochromes ont trouvé des applications croissantes en chimie, en sciences des matériaux, en biologie et en photopharmacologie grâce à la possibilité de photocontrôler d'une manière spatio-temporel et réversible de la conformation, des propriétés physicochimiques, de la réactivité chimique, et des activités biologiques et pharmacologiques des molécules d'intéret. Nous nous sommes intéressés au dévelopment de glucides photocommutables, en particulier la synthèse de glycomacrocycles photocommutables, afin de moduler leurs propriétés physicochimiques, chimiques et biologiques par la lumière. Dans cette thèse, nous avons étudié l'influence de l'irradiation lumineuse sur la stéréosélectivité de la glycosylation intramoléculaire en utilisant le *o,o'*-dihydroxyazobenzène comme photochrome, et préparé deux nouvels séries de glycomacrocycles photocommutables. L'efficacité et la stéréosélectivité de la glycosylation dépendent de la nature des liens et de l'accepteur de glycosyle, ainsi que de la configuration de l'azobenzène. Une excellente 1,2-*cis* mannosylation a été obtenue avec des accepteurs de glycosyle portant un groupe hydroxyle primaire. Des études photophysiques ont révélé que les glycomacrocycles synthétisés présentent d'excellentes propriétés photophromes et une grande résistance à la fatigue. Le transfert de chiralité du sucre à la partie azobenzène a également été observé. Les résultats préliminaires ont montré des propriétés de complexation des ions métalliques contrôlées par la lumière pour les glycomacrocycles, avec un changement de propriété chiroptique lors de la complexation.

Title: Photochromic glycomacrocycles: synthesis, characterization and light-controlled stereoselective glycosylation investigation

Keywords: azobenzene, carbohydrate, glycosylation, macrocycle, photochrome.

Abstract: Photochromic molecules have found increasing applications in chemistry, materials sciences, biology and photopharmacology through spatial and temporal photocontrol of conformation, physicochemical properties, chemical reactivity, biological and pharmacological activities of molecules in a reversible way. We are interested in the development of photoswitchable carbohydrates, in particular the synthesis of photoswitchable glycomacrocycles so as to modulate their physicochemical, chemical and biologic properties by light. In this thesis, we have investigated the influence of light illumination on the stereoselectivity of intramolecular glycosylation by using o,o'-dihydroxyazobenzene as photochromic template, and prepared two new series of photoswitchable glycomacrocycles. The efficiency and the stereoselectivity of glycosylation have been found to be dependent on the nature of the linkers and glycosyl acceptor, as well as the configuration of the azobenzene tether. Excellent 1,2-*cis* mannosylation has been obtained with glycosyl acceptors bearing a primary hydroxyl group. Photophysical investigations revealed that the synthesized glycomacrocycles show excellent photophromic properties with high fatigue resistance. Chirality transfer from sugar to azobenzene moiety has also been observed. Preliminary results showed light-controlled metal ion complexing properties of glycomacrocycle with chiroptical property switching upon ion-complexation.